CHAPTER 1

Introduction to Polyoxometalates and Scope of the Work

The impact of polyoxometalate chemistry since the synthesis of the first derivative in 1826 is beyond all doubt. Experimentalists have studied these complexes for a long time and much is known about their behaviour and applications. Experimental techniques were used to study their properties and knowledge rapidly increased. The unprecedented properties and the virtually unlimited structural possibilities of these compounds have focused the attention of a large number of chemists for decades. Furthermore, the complex nature of metal-oxide frameworks and their associated phenomena created considerable interest amongst the community of theoretical chemists that, in the early 90s, started to apply modern computational techniques to explain the intricacies of polyoxometalate chemistry. The present chapter introduces the reader to the general characteristics of polyoxometalates: for example, the patterns governing their structure, their redox behaviour and the most important applications discovered to date. We pay particular attention to their structural characteristics, the main focus of the study. Finally, the last section shows the main aims of this thesis.

1.1. Introduction

The great majority of inorganic compounds are constructed of metallic atoms as principal entities. This means that this subgroup of chemicals has considerable structural diversity, although it is still surpassed (in number of classified and characterised compounds) by organic compounds. However, inorganic molecules (a priori a much bigger field) have greater potential because the number of elements in *purely* inorganic molecules, combined with their structural diversity, make them more powerful, particularly as far as their applications are concerned. In fact, the search for new features puts more importance on the elements in a framework than on the structure itself. In the organic world, the principal variable that produces novel behaviour is the structure. In this sense, maybe the field of polyoxometalates (POMs) lies between the organic and the inorganic worlds.

Historical perspective

The first POM, the phosphomolybdate of formula $[PMo_{12}O_{40}]^{3-}$, was reported by Berzelius[1] in 1826. Marignac[2] observed two isomeric forms of $[SiW_{12}O_{40}]^{4-}$. In the early 1930s, Keggin solved the structure of the related anion $[PW_{12}O_{40}]^{3-}$.[3] Since then, countless structures have been synthesised and characterised. The turning point came when spectroscopic techniques were used for characterisation. The end of the 19th century and the early decades of the 20th century were fruitful in theories that explained coordination chemistry[4] and, particularly, the chemistry of POMs.[5] In the last 40 years, a lot of experimental information has been collected. Today, POMs constitute an immense class of polynuclear metal-oxygen clusters[6-8] usually formed by Mo, W or V and mixtures of these elements. They have potential applications in many fields including medicine, catalysis, multifunctional materials, chemical analysis, etc. According to Katsoulis' compilation,[9] in 1996 there were more than 700 communications (publications and patents) in the family of POMs. Most applications are related to their special ability to accept one or several electrons with minimal structural changes. Dozens of elements have been reported as taking part in POM compounds.[6] In addition, beyond this chemical flexibility, they have an 'organic-like' structural diversity and the number of frameworks synthesised increases daily.

1.2. Structural Principles of Polyoxometalates

Polyoxometalates are one set of inorganic molecules in the vast field of coordination chemistry compounds. They are characterised by a metallic centre, M, which is surrounded by some atoms or groups of atoms. In POMs, ligands are normally oxygen atoms, although some derivatives with S,[10-14] F,[15] Br[16] and other p-block elements are known. So, in general, we have MO_n units, where n indicates the coordination number of M. Usually, n = 6, although it can be 4, 5 or 7, as well. Apart from M and O, other elements, which are usually labelled as X, can be part of the POM framework. As a general rule, they are 4-fold- or 6-fold-coordinated and lie in the centre of the M_xO_y shell. Depending on whether X is present or not, we can distinguish two types of POM species. This classification is based on a purely structural criterion and this nomenclature will be used throughout the text:

Isopolyanions (IPAs)	$[M_nO_y]^{p-}$	(1)
Heteropolyanions (HPAs)	$[X_zM_nO_y]^{q-}$, with $z \leq n$	(2)

There are no chemical limitations for X and M by definition. The X elements are the so-called primary, central or *heteroatoms*. In general, any element can participate as X in a POM cluster since there are no strict physical requirements for this position. On the other hand, M are the so-called secondary, peripheral or *addenda* atoms and only some M elements are typically found in such compounds (see text below in this section). In a few cases, this distinction may be confusing or uncertain, but in the clusters dealt with here the distinction is clear. Despite the simplicity of formulas (1) and (2) above, the composition of a cluster can be highly complex, with various M elements taking part in the structure. In anions in which more than one M addenda-type is present in the framework, the molecule is known as a *mixed-addenda* cluster. The study of mixed-addenda anions is a fundamental part of this thesis, and will be discussed at length in Part II.

Basic structural units

POMs are a family of medium-to-large-sized molecular (discrete) metal-oxides. Metal-oxide aggregates with fewer than 3–4 metal centres are traditionally *not* POMs. Nevertheless, due to the increasing diversity of

structures classified as such in the literature, the unequivocal definition of this group of compounds becomes gradually more and more diffuse. Be that as it may, countless reports,[21] books[17] and reviews[18-19] have been published on this topic, showing an enormous molecular diversity amongst the inorganic family of molecules. This diversity is somehow a consequence of the rich, unprecedented and unusual properties associated to POMs. Many authors claim that they can be regarded as packed arrays of pyramidal MO_5 and octahedral MO_6 units (see Figure 1.1). These entities are, then, the fundamental structural units and are somewhat similar to the $-CH_2-$ unit in organic chemistry.

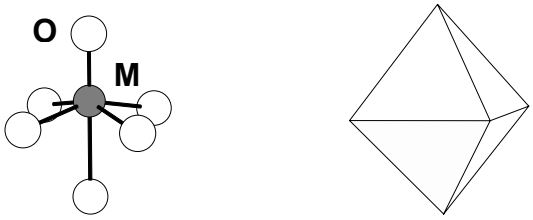

Figure 1.1. Ball-and-stick and polyhedral representations of the fundamental unit MO_6. Note that the M atom is displaced off the geometrical centre of the octahedron towards one of the oxygens, thus giving rise to a distorted C_{4v} unit.

The very important MO_6 units (and the MO_5 partner as well but to a lesser extent) are, then, packed to form countless shapes. They join to one another, apparently, in accordance with a few simple rules (as $-CH_2-$ does in organic molecules). Observing a representative set of POM clusters, and identifying the MO_6 blocks, we notice that the molecule as a whole is built by edge- and/or corner-sharing MO_6 octahedra. Figure 1.2 shows these simple unions. The most stable unions between two octahedra are the corner- and edge-sharing models,[20] in which the M^{n+} ions are far enough from each other, and their mutual repulsion is modest (Table 1.1). In case C of Figure 1.2, the metallic centres are closer than in any of the other two cases (A, B) and, at such distances, the repulsion is not balanced by the stabilisation due to the chemical bonding in the 2-block unit. The latter form of union is uncommon and all the structures presented in this text only deal with derivatives containing combinations of pairs of types A and B.

Table 1.1. Selected M–M distances (in angstrom units) of corner- and edge-sharing octahedra in POMs.

Metal(ON)	*corner-sharing*	*edge-sharing*
W(VI)	3.7	3.4
Mo(VI)	3.7	3.5
V(V)	3.5	3.2

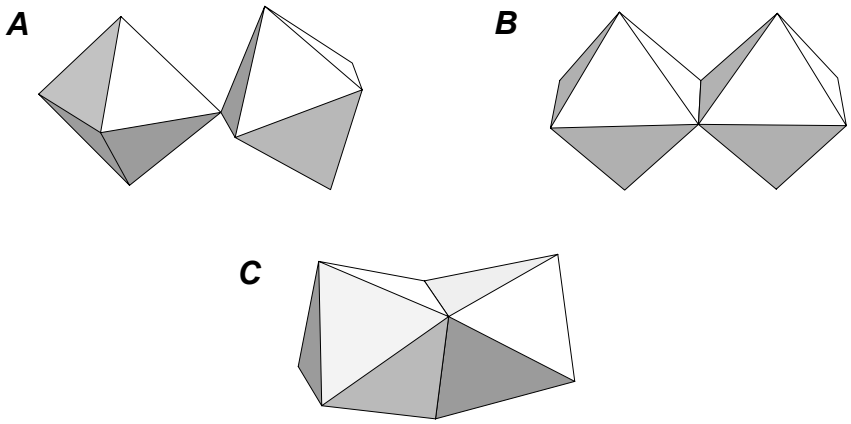

Figure 1.2. The polyhedral models represent the three possible unions between two MO_6 octahedral units. A) corner-sharing, B) edge-sharing and C) face-sharing. Each corner represents an oxygen position.

The clathrate-like structure

Clathrate-like systems are molecular or supramolecular arrangements in which an internal unit is encapsulated by an external core. In metal-oxide polynuclear clusters, it is a common phenomenon that has been discussed by experimentalists[21-24] and computational chemists.[25-27] A formulation for molecules that accomplish the requirements of a clathrate-like system was introduced in the way I@E, in which I and E are the internal and the external *fragments* (see Figure 1.3). Keggin, Wells–Dawson and Lindqvist anions were also formulated as

$[XO_4]^{n-}@M_{12}O_{36}$ Keggin,

$[XO_4]_2^{n-}@M_{18}O_{54}$ Wells–Dawson,

$O^{2-}@M_6O_{18}$ Lindqvist,

where the external M_xO_y core is free of metallic electrons if the cluster is fully oxidised. This assumption can be very advantageous in the study of complex phenomena like the isomerism, as shall be discussed in chapter 4.

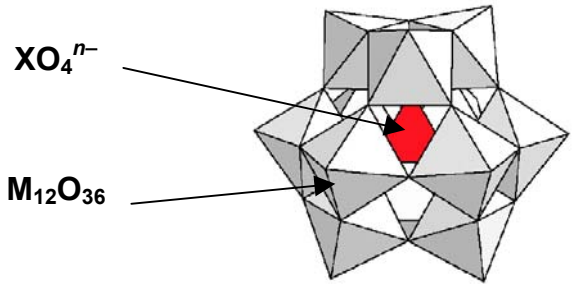

Figure 1.3. Polyhedral view of the clathrate-like structure of the Keggin anion. The external $M_{12}O_{36}$ core encapsulates the internal unit (represented as a red tetrahedron).

Chemical elements taking part in POMs

We have identified the addenda atom, M, as the most important entity in POMs. All the clusters included in this classification contain MO_n units, so the characteristics of M deserve further discussion. The fundamental structural block from which POM frameworks are built is the MO_6 unit,[28] where M is a transition-metal element. Many M elements are known to form six-fold, octahedral coordination compounds with oxygen, but not so many can take part, in MO_6 units, in a packed polynuclear metal-oxide aggregate. The structures of polyanions appear to be governed by the electrostatic and ionic radius principles of metal centres. That is, only selected values of the charge/radius ratio are observed in M^{n+} in combination with O^{2-} ligands, thus forming POMs. A few Ms are commonly found or routinely included in a structure since these physical limitations control the stability of the metal-

oxide framework (see the values listed in Table 1.2). It only contains early transition metal elements, from the left of the periodic table. In fact, there are other ions that have values of q and r with limits similar to those shown in Table 1.2. So, apart from other transition metals, some p-block elements could be, at least in principle, good candidates for being included in MO_6 units as addenda.

However, charge and radius are not the only considerations to rule these assemblages of metal-centred units. Actually, an additional parameter to be considered, related to M, is the ability to form metal-oxygen π-bonds. This affects the stability of these clusters, as well. It was observed long ago that, in octahedral MO_6 blocks, the metallic centre is not in the very middle of the polyhedron, but somewhat displaced from the geometrical centre towards one of the corners (see Figure 1.1). More precisely, it is displaced towards the corner that does not share another octahedron, and the oxygen at this position usually forms a double bond with the metal (see the cluster in Figures 1.2 and 1.4). This is another of the requirements that the M centre should comply with. These pπ–dπ interactions are of the greatest importance in the stability of metal-oxide clusters,[29] and only the elements listed in Table 1.2 are suitable for this purpose. The reader shall see in future chapters that terminal (unshared) oxygens are, in general, essentially non-basic since there is a strong inward polarisation of the oxygen's electron density. This accounts for the molecular (discrete) metal-oxide arrays of MO_6 units, instead of extended, insoluble infinite layers or solids.

Table 1.2. List of common metal cations, M^{n+}, taking part in POM frameworks. We especially highlight W and Mo for being the most typical as addenda atoms.

Metal ion	*Octahedral radius (Å)*	*Observed coordination numbers in POMs*
W^{6+}	**0.74**	**6**
Mo^{6+}	**0.73**	**4, 6, 7**
V^{5+}	0.68	4, 5, 6, 7
Ta^{5+}	0.78	6
Nb^{5+}	0.78	6

Table 1.2. Continued.

Tc^{7+}	0.70 [a]
Ti^{4+}	0.74 [a]
Sb^{5+}	0.74 [a]

a) Shannon–Prewitt effective ionic radii for sixfold coordination.

It is precisely the ability to form M=O double bonds that makes *small* POMs possible. Nevertheless, exceptions to this rule are discussed in chapter 6. Despite all of the above, after nearly two centuries of POM chemistry, almost all the elements of the periodic table have somehow been incorporated into a polyoxometalate framework.[30] This accounts for the chemical variability of this field.

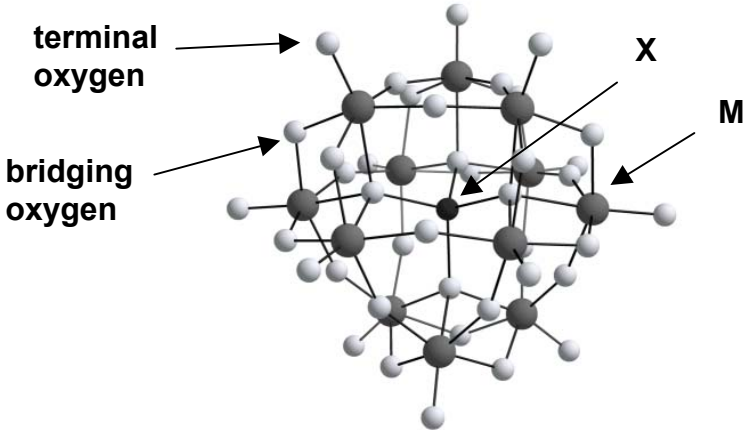

Figure 1.4. Ball-and-stick representation of the Keggin heteropolyanion. The terminal and bridging oxygen sites are indicated for further discussion.

A. **$M_6O_{19}^{n-}$ (Lindqvist)**

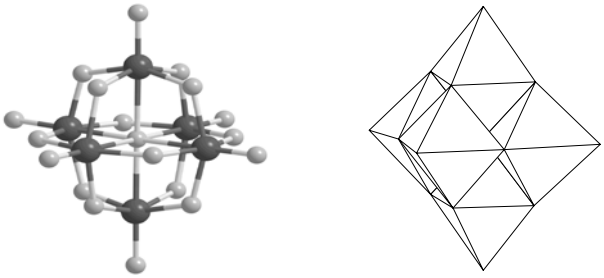

B. **$XM_6O_{24}^{n-}$ (Anderson)**

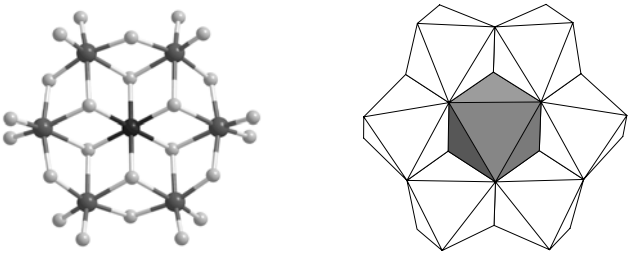

C. **$X_2M_{18}O_{62}^{n-}$ (Wells–Dawson)**

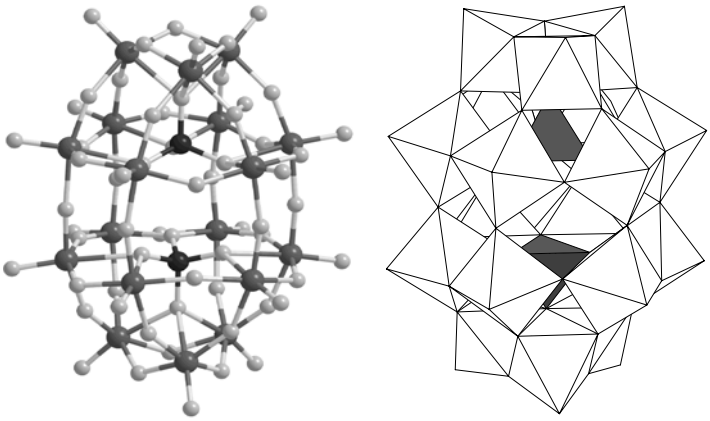

Figure 1.5. Ball-and-stick and polyhedral views of one isopolyanion (A) and two heteropolyanions (B, C). Dark grey spheres are metal centres, whereas light ones are oxygens. Black spheres (and the homologous dark polyhedra) contain the X heteroatom.

Fewer restrictions are found when the heteroatom X is part of a POM. Clusters with p-block elements (P, Si, Al, Ga, Ge...), transition metal elements (Fe(II/III), Co(I/II), Ni(II/IV), Zn(II)...), and even two H^+ have been synthesised. This position can be either tetrahedrally coordinated (as in Keggin and Wells–Dawson, or WD, anions) or octahedrally coordinated (as in the Anderson structure). Figure 1.5 shows a small collection of typical POMs including one isopolyanion (A) and two heteropolyanions (B and C). In B, atom X is surrounded by six oxo ligands in a pseudo-octahedral symmetry whereas, in C, two heteroatoms X are tetrahedrally coordinated. In Figure 1.4, only four oxygens surround the central atom. Form A only contains two structurally different atoms: M and O. However, the central atom (an oxygen) is chemically very different from the external ones since it is surrounded by six cations.

1.3. Features of Polyoxometalates

Preparation

Heteropoly- and isopolyanions are routinely prepared and isolated from both aqueous and non-aqueous solutions. The most common method of synthesis involves dissolving $[MO_n]^{m-}$ anions which, after acidification, assemble to yield a packed molecular array of MO_6 units. For example,

$$7MoO_4^{2-} + 8H^+ \rightarrow \left[Mo_7O_{24}\right]^{6-} + 4H_2O$$

$$12WO_4^{2-} + HPO_4^{2-} + 23H^+ \rightarrow \left[PW_{12}O_{40}\right]^{3-} + 12H_2O$$

In general, care must be taken with pH conditions so that the reaction can be controlled. Sometimes, the sequence in which the reagents are added to the reaction media is important. One of the latest steps in synthetic procedures, and maybe the most important if POMs are to be completely characterised, is the isolation of crystals so that their features can be studied in greater depth. Clusters are precipitated by adding countercations (alkali metals, organic cations like TBA, ammonia, etc.) and subsequent separation. The crystals can then be fully characterised. As far as preparation and storage conditions are concerned, it is worth stressing that POMs are stable

in the presence of oxidising agents (air, water), and also at modestly high temperatures.

Redox properties

Addenda metals, M, are present in their highest oxidation state in all POMs, typically in d^0 or d^1 electronic configurations. They are also bonded to O^{2-} ligands, which produces very ionic structures. Formally, we have pairs like W^{6+}–O^{2-} or V^{5+}–O^{2-}. They can be compared to metal-oxide crystals since the surface of molecular oxometal aggregates is similar to that of infinite surfaces. Thus, to what M_xO_y surfaces are interesting for, POMs can be as well with the great advantage of being soluble as discrete systems in liquid media. One can think in a powerful homogeneous catalyst with similar features to that of traditional crystalline surfaces.

There is little ligand-to-metal donation in their structure, so metal centres are willing to accept external electrons because their valence shell is empty. The overall charge of these anions depends on the heteroatom, X (formally P^{5+}, Al^{3+}, I^{7+}...), and on the addenda metal. Fully oxidised M atoms in POMs usually have formal charges between 4+ and 6+. Obviously, the state of reduction of the molecules can vary this number. Even though they are negatively charged, reductions are common, and often accompanied by protonation. This is the principal feature of POMs: they are strong oxidising agents. The low-lying empty d-type orbitals of addenda atoms can accept numerous electrons with no major changes in their geometry. These extra electrons, located in d-metal orbitals, are called metallic or *blue* electrons. The latter term has its origin in the intense blue colour that can be observed when a few electrons reduce some common POMs. However, we will use the term *blue* regardless of the true colour of a reduced species it merely indicates the presence of metallic electrons. The localisation of metallic electrons is extensively studied throughout this text, and the relationship between the degree of localisation and the presence of different addenda atoms is stressed. The willingness of a given M atom to trap a metallic electron depends on its physical nature. There are many examples in the literature of POM clusters with a high number of metallic electrons (see chapter 7). This is why it is often said that they are a *reservoir* of electrons. An extensive study of reduced states can be found in reference.[6] POMs, however, are stable in solution and in the solid state in their fully

oxidised forms, as well, obviously combined with countercations balancing the negative charge that, in general, POMs carry.

Basicity

Another characteristic of POMs is their acid strength. Many acid-base equilibria in liquid media have been reported, in which POMs appear as polyacids.[31] In most cases, their pK_a is lower than 0, which denotes strong acidity, although in very acidic media they can, of course, be protonated. Because of the chemical differences when POMS are bonded to M, not all oxygen sites in a POM framework are identically basic or acidic. This depends on the following parameters: the covalency/ionicity of the M–O bond, the number of neighbouring M atoms and the physical nature of M. This last point is especially important in the context of this thesis and will be dealt with in depth in the coming chapters. POMs are involved as catalysts in some organic reactions where proton transfer occurs. Incorporating a POM into acidic media can lead to polymerisation reactions, as well. Following similar chemical principles to those that govern the processes formulated in equations (1) and (2), molecular metal-oxides can self-assemble in the presence of protons and then produce larger oxometalates. The mechanics of this complex reaction are still not fully understood nowadays, although the parameters that govern the process are controlled quite well in solution. This phenomenon of polymerisation can, in principle, be attributed to many POMs in favourable conditions. After presenting the general results for the basicity of external oxo sites for a series of mixed-addenda Keggin anions, chapter 6 discusses the particular case of the Keggin dimerisation process.

Isomerism

The effect of isomerism on POMs is chemically subtle but it has been studied by both experimental and theoretical groups. The HPAs studied here have different isomeric forms: the Keggin and the Wells–Dawson anions (discussed in chapters 4 and 5). An assembly of four M_3O_{13} trimeric units forms the Keggin anion, $XM_{12}O_{40}^{n-}$ in general. Each of these trimers can be found in two possible orientations in the framework, thus giving five rotational isomers known as α, β, γ, δ and ε (see chapter 4). A similar rotational isomerism exists for the WD molecule. Differences in the

reduction potentials were found for different isomers of the same chemical formula, although the differences were smaller than those produced by changes in M. Isomers have some different properties, although in general they can be considered chemically similar. Nevertheless, the combination of isomerism and metal substitution make it possible for the properties of the cluster to be tuned.

1.4. Applications

All the value-adding properties presented above have many applications in the technological, chemical and medical fields. There are too many interesting applications to be listed here. At present, excluding medical and catalytic applications, there are nearly 20 categories in which POMs are attractive species.[9] One of the traditionally reported applications concerns elemental analysis aided by POM chemistry. A large set of species, mostly metal elements, can be determined in solution. The reduction potentials in POM species vary considerably as a function of the geometrical characteristics of the cluster and the addenda atoms that take part. Redox potentials are affected by the overall charge of the species, too. So the reduction/oxidation properties can be *tuned* by choosing the heteroatom X, the addenda metal M and the framework.

Some brief comments should be made here, although they are far from exhaustive. POMs have been applied to medicine with considerable success and efficacy. Their oxidising ability is of particular interest. They catalyse many organic reactions and give high yields of reaction and good selectivity.[32] Some POMs that contain vanadium centres have been investigated for environmental-friendly wood pulp bleaching.[33]

The medical or biological/chemical principles governing the interactions between target biomolecules and drugs are

redox potential,
polarity,
shape,
surface charge distribution and
acidity,

which are a set of attributes that chemists can skilfully control in POMs. So the features of POMs can be altered to fit the recognition rules for medical applications. An exhaustive compilation of the knowledge acquired in the field of medical applications of POMs can be found in the References.[34] The medical investigation of some oxometalates is promising although it is still in an initial stage. The *modus operandi* of POMs against viruses or tumoral agents, despite the amount of documentation on the subject, remains unclear. Some outlines of the mechanism have been proposed, though. In fact, POMs show high selectivity toward the target system, whether it is an enzyme or a membrane. The data collected over the years suggest that the overall charge and the charge density play a key role in the efficiency of the inhibition. Some reports have concluded that there is a lock-and-key mechanism between POMs and enzymes, so the size and the electrostatic properties of the oxometalate are determining factors for successful remedies.[34]

1.5. Scope of the Thesis

The main goal of this thesis is to help rationalise the general physical basis of the chemical properties of POMs. The whole study is based on density functional theory calculations that have been proven to be appropriate for studying large molecular systems. Other mathematical tools are used and even introduced to the reader where needed. The theoretical details concerning the computation are discussed in length in chapter 2. The electronic properties of two well-known heteropolyanions —the Keggin ($XM_{12}O_{40}^{n-}$) and the Wells–Dawson ($X_2M_{18}O_{62}^{n-}$) anions— are the fundamental topic of the work. . A rather large set of compounds is presented, with variable X, M and the isomerism. So, the results are not limited to the compounds studied but can be extended to apply to all HPA behaviour. The data shall allow those interested in POM chemistry to find out about the origin of some properties. The main results will concern the following topics:

- The description of the structural features (geometry, clathrate-like framework, localisation of the charge, etc.) and the electronic properties of the Keggin and Wells–Dawson anions, as well as the redox chemistry associated to those clusters.

- The implications of the rotational isomerism in a series of HPAs, with different X and M, rationalised on the basis of their molecular orbitals' scheme. Changes in the MO sequence and energy can explain the reduction potentials observed experimentally.

- The chemical effects of the addenda substitution in HPA frameworks. A series of clusters (M = W, Mo, V, Nb, Ti) are analysed in terms of their protonation energies in different oxygen sites, and relative basicity scales are proposed.

- The dimerisation of mixed-addenda Keggin clusters. From the experimental information available, an attempt to unravel some aspects of the dimerisation process is made. The results combine protonation energies and Molecular Electrostatic Potential visualisation of the substituted Ti-and Nb-derivatives, as well as energy reaction profiles of possible dimerisation pathways.

- The influence of the solvent on the HPA's properties. A continuum model is used to show the effects of the solvent. Calculations carried out in this way show the downshift of the orbital energies accompanied by the stabilisation of the anions. An alternative study was made to give an approximate picture of the structure of a solvent surrounding a Keggin anion.

References and Notes

[1] Berzelius, J. J. *Poggendorfs Ann. Phys. Chem.* **1826**, *6*, 369.

[2] Marignac, C. *Ann. Chim. P*hys. **1864**, *3*, 1.

[3] Keggin, J. F. *Nature*. **1933**, *131*, 908.

[4] Werner, A. *Z. Anorg. Chem*. **1893**, *3*, 267.

[5] Copaux, H. *Ann. Chim. Phys*. **1906**, *7*, 118. Werner, A. *Ber. Dtsch. Chem. Ges*. **1907**, *40*, 40. Miolati, A.; Pizzighelli, R. *J. Prakt. Chem*. **1908**, *77*, 417. Rosenheim, A. *Handbuch der Anorganischen Chemie*. Vol. IV, Part 1. Abegg, R.; Auerbach, F. Eds. Hirzel Verlag, Leipzig, **1921**, pp 977−1064. Pauling, L. *J. Am. Chem. Soc*. **1929**, *51*, 2868.

[6] Pope, M. T. *Heteropoly and Isopoly Oxometalates*, Springer-Verlag, Berlin. **1983**.

[7] Hill, C. L., ed., *Chem. Rev.*, **1998**, *98*, 1−390.

[8] Pope, M. T.; Müller, A. *Angew. Chem. Int. Ed. Eng.*, **1991**, *30*, 34.

[9] Katsoulis, D. E. *Chem. Rev.*, **1998**, *98*, 359.

[10] Halbert, T. R.; Ho, T. C.; Stiefel, E. I.; Chianelli, R. R.; Daage, M. J. *J. Catal.* **1991**, *130*, 116.

[11] Cadot, E.; Béreau, V.; Marg, B.; Halut, S.; Sécheresse, F. *Inorg. Chem.* **1996**, *95*, 3099.

[12] Cadot, E.; Béreau, V.; Sécheresse, F. *Inorg. Chim. Acta.* **1996**, *252*, 101.

[13] Cadot, E.; Salignac, B.; Halut, S.; Sécheresse, F. *Angew. Chem. Int. Ed.* **1998**, *37*, 611.

[14] Béreau, V.; Cadot, E.; Bögge, H.; Müller, A.; Sécheresse, F. *Inorg. Chem*. **1999**, *38*, 5803.

[15] Bino, A.; Ardon, M.; Lee, D.; Spingler, B.; Lippard, S. J. *J. Am. Chem. Soc.* **2002**, *124*, 4578.

[16] Errington, R. J.; Wingad, R. L.; Clegg, W.; Elsegood, M. R. J. *Angew. Chem. Int. Ed.* **2000**, *39*, 3884.

[17] Pope, M. T.; Müller, A., eds. *Polyoxometalate Chemistry*. Kluwer Academic Publishers, the Netherlands, **2001**.

[18] Hill, C. L., ed. *Chem. Rev.* **1998**, *98*, 1.

[19] Rohmer, M.-M.; Bénard, M.; Blaudeau, J.-P.; Maestre, J. M.; Poblet, J. M. *Coord. Chem. Rev.* **1998**, *178–180*, 1019.

[20] Kepert, D. L. *Inorg. Chem*. **1962**, *4*, 199. Kepert, D. L. *Inorg. Chem*. **1962**, *8*, 1556. Tézé, A.; Hervé, G. *J. Inorg. Nucl. Chem*. **1977**, *39*, 2151. Pope, M. T. *Inorg. Chem*. **1976**, *15*, 2068.

[21] Clark, C. J.; Hall, D. *Acta Crystallogr. B*. **1976**, *32*, 1454.

[22] Day, V. W.; Klemperer, W. G. *Science*. **1985**, *228*, 533.

[23] Müller, A. *Nature*. **1991**, *352*, 115.

[24] Pope, M. T. *Nature*. **1992**, *355*, 27.

[25] Jansen, J. A.; Singh, D. J. Wang, S.-H. *Chem. Mater.* **1994**, *6*, 146.

[26] López, X.; Maestre, J. M.; Bo, C.; Poblet, J. M. *J. Am. Chem. Soc.* **2001**, *123*, 9571.

[27] Maestre, J. M.; López, X.; Bo, C.; Casañ-Pastor, N.; Poblet, J. M. *J. Am. Chem. Soc.* **2001**, *123*, 3749.

[28] In some cases, the MO_5 unit is also presented as a fundamental building block in the chemistry of POMs. We will assume that considering only the MO_6 unit is general enough to understand the main features and rules of POM chemistry.

[29] Kepert, D. L. *The Early Transition Elements*. Academic Press, New York, **1972**.

[30] A comprehensive list of elements known (20 years ago) to be added in POM structures appears in ref.6, p. 58.

[31] For example, heteropolyanions are also known as heteropolyacids.

[32] Kozhevnikov, I. V. *Chem. Rev*. **1998**, *98*, 171–198.

[33] Weinstock, I. A.; Atalla, R. H.; Reiner, R. S.; Moen, M. A.; Hammel, K. E.; Houtman, C. J.; Hill, C. L. *J. Mol. Catal. A: Chem*. **1997**, *116*, 59. Weinstock, I. A.; Atalla, R. H.; Agarwal, U. P.; Minor, J. L.; Petty, C. *Spectrochim. Acta, Part A*. **1993**, *49A*, 819. Weinstock, I. A.; Atalla, R. H.; Reiner, R. S.; Moen, M. A.; Hammel, K. E.; Houtman, C. J.; Hill, C. L. *New J. Chem*. **1996**, *20*, 269. Weinstock, I. A.; Atalla, R. H.; Hill, C. L. World Patent WO 9526438 A1, **1995**. *Chem. Abstr*. **1995**, 124, 59630. Atalla, R. H.; Weinstock, I. A.; Hill, C. L.; Reiner, R. S. U.S. Patent 5549789, **1996**; *Chem. Abstr*. **1996**, 125, 250734. Weinstock, I. A.; Hill, C. L.; Atalla, R. H. U.S. Patent 5552019, **1996**;

Chem. Abstr. **1996**, 125, 250735. Weinstock, I. A.; Hill, C. L. World Patent WO 9405849 A1, 1994; *Chem. Abstr*. **1994**, 121, 2333328.

[34] Rhule, J. T.; Hill, C. L.; Judd, D. A.; Schinazi, R. F. *Chem. Rev*. **1998**, *98*, 327–357.

CHAPTER 6

Basicity of the External Oxo Sites. Dimerisation Reactions

The applications of polyoxometalates are often related to their ability to be protonated. This chapter is aimed at studying a series of Keggin anions protonated at different positions. In section 6.1, the basicity of the oxygen sites of the Keggin framework is studied by means of various methods: qualitatively through the analysis of molecular electrostatic potentials and quantitatively, computing protonation energies at different sites of the external Keggin core. It showed that not all the oxo sites in a POM have the same predisposition to be protonated. The reader shall find a basicity scale for the set of oxo sites in $SiM_3W_9O_{40}$ frameworks, with M = Mo, V and Nb. A phenomenon associated to protonation, the dimerisation of Keggin anions, is studied in deep in sections 6.2 and 6.3. $[SiNb_3W_9O_{40}]^{7-}$ and $[PTiW_{11}O_{40}]^{5-}$ are known to dimerise, and this reaction is investigated to unravel when and how two monomers link to each other. This study is based on the relative protonation energies of different oxo sites in the external metal-oxide core and in the study of some reaction intermediates. The effect of the solvent is taken into account to get realistic reaction energy profiles.

6.1. Basicity of the External Oxygen Sites in Mixed-addenda Keggin Anions

This section is addressed to the study of the basicity of oxo sites in the Keggin anion. For the sake of generality, various compounds are studied, taking the $[SiW_{12}O_{40}]^{4-}$ anion as a reference, and studying various addenda substitutions. The recent history of polyoxometalates has demonstrated that mixed-metal anions are far more interesting than single-addenda ones from the redox and the acid-base properties. Following the same scheme of section 4.2, several $SiM_3W_9O_{40}^{n-}$ clusters are presented and their basicities explored. The vast literature concerning the study of the basicity and the chemistry are a good proof for the importance of this phenomenon. Amongst other chemists, Walter Klemperer performed systematic studies on various types of anions during decades in order to unravel, amongst other features, the chemical properties related to the basicity (or nucleophilicity) of the external oxo sites.[1-14] Klemperer studied functionalised compounds with organic fragments and Ti-derived ligands.

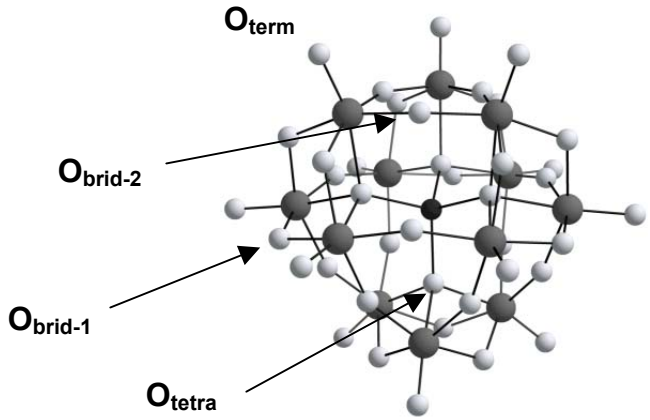

Figure 6.1. Ball-and-stick representation of the single-addenda $SiW_{12}O_{40}^{4-}$ Keggin anion. White spheres represent oxygens, and grey ones metal atoms. The internal dark sphere is the silicon atom. The four oxygen positions are labelled for further discussion.

In single-addenda Keggin anions there are two different external oxo sites, the bridging OM_2 oxygens and the terminal OM ones. In fact, there are two distinct bridging oxygens but, a priori, the differences between them are rather small (Figure 6.1). They are different since those labelled $O_{brid\text{-}1}$ belong to two edge-sharing octahedra, whereas the $O_{brid\text{-}2}$ are shared by corner-sharing MO_6 units. This mere fact leads to differences that will be discussed later. The relative basicity scale of the single-addenda tungstate is not a matter of discussion in this chapter since our interest is centred on mixed-addenda anions. Nevertheless, recent theoretical work performed by Bardin *et al*.[15] and Ganapathy *et al*.[16] analyses this point in the PW_{12} cluster. From these works it arises that bridging oxygens appear to be the most basic at the DFT level. However, the very recent work of Ganapathy *et al*.[16] compares the theoretical results with experimental data, leading to unprecedented conclusions, since they claim from NMR measurements that terminal oxygens could be the first to be protonated.

By removing one or various tungsten centres from the parent SiW_{12} structure and replacing them with different elements we can modify the properties of the cluster. Not only the redox properties or the localisation of the blue electrons are, as we described in section 4.2, but also the surface properties of the POM. This concerns especially the electron density, which is strongly dependent on the intrinsic properties of all the atoms of the framework. The key properties taking part in these changes are the formal charge of the metal centre, its size and the energy of its electronic levels. We will show in the present section how the basicity is affected by the substitution of three Ws by Mo or V. Mo is holding the same formal charge and the size is nearly equivalent, so no great changes are expected in the basicity. Vanadium, on the other hand, is pentavalent and considerably smaller. Both parameters are determinant in the V–O distances and the charge density in the region of substitution, as well. It is worth noting that $SiMo_3W_9O_{40}^{4-}$ has exactly the same charge as the single-addenda SiW_{12}^{4-}. This fact indicates a priori minor changes in the *absolute* basicity after substitution. On the other hand, $SiV_3W_9O_{40}^{7-}$ is highly negatively charged, and its basicity is expected (and well known) to be greater. But the interesting point here is to provide a basicity scale between the different oxo sites of each cluster, having a better approximation to the ordering of protonation in the different sites.

Figure 6.2 shows a three-times-substituted Keggin anion. Notice that the substituted centres belong to corner-sharing octahedra. Addenda metals

in Keggin clusters are more commonly substituted in this fashion. The aim of this section is to contribute to enlarge the knowledge on a well-known family of molecules, to which much effort is invested amongst the experimentalists.

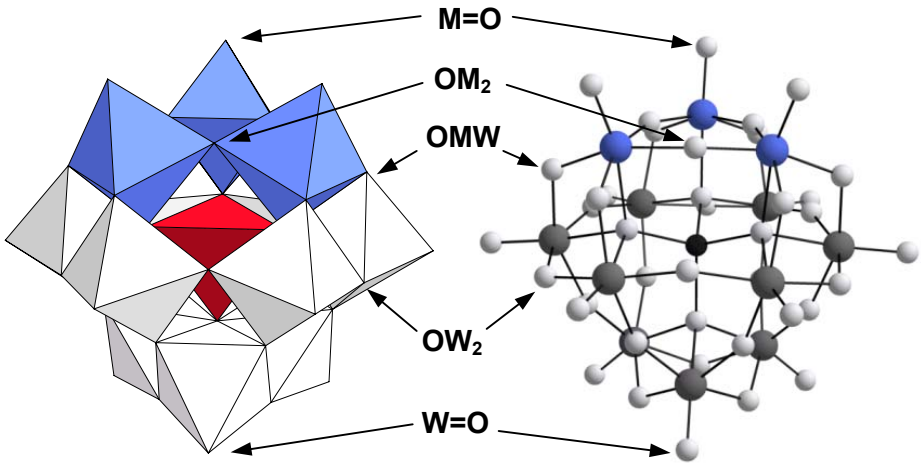

Figure 6.2. Polyhedral and ball-and-stick representation of the mixed-addenda A-α-$SiM_3W_9O_{40}^{n-}$ Keggin anion. The M centres are in blue and grey spheres are the tungsten atoms.

The Keggin structure may be viewed as the assembly of four M_3O_{13} edge-sharing triads (*B-triads*) or as the packing of four M_3O_{15} corner-sharing triads (*A-triads*). Of the lacunary XM_9 units, the anions that contain A-fragments are the most frequent, although many aggregates of the B-XM_9 precursor are also known.[17-19] All the structures reported in the present work are formal derivatives of the Keggin anion: the A-$[SiM_3W_9O_{40}]^{n-}$ species maintain their shape after the substitution. The substitution of a W or a Mo by another metal may modify the charge density throughout the POM and alter the relative basicity of various sites in the molecule. In general, the basicity of the oxygen sites depends on the number of metals linked to the oxo ligand. Hence, for example, experimental[11] and theoretical[20] studies on the decavanadate anion $[V_{10}O_{28}]^{6-}$ showed that the oxygen bonded to three vanadiums is more basic than bridging oxygens and the terminal oxygens are the least basic sites.

Molecular electrostatic potentials

A brief introduction to the electrostatic potential function can be found in chapter 2. From the theoretical point of view, the qualitative study of molecular electrostatic potentials (MESP) proved to be very useful for detecting the most nucleophilic regions of a POM. Electrophilic species —those positively charged— tend to minimise its potential energy by approaching as much as possible a minimum of a MESP distribution. Figure 6.3 shows three views of the MESP distribution on an isodensity 3D-surface for the mixed-addenda anions SiM_3W_9 (M = Mo and V). The colour of the electronic density isosurface (ρ = 0.017 e/ua) in the figure is a function of the MESP value. Red colour identifies regions in which the electrostatic potential is negative (nucleophilic regions) and blue denotes positive or less negative electrostatic potentials (electrophilic regions).

When molybdenums substitute tungstens in SiW_{12}, the electronic reorganisation is quite small and the basicity of the substituted anion is not much different from that of the parent anion. It can be easily deduced from the MESP function that bridging oxygens are generally more basic than terminal oxygens since the regions close to terminal OMo and OW oxygen sites (dark blue) are the least basic. Contrarily, the accessible nucleophilic regions (red) are close to the bridging oxygens. Recall that the more intense red colour —in the vicinity of the internal region— is dominated by the potential of the tetrahedral oxygens, which are the only oxo ligands in the cluster bonded to four positive ions. This oxygen is not easily accessible for a proton, though.

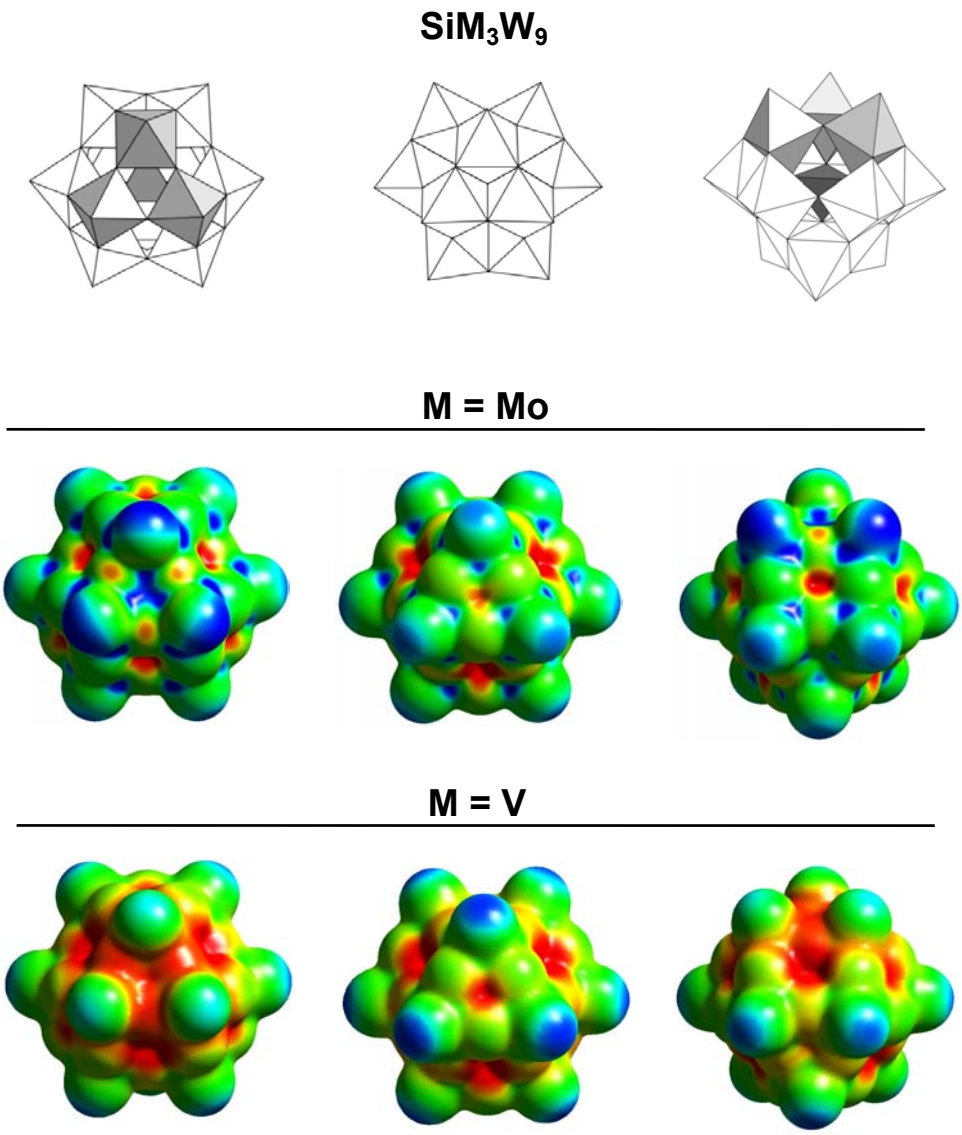

Figure 6.3. Polyhedral representations and Molecular Electrostatic Potentials from three different viewpoints for the $SiMo_3W_9$ and SiV_3W_9 derivatives. See text for further details.

Protonation energies

The qualitative analysis of the MESP just indicated that, on the one hand, the bridging OMo_2 would be the most nucleophilic sites and, on the other, that the terminal OMo oxygen is not a good position for protonation. Computation of the fully optimised structures of the corresponding protonated forms could reinforce this hypothesis. Table 6.1 lists the values of the relative protonation energies for the five isomers H–OM_2, H–OM, H–OW_2, H–OWM, H–OW. The energy sequence matches the qualitative ideas that emanate from the MESP distribution analysis. The most stable protonated complex is the isomer in which the proton is attached to the bridging oxygen linked to two molybdenum ions. The next preferred site is OMoW with a relative energy of only 3.7 kcal mol^{-1} and OW_2 is the least basic of the bridging oxygens and lies at 6.8 kcal mol^{-1}. The energies of H–OMo and H–OW isomers were computed to be 19.8 and15.9 kcal mol^{-1} above the energy

Table 6.1. Relative protonation energies (in kcal mol^{-1}) for all the distinct external oxygens of $[SiM_3W_9O_{40}]^{n-}$, with M = Mo and V. For a better comparison between the two clusters, the zero-energy protonation site was arbitrarily chosen to be OW_2.

M	*Site*	*Relative Energy*
Mo	OMo_2	–4.9
	OMoW	–1.2
	OW_2	0.0
	OW	+11.0
	OMo	+15.0
V	OV_2	–12.4
	OVW	–1.4
	OW_2	0.0
	OV	+5.6
	OW	+19.2

of H–OMo_2, respectively. These results are consistent with the acidity ordering of HPAs, where tungstates are slightly more acidic than molybdates.[21]

It is clear in the MESP distribution of the group 5 SiV_3W_9 derivative (Figure 6.3) that the differences in proton affinity between the most basic and the least basic sites are larger than in W/Mo mixed anions. The blue colour in the vicinity of terminal OW oxygens indicates that these sites might be the least basic ones. In contrast, the wide read area in the region of OV_2 sites is a clear signal that these sites might have the strongest proton affinity. Once again, the calculations carried out on the protonated forms fully confirm the predictions made from MESP since H–OV_2 is the most stable isomer for $HSiV_3W_9$. Our calculations suggest the following basicity scale of the oxo sites in SiV_3W_9: OV_2 > OVW > OW_2 > OV > OW. The difference in the proton affinity between the most and least basic sites is ~30 kcal mol^{-1}. The range is ~10 kcal mol^{-1} wider than in $SiMo_3W_9$.

One proton residing on a bridging oxygen OM_2 with M = W, Mo or V and on a terminal OM has energy differences, according to present DFT calculations, ranging between 9 and 20 kcal mol^{-1}. This is a considerable amount of energy but significantly lower than the 71 kcal mol^{-1} suggested by Davis *et al*. by means of model clusters.[15] These authors, however, performed calculations on triprotonated H_3PM_{12} clusters to determine a reliable proton affinity difference between the bridging oxygens in PMo_{12} and PW_{12} of 9 kcal mol^{-1}. Such a value is fairly similar to the ~6 kcal mol^{-1} computed in the present work for the mixed-addenda $SiMo_3W_9$ cluster. Another important point is that, when the proton attaches to bridging oxygens, there is an additional stabilisation via a weak hydrogen bond with the nearest bridging oxygen. In H–OMo_2, the H–O bond length is 0.99Å and the H···OW_2 distance is 2.03 Å. The conformation with the H oriented outwards from the molecular framework is notably higher in energy, more than 10 kcal mol^{-1}. This additional stabilisation is similar in H–OMo_2 and H–OW_2 and, therefore, does not modify their relative stability, but it is an important factor in the difference of affinity between a proton residing on a terminal and in bridging oxygen. The important stabilisation energies computed in protonated clusters with H···O bonds account for the importance of this weak interaction. Notably, Keggin anions protonated at terminal M=O bonds do not allow H···O bond formation, thus they remain higher in energy. See Figure 6.4 for a visualisation of the interactions.

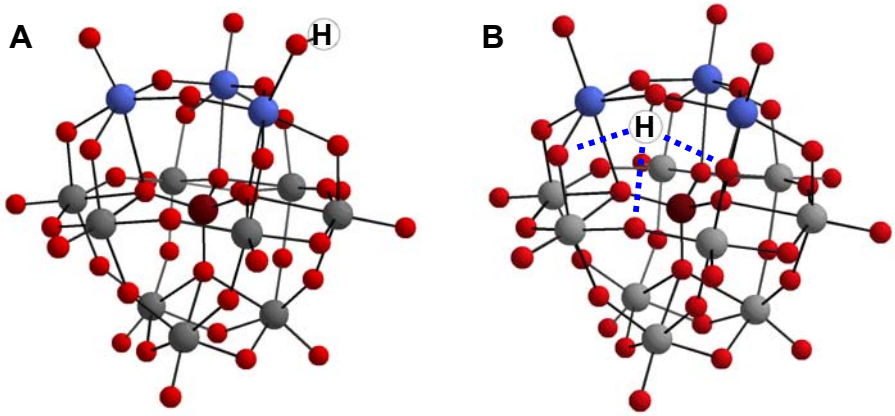

Figure 6.4. SiM_3W_9 model clusters protonated at a (A) terminal or a (B) bridging oxo site. White spheres are hydrogen atoms. Notice the H···O stabilising interactions in the latter case.

6.2. Dimerisation Processes in Mixed-addenda Keggin Anions

Introduction

The acid-base properties in POMs have been deeply investigated in history with the aim of exploiting their associated features. One of them is the inclusion of POMs in reactions acting as catalysts. Many experimental works have shown that the likeliness of a Keggin anion to be protonated is strongly dependent on its chemical composition. Furthermore, different oxo sites in the metal-oxide core of POMs have different affinity to protons, so POM chemists have learnt to vary composition and structure to tune the properties.

In the middle 80's, the first successful attempts to obtain a Keggin dimer were reported by Richard G. Finke[22] and Walter G. Klemperer.[10-23] Even though, the dimerisation and the rules governing this reaction are not fully understood since serious difficulties are found to elucidate intermediate species. Nevertheless, valuable experimental hints are available concerning the capability of the external oxo sites to be protonated in POMs. In this section we analyse and discuss the relationship existing

between the basicity in Keggin anions and the dimerisation processes. It is well known that the synthesis of mixed-addenda anions led to the possibility of discovering new ways of assembly, in which the physical nature of the substituting metal element plays a fundamental role.

In the single-addenda Keggin tungstate, a protonation at the terminal W=O site is very unfavourable since the bridging OW_2 oxygen is notably more basic. Even though, the presence of other metals, M, in the framework ($XM_xW_{12-x}O_{40}$) can modify the relative basicity of the oxygen sites, favouring the protonation at regions close to the substituted metal. Many mixed-addenda Keggin structures have been synthesised and characterised,[24-25] but only derivatives containing Nb, Ti and Cr dimerise to form M–μ-O–M unions,[22-27] indicating that the nature of M is very important (see Figure 6.5).

This section is devoted to the study of two monomeric systems and their dimeric partners as well as the reaction pathways of dimerisation. $PTiW_{11}O_{40}^{5-}$ and $SiNb_3W_9O_{40}^{7-}$ are known to dimerise under suitable conditions. First of all, the data related to the basicity of the various relevant oxo sites is presented for both clusters. Afterwards, the reader shall find possible dimerization pathways for the Ti- and Nb-derivatives. All the calculations presented take into account solvent effects since the relative energy of the species considered is of much importance. The solvent is considered by means of a continuum model as implemented in the COSMO method.[28] See chapter 8 for details.

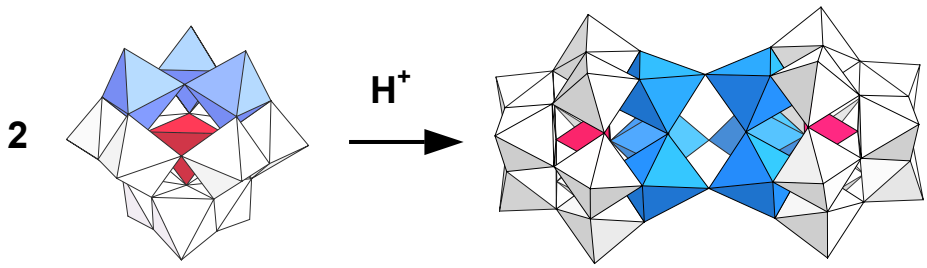

Figure 6.5. Polyhedral representation of a generic dimerisation reaction to form the $X_2M_6W_{18}$ anion. Blue octahedra contain the M centres.

6.2.1. Dimerisation of $PTiW_{11}O_{40}^{5-}$

In 2000, Kholdeeva *et al*.[27] reported the dimerisation of the monosubstituted Ti-derivative of the Keggin anion. It was achieved under acidic conditions and a single M–μ-O–M linkage was formed. From subsequent characterisation, it was found to be a Ti–O–Ti bridge and the overall yield was of 98% conversion. This dimer exhibited catalytic properties in the presence of H_2O_2. Contrarily, the monomer did not have so much activity. Other titanopolytungstates have been found to catalyse oxidation reactions of thioethers with hydrogen peroxide[29] in nearly quantitative yield.

The authors of that study assumed that protonation occurs at the Ti=O site prior to Ti–O–W. Even though, no strong evidence of the compounds formed at intermediate steps of the process is yet available. The aim of this section is to present the DFT results obtained on the protonation of the monomer and the reaction pathway to form the dimer $(PTiW_{11}O_{39})_2(\mu\text{-OH})$ from the monomer $PTiW_{11}O_{40}$. Figure 6.6 shows a schematic view of the dimerisation reaction for $PTiW_{11}$.

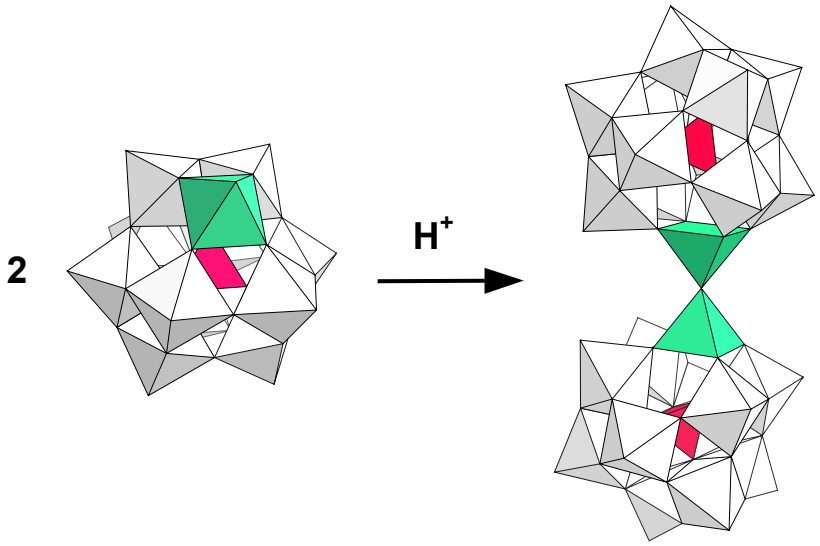

Figure 6.6. Polyhedral representation of the monomeric $PTiW_{11}$ and the dimeric $(PTiW_{11})2(\mu\text{-O})$ forms discussed in this section. Green polyhedra contain the titanium atoms.

Basicity of the oxo sites in $PTiW_{11}O_{40}^{5-}$

The dimerisation reaction starts with the protonation of $PTiW_{11}$. The detailed analysis of the most basic sites of the monomer is performed, as in section 6.1, determining the MESP distribution and the protonation energies at different sites. A 3D representation of the MESP function (Figure 6.7) shows a high proton affinity in the vicinity of the external oxygen of the octahedron that contains the Ti^{4+}. The bridging OTiW sites appear as competitive nucleophilic sites, whereas the next most basic sites are the bridging oxygens bonded to two tungstens. As previously described for other mixed-addenda systems, the terminal W=O atoms are the least basic sites.

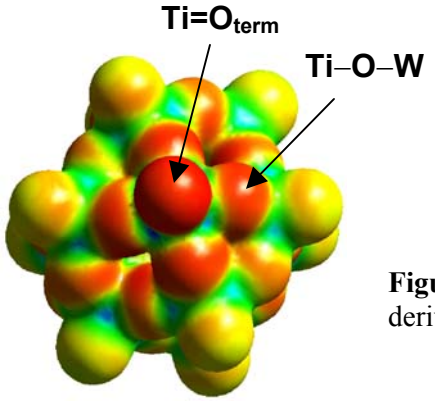

Figure 6.7. MESP for the $PTiW_{11}$ derivative.

Table 6.2. Protonation energies computed (kcal mol^{-1}) for $PTiW_{11}$. Note the effect of the introduction of a solvent in the relative protonation energies.

Protonation Site	*Gas phase*	*Acetonitrile*
OW_2	0.0	0.0
OTiW	–2.9	–2.2
OTi	–8.5	–13.1

Assuming that the Ti=O, OTiW and OW_2 are the most basic sites, the geometries for the three corresponding protonated isomers were fully optimised. According to the MESP distribution, the cluster with the proton bonded to the Ti=O oxygen is the most stable. Table 6.2 shows that

protonation at the bridging OTiW site is 5.6 kcal mol^{-1} less favourable, energy that increases up to 11.4 kcal mol^{-1} in a solution of acetonitrile (dielectric constant of 37.0).

The additional relative stabilisation of the Ti=OH form is attributed to a more efficient interaction between the proton and the solvent in this isomer. The inward orientation of the proton when it is linked to a bridging site does not favour its stabilisation by electrostatic interaction with the solvent molecules. So, the qualitative analysis through the electrostatic potential function and the relative protonation energies coincide, reinforcing the experimental assumption that the Ti=O site is the most basic on the Ti-derivative.

Dimerisation pathways

According to the scheme proposed by Kholdeeva *et al.*,[27] the formation of the dimer $(PTiW_{11}O_{39})_2O$ occurs after protonation of the monomer $PTiW_{11}O_{40}$ at the terminal Ti=O site. Then, two protonated molecules $HPTiW_{11}O_{40}$ react to give the dimer. The reaction could also start from H–OTiW, the second protonated monomer in stability. The next step in both cases would be the loss of a water molecule to give $(PTiW_{11}O_{39})_2(\mu\text{-}O)^{8-}$. This cluster has been also observed in its protonated (μ-OH) form. The plausible mechanism for the formation of the dimer may be described, therefore, by the next four equations

Chart 6.1

$$2\,[PTiW_{11}O_{40}]^{5-} + 2\,H^{+} \longrightarrow 2\,H[PTiW_{11}O_{40}]^{4-} \quad (1)$$

$$2\,H[PTiW_{11}O_{40}]^{4-} \longrightarrow H_2[(PTiW_{11}O_{39})_2(\mu\text{-}O)_2]^{8-} \quad (2)$$

$$H_2[(PTiW_{11}O_{39})_2(\mu\text{-}O)_2]^{8-} \longrightarrow [(PTiW_{11}O_{39})_2(\mu\text{-}O)]^{8-} + H_20 \quad (3)$$

$$[(PTiW_{11}O_{39})_2(\mu\text{-}O)]^{8-} + H^{+} \longrightarrow [(PTiW_{11}O_{39})_2(\mu\text{-}OH)]^{7-} \quad (4)$$

The product of step 2 will be different depending on the protonation site of the monomer. If the reaction starts with the protonation at Ti=OH, the intermediate III-1 is formed, but if the protonation at the bridging OTiW oxygen happens, III-2 is the intermediate (Figure 6.8). Step 2 is shown in more detail in Chart 6.2. A great computational effort was made to fully optimise all reactants, intermediates and products involved in the reactions in Chart 6.1.

Chart 6.2

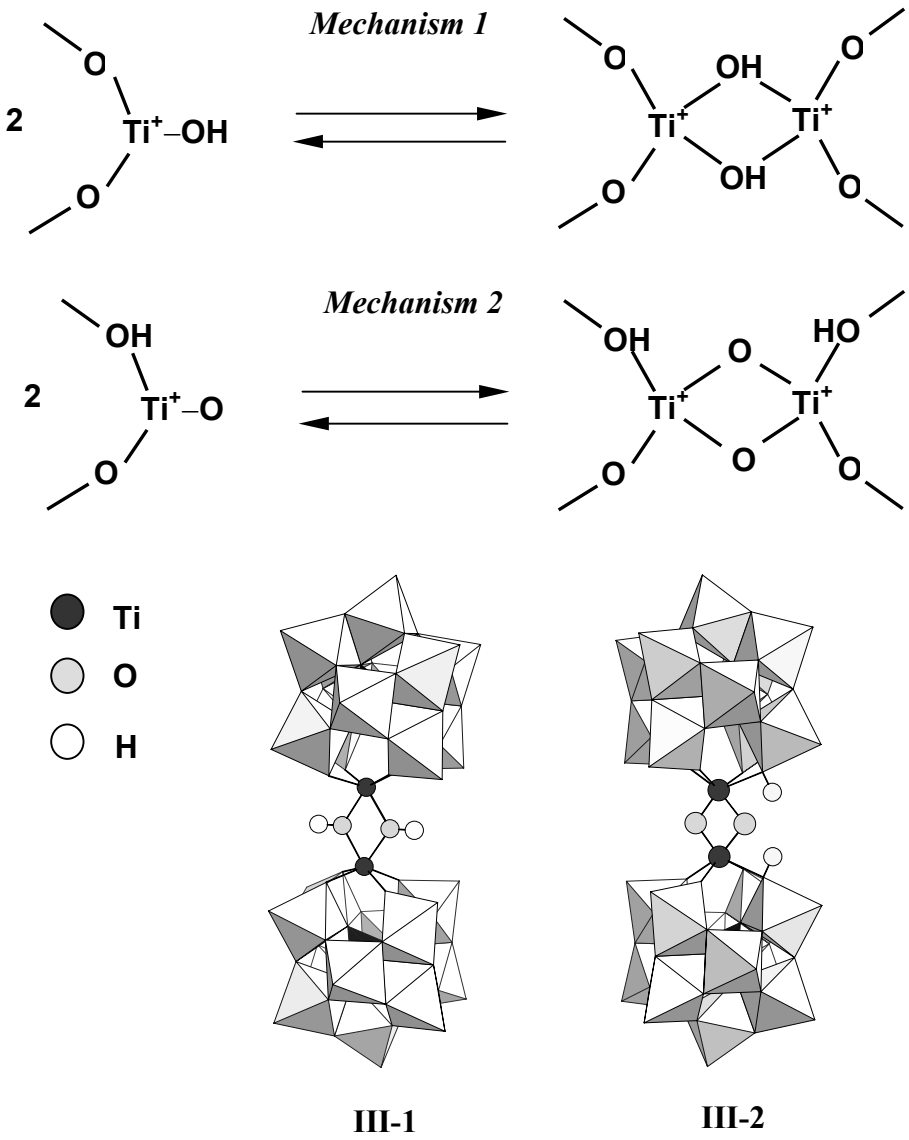

Figure 6.8. Polyhedral view of intermediates III-1 and III-2. They are associated to mechanisms 1 and 2, respectively.

The energy profiles associated to pathways 1 and 2 are represented in Figures 6.9 and 6.10. The energies correspond to single-point calculations of the molecules in acetonitrile media (ε = 37.0). The energies of all points are referred to that of point I, which is the same in both pathways. Labels I, II-1, II-2, III-1, etc. denote monomers, intermediates and dimers involved in reactions 1-4. The reader, however, must take in mind that the energy for points I-V in Figures 6.9 and 6.10 were computed taking into account all the species necessary for charge and matter conservation (Chart 6.3).

Chart 6.3

Pathway 1

I: 2 $PTiW_{11}O_{40}^{5-}$ + 3 H_3O^+

II-1: 2 $[P(TiOH)W_{11}O_{39}]^{4-}$ + H_3O^+ + 2 H_2O

III-1: $[(PTiW_{11}O_{39})_2(\mu\text{-}OH)_2]^{8-}$ + H_3O^+ + 2 H_2O

IV: $[(PTiW_{11}O_{39})_2\mu\text{-}O]^{8-}$ + H_3O^+ + 3 H_2O

V: $[(PTiW_{11}O_{39})_2\mu\text{-}(OH)]^{7-}$ + 4 H_2O

Pathway 2

I: 2 $PTiW_{11}O_{40}^{5-}$ + 3 H_3O^+

II-2: 2 $[HPTiW_{11}O_{40}]^{4-}$ + H_3O^+ + 2 H_2O

III-2: $H_2[(PTiW_{11}O_{39})_2(\mu\text{-}O)_2]^{8-}$ + H_3O^+ + 2 H_2O

IV: $[(PTiW_{11}O_{39})_2\mu\text{-}O]^{8-}$ + H_3O^+ + 3 H_2O

V: $[(PTiW_{11}O_{39})_2\mu\text{-}(OH)]^{7-}$ + 4 H_2O

From the energy profiles in Figures 6.9 and 6.10 is clear that the overall process is quite exothermic, since the reaction products IV and V are about 50 kcal mol^{-1} more stable than the reactants. Another significant fact is that the initial step is also very exothermic (–49.7 kcal mol^{-1}) when the protonation occurs at Ti=O (pathway 1). However, the formation of III-1 requires a significant amount of energy (~25 kcal mol^{-1}). Contrarily, the protonation at OTiW is less stabilising (–28.0 kcal mol^{-1}) and intermediate III-2 is quite high in energy (–4.9 kcal mol^{-1}). Figure 6.11 compares the

energy profiles associated to pathways 1 and 2. This plot clearly indicates that dimerisation of the mixed-addenda Ti-derivative should occur mostly through protonation at Ti=O and formation of III-1. To sum up, present calculations strongly suggest that the major basicity of the terminal Ti=O oxygen site determines the mechanism of dimerisation.

Table 6.3 shows computed distances and angles for the species involved in the dimerisation of the Ti-derivative. Only parameters of the local region of linkage between monomers are listed since the rest of the molecule does not change with regard to the monomer. Notice the enlargement of the Ti···Ti distance when forming the protonated dimer (V) and the great difference between intermediates III-1 and III-2 in the region of linkage. The formation of Ti–μ-(OH)–Ti shortens the Ti···Ti distance by more than 0.5 Å.

Table 6.3. Selected distances (in Å) and angles for the Ti-species involved in points I–V of pathways 1 and 2 of dimerisation.

		III-1	III-2	IV	V
distance					
	Ti···Ti	3.53	2.97	3.69	4.07
	Ti–(μ-O)	2.06	1.92	1.85	2.06
	P···Ti	3.94	4.24	3.68	3.57
	(μ-O)–H	0.98	–	–	0.98
angle					
	Ti–(μ-O)–Ti	108.4	105.7	179.5	161.6

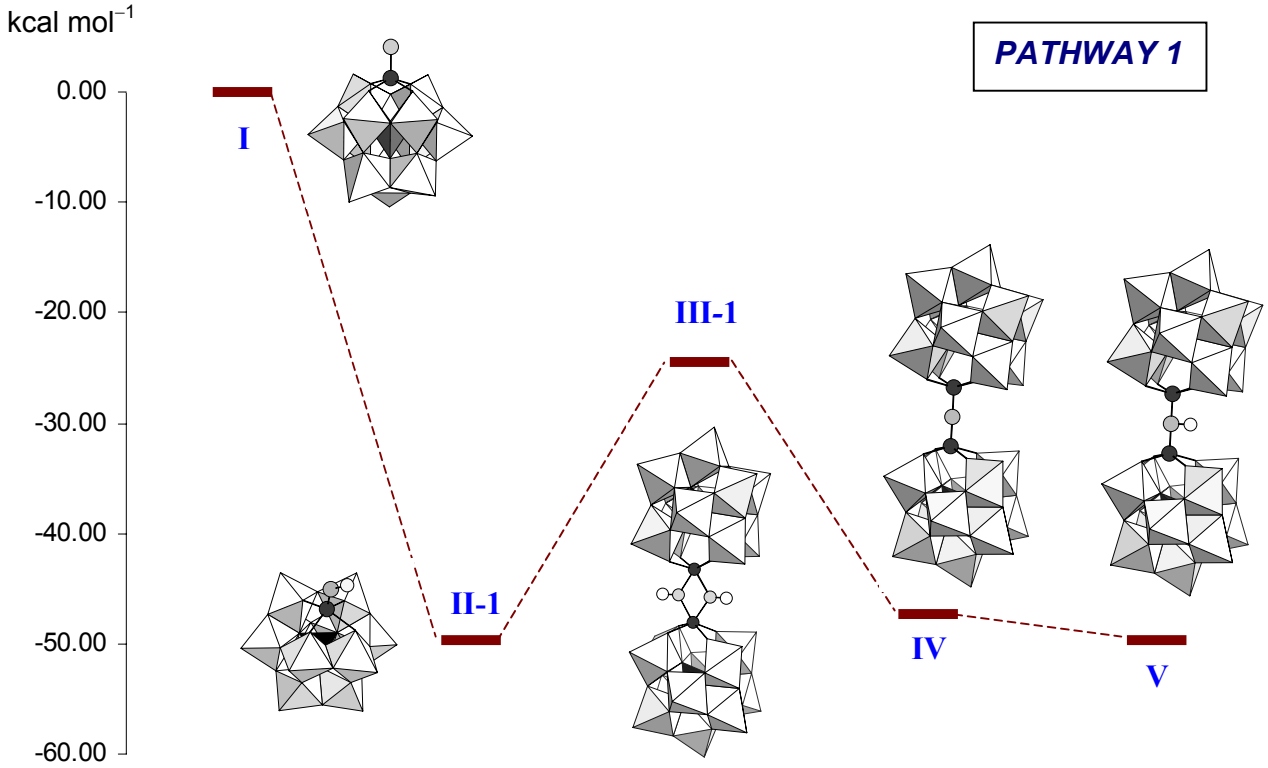

Figure 6.9. Reaction energy profile computed for pathway 1 of formation of $(PTiW_{11}O_{39})OH^{7-}$. Each point I-V contains all the necessary chemical species for charge and matter conservation. See Chart 6.3 for a detailed description of each point.

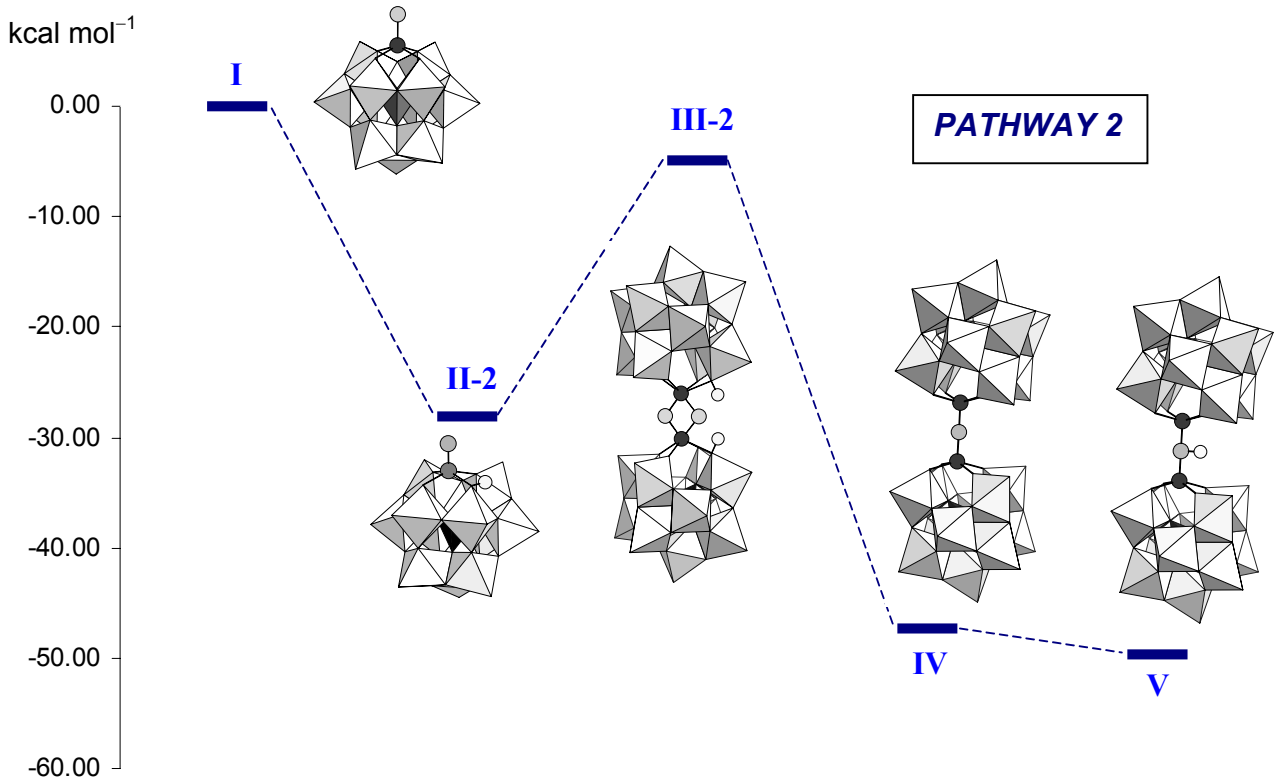

Figure 6.10. Reaction energy profile for pathway 2. Intermediates II-2 and III-2 are different from pathway 1, whereas species I, IV and V are equivalent to the homologous species in Figure 6.9.

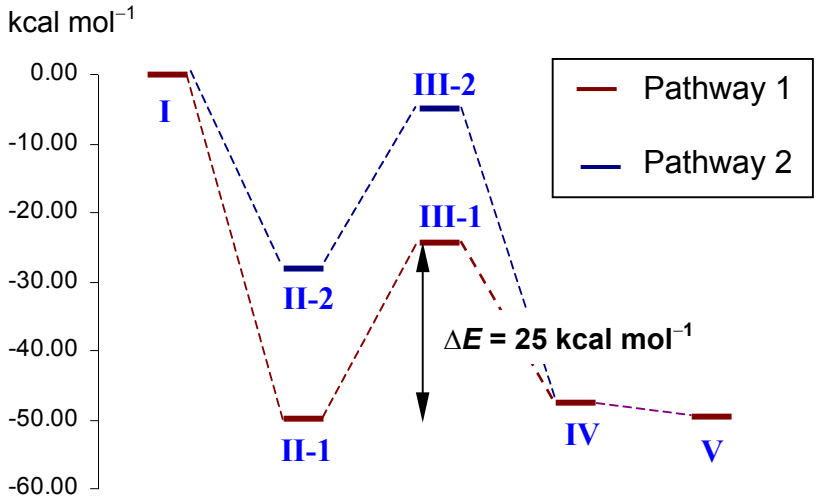

Figure 6.11. Combined reaction profiles for pathways 1 and 2 for the dimerisation of $PTiW_{11}$.

6.2.2. Dimerisation of $SiNb_3W_9O_{40}^{7-}$

The synthesis of $(SiNb_3W_9O_{37})_2O_3^{8-}$ reported by Finke *et al.*[22] in 1984 was the landmark work on the formation of Keggin dimers. That work opened a novel class of reactions in HPAs. Later studies related to the dimerisation reaction of Keggin clusters have been reported.[26d-e] Very recently, Weinstock and co-workers addressed an exhaustive study about the formation of Nb–μ-O–Nb bonds.[30] The authors report pH-controlled reversible and stepwise formation of individual linkages. The monomer, $SiNb_3W_9$, and the dimer, $Si_2Nb_6W_{18}$, are represented in Figure 6.5.

This subsection presents the results about the formation of the Nb–μ-O–Nb linkage in Nb-substituted Keggin anions. The study is conducted in the same fashion as section 6.2.1, dealing with data from MESP, protonation energies and, finally, the reaction energy profile.

Basicity of the oxo sites in $SiNb_3W_9O_{40}^{7-}$

The case of $SiNb_3W_9$ is slightly different from that of the monosubstituted Ti-derivative. In the present anion, three neighbouring Nb atoms form a corner-sharing triad, so three Nb–O–Nb bridging oxygen sites link the niobium centres. These oxygens are supposed to be rather basic since the excess of negative charge of the cluster is somewhat concentrated in the region of substitution. The electrostatic potential function showed in Figure 6.12 supports this statement. Blue regions are localised around terminal W=O oxo sites, which are, *a priori*, the least basic in this anion. From the MESP, other sites competing with ONb_2 for an incoming H^+ could be ONbW and Nb=O, as well.

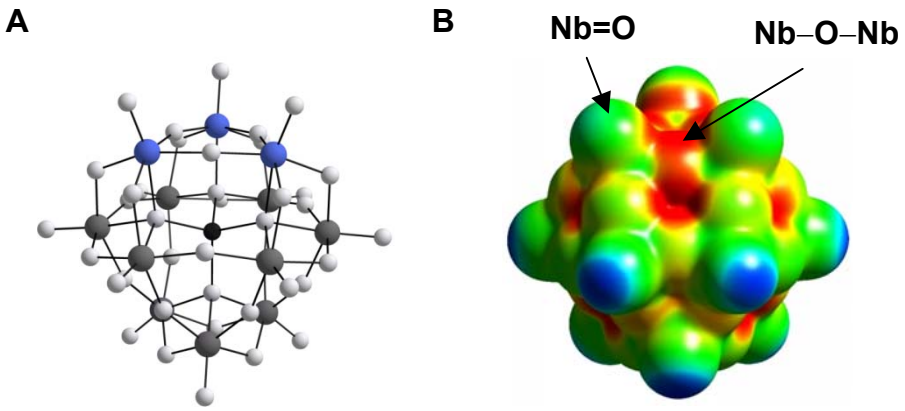

Figure 6.12. (A) Ball-and-stick view of $SiNb_3W_9$ (blue spheres are Nb atoms), and (B) MESP plotted in colour over an isodensity surface of $SiNb_3W_9$.

The relative energies computed for the most suitable isomers of $HSiNb_3W_9^{6-}$ is listed in Table 6.4. The Nb–O–Nb oxygen is the most basic, followed by the terminal Nb=O site in acetonitrile media. The effect of the solvent favours the stabilisation of the most exposed protons like in preceding examples. We assume that protonations at W=O oxygen sites are much higher in energy and they would not attach the proton preferentially.[31]

Table 6.4. Relative protonation energies (in kcal mol^{-1}) of $SiNb_3W_9$ at three oxo sites, computed in the gas phase and in a solvent (ε = 37) with the COSMO program.

Protonation Site	*Gas phase*	*Solvent*
OW_2	0.0	0.0
ONb_2	−11.5	−7.8
ONb	+3.6	−4.4

Data concerning the protonation energies reinforce the fact that this cluster behaves rather differently from $PTiW_{11}$. Now, the competition between ONb_2 and Nb=O for the proton is possible. The energies of protonation between these two sites only differ in 3.4 kcal mol^{-1}, which is a small value. In a series of papers, Klemperer's group studied the reactivity of the $Nb_2W_4O_{19}^{4-}$ Lindqvist anion,[4,10,13-14] concluding that the ONb_2 site is the most basic, nucleophilic oxo site. From a Hartree–Fock study, Maestre *et al*.[32] found the same trend for the basicity of the external oxygens of that Nb-derivative.

Dimerisation pathways

The case we deal with in this section is somewhat more complex because three μ-O bridges are ready to be formed in a stepwise process.[30] For the sake of simplicity, we will only discuss here the formation of a single μ-O bridge between two monomeric units for analogy with the case of the Ti-derivative. For this purpose, the energies in solution were computed for the monomer, the protonated monomer and two reaction intermediates as well as the product of reaction, $(SiNb_3W_9)_2(\mu\text{-}O)$.

Let us take into account again the mechanisms showed in Chart 6.2. If we replace Ti by Nb in that scheme, equivalent intermediates are formed, but in the present case are labelled as VIII-1 and VIII-2. We represent these two species in Figure 6.13 in polyhedral view.

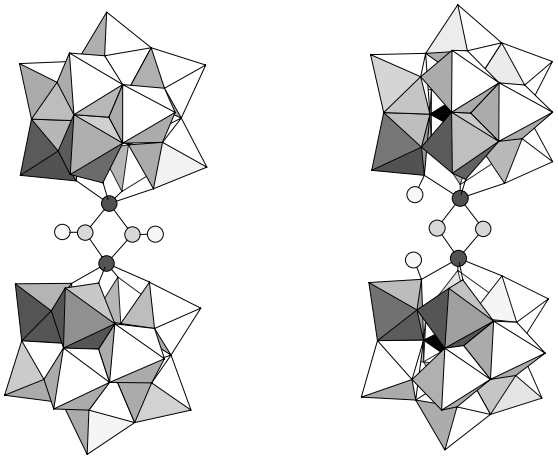

Figure 6.13. The two intermediates, VIII-1 (left) and VIII-2 (right), participating in the formation of the first μ-O bridge in the dimerisation of $SiNb_3W_9O_{40}^{7-}$. Dark polyhedra and dark spheres contain the Nb centres. Light grey spheres represent oxygens, and the white ones hydrogens.

The formation of $(SiNb_3W_9)_2\mu$-O might occur through these two intermediates. At each stage the following species are present:

Chart 6.4

Pathway 1

VI: 2 $[SiNb_3W_9O_{40}]^{7-}$ + 3 H_3O^+

VII-1: 2 $[Si(NbOH)Nb_2W_9O_{39}]^{6-}$ + H_3O^+ + 2 H_2O

VIII-1: $[(SiNb_3W_9O_{39})_2(\mu\text{-}OH)_2]^{12-}$ + H_3O^+ + 2 H_2O

IX: $[(SiNb_3W_9O_{39})_2\mu\text{-}O]^{12-}$ + H_3O^+ + 3 H_2O

Pathway 2

VI: 2 $[SiNb_3W_9O_{40}]^{7-}$ + 3 H_3O^+

VII-2: 2 $[HSiNb_3W_9O_{40}]^{6-}$ + H_3O^+ + 2 H_2O

VIII-2: $H_2[(SiNb_3W_9O_{39})_2(\mu\text{-}O)_2]^{12-}$ + H_3O^+ + 2 H_2O

IX: $[(SiNb_3W_9O_{39})_2\mu\text{-}O]^{12-}$ + H_3O^+ + 3 H_2O

The energy profiles for both pathways of dimerisation (Figure 6.14) show that the step of protonation (VI → VII) of the monomer is quite exothermic (more than 50 kcal mol^{-1}). Point VII of reaction is slightly more stable for pathway 2 by about 7 kcal mol^{-1}, as has been showed in the study of the relative basicity of $SiNb_3W_9$ oxo sites. The formation of intermediates VIII-1 and VIII-2 from their protonated monomers is very endothermic, though. After the second step, species VIII-1 turns to be the most stable by ~12.6 kcal mol^{-1} at this point of the reaction, which implies a crossing of both profiles in step 2. The energy difference at point VIII is moderate between both pathways. So, the intermediate species formed by two μ-(OH) linkages is again the most stable. This may indicate that the protonation at Nb=O (first step of reaction), although being less favoured, is more willing to yield the product dimer than the $H–ONb_2$ form.

In the last step, intermediates VIII-1 and VIII-2 lose a H_2O molecule to give the dimer IX. The energy loss is only 4.1 kcal mol^{-1} for pathway 1, and 16.7 kcal mol^{-1} for pathway 2. The energy of IX, in relation to VI, is –5.9 kcal mol^{-1}. We attribute this small exothermicity to the high negative charge (−12) of the final product.

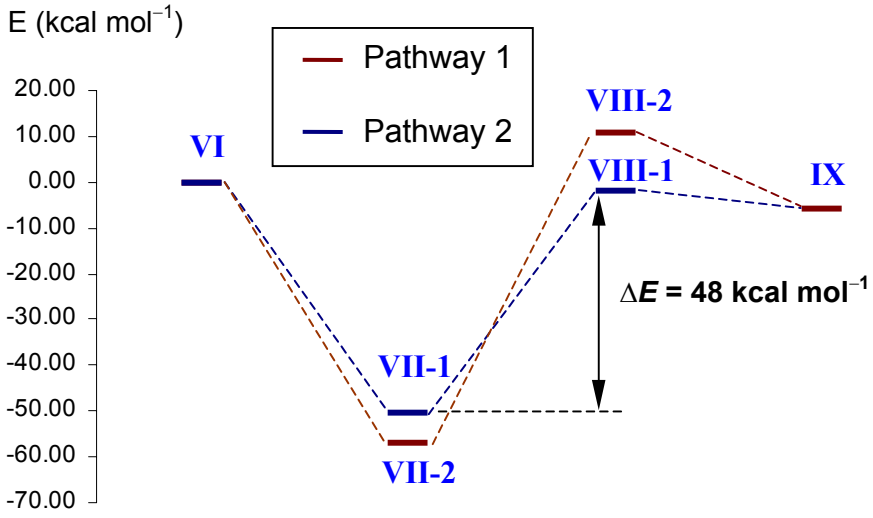

Figure 6.14. Combined energy profiles for pathways 1 and 2 for dimerisation of $SiNb_3W_9$.

Table 6.5 shows computed parameters for the species involved in the dimerisation of the Nb-derivative. These geometric data correspond to the region of formation of the μ-O linkage. The regions far from the Nb centres remain fairly unchanged. The Si···Nb_1 distance changes notably from the monomeric forms, VI-VII, to the dimerised species. In the former cases, it was computed to be 3.70 Å, whereas, as shown in the table, it becomes 4.12 Å for the final dimer. Neither the Si···Nb_2 nor the Nb_2···Nb_2 distances change appreciably.

Table 6.5. Selected distances (in Å) and angles for the Nb-species involved in points VI–IX of pathways 1 and 2 of dimerisation.

	VIII-1	VIII-2	IX
distance[a]			
Nb_1···Nb_1	3.95	3.31	4.09
Nb_1–(μ-O)	2.26	2.00	2.05
Si···Nb_1	4.17	4.44	4.12
Si···Nb_2	3.70	3.66-3.75	3.70
Nb_1···Nb_2	3.83	3.92-4.23	3.82
Nb_2···Nb_2	3.77	3.77	3.78
(μ-O)–H	0.98	–	–
angle			
Nb-(μ-O)-Nb	121.5	106.5	175.8

a) Nb_1 is the centre directly bonded to μ-O, whereas Nb_2 are the neighbouring atoms.

In more acidic conditions, the remaining Nb=O sites are protonated and the di-μ-O bridged dimer $[Si_2Nb_6W_{18}O_{78}]^{10-}$ and the tri-μ-O $[Si_2Nb_6W_{18}O_{77}]^{8-}$ dimer are formed. The complete reaction is accomplished following the process:

$$2\ [SiNb_3W_9O_{40}]^{7-} + 6\ H_3O^+ \rightarrow [(SiNb_3W_9O_{37})_2(\mu\text{-}O)_3]^{8-} + 9\ H_2O$$

It is worth noting that the formation of the three Nb–μ-O–Nb linkages is highly exothermic, $\Delta E = -158$ kcal mol^{-1}. This value contrasts with the

stabilisation found for the mono-μ-O dimer, –5.9 kcal mol^{-1} (Figure 6.14). We believe that this difference in stability originates in the different charges of the clusters. Although in a POM the total charge is stabilised by the solvent, the anions with larger charges gain stability if they transform to less charged clusters. Therefore, this energetic behaviour would explain why the tri-μ-O dimer is found preferentially. Thus, for obtaining the mono- or di-μ-O dimers, the pH conditions must be carefully controlled.[30] From present discussion we wonder whether the simple substitution of the central Si atom by P in XNb_3W_9 would favour the self-assembly of the cluster because in this case the charge of the mono-μ-oxo dimer would be –10 instead of –12. Finally, another question remains still open: why the $XV_3W_9O_{40}^{n-}$ anions do not dimerise? We believe that the strong difference in the basicity of terminal V=O and OV_2 oxygen sites could be the responsible. Calculations are underway to solve this puzzle question.

Table 6.6 lists computed geometrical parameters for the tri-μ-O dimer that are in excellent agreement with the available X-ray data.[26d]

Table 6.6. Selected computed and experimental distances (in Å) and angles for the $[(SiNb_3W_9O_{37})_2(\mu\text{-}O)_3]^{8-}$ dimer.

	Calculated	Experimental[a]
distance[a]		
$Nb_1\cdots Nb_2$[b]	3.67	3.55
$Nb_1\cdots Nb_1$[c]	3.77	–
Nb–(μ-O)	1.95	1.91
Si···Nb	3.50	–
Nb···O	1.95	–
angle		
Nb-(μ-O)-Nb	140.2	137.0

a) X-ray averaged parameters from the crystal structure of reference 26d.
b) Nb_1 and Nb_2 correspond to two Nb centres linked through a μ-O site.
c) Two Nb_1 centres are neighbours in the same Keggin unit.

Finally, we remark that no significant electronic differences were found between the dimers and the corresponding monomers. Hence, the HOMO-LUMO gap in $[(PTiW_{11}O_{39})_2(\mu\text{-}OH)]^{6-}$ and both the mono- and tri-μ-O Nb-dimers is almost identical to that determined for the monomers. This means that the differences in the redox properties between the monomers and dimers would originate exclusively in the whole charge of the cluster.

6.3. Basicity of the $PTi(O_2)W_{11}O_{39}^{5-}$ Peroxo Derivative

A DFT study of the mixed-addenda $[PTi(O_2)W_{11}O_{39}]^{5-}$ (**1**) peroxo derivative was performed to identify the most basic site of this anion in collaboration with Kholdeeva *et al*.[33] The unprotonated and various protonated clusters were computed. This study is aimed at characterising this species, which possesses catalytic activity. The selective catalytic oxidation of organic compounds with an environmentally attractive oxidant, aqueous H_2O_2, is of both academic and industrial interest.[34]

Conclusions concerning the structure of **1** based on the experimental findings are supported by DFT calculations performed for $[PTi(O_2)W_{11}O_{39}]^{5-}$ and its protonated partner. To obtain the geometry of minimal energy for the non-protonated complex, three orientations of the peroxo group were explored for the $[PTi(O_2)W_{11}O_{39}]^{5-}$ anion. Two orientations were computed under the restrictions of the C_s point group, labeled **2a** and **2b** in Chart 6.5 (their relative energies are indicated in kcal mol^{-1}), one of them with the σ-plane containing the Ti center and the O_2 group (**2a**), and the other one with the peroxo group perpendicular to σ (**2b**). Both conformations are very similar in energy, only differing by a mere 1.15 kcal mol^{-1}. The third structure, **2c**, of C_1 symmetry in which the peroxo group is almost aligned with the Ti–O–W plane, is clearly more stable (6–7 kcal mol^{-1}) than the conformations where the O_2 ligand is rotated ~45º with respect to the eclipsed conformation.

Chart 6.5

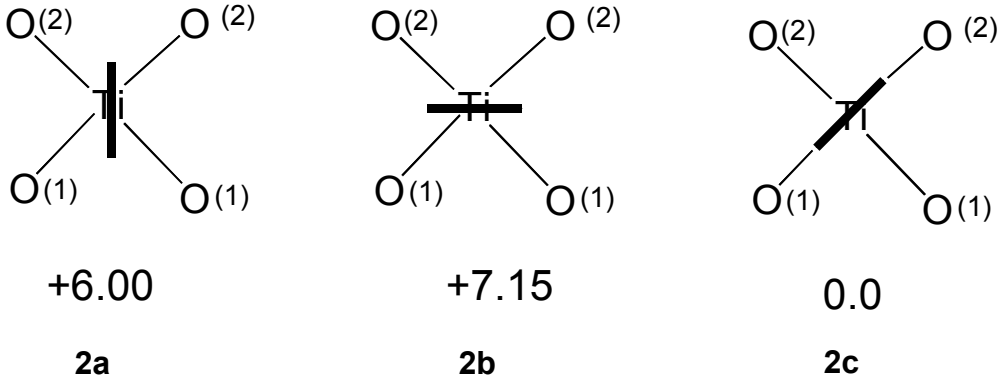

The latter orientation permits electron donation from the occupied π^*_{O-O} orbital to the vacant d_{xy}(Ti)-like orbital by in-phase π^*-d overlapping (Figure 6.15). Such an effect produces an extra stabilisation of the HOMO of the **2c** form, being 0.3–0.4 eV lower in energy than in the *alternated* homologues (Figure 6.16).

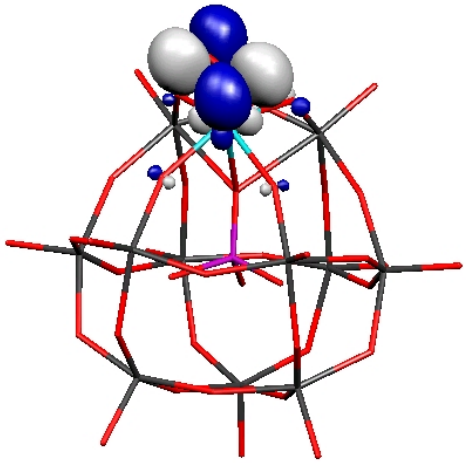

Figure 6.15. Representation of the HOMO for the eclipsed peroxo form **2c**.

The bond lengths computed for O–O and O–Ti in the most stable eclipsed conformation are 1.50 and 1.90 Å, respectively. It is worth

mentioning that POM geometries are very well reproduced by DFT methods, with average deviations from X-ray data of about 0.03 Å.[35-37] The only exception corresponds to the metal-terminal oxygen distances, which are in general, overestimated by ~0.05 Å. The O(1) oxygens link the TiW_2 triad with another triad whereas O(2) are bridging oxygens inside the TiW_2 triad.

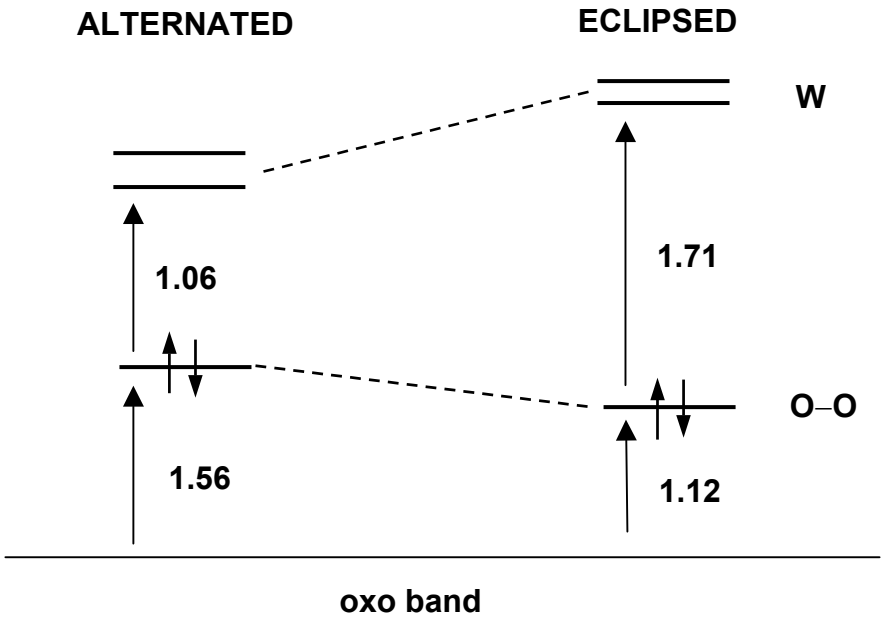

Figure 6.16. Relative frontier orbitals energies (in eV) for the alternated and eclipsed peroxo $[PTiOOW_{11}O_{39}]^{5-}$ anion. See Figure 10 for a 3D representation of the HOMO in the eclipsed conformation.

According to the formal IV and VI oxidation states for Ti and W, respectively, the electronic structure of $[P(TiO_2)W_{11}O_{39}]^{5-}$ is characterised by two sets of orbitals relatively close in energy. The HOMO in the non-protonated species is fairly localised over the O–O group, and the empty set of d-metal orbitals appear 1.71 eV above the occupied band at the DFT level, which is a somewhat small value compared to ~2.90 eV of the related $[PTiW_{11}O_{40}]^{5-}$ Keggin anion. This could be a sign of higher reactivity of the

peroxo derivative. Structures **2a** and **2b** have smaller HOMO-LUMO gaps, very close to 1.0 eV. The structure of the related $[P(WO_2)TiW_{11}O_{39}]^{5-}$ peroxo complex was computed for comparison. There are five distinct isomers according to the position of the W in relation to Ti. Since we do not expect a strong energy dependence of the cluster with the WOO position, we have arbitrarily chosen one non-neighbouring WOO–Ti form. In the eclipsed conformation for the O_2 group, the WOO complex was computed to be 13.7 kcal mol^{-1} higher in energy in relation to the most stable conformation for $[PTi(O_2)W_{11}O_{39}]^{5-}$. This important energy excludes the $[P(WO_2)TiW_{11}O_{39}]^{5-}$ peroxo complex as a result of the reaction of $[Bu_4N]_8[(PW_{11}O_{39}Ti)_2O]$ with H_2O_2.

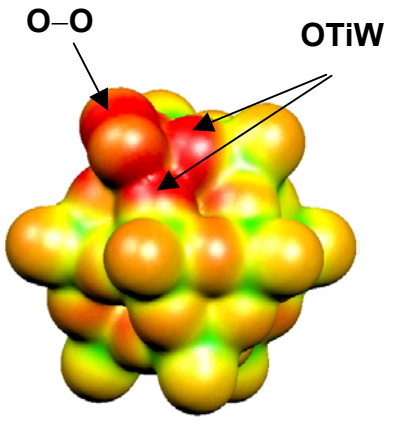

Figure 6.17. MESP function plotted over an isodensity surface for structure **2c**. Red regions represent proton-attractive sites.

A priori, the protonation of $[PTiW_{11}O_{40}]^{5-}$ could yield several isomers depending on the protonation site and the orientation of the proton. The electrostatic potential (EP) function is an useful tool in the prediction of protonation sites in a POM, allowing a qualitative classification of the relative nucleophilicity of the external regions of the POM core.[31,37] Alternatively, the protonation sites can be studied by explicit addition of protons in an attempt to find quantitative relative protonation energies.[15-16,31] Again, the relative basicity order found with the DFT methodology for several Keggin anions is in accordance with the experimental evidence.[35] In

the present case, the preferred site for protonation in $[PTi(O_2)W_{11}O_{39}]^{5-}$ was studied taking into account several isomers and orientations of the hydrogen atom. The EP function was appropriated in discriminating the most from the least favourable protonation sites in $[PTi(O_2)W_{11}O_{39}]^{5-}$.[32,35b] The EP distribution was plotted over a 3D-isodensity surface (Figure 6.17). The red colour identifies the most favourable protonation sites (nucleophilic regions). This representation suggests that the most likely positions to accept an incoming proton are the four oxygen atoms bridging the Ti and W atoms, indicated by the intense red colour in those regions. Contrarily, terminal W=O sites would be the least basic ones and, in general, the protonation in these terminal oxygens is very unlikely.[31] The O_2 group could compete in the protonation process because the EP takes similar values compared to OTiW sites.

A more quantitative description was obtained through the study of the protonated species, $[HPTi(O_2)W_{11}O_{39}]^{4-}$. When the OTiW oxygens were protonated several local minima were found. In the most stable structure A (Figure 6.18) the hydrogen is oriented towards the centre of the nearest M_4O_4 ring, a region with a high proton affinity. Notice in Figure 6.17 the intense red area nearby the M_4O_4 ring, especially in the vicinity of the OTiW sites. In structure B, the proton is equidistant from two bridging oxygens and from one of the oxygens of the peroxo group. This form is 3.7 kcal mol^{-1} above the most stable structure A in the gas phase. The relative energy of these two proton orientations changes when the solvent is included via a continuum model.[28] In acetonitrile (ε = 37.0) the two conformations are only separated by 0.4 kcal mol^{-1}. The interaction between the solvent and the anion is more efficient in structure B because the proton is oriented outwards from the anion surface.

The protonation in the peroxo ligand was also amply studied. All attempts to obtain a TiOO–H side-on coordination structure were, however, unsuccessful because the optimisation always evolved towards geometries with a η^1-coordination. This result contrast with the very recent B3LYP study of Sever and Root on the $Ti(OH)_3OOH$ model clusters, who also found structures with a η^1-coordination for the OOH group.[38]

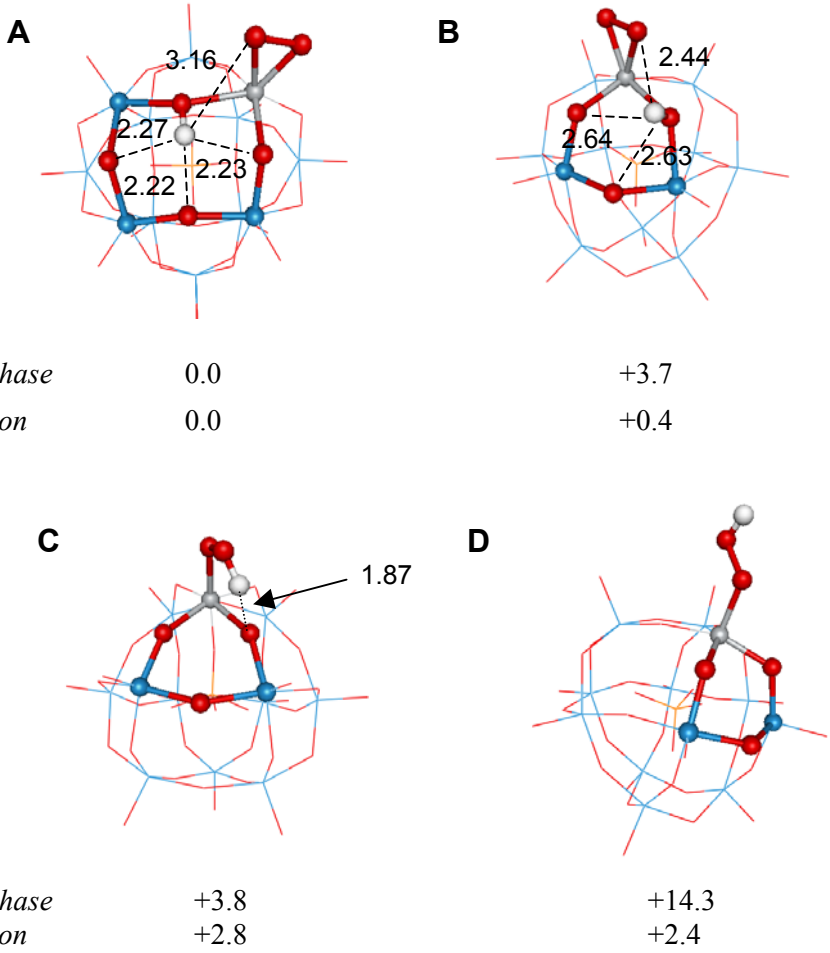

Gas phase	0.0	+3.7
Solution	0.0	+0.4

Gas phase	+3.8	+14.3
Solution	+2.8	+2.4

Figure 6.18. Optimised structures, relative energies (in kcal mol^{-1}) and H···O distances (in Å) for several isomers of $[HPTi(O_2)W_{11}O_{39}]^{4-}$. Notice the existence of a correlation between the number of H···O interactions and the stability of anion.

The larger coordination of the titanium centre in the polyoxometalate probably originates this different behaviour. The relative energy of C (Figure 6.18) in relation to A is +3.8 kcal mol^{-1} in the gas phase and only +2.8 kcal mol^{-1} in acetonitrile solution. Structure D is quite unstable, presumably due to the lack of any stabilising O···H interaction. But again, a

large stabilisation happens when the effect of the solvent is included in the calculations. In this latter case, the proton is very exposed to the solvent molecules and the relative energy for D goes from +14.3 kcal mol^{-1} in the isolated anion to only +2.4 kcal mol^{-1} in solution. Therefore, although the calculations point to OTiW as the most basic site, both H–OTiW and TiOO–H protonated anions could coexist in solution. Present calculations clearly show that, in addition to the intrinsic basicity of an oxygen site, inter and intra O···H interactions in POM clusters are of great importance in determining the protonation site in a POM.

It is worth noting that structure C (in which the O–O group has been protonated) yields the larger HOMO-LUMO gap of the series, a sign of stability of the cluster. The protonation at the peroxo ligand stabilises the energy of the HOMO, which is only 0.1 eV above the oxo band. Contrarily, the protonation in the Keggin core, as expected, does not modify the relative energy of the frontier orbitals. Finally, let us comment that the Mulliken population analysis shows a small increment of the positive charge in all the metal centres after protonation, particularly in those centres closest to the proton. Namely, the titanium atom and two of the four neighbouring W atoms. The largest change amounts 0.07 e

References and Notes

[1] Klemperer, W. G.; Shum, W. *J. Am. Chem. Soc.* **1977**, *99*, 3544.

[2] Klemperer, W. G.; Shum, W. *J. Am. Chem. Soc.* **1978**, *100*, 4891.

[3] Filowitz, M.; Ho, R. K. C.; Klemperer, W. G. *Inorg. Chem.* **1979**, *18*, 93.

[4] Besecker, C. J.; Klemperer, W. G. *J. Am. Chem. Soc.* **1980**, *102*, 7598–7600.

[5] Day, V. W.; Fredrich, M. F.; Thompson, M. R.; Klemperer, W. G.; Liu, R.-S.; Shum, W. *J. Am. Chem. Soc.* **1981**, *103*, 3597–3599.

[6] Besecker, C. J.; Klemperer, W. G.; Day, V. W. *J. Am. Chem. Soc.* **1982**, *104*, 6158–6159.

[7] Besecker, C. J.; Day, V. W.; Klemperer, W. G.; Thompson, M. R. *J. Am. Chem. Soc.* **1984**, *106*, 4125–4136.

[8] Day, V. W.; Klemperer, W. G.; Maltbie, D. J. *Organometallics.* **1985**, *4*, 104.

[9] Besecker, C. J.; Day, V. W.; Klemperer, W. G.; Thompson, M. R. *Inorg. Chem.* **1985**, *24*, 44.

[10] Day, V. W.; Klemperer, W. G.; Schwartz, C. *J. Am. Chem. Soc.* **1987**, *109*, 6030–6044.

[11] Day, V. W.; Klemperer, W. G.; Maltbie, D. J. *J. Am. Chem. Soc.* **1987**, *109*, 2991.

[12] Day, V. W.; Klemperer, W. G.; Lockledge, S. P.; Main, D. J. *J. Am. Chem. Soc.* **1990**, *112*, 2031.

[13] Day, V. W.; Klemperer, W. G.; Main, D. J. *Inorg. Chem.* **1990**, *29*, 2345–2355.

[14] Day, V. W.; Klemperer, W. G.; Main, D. J. *Inorg. Chem.* **1990**, *29*, 2355–2360.

[15] Bardin, B. B.; Bordawekar, S. V.; Neurock, M.; Davis, R. J. *J. Phys. Chem. B.* **1998**, *102*, 10817–10825.

[16] Ganapathy, S.; Fournier, M.; Paul, J. F.; Delevoye, L.; Guelton, M.; Amoureux, J. P. *J. Am. Chem. Soc.* **2002**, *124*, 7821–7828.

[17] (a) Hervé, G.; Tézé, A. *Inorg. Chem.* **1977**, *16*, 2115. (b) Massart, R.; Contant, R.; Fruchart, J. M.; Ciabrini, J. P.; Fournier, M. *Inorg. Chem.* **1977**, *16*, 2916. (c) Jeannin, Y.; Martin-Frère, J. *J. Am. Chem. Soc.* **1981**, *103*, 1664–1667. (d) Martin-Frère, J.; Jeannin, Y. *Inorg. Chem.* **1984**, *23*, 3394–3398. (e) Weakley, T. R. J. *J. Chem. Soc., Chem. Commun.* **1984**, 1406. (f) Kortz, U.; Tézé, A.; Hervé, G. *Inorg. Chem.* **1999**, *38*, 2038–

2042.

[18] Weakley, T. J. R.; Evans, H. T.; Showell, J. S.; Tourné, C. M.; Tourné, G. F. *J. Chem. Soc. Chem. Commun.* **1973**, 139. Finke, R. G.; Droege, M.; Hutchinson, J. R.; Gansow, O. *J. Am. Chem. Soc.* **1981**, *103*, 1587–1589. Evans, H. T.; Tourné, C. M.; Tourné, G. F.; Weakley, T. J. R. *J. Chem. Soc. Dalton Trans.* **1986**, 2699–2705. Finke, R. G.; Droege, M. W.; Domaille, P. J. *Inorg. Chem.* **1987**, *26*, 3886–3896. Weakley, T. J. R.; Finke, R. G. *Inorg. Chem.* **1990**, *29*, 1235–1241. Gómez-García, C. J.; Coronado, E.; Borrás-Almenar, J. J. *Inorg. Chem.* **1992**, *31*, 1667.

[19] Domaille, P. J. *J. Am. Chem. Soc.* **1984**, *103*, 7677–7687.

[20] Kempf, J. Y.; Rohmer, M.-M.; Poblet, J.-M.; Bo, C.; Bénard, M. *J. Am. Chem. Soc.* **1992**, *114,* 1136.

[21] Okuhara, T.; Mizuno, N.; Misono, M. *Adv. Catal.* **1996**, *41*, 113.

[22] Finke, R. G.; Droege, M. W. *J. Am. Chem. Soc.* **1984**, *106*, 7274–7277.

[23] Edlund, D. J.; Saxton, R. J.; Lyon, D. K.; Finke, R. G. *Organometallics.* **1988**, *7*, 1629–1704.

[24] See references 22-30 of chapter 4.

[25] Finke, R. G.; Rapko, B.; Weakley, T. J. R. *Inorg. Chem.* **1989**, *28*, 1573 and see Barnard, D. L.; Hill, C. L.; Cage, T.; Matheson, J. E.; Huffman, J. H.; Sidwell, R. W. Otto, M. I. Schinazi, R. F. *Intl. Antiviral News.* **1995**, *3*, 159–161.

[26] (a) Yamase, T.; Ozeki, T.; Sakamoto, H.; Nishiya, S.; Yamamoto, A. *Bull. Chem. Soc. Jpn*. **1993**, *66*, 103–108. (b) Lin, Y.; Weakley, T. J. R.; Rapko, B.; Finke, R. G. *Inorg. Chem.* **1993**, *32*, 5095–5101. (c) Müller, A.; Krickemeyer, E.; Dillinger, S.; Meyer, J.; Bögge, H.; Stammler, A. *Angew. Chem., Int. Ed. Engl.* **1996**, *35*, 171–173. (d) Kim, G.-S.; Zeng, H.; Rhule, J. T.; Weinstock, I. A.; Hill, C. L. *J. Chem. Soc., Chem. Commun.* **1999**, 1651–1652. (e) Kim, G.-S.; Zeng, H.; VanDerveer, D.; Hill, C. L. *Angew. Chem., Int. Ed. Engl.* **1999**, *38*, 3205–3207.

[27] Kholdeeva, O. A.; Maksimov, G. M.; Maksimovskaya, R. I.; Kovaleva, L. A.; Fedotov, M. A.; Grigoriev, V. A.; Hill, C. L. *Inorg. Chem.* **2000**, *39*, 3828–3837.

[28] Pye, C. C.; Ziegler, T. *Theor. Chem. Acc.* **1999**, *101*, 396. ADF 2000.01. Department of Theoretical Chemistry. Vrije Universiteit. Amsterdam. Baerends, E. J.; Ellis, D. E.; Ros, P. *Chem. Phys.* **1973**, *2*, 41. Versluis, L.; Ziegler, T. *J. Chem. Phys.* **1988**, *88*, 322. Te Velde, G.; Baerends, E. J. *J. Comput. Phys.* **1992**, *99*, 84. Fonseca Guerra, C.; Snijders, J. G.; Te Velde, G.; Baerends, E. J. *Theor. Chem. Acc.* **1998**, *99*, 391.

[29] Kholdeeva, O. A.; Maksimovsaya, R. I.; Maksimov, G. M.; Zamarev, K. I. *React. Kinet. Catal. Lett*. **1998**, *63*, 95.

[30] Kim, G.-S.; Zeng, H.; Cowan, J. J.; Neiwert, W. A.; VanDerveer, D.; Hill, C. L.; Weinstock, I. A. *Inorg. Chem.* **2003**, *42*, in press.

[31] López, X.; Bo, C.; Poblet, J. M. *J. Am. Chem. Soc.* **2002**, *124*, 12574.

[32] Maestre, J. M.; Sarasa, J. P.; Bo, C.; Poblet, J. M. *Inorg. Chem.* **1998**, *37*, 3071.

[33] Manuscript in preparation.

[34] Sheldon, R. A.; Kochi, J. K. *Metal-Catalyzed Oxidations of Organic Compounds,* Academic Press, New York, **1981**. Sheldon, R. A.; Dakka, J. *Catal. Today.* **1994**, *19*, 215. Notari, B. *Adv. Catal.* **1996**, *41*, 253. Centi, G.; Misono, M. *Catal. Today* **1998**, *41*, 287. Clerici, M. G. *Topics in Catalysis* **2000**, *13*, 373. Sanderson, W. R. *Pure and Appl. Chem.* **2000**, *72*, 1289. Arends, I. W. C. E.; Sheldon, R. A. *Appl. Catal. A: General.* **2001**, *212*, 175.

[35] (a) Poblet, J. M.; López, X.; Bo, C. *Chem. Soc. Rev.* **2003**, 297; (b) Rohmer, M.-M.; Bénard, M.; Blaudeau, J.-P.; Maestre, J. M.; Poblet, J. M. *Coord. Chem. Rev.* **1998**, *178–180*, 1019.

[36] López, X.; Maestre, J. M.; Bo, C.; Poblet, J. M. *J. Am. Chem. Soc.* 2001, **123***,* 9571.

[37] Maestre, J. M.; López, X.; Bo, C.; Casañ-Pastor, N.; Poblet, J. M. *J. Am. Chem. Soc.* **2001**, *123*, 3749. Bridgeman, A. J.; Cavigliasso, G. *Inorg. Chem.* **2002**, *41*, 1761. Bridgeman, A. J.; Cavigliasso, G. *Inorg. Chem.* **2002**, *41*, 3500.

[38] Sever, R. R.; Root, T. W. *J. Phys. Chem*. **2003**, *107*, 4090

CHAPTER 8

Solvent Effects

This chapter provides a first attempt to deal with the environmental factors acting on POMs. In the previous chapters 4-7 we mostly studied polyoxometalates in the gas phase. Such a crude treatment is valid to study some properties but, in some cases, it may not be sufficient. The introduction of the solvent effects by means of theoretical tools has been studied for a long time. Amongst others, two theoretical approaches can be used nowadays to model the solvent effects. This chapter presents tests performed with POMs making use of a continuum model, on the one hand, and with molecular dynamics, on the other hand. In section 8.2 we discuss a few examples in which the COSMO method is utilised for recomputing the cluster energies. Section 8.3 describes the solvation of two Keggin anions treated with molecular dynamics. In this method, the solvent molecules are treated as discrete units. From this data, one can get a general picture of the disposition of water molecules around a POM.

8.1. Introduction

The results presented in previous chapters of this thesis dealt with molecules in the gas phase, just getting rid off the external factors like counterions or solvent molecules. For many considerations, it is a fairly good approximation, but for some purposes it is obligatory to go beyond this simple model, thus including the effect of the environment. Since polyoxometalates are known to exist only in solution or in crystalline matrices, an approach to reality passes through the inclusion of the molecules that surround them. Of course, the media they are in influences not only some inherent properties of POMs, but also the way they interact or react with other species. An example is the electron transfer reaction, which is discussed below. Maestre *et al.*[1] and Rohmer *et al.*[2] published the pioneering works where an external field was applied to a POM cluster. The method proposed takes into account the stabilising effects of the environment by reproducing the external potential field with a set of point charges (see chapter 3).

The aim of this chapter is to present the results obtained by using two well-known models that enable the introduction of the solvent effects to POMs. These two methodologies are briefly introduced, together with illustrative results, in sections 8.2 and 8.3. These resorts for including the environmental effects are inherently very different in their assumptions of how the solvent is treated. The information obtained from these two techniques is valuable since scarce information is available. Section 8.3 is based on unpublished results.

8.2. Solvent Treated with a Continuum Model

8.2.1. The COSMO model of solvation

When treating a solvent as a continuum material, the number of degrees of freedom associated to the solvent molecules is dramatically reduced. The computational cost of such technique is modest compared to methods that explicitly consider all molecules. The idea of approximating the solvent as a continuum material surrounding a solute molecule is ancient. Starting from the original conception of Born,[3] Kirkwood[4] and Onsager[5] for modelling the solvent at a theoretical level, countless reports inspired in those primary

approaches have been published.[6-7] In the middle 1990's, Klamt and others[8-11] applied new approaches on the definition of the molecule-shaped cavity of the solvent, thus developing a quantitative description of the solvation phenomenon. It is the so-called *conductor-like screening model* of solvation (COSMO). This model has been implemented in various programs, as in the MOPAC[12] and ADF[13] packages. The model of Klamt *et al*. assumes that a molecule in solution may be regarded as being encapsulated in a cavity surrounded by the solvent molecules. This solvent, instead of being treated as a set of discrete molecules, is viewed as constituting a continuum material with a characteristic dielectric constant, ε. The target molecule plays the role of the solute that induces a charge distribution at the surface of the continuum material, which is opposite to the charge inside the cavity. Conceptually, this charge distribution corresponds to the polarisation of the continuum material. In principle, the total charge distributed along the solvent cavity surface is equal to the charge of the molecule inside.

The model is transcribed to a mathematical expression accounting for the total electrostatic energy, expressed as

$$E^S = \int_S \sum_A \frac{Z_A \rho_S(r_S)}{|R_A - r_S|} dr_S + \int_S \int_S \frac{\rho_S(r_S)\rho_S(r_S')}{|r_S - r_S'|} + \int_V \int_S \frac{\rho(r)\rho_S(r_S)}{|r - r_S|}$$

The first term represents the interaction of the surface charges, $\rho_s(r_s)$, with the nuclei of the solute molecule, Z_A. The second term accounts for the self-interaction between solvent charges, and the third one is the electrostatic interaction of the solvent charges with the electron density of the solute, $\rho(s)$. For practical purposes, the charge distribution over the surface of the solvent cavity is depicted by discrete point charges. It is very important, in assessing the performance of the model, the level of description of the surface surrounding the solute. The fundamental approximation is to consider the cavity as the union of van der Waals (vdW) spheres centred on the atoms of the solute molecule. Connolly,[14] Gibson and Scheraga,[15] Kundrot *et al*.,[16] and Perrot *et al*.[17] have investigated the analytical properties of vdW surfaces. The basic approach consists in converting the surface of the cavity in a discrete ensemble of polyhedrons. Figure 8.1 shows the vdW surface of the Keggin anion. Some methods have been reported to reproduce this surface, although one of the most common is to generate a family of triangles, each one holding a given charge. Silla and co-

workers developed a more efficient algorithm (GEPOL) to compute the surface and volume of the cavity, with better accuracy and lower cost than Connolly's method.[18] Thus, the mathematical expression above can be reformulated in terms of this formulation.

8.2.2. Application of the COSMO to POMs

Computational details

The results showed in this section were obtained by means of the implementation of the COSMO method in the ADF program.[13] For the description of the Keggin anions, we made use of the regular TZP/STO basis sets for all atoms. The strategy conducted for obtaining the energies in solution is composed of two steps. First, geometry optimised structures were obtained in the gas phase. In a second step, single-point variational calculations were performed including the surface charges in the Fock operator self-consistently, i.e., recomputing the charges of the cavity at every SCF step. The solvent is characterised by a set of parameters. We constructed the Keggin-containing cavity with the solvent-excluding surface method, constructed by means of the GEPOL93 algorithm,[18c] in which the radius of the solvent is taken as 1.4 Å. The solvent-excluding surface converts the cusps appearing in vdW surfaces in smooth concave parts. The discretisation of the surface cavity (also know as tessellation) is also characterised by how fine the spheres are partitioned in triangles. We used a value of 5, which represents a smoother description than the default option in the ADF code. The solute is characterised by the radii of the composing atoms. In fact, the Keggin structure has only oxygens exposed to the solvent, so it is more important the choice of the oxygen radius than any other one in the framework. It is fixed at a value of 1.52 Å considering a formal charge of –2. For W^{6+} and Nb^{5+}, the radii were 1.26 and 0.78 Å, respectively. These values are taken from standard libraries of atomic data.[19] The internal atoms like P and Si do not need an accurate value of radius since they are far from interact with the solvent.

The polarisability of the continuum material is governed by its dielectric constant, ε. The value utilised for water is 78.4 and, for acetonitrile, another common solvent, it is 37.0. Provided that the COSMO equation is strictly correct for conductors, a scaling function is introduced to

the dielectric solvent-related terms. In the total energy expression for the system (solute + solvent), the factor

$$f(\varepsilon) = \frac{\varepsilon - 1}{\varepsilon + x}$$

where x is an empirical parameter, is introduced. Some authors choose x = 0.5,[8-9,11,20] whereas others take 0.0.[21-22] We utilised the latter value in our calculations.

Pye *et al*.[13] tested several ionic and neutral compounds with the various surfaces commented above, obtaining modest differences in the solvation energies for small molecules, although notably differing for large systems.

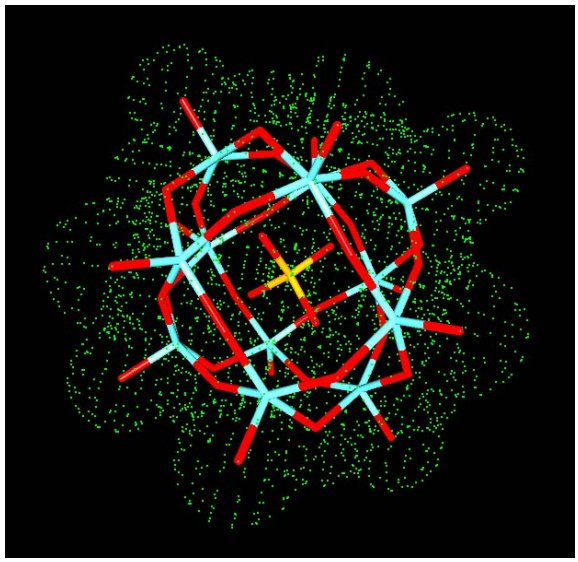

Figure 8.1. Representation of the van der Waals surface (represented as green dots) that surrounds the Keggin anion.

The electronic structure in solution

The case of POMs is especially interesting because they are, in general, molecules with a high negative charge that do not exist in the gas phase. This implies an upshift of the molecular orbital energies that is unrealistic, a

deviation being larger with the negative charge. An external field generated by the counterions and the solvent is crucial to stabilise the POMs. Therefore, for a realistic comparison of the orbital energies, the solvent has to be taken into account. In solution, many of the properties of POMs depend on the concentration, the ionic strength, the pH of the solution, etc. At present it is still not possible to take all these factors into account in a quantum chemistry study. However, a first order approximation for dilute solutions is to model the solvent effect by a polarizable continuum. The main goal of the application of the COSMO method is to put MO energies at the correct level, thus allowing the study of electron transfer reactions between POM species.

Let us take, for example, the $[PW_{12}O_{40}]^{3-}$ Keggin anion.[23] In the gas phase, the molecular orbitals are very high in energy due to the negative charge of the species. In general, POMs may be viewed as a neutral cage encapsulating an anion in its interior; this is the so-called clathrate model that allows $[PW_{12}O_{40}]^{3-}$ and $[P_2W_{18}O_{62}]^{6-}$ to be reformulated as $[PO_4]^{3-}@W_{12}O_{36}$ and $[PO_4]_2^{6-}@W_{18}O_{54}$, respectively (see chapters 1 and 4). The unoccupied metallic band of the *neutral* $W_{12}O_{36}$ and $W_{18}O_{54}$ cages appears very low in energy in the gas phase. The LUMO lies near –6.5 eV in both frameworks. The encapsulation of the phosphate anion inside the neutral cages shifts all the molecular orbitals of the POM toward higher energies. Hence, the absolute energies of the frontier orbitals in PW_{12} are +0.06 eV and +2.85 eV, respectively. When $W_{12}O_{36}$ encapsulates the SiO_4^{4-} unit, the shift is even more considerable but the H-L gap is still independent of the total charge of the encapsulated anion. Keeping in mind that POMs are *easily reducible* chemical species, the energy of the lowest unoccupied orbitals must be low enough to accept the incoming electron. The crystal field in the solid state[1] and the solvent molecules in dilute solutions stabilise the anion, and a downshift of the MOs' energies occurs. Figure 8.2 gives the orbital energies computed in the gas phase compared to those obtained including solvent effects. There is a considerable decrease in the MO energies after the solvation and the magnitude of this decrease parallels the charge of the anion. Note from those values that the LUMO and the rest of orbitals with metallic character above appear at quite negative energies after solvation (about –4 eV). This is a necessary condition for an incoming electron to be trapped in the framework.

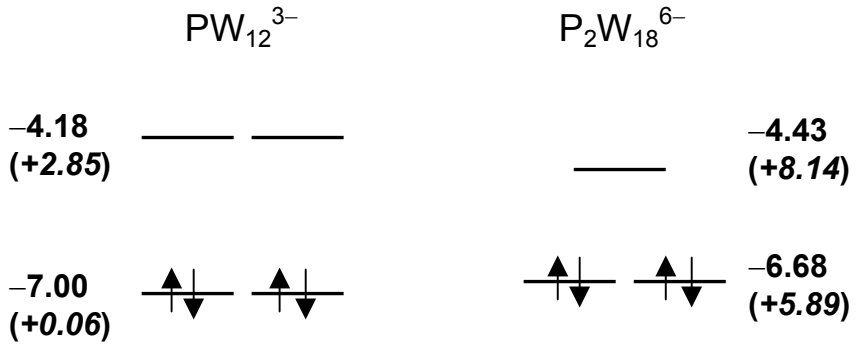

Figure 8.2. Energy of the HOMO and the LUMO for the Keggin PW_{12} and the WD P_2W_{18} anions in solution and in the gas phase (in parentheses). Values are in kcal mol^{-1}.

One goal in the introduction of the COSMO is to reproduce the correct direction of a reaction. Let us take as an example the electron transfer reaction between two POMs. It is well known that P_2W_{18}, although has a higher negative charge, is more oxidant than PW_{12}. In the gas phase, the process:

$$[PW_{12}\ 1e]^{4-} + [P_2W_{18}]^{6-} \rightarrow [PW_{12}]^{3-} + [P_2W_{18}\ 1e]^{7-}$$

was computed to be highly endothermic (ΔE = +5.07 eV) because, in absolute value, the LUMO in the WD anion lies at a higher energy. Consequently, in the absence of external fields, the extra electron simply prefers to go to the least charged PW_{12} anion. On the other hand, the frontier orbitals have similar energies in solution (Figure 8.2) and the electron transfer reaction becomes slightly exothermic (ΔE = –0.11eV), thus reproducing the experimental trend.

We also checked whether the solvent has an effect on the inner reduction properties of WD anions. The difference in stability of a P_2W_{18}1e reduced at a polar site and its partner reduced at an equatorial site is not altered by the presence of the solvent. Neither we did observe any difference in the relative stability of the reduced anions of the mixed cluster $P_2W_{15}V_3$. These results are consistent with the almost isotropic field generated by the continuum model that modifies the absolute MO energies but does not change their relative values. Therefore, in the absence of short

intermolecular contacts (such as ionic pairing or weak hydrogen bonds), the study of isolated anions suffices to understand many redox properties of POMs. Often their properties may simply be described by the electronic properties of the corresponding neutral cage. For example, the difference in the reduction energy between the polar and equatorial sites in the neutral cage $W_{18}O_{54}$ of the WD framework was computed to be 0.71 eV, a value that is very similar to the energy difference computed for the complete cluster $[PO_4]_2^{6-}@W_{18}O_{54}$, 0.84 eV.

Table 8.1. Energy change for the HOMO and LUMO for several POMs. The energy downshift fairly equalises the energy of the HOMO.

	E_{HOMO} *(eV)*		E_{LUMO} *(eV)*	
anion	$\varepsilon_o = 0$	$\varepsilon_w = 78.4$	$\varepsilon_o = 0$	$\varepsilon_w = 78.4$
$[PW_{12}]^{3-}$	0.06	–7.00	2.86	–4.18
$[PW_{12}\ 1e]^{4-}$	2.98	–6.68	5.74	–3.88
$[SiW_{12}]^{4-}$	2.99	–6.22	5.83	–3.78
$[AlW_{12}]^{5-}$	6.43	–6.26	9.24	–3.40
$[SiW_{12}\ 1e]^{5-}$	5.89	–6.43	8.70	–3.61
$[Co^{III}W_{12}]^{5-}$	5.85	–6.43	8.58	–3.65
$[AlW_{12}\ 1e]^{6-}$	9.25	–5.97	11.99	–3.17
$[Co^{II}W_{12}]^{6-}$	8.64	–6.21	11.34	–3.44
$[SiW_9Ti_3O_{40}]^{10-}$	19.36	–5.16	21.67	–2.21

Table 8.1 summarises some orbital energies of a set of polyoxoanions computed both in the gas phase and with the COSMO solvation method. The energies of HOMO and LUMO before and after inclusion of the solvent are illustrative of the effect that the COSMO has on the energy of the orbitals. The dielectric constant, ε, was chosen to be 78.4. In the gas phase, the HOMOs and LUMOs (listed in the table) are very high in energy and thus not representing realistic situations. After the COSMO calculation, the energy of the HOMOs is shifted to negative energies, which is a necessary condition for stability. Also notice that all the HOMO energies for this family of POMs lie at energies between –7 and –6 eV. This is another fact reinforcing the improvement achieved by including the external field. The

energies of the LUMOs are shifted to negative energies, as well. Taking into account that POMs are strong oxidant species, it is another necessary fact to correct in the gas-phase calculation. At the COSMO level, the energy of the LUMO allows them to accept metallic electrons and to locate them in low-lying orbitals.

However, the utilisation of this technique must be carried out with care. Some highly charged anions could be overstabilised, which could be an artefact of the model. Despite this, we claim that the study of energy reaction profiles of charged systems (see section 6.2) are realistic only if a model of solvation is taken into account.

8.3. Molecular Dynamics Simulations

8.3.1. Introduction and details of the simulations

A different point of view for studying the solvent is provided by molecular dynamics (MD). This technique does not take into account quantum considerations to study the molecular interactions. Therefore, no electron density is present and this model is not able to create or destroy bonds. It has been utilised for the study of different phenomena, such as the modelling of large ensembles of molecules. The motion of the solvent molecules can be simulated according to a standard energetic criterion and a distribution of molecules is obtained referring to their position. The information provided by MD is somewhat more qualitative than that of the COSMO model because it provides averaged statistical information although it represents in a more realistic way the behaviour of the solvent around the solute.

The solvent is not modelled as a continuum material but by a discrete ensemble of molecules in which each atom is characterised by empirical or calculated parameters. In the present case, the modelisation deals with solute molecules, as well. In the model we applied, all the molecules were left absolutely rigid, were the solvent molecules are only able to rotate and translate, whereas the solute molecule was fixed at the centre of a cell (Figure 8.3).

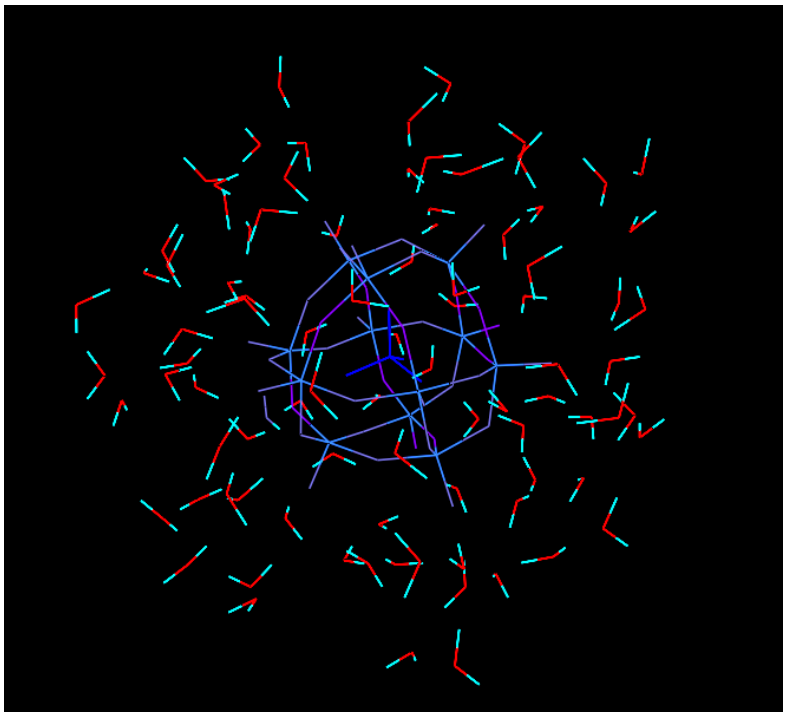

Figure 8.3. Snapshot of a molecular dynamics run. The Keggin anion is shown in blue, whereas (a few) water molecules are represented surrounding the solute molecule.

Computational details

One way for visualising the information provided by MD is to represent the *radial distribution* of the solvent molecules around the central cluster. Each MD run in the present results is characterised by the following parameters. Assuming that the total energy can be approximated by a pair-potential, we have:

$$E_{pot} = \frac{1}{2}\sum_{\substack{i,j \\ i \neq j}} \phi(r_{ij})$$

In general, $\phi(r_{ij})$ is approximated to: $\Phi(r) = \frac{\lambda^n}{r^n} - \frac{\lambda^m}{r^m}$

The van der Waals forces arising from the dipole interaction, the attractive part, corresponds to $m = 6$. The most common general potential obeys the 12-6-Lennard–Jones (LJ) potential.[24] Thus, the total potential energy is

$$\Phi(r) = \sum_i \sum_j \left(4\varepsilon_{ij} \left[\left(\frac{\sigma_{ij}}{r_{ij}} \right)^{12} - \left(\frac{\sigma_{ij}}{r_{ij}} \right)^{6} \right] + \frac{q_i q_j}{r_{ij}} \right)$$

with

$$\sigma_{ij} = \frac{1}{2}(\sigma_{ii} + \sigma_{jj}) \text{ and } \varepsilon_{ij} = \sqrt{\varepsilon_{ii}\varepsilon_{jj}}$$

In the expression of $\Phi(r)$, r_{ij} is the distance between site i and j, and q is the atomic charge, obtained by means of the Mulliken population analysis. The values of ε and σ for each element are fitted to experimental data. See Table 8.2 for a list of the parameters utilised for the MD calculations. The potential parameters for the Keggin-oxygen (water) interactions in the present calculations are:

Table 8.2. ε, σ and q parameters utilised for the molecular dynamics calculations. The atomic charges listed were calculated by Mulliken population analysis.

	ε *(kJ mol^{-1})*	σ	q	
Atoms in the Keggin			PW_{12}	$SiNb_3W_9$
P	123.45	3.000	+1.94	–
Si			–	+2.08
W	111.26	2.337	+2.85	+2.77/+2.81
Nb			–	+2.24
O_{tetra}			–0.90	–1.14
O_{bridge}	107.95	3.169	–1.06/–1.12	–0.99/–1.12
O_{term}			–0.78	–0.89/–0.91

The LJ interactions were assumed to be the same for both Keggin clusters tested (see below). The electrostatic interactions are usually much stronger than the LJ potential and the error introduced with this approximation is negligible. Since the potential decreases rapidly with r, we can apply a cut-off to the potential. For avoiding discontinuity, we choose a given value for r_0 and the termination of the potential is smoothed using a tail potential, say $\Psi(r)$ such that $\Psi(r) = \Phi(r)$ at r_0. The truncation of the forces was chosen at a cut-off intermolecular distance of 9.0 Å. The long-range electrostatic interactions were calculated by a standard Ewald summation.[25]

We constructed a (27.929 x 27.929 x 27.929) $Å^3$ cubic unit cell. The total number of water molecules inside this cage is fixed at 665. An extended simple-point-charge (SPC/E) force-field model was used for water.[26] For constructing the radial distribution curve for water, the Keggin was assumed to be spherical. The positions for all atoms of the solvent were averaged at each step of the run (excluding the positions during the equilibration time). The temperature of the experiment was fixed by means of the Berendsen thermostat[27] at 298 K, in which the instantaneous temperature is pushed towards the desired T by scaling the molecular velocities at each step of the run. The time constant was fixed at 0.2 ps. The equilibration time was fixed at 50 ps, whereas the total runtime for each experiment was 700 ps with a time step of 2.0 fs.

8.3.2. MD study of the solvation of Keggin clusters

MD calculations were carried out to obtain additional information concerning the fashion in which Keggin anions are solvated. The study was performed in collaboration with Dr. Christoph Hartnig,[28] from the Juelich Research Centre, Germany. From each MD run, the information is transformed into averaged radial distributions for the molecules of solvent around the solute anion. These curves can be plotted representing H- and O-distributions in order to identify accumulations of hydrogen or oxygen atoms of the water molecules separately. MD was used for comparing the effects of the solvent in two cases: the single-addenda $PW_{12}O_{40}^{3-}$ and the mixed-addenda $SiNb_3W_9O_{40}^{7-}$ anions. The overall charge was chosen to be different in both clusters with the aim of finding differences in the way they are solvated by water. In principle, we can expect that the solvent molecules will behave somehow differently.

MD study of $PW_{12}O_{40}^{3-}$ in water

We start the discussion of the MD results with the most symmetric single-addenda PW_{12} anion. The discussion of the results in this section is referred to oxygen positions in the Keggin anions showed in Figure 8.4.

Table 8.3. Average distances computed (in Å) from the central X atom to the terminal (O_{term}), bridging-1 (O_{brid-1}) and bridging-2 (O_{brid-2}) oxygens in PW_{12} and $SiNb_3W_9$.

	$X–O_{term}$	$X–O_{brid-1}$	$X–O_{brid-2}$
$PW_{12}O_{40}^{3-}$	5.29	3.97	3.42
$SiNb_3W_9O_{40}^{7-}$	5.52	4.10	3.40–3.59

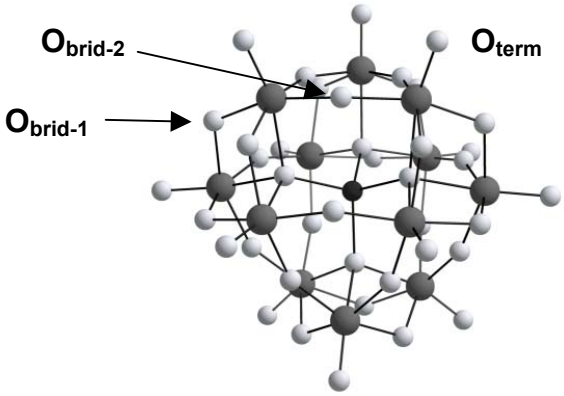

Figure 8.4. Ball-and-stick view of the Keggin anion. The three external oxygen sites are labelled.

The radial distribution of H_2O molecules around $PW_{12}O_{40}^{3-}$ is shown in Figure 8.5. Three peaks appear in the H-distribution. At distances larger than 8.6 Å from the central phosphorous, the H-distribution is almost constant indicating that the perturbations generated by the anion on the solvent are almost negligible at 4–5 Å from the Keggin surface. The first breaking of the solvent structure is found at 8.5 Å, giving rise to a band

centred at 8.3 Å and a most pronounced maximum at 7 Å. This latter peak must be mainly associated with hydrogen atoms directly interacting with terminal oxygen sites.

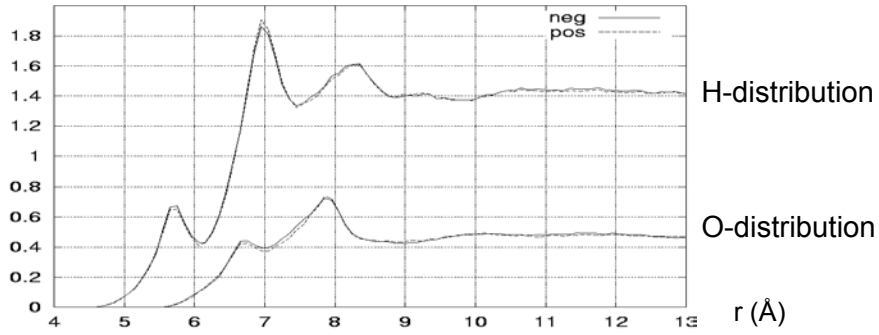

Figure 8.5. Radial distribution of H and O atoms of solvent around $PW_{12}O_{40}^{3-}$. We will discuss only de H-distribution. The origin of the x-axis is the P atom inside the Keggin. It is only represented from 4 to 13 Å, provided that at r < 4 Å we have the cluster and there are no solvent molecules.

The presence of a unique maximum in the region 7–8.5 Å in the O-distribution centred at 8 Å would indicate that both in the H-distribution belong to the same water molecule. So, the broad peak at 8.3 Å may not correspond to a H atom directly linked to one of the Keggin oxo sites. A third peak of minor intensity appears at ~5.6 Å. This accumulation must be attributed to the electrostatic interaction between the bridging sites and the water molecules. As shown in Figure 8.4, there are two distinct bridging oxygens in a Keggin framework: $O_{brid\text{-}1}$ that is at 3.97 Å from P and the more internal $O_{brid\text{-}2}$, with a P···O separation of 3.42 Å (Table 8.3). Most water molecules owning H atoms between 5 and 6 Å from the centre of the cluster would be in contact with the more external $O_{brid\text{-}1}$ oxygen, with H···O distances between 1.1 and 2 Å. The lack of a significant number of water molecules under 5 Å would be indicative of the minor accessibility of water molecules to the most internal bridging $O_{brid\text{-}2}$ oxygens. Therefore, although the two types of bridging sites have almost the same intrinsic basicity (see discussion in chapter 6) $O_{brid\text{-}1}$ and $O_{brid\text{-}2}$ would behave differently, for example, in acid-base catalysis. Taking into account that there is the same

number of terminal and O_{brid-1} sites, the affinity of water molecules for O_{term} and O_{brid-1} is approximately in a ratio 3:1. All the assignments were made taking into account a O···H distance between 1.4 and 1.8 Å. We have already mentioned in preceding chapters that terminal oxygen sites are the most exposed to the solvent molecules, which is plenty confirmed by the present MD calculations.

MD study of $SiNb_3W_9O_{40}^{7-}$ in water

The MD study of $SiNb_3W_9O_{40}^{7-}$ in a solution of water gives similar results to those found in the single-addenda anion. The radial distributions of O and H atoms of solvent were analysed making a distinction between the two *hemispheres* of the cluster: one containing the 3 Nb ions and the other only containing tungsten ions, denoted by solid and dashed lines in Figure 8.6. The larger negative charge in the Nb-derivative induces, however, some changes in the water distributions around the anion:

(i) All the peaks are shifted to smaller radial values in comparison to the distribution found for $PW_{12}O_{40}^{3-}$.

(ii) There is a new shoulder in the H-distribution, marked with an arrow in Figure 8.6, at 5 Å

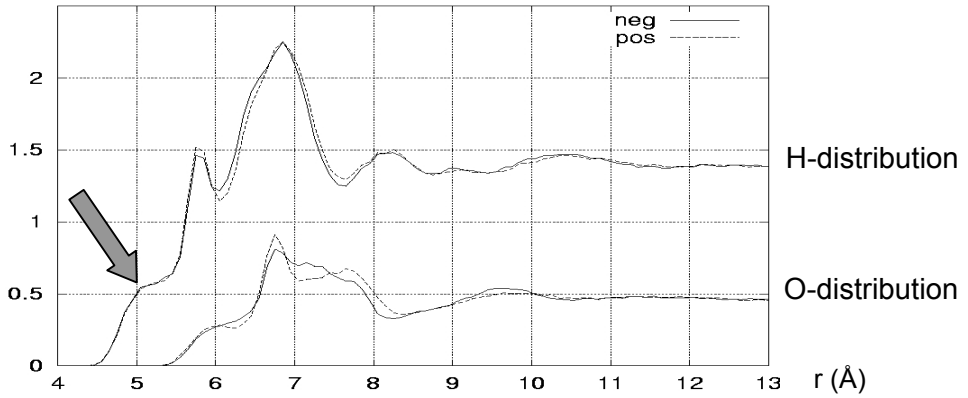

Figure 8.6. Radial distribution of H and O atoms of solvent around $SiNb_3W_9^{7-}$. The general picture resembles that of Figure 8.5, although slight changes appear.

The terminal sites keep on being surrounded by a large number of solvent molecules, but by the effect of the larger negative charge, now the local accumulation of water molecules is greater and closer to the surface of the Keggin cluster. The peak is centred at r = 6.8 Å, which means that, in average, the H···O_{term} distance is notably shorter in the substituted cluster, 1.3 Å in comparison to the value of 1.7 Å in the unsubstituted anion (see Si···O_{term} distances in Table 8.2). The number of water molecules also significantly increases in the regions near O_{brid-1} and near O_{brid-2}, as well, which is manifested by the shoulder in the H-distribution at 5 Å. Thus, we believe that this relative accumulation of water molecules would correspond to an effective interaction with the most internal O_{brid-2} site. The average H···O_{brid-2} distances are ~1.5 Å. In addition, the distribution of water molecules is almost equivalent in the two hemispheres of the anion. Despite that the negative charge is somewhat more concentrated in the Nb-region, the water molecules with the present model do not experience different forces between the *hemispheres*.

References and Notes

[1] Maestre, J. M.; Sarasa, J. P.; Bo, C; Poblet, J.-M. *Inorg. Chem.* **1998**, *37,* 3071.

[2] Rohmer, M.-M.; Bénard, M.; Blaudeau, J.-P.; Maestre, J. M.; Poblet, J. M. *Coord. Chem. Rev.* **1998**, *178–180*, 1019.

[3] Born, M. *Z. Phys*. **1920**, *1*, 45.

[4] Kirkwood, J. G. *J. Chem. Phys*. **1934**, *2*, 351.

[5] Onsager, L. *J. Am. Chem. Soc*. **1936**, *58*, 1486.

[6] Tomasi, J.; Persico, M. *Chem. Rev.* **1994**, *94*, 2027.

[7] Cramer, C. J.; Truhlar, D. G. *Chem. Rev.* **1999**, *99*, 2161.

[8] Klamt, A.; Schüürmann, G. *J. Chem. Soc, Perkin Trans*. *2*. **1993**, 799.

[9] Andzelm, J.; Kölmel, C.; Klamt, A. *J. Chem. Phys*. **1995**, *103*, 9312.

[10] Klamt, A. *J. Chem. Phys*. **1995**, *99*, 2224.

[11] Klamt, A.; Jonas, V. J. *Chem. Phys*. **1996**, *105*, 9972.

[12] Stewart, J. J. P. *QCPE Bull*. **1993**, *13*, 42.

[13] Pye, C. C.; Ziegler, T. *Theor. Chem. Acc*. **1999**, *101*, 396. ADF 2000.01. Department of Theoretical Chemistry. Vrije Universiteit. Amsterdam. Baerends, E. J.; Ellis, D. E.; Ros, P. *Chem. Phys.* **1973**, *2*, 41. Versluis, L.; Ziegler, T. *J. Chem. Phys.* **1988**, *88*, 322. Te Velde, G.; Baerends, E. J. *J. Comput. Phys.* **1992**, *99*, 84. Fonseca Guerra, C.; Snijders, J. G.; Te Velde, G.; Baerends, E. J. *Theor. Chem. Acc.* **1998**, *99*, 391.

[14] Connolly, M. L. *J. Appl. Crystallogr*. **1983**, *16*, 548. Connolly, M. L. *J. Am. Chem. Soc.* **1985**, *107*, 1118. Connolly, M. L. *J. Appl. Crystallogr*. **1986**, *18*, 499.

[15] Gibson, H. D.; Scheraga, H. A. *Mol. Phys*. **1987**, *62*, 1247. Gibson, H. D.; Scheraga, H. A. *Mol. Phys*. **1986**, *64*, 641.

[16] Kundrot, C. E.; Ponder, J. W.; Richards, F. M. *J. Comput. Chem*. **1991**, *12*, 402.

[17] Perrot, G.; Cheng, B.; Gibson, K. D.; Vila, J.; Palmer, K. A.; Nayeem, A.; Maigret, B.; Scheraga, H. A. *J. Comput. Chem*. **1992**, *13*, 1.

[18] Pascual-Ahuir, J. L.; Silla, E. *J. Comput. Chem*. **1990**, *11*, 1047. Silla, E.; Tuñón, I.; Pascual-Ahuir, J. L. *J. Comput. Chem*. **1991**, *12*, 1077. Tuñón, I.; Silla, E.; Pascual-Ahuir, J. L. *Protein Eng*. **1992**, *5*, 715. Pascual-Ahuir, J. L.; Silla, E.; Tuñón, I. *J. Comput. Chem*. **1994**, *15*, 1127.

[19] A survey of atomic data can be found in www.webelements.com.

[20] Baldridge, K.; Klamt, A. *J. Chem. Phys*. **1997**, *106*, 6622.

[21] Truong, T. N.; Stefanovich, E. V. *Chem. Phys. Lett*. **1995**, *240*, 253.

[22] Barone, V.; Cossi, M. *J. Phys. Chem. A*. **1998**, *102*, 1995.

[23] López, X.; Bo, C.; Poblet, J. M. *J. Am. Chem. Soc.* **2002**, *124*, 12574.

[24] Lennard-Jones, J. E. *Proc. Roy. Soc*. **1924**, *106*, 463.

[25] Allen, M.; Tildesley, D. *Computer Simulation of Liquids*. Oxford, **1987**. Tosi, M. P. *Solid State Physics*. Vol 16, Springer, **1964**. Kittel, C. *Introduction to Solid State Physics*. Wiley, **1986**.

[26] Berendsen, H. J. C.; Grigera, J. R.; Straatsma, T. P. *J. Phys. Chem*. **1987**, *91*, 6269. Kusalik, P. G.; Svishev, I. M. *Science*, **1994**, *265*, 1219.

[27] Berendsen, H. J. C.; Postma, J. P. M.; van Guntseren, W. F.; DiNola, A.; Haak, J. *J. Chem. Phys*. **1984**, *81*, 3684.

[28] Vassilev, P.; Hartnig, C.; Koper, M. T. M.; Frechard, F.; van Santen, R. A. *Journal of Chemical Physics*. **2001**, *115*, 9815. Hartnig, C.; Koper, M. T. M. *Journal of Chemical Physics*. **2001**, *115*, 8540.

Conclusions

Compared to other fields, the application of quantum chemistry methods to polyoxoanions is in its initial stages. This may be because the theoretical treatment of these species has some intrinsic difficulties. POMs are, from a computational viewpoint, large molecules. In addition, because they are transition metal oxides, they are often highly charged anionic species that can exhibit open-shell electronic states. Since the pioneering work of Bénard on the decavanadate anion, published in the early 1990s, the continuous advances in computational power, the evolution of quantum chemistry software and the wide acceptance of DFT methods by the scientific community have enabled other topics and more sophisticated structures to be studied. The compilation of results in this book is proof that DFT has been skilfully applied to POMs.

The results presented in this thesis give definitive impetus to the study of POMs with first-principles methods. The fact that the work published in the last four years has been well accepted shows the quality of the conclusions and the information. All the work was aimed at complementing the experimental observations, providing additional data so that the physical basis of the behaviour of large metal-oxide molecular clusters could be fully understood.

For the theoretical study of medium-to-large molecules like POMs, the DFT method proved to be an excellent computational tool. It provided good geometries and reproduced experimental observations about the redox properties and basicity. The whole investigation focused on obtaining general rules of behaviour. Families of compounds with different addenda metals, heteroatoms, isomers and shapes made it possible to draw valuable conclusions that could be extrapolated to other systems. The principal conclusions about the systems studied are:

- **α/β-Keggin relative stability**. Changes in the addenda metal, M, and the internal atom, X, reveal that the energy of reduction is independent of X. It is a consequence of the constant HOMO-LUMO gap computed. The substitution of W by Mo decreases this magnitude by 0.8 eV at the DFT level, thus confirming that molybdates are more oxidant species. The β-Keggin forms are always more easily reducible than their α partners. In addition, the stability of the β form with

respect to α is a function of X. The clathrate-model proved to be useful for rationalising the larger oxidant character of the β frameworks.

- **Redox properties of mixed-addenda Keggin anions**. The oxidative character of SiM_3W_9 anions was found to be correlated with the physical nature of M. The localisation of the blue electrons is driven by the affinity of the various metal centres of the cluster, with V being the most willing to trap the first incoming electron, and Nb the least.

- **Basicity of the oxygens in SiM_3W_9 anions**. A relative basicity scale is proposed for the various oxo sites in Keggin anions. The proton affinity of the oxygens depends on the type and number of metals to which they are bonded. In general, bridging OM_2 sites are more basic than terminal M=O positions. On the other hand, oxygens bonded to V, Nb or Ti are much more basic than those linked to Mo or W.

- **Redox properties and α/β isomerism in Wells–Dawson anions**. The presence of non-equivalent metal centres in WD anions means that the electron affinity depends on the reduction site. The belt sites in these frameworks are the first to accept the blue electrons. The substitution of addenda metals in the least reducible sites by V inverts this trend and the blue electron is trapped in the cap sites. Unlike Keggin clusters, the α/β isomerism in WD does not greatly affect the oxidant power. This is because the HOMO-LUMO gap is nearly independent of the rotation of a capping triad.

- **Dimerisation reactions in Keggin clusters**. The study of reaction energy profiles for the dimerisation of substituted $PTiW_{11}$ and $SiNb_3W_9$ anions showed that protonation is the first step, and that the most accessible protonation site can be crucial if the dimerisation is to occur. This process is completed after an intermediate species forms, the energy of which determines the formation of the μ-O linkages. In the Ti-derivative, Ti=OH must be formed if the process is to be completed, whereas for the Nb-partner, the energies of the species Nb=OH and HO–Nb_2 is similar, and the two pathways studied are both plausible ways of forming the dimer.

- **Highly-reduced polyoxometalates**. DFT and *ab initio* preliminary results for the complex $[PMo_8V_4O_{40}(VO)_4]^{5-}$, with 10 metal electrons, show a highly stable repartition of 4 e^- over Mo and 6 e^- over V. The six V-electrons are antiferromagnetically coupled along the 8-membered ring of V centres. CASSCF calculations are in progress to confirm this result.

- **Solvent effects**. The introduction of the environment carried out by means of the COSMO model provides more realistic orbital energies and makes it possible to study reaction energies such as electron-transfer processes in POM clusters. Molecular dynamics provides a picture of the disposition of water molecules solvating a Keggin cluster, with a shell-shaped nature. Terminal oxygens are the most exposed and, therefore, they interact most with the solvent, whereas bridging oxo sites are water-free because they are more internal.

Perspectives

In spite of the current position of the first-principles study of POMs, the process has just begun and POM chemistry still offers considerable challenges. To date, most quantum chemical studies have considered anions in the gas phase, but POMs only exist in solution, or in the solid state stabilised by the field that is generated by the solvent molecules and counterions. This crude representation has provided invaluable information about the relative properties of POMs. But to determine absolute values —or to compare anions with different charges— we need to consider surrounding molecules. The environment of a POM needs to be properly described if we are to make progress in the modelling of such clusters.

POMs can be giant molecules. Some of them comprise more than 150 metal ions and about 500 oxygen atoms. The proper theoretical description of these nanostructures is another big challenge in the coming years. DFT-based methods have helped us to understand the electronic structure of POMs with paramagnetic ions, but for a rigorous analysis we need to use classical multiconfigurational *ab initio* methods that today can only be applied to the smallest structures like the Lindqvist $[M_6O_{19}]^{n-}$ or Anderson $[XM_6O_{24}]^{m-}$ anions.

In summary, the modelling of polyoxometalate chemistry will require contributions from specialists in a number of fields including molecular dynamics, multiconfigurational quantum chemistry methods and magnetism. The powerful computers of the 21st. century will permit accurate CASSCF or CASMP2 calculations in such large systems. This means that multi-determinantal wavefunctions may be used as a part of routine work.

Resum

La tesi que porta per títol "*Theoretical Study of the Basicity and the Redox Properties of Heteropolyanions*" està enfocada a oferir informació valuosa a la comunitat científica relacionada amb la química de coordinació amb metalls de transició en general, i particularment a experts en òxids metàl·lics d'elevada nuclearitat. Dades experimentals sobre polioxometal·lats (POMs) han estat disponibles des de fa més de 150 anys, quan Berzelius, Marignac i altres van començar a estudiar aquest nou camp de la química. Des de llavors, molts compostos tipus POM han estat caracteritzats. Aquesta família de molècules és atractiva pels científics des d'un punt de vista acadèmic però també han demostrat tenir propietats amb un gran valor afegit, que han estat explotades en aplicacions tecnològiques. Per exemple, els POMs poden associar-se selectivament a espècies iòniques i catalitzar certes reaccions orgàniques; també són agents blanquejadors de la polpa de fusta respectuosos amb el medi ambient, funcionen com a membranes, sensors, etc. En el futur, podrien ser aplicats amb èxit en medecina ja que estan sent *testats* com a agents antivirals. La llista de possibles aplicacions és interminable. Sigui com sigui, molts grups estan treballant per l'aprofitament de les propietats d'aquests òxids metàl·lics. Per tant, un coneixement acurat de les propietats fonamentals dels POMs és necessari si es pretén el desenvolupament de noves tecnologies.

Els químics teòrics van iniciar la seva contribució fa poques dècades amb l'ús rutinari dels ordinadors. Quan vaig començar aquesta tesi doctoral el 1999, els estudis teòrics de primers principis sobre POMs eren realment escassos. Estaven limitats a alguns treballs publicats principalment pels grups d'en Marc Bénard, Serguei A. Borshch i Josep M. Poblet. Tot i així, ells van establir les bases per futures investigacions en aquest camp. La tesi aquí presentada és un recull del treball realitzat durant els darrers quatre anys sobre les propietats generals de dos heteropolianions: els anions de Keggin i de Wells–Dawson i alguns dels seus derivats. El desenvolupament de programes de càlcul cada cop més eficients, juntament amb el creixement del poder de càlcul dels ordinadors, ha permès que la química computacional jugui un paper destacat en la ciència. Com sempre ha estat, la precisió de les mesures de laboratori està limitada dels instruments utilitzats. Per això val a dir que la informació facilitada pels càlculs d'alt nivell és essencial si es vol tenir una idea completa d'un problema químic. En l'actualitat, les dades facilitades pels químics teòrics poden corroborar o

explicar observacions experimentals. L'objectiu final de la química computacional és tenir un paper predictiu real.

De tota manera, el tractament teòric dels POMs és encara en la seva etapa inicial, probablement per les dificultats intrínseques associades al càlcul d'aquestes espècies. Elles són, des del punt de vista computacional, molècules grans. A més, degut a que són òxids de metalls de transició, acostumen a ser anions altament carregats amb, de vegades, estats electrònics de capa oberta. Des del treball pioner de Bénard sobre l'anió decavanadat, publicat a principis dels anys 90, els avenços en el poder de càlcul, el desenvolupament del *software* i l'acceptació general de la teoria del funcional de la densitat (DFT) per la comunitat científica han facilitat l'estudi de compostos de major complexitat. Els resultats recopilats aquí són una prova de que el DFT es pot aplicar amb èxit a l'estudi dels POMs. Per l'estudi teòric de molècules mitjanes a grans, el mètode DFT és una eina excel·lent. En general, dóna bones geometries i reprodueix les observacions experimentals sobre la química redox i les propietats de basicitat. Tot el treball ha estat enfocat a donar pautes generals de comportament. Han estat estudiades famílies de compostos amb diferents metalls perifèrics (anomenats *addenda*), metalls centrals (heteroàtoms), isòmers i estructures, de manera que s'han traçat conclusions valuoses i extrapolables a altres sistemes no estudiats. Les conclusions principals del treball són les següents:

- **Estabilitat relativa dels isòmers α/β-Keggin**. Els canvis en els *addenda*, M, i en l'àtom intern, X, han mostrat que l'energia de reducció és independent d'X. Això és una conseqüència del *gap* HOMO-LUMO calculat invariable. La substitució de tungstens per molibdens redueix aquesta diferència en 0.8 eV a nivell DFT, confirmant que els molibdats són espècies més oxidants. Les formes β-Keggin són sempre més fàcilment reduïbles que els seus homòlegs α. A més, l'estabilitat de la forma β respecte a l'α és una funció d'X. El model de clatrat va demostrar ser útil per racionalitzar el major caràcter oxidant de les estructures β.

- **Propietats redox dels anions Keggin amb metalls mesclats**. Es va trobar correlació entre el caràcter oxidant dels anions SiM_3W_9 i la naturalesa física d'M. La localització dels electrons metàl·lics (electrons *blue*) es veu afectada per l'afinitat dels diversos centres

metàl·lics del cluster, essent el V el més predisposat a retenir un primer electró extern, i el Nb el que menys.

- **Basicitat dels oxígens en anions SiM_3W_9**. S'ha proposat una escala de basicitats relatives per diverses posicions oxo en anions de Keggin. L'afinitat dels oxígens pels un protons depèn del tipus i nombre de metalls als quals els primers estan connectats. En general, posicions OM_2 pont són més bàsiques que les terminal M=O. Per altra banda, els oxígens enllaçats a V, Nb o Ti són molt més bàsics que els units a Mo o W.

- **Propietats redox i isomeria α/β en anions Wells–Dawson**. La presència de centres metàl·lics no equivalents en anions WD implica que l'afinitat electrònica depèn del lloc de reducció. Les posicions del *belt* en aquests esquelets són les primeres en acceptar els electrons *blue*. La substitució en les posicions menys afins als electrons de metalls addenda per V inverteix aquesta tendència i l'electró és atrapat a una posició del *cap*. Contràriament a les observacions en anions Keggin, la isomeria α/β en WD no afecta notablement el poder oxidant. Això és degut a que el *gap* HOMO-LUMO és pràcticament independent de la rotació d'una triada en la regió del *cap*.

- **Reaccions de dimerització en clusters Keggin**. L'estudi de perfils energètics de reacció per la dimerització d'anions substituïs com $PTiW_{11}$ i $SiNb_3W_9$ ha mostrat que la protonació és el primer pas, i que el lloc de protonació més accessible pot ser crucial per que es doni la dimerització. Aquest procés té lloc després de la formació d'una espècie intermèdia, l'energia de la qual determina la formació de les unions μ-O. En el derivat de Ti, el compost Ti=OH ha de formar-se de forma preferent per completar-se el procés, mentre que pel derivat de Nb, les energies de les espècies Nb=OH i HO–Nb_2 són similars, i els camins de reacció són ambdós plausibles per formar el dimer.

- **Polioxometal·lats altament reduïts**. Els resultats preliminars DFT i *ab initio* per al complex $[PMo_8V_4O_{40}(VO)_4]^{5-}$, amb 10 electrons metàl·lics, mostren una repartició molt estable amb 4 e^- sobre els Mo i 6 sobre els V. Els sis e^- metàl·lics presenten un acoblament

antiferromagnètic al llarg de l'anell de 8 vanadis. Càlculs CASSCF estan en progrés per confirmar aquest resultat.

- **Efectes del dissolvent**. La introducció de l'entorn duta a terme mitjançant el model COSMO dóna energies orbitals més realistes i fa possible estudiar energies de reacció com processos de transferència electrònica en POMs. La dinàmica molecular dóna una idea de la disposició de les molècules d'aigua solvatant un anió de Keggin, amb una naturalesa en capes. Els oxígens terminals són els més exposats i, per tant, són els que més fortament interaccionen amb el dissolvent, mentre que els oxígens pont són lliures d'aigües ja que són més interns.

Publications in journals

Articles directly related to this thesis

"Electronic properties of polyoxometalates: a DFT study of α/β-$[XM_{12}O_{40}]^{n-}$ relative stability (M = W, Mo and X a main group element)".
López, X.; Maestre, J. M.; Bo, C.; Poblet, J. M. *J. Am. Chem. Soc.* **2001**, *123*, 9571–9576.

"Electronic properties of polyoxometalates: electron and proton affinity of mixed-addenda Keggin and Wells–Dawson anions".
López, X.; Bo, C.; Poblet, J. M. *J. Am. Chem. Soc.* **2002**, *124,* 12574–12582.

"Relative Stability in α- and β-Wells–Dawson Heteropolyanions: A DFT Study of $[P_2M_{18}O_{62}]^{n-}$ (M = W and Mo) and $[P_2W_{15}V_3O_{62}]^{n-}$".
López, X.; Bo, C.; Poblet, J. M.; Sarasa, J. P. *Inorg. Chem*. **2003**, *42*, 2634–2638.

"Ab initio and DFT Modelling of Complex Materials: Towards the Understanding of Electronic and Magnetic Properties of Polyoxometalates".
Poblet, J. M.; López, X.; Bo, C. *Chem. Soc. Rev.* **2003**, *32*, 297.

"The First Isolated Active Titanium Peroxo Complex: Synthesis, Characterization and Theoretical Study".
Kholdeeva, O. A.; Arapova, T. A.; Maksimovskaya, R. I.; Golovin, A. V.; Neiwert, W. A.; Kolesov, B. A.; López, X.; Poblet, J. M. *submitted to publication.*

Other articles published

"Electronic and magnetic properties of α-Keggin anions: a DFT study of $[XM_{12}O_{40}]^{n-}$, (M = W, Mo; X = Al^{III}, Si^{IV}, P^{V}, Fe^{III}, Co^{II}, Co^{III}) and $[SiM_{11}VO_{40}]^{m-}$ (M = Mo and W)".
Maestre, J. M.; López, X.; Bo, C.; Poblet, J. M.; Casañ-Pastor, N. *J. Am. Chem. Soc.* **2001**, *123*, 3749–3758.

"A DFT study of the electronic spectrum of the α-Keggin anion $[Co^{II}W_{12}O_{40}]^{6-}$".
Maestre, J. M.; López, X.; Bo, C.; Daul, C.; Poblet, J. M. *Inorg. Chem.* **2002**, *41*, 1883–1888.

Agraïments

Al llarg de tot el camí recorregut durant els darrers quatre anys he rebut el recolzament de molta gent, tant moralment com a nivell de coneixements. És ben cert que l'un sense l'altre no són res, per això agraeixo els meus familiars i amics que m'han donat ànims constantment. Tanmateix, per formar-me com a químic, m'han acompanyat com a directors de la tesi en Josep Maria Poblet i en Carles Bo, dels que sempre he rebut un tracte immillorable i amb qui he après com es realitza un treball científic des de la concepció de la idea primitiva fins a la publicació d'un article. A la resta dels *seniors* de la planta 4, gràcies sense excepció ja que de tots he après. Menció especial mereix en José C. Ortiz, tècnic informàtic i *master* de la maquinària computacional del grup. Gràcies com no al Joan Iglesias, programador del C-Lab i co-*master* de tota la part informàtica.

El meu agraïment més especial és per a tots els companys de la planta 5. Als que han passat pel meu grup: Jordi Muñoz, José Gracia, Josep Maria Campanera, Elías Daura, Joan Miquel Maestre, Susanna Romo i Jorge Fernández. També als de les 'superfícies': Daniel Curulla, Alfred Gil, Paco Ample i Ana Valcárcel. Els 'post-HF', Esther Bordas, Isabel Gómez, Jesús Cabrero, Elena Rodríguez, Coen de Graaf, Engelbert Sans, David Taratiel i Núria Queralt. Gràcies pel companyerisme i bon ambient.

Durant la meva estada a l'Institut Le Bel de Strasbourg vaig rebre un tracte molt hospitalari per part dels doctors M. Bénard i M-M. Rohmer, així com de la resta del grup. A això li hem d'afegir les profitoses converses sobre temes molt diversos (especialment amb en Julien i en Gaétan). Part del capítol 6 d'aquesta tesi, corresponent a un treball en vies de preparació, ha comptat amb la inestimable aportació del Dr. I. A. Weinstock sobre els mecanismes de dimerització dels Keggin. Vull destacar també el treball realitzat pel Dr. C. Hartnig, qui va dur a terme els càlculs de dinàmica molecular. Gràcies a la Dra. O. Kholdeeva, amb la qual hem realitzat un treball conjunt sobre peròxids de titani, a en J. F. Paul i al Dr. José P. Sarasa, col·laborador habitual en els nostres treballs.

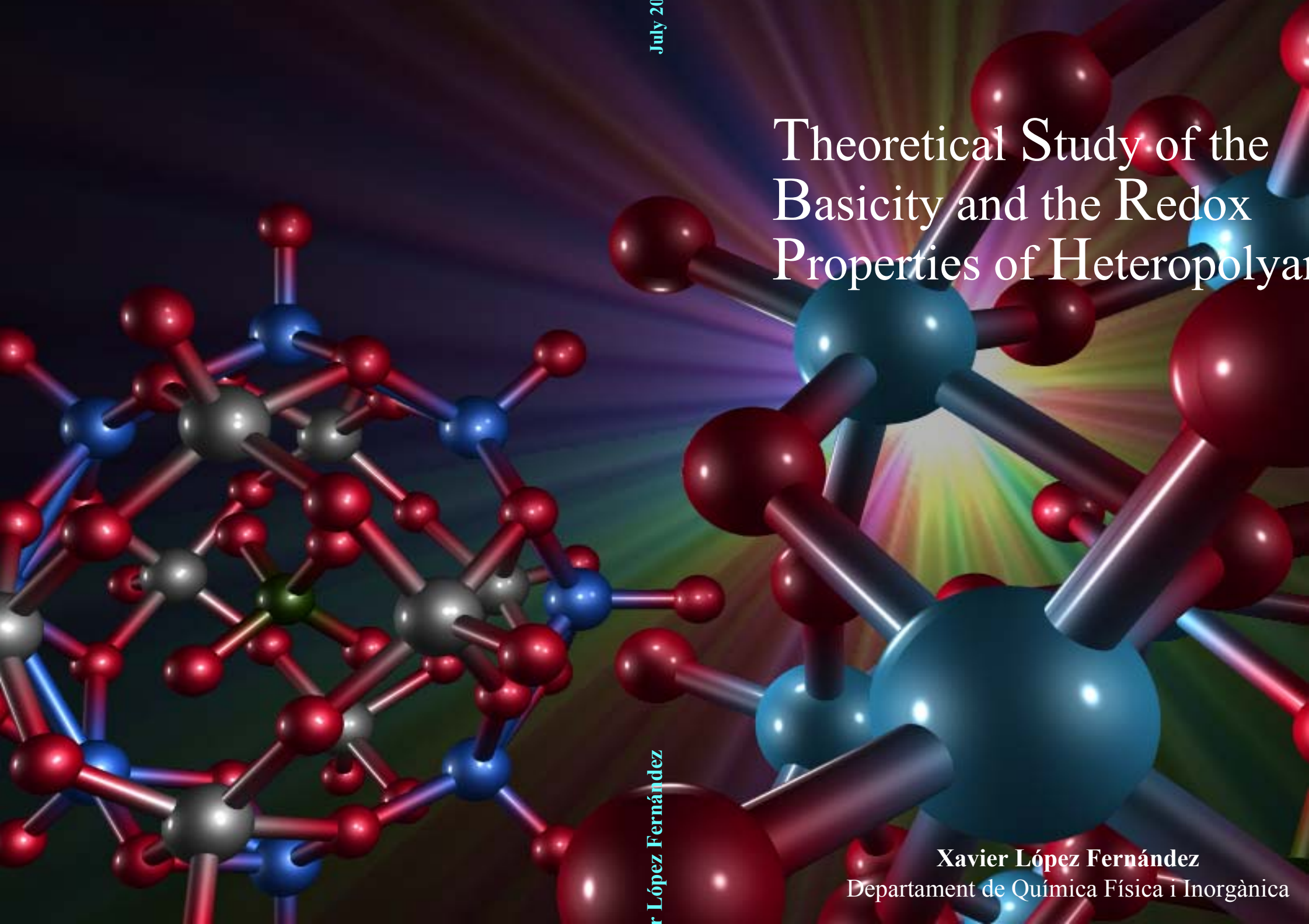

Theoretical Study of the Basicity and the Redox Properties of Heteropolyan

Xavier López Fernández
Departament de Química Física i Inorgànica

July 20

r López Fernández

CHAPTER 7

Highly-reduced Polyoxometalates: Study of $[PMo_8V_4O_{40}(VO)_4]^{5-}$

In the present chapter, a preliminary DFT/*ab initio* study to characterise the electronic structure of the 10e$^-$-reduced $[PMo_8V_4O_{40}(VO)_4]^{5-}$ cluster (**1**) is reported. This molecule may be viewed as a Keggin-like $[PMo_8V_4O_{40}]$ structure capped by four VO units. In mixed V/Mo clusters it is accepted that the first reductions occur at the V^{5+} ions. This behaviour was found in the 8e$^-$-reduced bicapped cluster $[PMo_{12}O_{40}(VO)_2]^{5-}$ for which DFT calculations showed that each V has formally an oxidation state of +4, whereas the 12 Mo atoms share 6 electrons. Here we show that this principle is not fully accomplished when the number of V^{5+} centres increases. On the other hand, highly reduced clusters can present several configurations close in energy. In these circumstances, monoconfigurational methods like DFT or HF only give an approximate representation of the wave function and multi-reference SCF techniques are, in general, needed for an accurate treatment of the electron correlation. Part of this work was performed during a stay of three months at the Louis Pasteur University (Strasbourg) in the group of Dr. Marc Bénard.

7.1. Introduction

Mixed-addenda capped Keggin anions

Modified cluster structures belonging to the family of POMs enrich and broaden the scope of this field. Several strategies are driven to alter the traditional characteristics of these inorganic systems. One of them incorporates capping units. It consists in the addition of M_xO_y units to the surface of a given POM cluster. Multiple capped clusters have been synthesised and characterised during the last ten years. Let us point out that these systems are restricted to compounds containing Mo, V and As atoms. A benchmark bicapped anion was characterised by Hill and co-workers in the middle 1990's,[1] composed of molybdenum and vanadium addenda atoms (Figure 7.1), with formula $[PMo_{12}O_{40}(VO)_2]^{5-}$. The special electronic features of this anion were analysed with the DFT methodology by Maestre *et al*.[2] Other derivatives were reported with similar molecular composition, with capping V or Mo units.[3-12] Some of them are not only capped structures but also substituted in the parent POM core. Novel capped clusters containing V and Ge centres were reported by Whitfield *et al*. in 2003.[13] $[Ge_4V_{16}O_{42}(OH)_4]^{8-}$ constitutes the first example of Ge_2O_7 capping units incorporated to vanadate derivatives based on the Keggin anion.

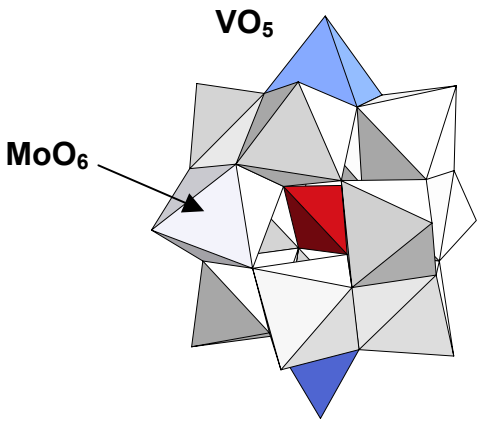

Figure 7.1. Bicapped phosphomolybdate Keggin anion obtained by Hill's group. The apical groups (blue pyramids) are, formally, VO_5 units.

As a new V-capped molybdate Keggin anion, Xu *et al*. reported the synthesis of the first polyanion with a tetra-capped Keggin structure in 1999.[14] This species consists of a $[PMo_8V_4O_{40}]^{7-}$ mixed-addenda cluster in which, formally, four additional VO^{3+} units are added to the external core. The four VO^{3+} capping units hold a charge of +12, which converts the parent oxidised $PMo_8V_4O_{40}$ cluster into the $[PMo_8V_8O_{44}]^{5+}$ cation. The resulting compound is indeed a $10e^-$-reduced molecule with a net charge of −5. More recently, the same group published a related compound with similar electronic structure[8] and, in 2003, Yuan *et al*. reported three novel V-capped Keggin derivatives with paramagnetic metal complexes attached to the surface of the cluster.[15] Perhaps, the most important feature of those clusters is that they are found in highly reduced forms.

The structure reported for **1** may be viewed as a V_8 equatorial ring plus two polar units made of 4 Mo atoms each. Notice in Figure 7.2 that all Mo atoms are equivalent whereas there are two different vanadium types, four pseudo-octahedrally coordinated and four in a square-pyramidal environment, that are labelled as V_o and V_p from now on, respectively. These V centres are alternatively disposed in the V_8-ring, like V_o-V_p-V_o-... Of course, all Mo centres have pseudo-octahedral environments.

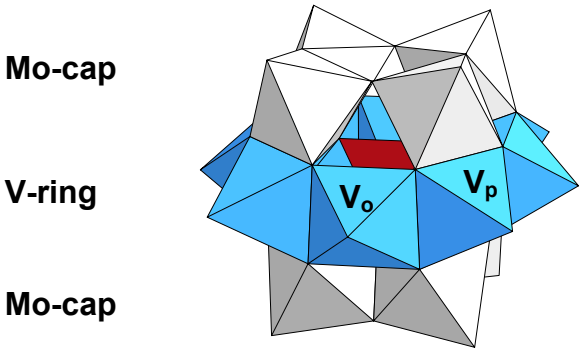

Figure 7.2. Polyhedral representation of the $[PMo_8V_4O_{40}(VO)_4]^{5-}$ anion, **1**. This viewpoint permits to see the equatorial ring of 8 alternating Vo-Vp vanadiums (see text for details), as well as the two polar molybdenum caps. The overall symmetry of the cluster is D_{2h}.

In general, it is difficult to unequivocally characterise the number and nature of the reduced centres in a partly reduced cluster and today this is still

a matter of debate.[16] Electrochemical reductions and EPR spectroscopy have usually been used to determine the localisation, or delocalisation, of the metal electrons in reduced HPAs. For example, Hervé and co-workers[17] found in electrochemical reductions on XMo_2VW_9 and $XMoV_2W_9$ anions (X = P, Si) that the V centres are commonly reduced in first place. However, in $PMoV_2W_9$, the authors assigned the first reduction process to $Mo^{VI} \rightarrow Mo^{V}$. In this line of thought, Xu *et al.*,[14] from X-ray diffraction and EPR spectra analysis, claimed that the electronic structure for **1** corresponds to the 10 metal electrons delocalised over the whole system. In fact, after valence sum calculations they attributed oxidation states to Mo and V metal atoms of the structure, thus concluding that all vanadium atoms have an oxidation state of +4. This means that the 8 Mo ions should share two electrons. With the analysis of **1** we pursue two objectives: to rationalise reduced mixed-addenda Mo/V derivatives[2,18] and to progress in the understanding of capped clusters.[1-2]

7.2. Study of the Electronic Structure

7.2.1. Structure of $[PMo_8V_4O_{40}(VO)_4]^{5-}$

The local geometry is, thus, slightly different between V_o and V_p centres. Apart of the coordination number, the degree of pyramidalisation is also different. Figure 7.3 shows geometrical parameters of both units computed as taking part in Xu's molecule at the DFT level. The rest of the parameters are similar to those of the uncapped Keggin partner.

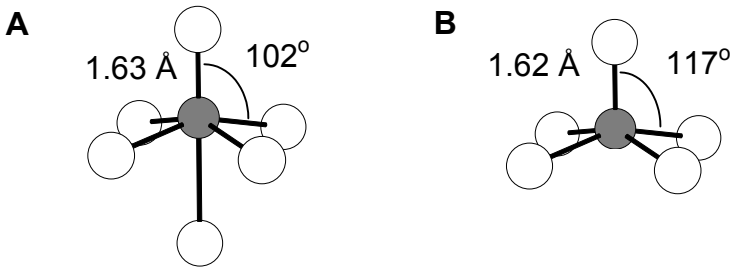

Figure 7.3. Geometric parameters computed for the pseudo-octahedral VO_6 (A) and pyramidal VO_5 (B) units.

7.2.2. Computational details

DFT calculations were carried out with the same computational strategy described in chapter 2. We utilised triple-ζ + polarisation basis functions and the BP86 functional commonly employed in our work within the scope of the LDA formalism. In addition, HF calculations were conducted to complement the DFT analysis. The Gaussian 98 program[19] was used. Double-ζ basis functions of the type LANL2DZ[20] with effective core potentials describe vanadium and molybdenum atoms. For the purpose of *ab initio* calculations, DFT-optimised structures were utilised and single point runs performed. The main goal of the HF calculations presented here is to get a set of molecular orbitals, in which the exact exchange is included, although the electrons are described by a poorer wavefunction. HF results are a starting point for further improvement of the wavefunction by means of multi-reference calculations.

Electronic configurations

In the most stable closed-shell configuration for **1**, the two lowest metal orbitals are delocalised over Mo atoms. The next three doubly occupied MOs are d_{xy}-like combinations of V orbitals (Figure 7.4). This will be the reference configuration in the present discussion.

Figure 7.5-A shows orbital $26b_1$, which has a non-bonding character. The bridging Mo–O–Mo oxo sites have no contribution to this orbital because they lie in a node. Orbital 26 a_2 is almost degenerate to 26 b_1 and has the same nature. Orbital 36 a_1 (part B of the figure) shows slightly antibonding d(V)-p(O) interactions, and lies above in energy despite that the all the d_{xy} orbitals of vanadiums are in phase. Orbitals of this nature accommodate six metal electrons. It is worth noting that V_o and V_p share the 6 upper electrons nearly in the same fashion. An analysis of the contributions to each of the 4 highest molecular orbitals occupied, leads to 71% Mo for 26 a_2, 73% Mo for 26 b_1, whereas for 36 a_1 we find 33% V_p + 33% V_o. The HOMO is formed by 27% V_o + 29% V_p. Despite their different coordination to O^{2-}, they are chemically very similar, and metallic electrons are delocalised over vanadiums irrespective of their type. The first empty orbitals, the LUMO and LUMO+1, are formed by 75% of V_o and 73% V_p, respectively. The first relevant result in this study is that Mo atoms share 4 electrons, instead of 2 as the experimental data suggest.

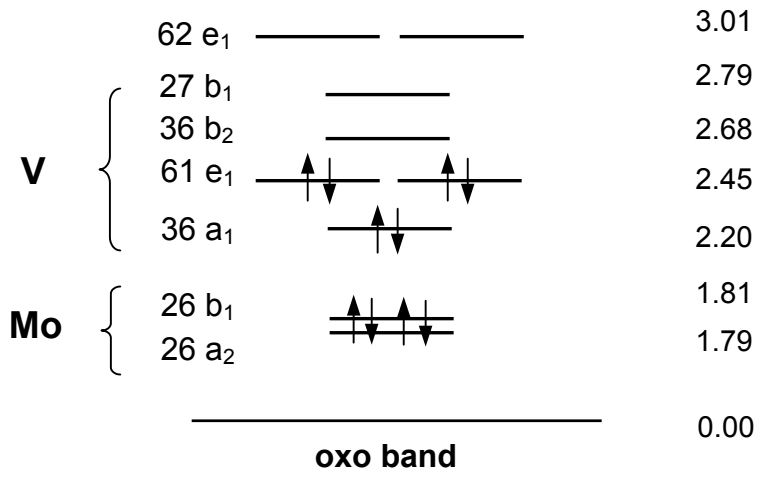

Figure 7.4. Closed-shell configuration (**C1**) for $[PMo_8V_4O_{40}(VO)_4]^{5-}$. Four electrons are localised on Mo atoms, whereas vanadium centres share the other six. Relative orbital energies are in eV.

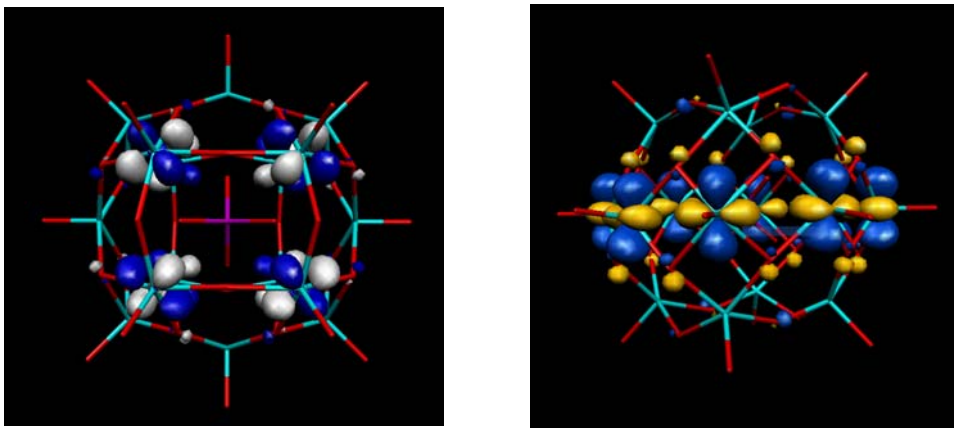

Figure 7.5. (A) Representation, perpendicular to the V-ring, of the doubly occupied 26 b_1 metal orbital, delocalised over the Mo atoms. (B) View of orbital 36 a_1 in the plane containing the vanadiums.

The promotion of two electrons from the 26 b_1 and 26 a_2 orbitals to 36 b_2 vanadium orbital requires 2.2 eV. This high energy clearly excludes the electron distribution ($2e^-$ Mo/ 8 e^- V) proposed by Xu *et al*.[14] The general assumption that in a mixed Mo/V anion the Mo ions are only reduced after all V ions have at least one electron[17] is not always accomplished as present DFT calculations strongly suggest.

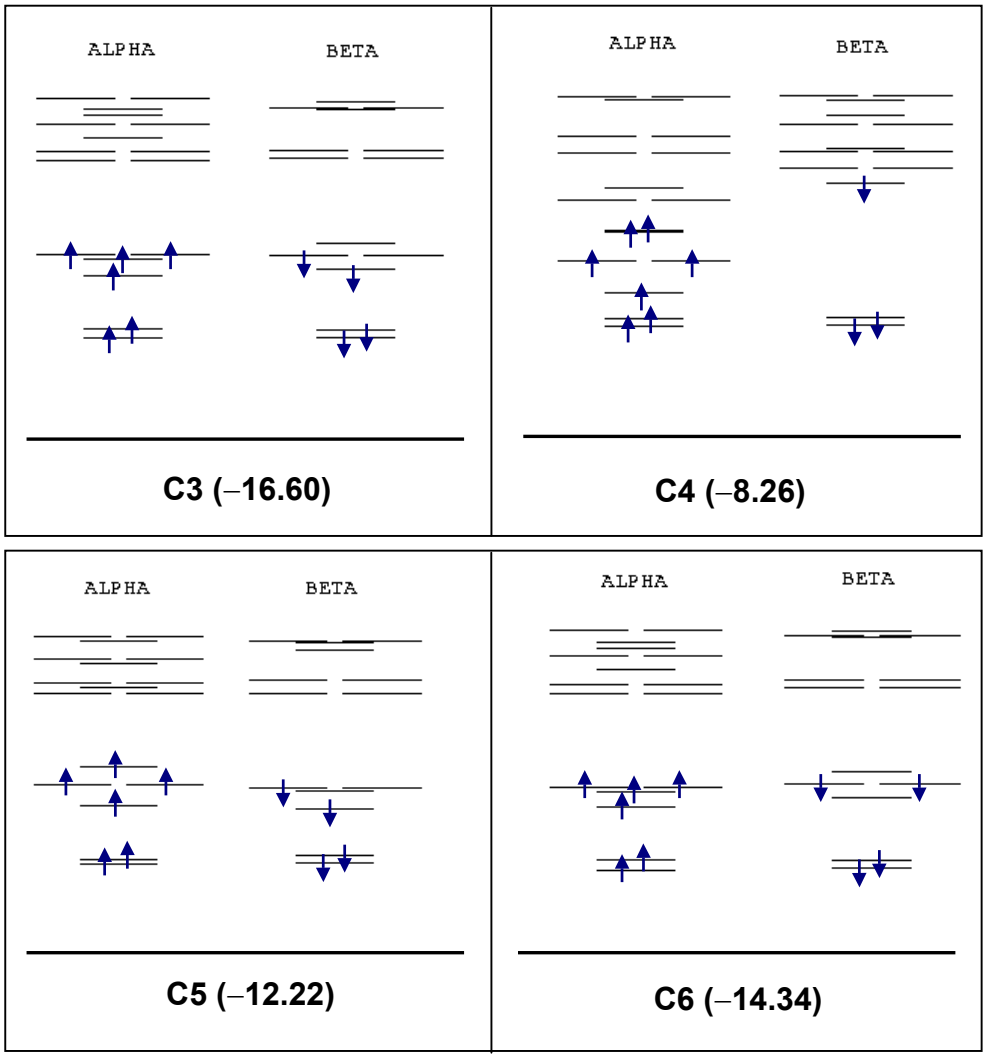

Figure 7.6. DFT-computed electronic configurations **C3**-**C6** and relative energies (referred to that of **C1**), in kcal mol^{-1}. Thick lines represent the O^{2-} band.

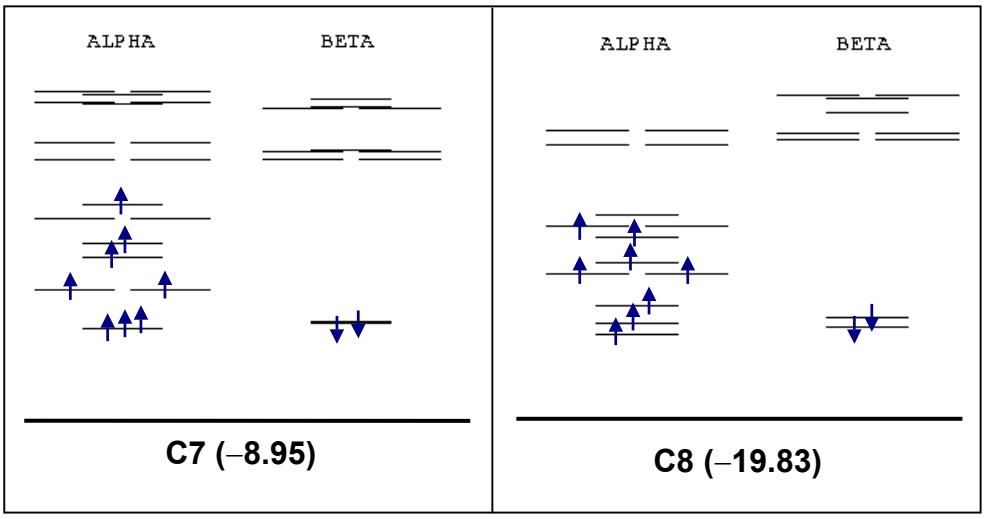

Figure 7.6. Continued. Configurations **C7** and **C8**.

Another important question concerns the six vanadium electrons. Is the ground configuration actually a closed-shell? Or has the compound any kind of magnetic behaviour? Unfortunately, we are not able to give a definitive answer to this question, yet. When orbitals are nearly degenerate, the monoconfigurational treatment always favours the high-spin state. Consequently, the high-spin C8 configuration (Figure 7.6) was found to be the most stable at the DFT level, with relative energy of –19.8 kcal mol^{-1} with respect the closed-shell C1 configuration. The spin polarisation of the septuplet showed that the 6 unpaired electrons are fully localised on the V_8-ring (0.88 e and 0.79 e on each V_o and V_p, respectively). As the figure shows, the stability of the configurations increases with the number of unpaired electrons. Some of the cases calculated could present Jahn–Teller distortion. However, the reader can take for granted that it would be very small.[21] Calculations were also performed at HF level yielding similar results with the septuplet state (C8) as the most stable one.

Various singlet open-shell configurations were also studied. Within the framework of the DFT, a Broken-symmetry solution[22] might be calculated since it can evenly reproduce electron couplings of this type. Some authors made use of this approach in binuclear complexes and in polyoxometalates.[23-24] The most stable singlet open-shell calculation

corresponds to a distribution of three alpha spin electrons localised on the four V_o centres, and the beta partners at V_p ions as shown in Figure 7.7. This solution was computed to be 0.32 eV above the septuplet. The Mulliken population analysis indicates a spin polarisation of 0.80 alpha and 0.77 beta electrons over V_o and V_p, respectively. It was shown that cluster **1** was EPR silent, and therefore it was assumed to be diamagnetic. Present Broken-symmetry calculations prove that an antiferromagnetic coupling of metal electrons would explain the lack of EPR signal mentioned by experimentalists.[14] Nevertheless, it would be desirable that the open-shell state be lower in energy than the septuplet state.

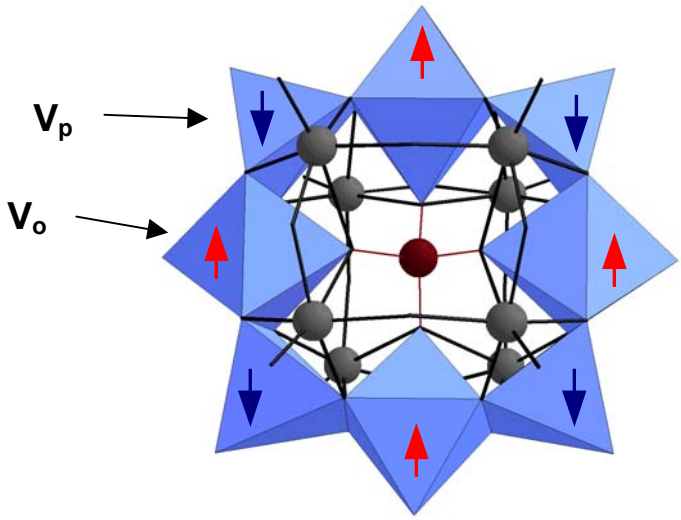

Figure 7.7. Schematic view showing the antiparallel coupling (coloured arrows) of the electrons in a singlet open-shell calculation. They are localised over the V-ring (blue polyhedra). Grey spheres represent molybdenum centres.

Figure 7.8 shows the nature of the V-centred metallic orbitals where the 6 electrons are located. Both V_o and V_p sites contribute to the same molecular orbital but the spatial parts describing the α and β electrons are separated.

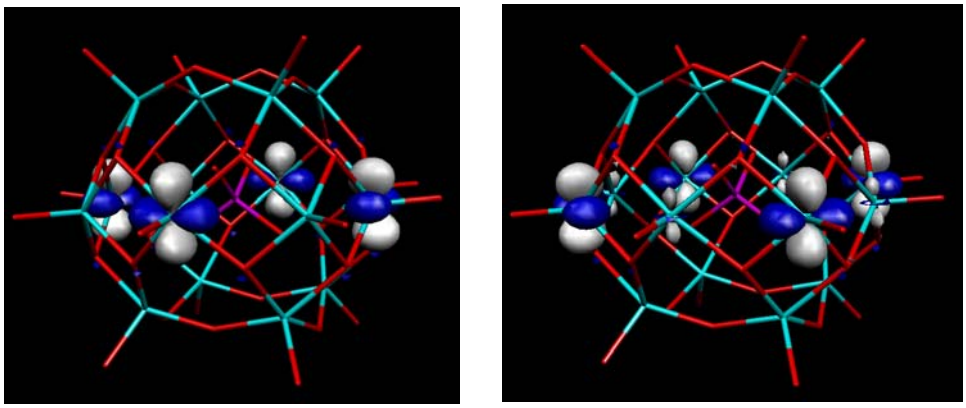

Figure 7.8. Doubly-occupied molecular orbital localised in the V-ring computed with Unrestricted DFT formalism. The left-hand picture corresponds to the spin-α, and the right-hand one to spin-β. The pseudo-octahedral V-sites (V_o) and the pyramidal positions (V_p) do not share the spatial part of this MO.

To fully determine the ground state for this system, it is necessary to carry out a multi-reference calculation for including non-dynamical (or *static*) electron correlation to the wavefunction. With the collaboration of Dr. Coen de Graaf, a *Complete Active Space SCF* (CASSCF) calculation is under way. The active space will include the 8 lowest lying virtual orbitals and the 3 highest occupied orbitals of the closed-shell RHF run. This set of MOs contains the 6 metal electrons located on vanadiums. This calculation requires an enormous computational effort and represents a great challenge. For example, the storage of molecular orbital integrals needs more than 160 Gbytes. Nevertheless, if this test succeeds, new doors will be open to the study of magnetism in POMs, going further than the use of model fragments to represent the whole molecule.[25]

References and Notes

[1] Chen, Q.; Hill, C. L. *Inorg. Chem*. **1996**, *35*, 2403.

[2] Maestre, J. M.; Poblet, J. M.; Bo, C.; Casañ-Pastor, N.; Gómez-Romero, P. *Inorg. Chem*. **1998**, *37*, 3444.

[3] Khan, M. I.; Zubieta, J. *Inorg. Chim. Acta*. **1992**, *193*, 17.

[4] Xu, Y.; Xu, J. Q.; Yang, G. Y.; Wang, T. G. Xing, Y.; Lin, Y. H.; Jia, H. Q. *Polyhedron*. **1998**, *17*, 2441.

[5] Dolbecq, A.; Cadot, E.; Eisner, D.; Sécheresse, F. *Inorg. Chem*. **1999**, *38*, 4217.

[6] Luan, G. Y.; Li, Y. G.; Wang, E. B.; Han, Z. B. *Inorg. Chem. Commun*. **2001**, *4*, 632.

[7] Müller, A. *Z. Anorg. Allg. Chem*. **1994**, *620*, 599.

[8] Xu, Y.; Zhu, D-R.; Guo, Z-J.; Shi, Y-J.; Zhang, K-L.; You, X-Z. *J. Chem. Soc., Dalton Trans*. **2001**, 772.

[9] Huang, G. Q.; Zhang, S. W.; Wei, Y. G.; Shao, M. C. *Polyhedron*. **1993**, *12*, 1483.

[10] Khan, M. I.; Chen, Q.; Zubieta, J. *Inorg. Chim. Acta*. **1993**, *212*, 199.

[11] Khan, M. I.; Chen, Q.; Zubieta, J. *Inorg. Chem*. **1993**, *32*, 2924.

[12] Müller, A.; Beugholt, C.; Kögerler, P.; Bögge, H.; Bud'ko, S.; Luban, M. *Inorg. Chem*. **2000**, *39*, 5176.

[13] Whitfield, T.; Wang, X.; Jacobson, A. J. *Inorg. Chem*. **2003**, *42*, 3728.

[14] Xu, Y.; Zhu, H-G.; Cai, H.; You, X-Z. *Chem. Commun*. **1999**, 787.

[15] Yuan, M.; Li, Y.; Wang, E.; Tian, C.; Wang, L.; Hu, C.; Hu, N.; Jia, H. *Inorg. Chem*. **2003**, *42*, 3670.

[16] Poblet, J. M.; López, X.; Bo, C. *Chem. Soc. Rev*. **2003**, *32*, 297.

[17] Cadot, E.; Fournier, M.; Tézé, A.; Hervé, G. *Inorg. Chem*. **1996**, *35*, 282.

[18] López, X.; Bo, C.; Poblet, J. M. *J. Am. Chem. Soc.*, **2002**, *124*, 12574.

[19] Frisch, M. J.; Trucks, G. W.; Schlegel, H. B.; Scuseria, G. E.; Robb, M. A.; Cheeseman, J. R.; Zakrzewski, J. A.; Montgomery, J. A.; Stratman, R. E.; Burant, J. C.; Dapprich, S.;

Millam, J. M.; Daniels, A. D.; Kudin, K. N.; Strain, M. C.; Farkas, O.; Tomasi, J.; Barone, V.; Cossi, M.; Cammi, R.; Mennucci, B.; Pomelli, C.; Adamo, C.; Clifford, S.; Ochterski, J.; Petersson, G. A.; Ayala, P. Y.; Cui, Q.; Morokuma, K.; Malick, D. K.; Rabuck, A. D.; Raghavachari, K.; Foresman, J. B.; Cioslowski, J.; Ortiz, J. V.; Stefanov, B. B.; Liu, G.; Liashenko, A.; Piskorz, P.; Komaromi, I.; Gomperts, R.; Martin, R. L.; Fox, D. J.; Keith, T.; Al-Laham, M. A.; Peng, C. Y.; Nanayakkara, A.; González, C.; Challacombe, M.; Gill, P. M. W.; Johnson, B. G.; Chen, W.; Wong, M. W.; Andres, J. L.; Head-Gordon, M.; Replogle, E. S.; Pople, J. A. *Gaussian 98*. Gaussian, Inc. Pittsburgh, PA, **1998**.

[20] Dunning/Huzinaga full double-ζ functions for oxygen: Dunning, Jr., T. H.; Hay, P. J. *Modern Theoretical Chemistry*, *Vol. 3*. Schaefer III, H. F., ed. Plenum, New York, **1976**. Heavy atoms described by Los Alamos ECP plus double-ζ: Hay, P. J.; Wadt, W. R. *J. Chem. Phys*. **1985**, *82*, 270. Wadt, W. R.; Hay, P. J. *J. Chem. Phys*. **1985**, *82*, 284. Hay, P. J.; Wadt, W. R. *J. Chem. Phys*. **1985**, *82*, 299.

[21] López, X.; Maestre, J. M.; Bo, C.; Poblet, J. M. *J. Am. Chem. Soc.*, **2001**, *123,* 9571.

[22] Noodleman, L. J. *Chem. Phys*. **1981**, *74*, 5737. Noodleman, L.; Davidson, E: R. *Chem. Phys*. **1986**, *109*, 131. Noodleman, L.; Case, D. A. *Adv. Inorg. Chem*. **1992**, *38*, 423. Noodleman, L.; Pen, C. Y.; Case, D. A. Mouesca, J. M. *Coord. Chem. R*ev. **1995**, *144*, 199.

[23] Ruiz, E.; Cano, J.; Alvarez, S.; Alemany, P. *J.Comput.Chem.* **1999**, *20,* 1391. Ruiz, E.; Alemany, P.; Alvarez, S.; Cano, J.; *J. Am. Chem. Soc.* **1997**, *119*, 1297. Ruiz, E.; Alemany, P.; Alvarez, S.; Cano, J.; *Inorg. Chem.* **1997**, *36*, 3683. Ruiz, E.; Alemany, P.; Alvarez, S.; *Chem. Commun.* **1998**, 2767. Cano, J.; Ruiz, E.; Alemany, P.; Lloret, F; Alvarez, S. *J. Chem. Soc. Dalton Trans*. **1999**, 1669. Cano, J.; Alemany, P.; Alvarez,, S.; Verdaguer, M.; Ruiz, E. *Chem. Eur. J.* **1998**, *4*, 476. Ruiz, E.; Cano, J.; Alvarez,, S.; Alemany, P. *J. Am. Chem. Soc.* **1998**, *120*, 11122.

[24] Duclusaud, H.; Borshch, S. A. *J. Am. Chem. Soc*. **2001**, *123*, 2825.

[25] Suaud, N.; Gaita-Ariño, A.; Clemente-Juan, J. M.; Sánchez-Marín, J.; Coronado, E. *J. Am. Chem. Soc.* **2002**, *124*, 15134.

UNIVERSITAT ROVIRA I VIRGILI

Theoretical Study of the Basicity and the Redox Properties of Heteropolyanions

Xavier López Fernández

Departament de Química Física i Inorgànica

Memòria presentada per optar al títol de Doctor en Química

El Dr. Josep Maria Poblet Rius, Catedràtic de Química Física, i el Dr. Carles Bo Jané, Professor Titular de Química Física del Departament de Química Física i Inorgànica de la Universitat Rovira i Virgili

Fem constar que la present memòria, que porta per títol:

"**Theoretical Study of the Basicity and the Redox Properties of Heteropolyanions**",

ha estat realitzada sota la nostra direcció al Departament de Química Física i Inorgànica de la Universitat Rovira i Virgili pel llicenciat en química Xavier López Fernández per obtenir el grau de Doctor en Química.

Tarragona, 10 de Juliol de 2003

Dr. Josep Maria Poblet Rius Dr. Carles Bo Jané

Preface

This thesis aims to provide valuable information to the community concerned with transition-metal coordination chemistry in general, and high nuclearity molecular metal oxides in particular. Experimental data on polyoxometalates (POMs) has been available for more than 150 years, when Berzelius, Marignac and others first started to study this new field in chemistry. Since then, countless POM compounds have been characterised. This family of molecules is appealing for scientists from an academic point of view but they have also proved to have some very interesting value-adding features that can be used for technological purposes. For example, they can selectively encapsulate ionic species and catalyse many organic reactions and they are environmentally-friendly wood pulp bleachers, membranes, sensors, etc. In the future, they may be successfully applied to medicine because they are now being tested as antiviral agents. The list of possible applications is endless. Be that as it may, many groups are working to exploit the properties of these metal oxides. Therefore, accurate knowledge of the fundamental properties of POMs is required if experimentalists are to develop new technologies.

Theoretical chemists started to make a contribution just a few decades ago with the routine use of computers. When I began this PhD. thesis in 1999, first-principles theoretical studies on POMs were really scarce. They were limited to a few articles published by the groups of Marc Bénard, Serguei A. Borshch and Josep M. Poblet. Nevertheless, they laid the basis for further investigation in the field of POMs. This book, entitled "*Theoretical Study of the Basicity and the Redox Properties of Heteropolyanions*", summarises the work I have done in the last four years on the general properties of the two title clusters. The development of increasingly efficient software, together with the increasing power of computers, enables computational chemists to play an important role in science. Nowadays, the accuracy of some calculations depends on the instruments used in the laboratory. It goes without saying that the information provided by high-performance calculations is essential if we are to have the complete picture of a chemical problem. For the time being, the data provided by theoreticians can corroborate or explain experimental observations. The ultimate goal of computational chemistry is to have a true predictive role.

This thesis is structured in two main parts. Part I introduced the work. Chapter 1 is an overview to the field of polyoxometalates and provides basic information about their structure and principal properties. Chapter 2 deals with the first-principles method of calculation used throughout this work, the density functional theory. It also describes the fundamentals of the methodology, computational details and some useful analytical tools. The last chapter in this section discusses the theoretical studies that have been made on POMs to date. Part II presents and discusses the results arising from this PhD, and is structured in five chapters. The first two describe the electronic properties and the α/β-isomerism of single-addenda clusters. They also discuss the redox properties of their mixed-addenda partners. The third block (chapter 6) deals with the basicity of the oxygen atoms in these anions and the study of the dimerisation reaction in some Keggin clusters. Chapter 7 is a study of a mixed-metal Mo/V cluster which was found to have special electronic properties. Finally, chapter 8 discusses two methodologies applied in the field of computational chemistry. They are aimed at including the effects of the environment to molecules.

While working on this PhD. thesis —some parts in collaboration with other groups— I have had six articles published in international journals or recently accepted for publication. Three manuscripts are in preparation.

Tarragona, July 2003

Table of Contents

PART II. RESULTS

A la meva família i amics

Nothing exists but atoms and empty space. All the rest are opinions

No existeix res més que àtoms i espai buit. La resta són opinions

Demokritos

CHAPTER 3

Overview to the Theoretical Studies on Polyoxometalates

During the last ten years, a few theoretical groups settled the basis for a new viewpoint in the understanding of polyoxometalates' characteristics. The aim of computational chemistry applied to such molecules is to give explanations to partially unknown phenomena, as well as general guidelines of behaviour. Computational chemistry has proven to be a powerful tool to the analysis of chemical systems. Various techniques have been developed and successfully applied to study systems ranging from small molecules to extended solids. In this chapter we summarise the quantum chemistry studies carried out by several groups before and during the realisation of this thesis. Here, we discuss in brief the most significant results obtained by means of the *ab initio* and the density-functional theory formulations. The acceptance of these works amongst the experimental community is growing and, for the time being, the information obtained by means of computational and *traditional* chemistry complements each other.

3.1. Introduction

Computational Transition Metal Chemistry has reached its maturity, basically due to the widespread acceptance of methods based on the density functional theory (DFT). In the 1970's, the *ab initio* Hartree–Fock (HF) approximation provided a reasonable starting point for studying small- to medium-sized organic molecules and for understanding reaction mechanisms involving small organic molecules. Later, Møller–Plesset perturbation theory, configuration interaction, coupled cluster theory and other methods provided a more quantitative description. For transition metals, the error in HF methods, the so-called *correlation energy*, is generally too large. Part of the correlation energy can be introduced using DFT methods. These give reliable structures and bonding energies with only moderate computational effort. Many organometallic and polynuclear structures have been described using DFT.[1] However, the number of high-level computational studies on POMs can be considered still quite low. A combination of three factors —the large size of polyoxoanions, the presence of transition metal ions and the high negative charge— produce, in practice, important computational limitations. In the last ten years, a few groups have been especially active and have made important progress in describing and rationalising the electronic and magnetic properties of POMs. The first studies by Marc Bénard were performed at the HF level. Later investigations preferentially used density functional methods, as implemented in the ADF set of programs.[2] Even though, some extended-Hückel calculations were carried out applied to heteropolyanions, as well.[3-5] In this chapter we review the most significant theoretical studies in the field of POMs. To do this, we stress more on the results achieved and less on the methods used. This chapter is based on a recently published review performed by our group in the context of the present thesis.[6]

This chapter is divided into two main parts. In section 3.2 we summarise works released previous to the beginning of the present PhD. work in 1999. Section 3.3 contains publications dating from that year to present except those published by the author of this thesis, which are discussed in chapters of Part II.

3.2. Previous Theoretical Studies

Relative basicity of the oxo sites in $V_{10}O_{28}$

Heteropoly acids are considered to be significantly stronger than typical inorganic acids such as H_2SO_4, HNO_3, HCl, etc. The negative charge of HPAs, which are larger than inorganic acids, is delocalised among a large number of oxygen sites, so the electrostatic interactions between the proton and the anion are weaker. In general, heteropolytungstates are more acidic than molybdates, whereas the effect of the heteroatom is less important. The order of acid strength for some heteropoly acids is $H_3PW_{12}O_{40}$ > $H_4SiW_{12}O_{40}$ > $H_4GeW_{12}O_{40}$ > $H_6P_2W_{16}O_{62}$ and $H_3PW_{12}O_{40}$ > $H_3PMo_{12}O_{40}$. Davis and co-workers[7] evaluated the acidity of $H_3PW_{12}O_{40}$ > $H_3PMo_{12}O_{40}$ by calculating the proton affinity from the process $H_3PM_{12}O_{40} \rightarrow H_2PM_{12}O_{40}^- + H^+$. The protons in $H_3PM_{12}O_{40}$ were placed at bridging positions far away from one another. The cluster energies were computed after the complete optimisation of the diprotonated and triprotonated species. The value of 1126 kJ mol^{-1} for the third bridging site in the phosphomolybdate was 38 kJ mol^{-1} larger than the proton affinity found for the tungstate. These results are fully consistent with the larger acidity of tungstates.

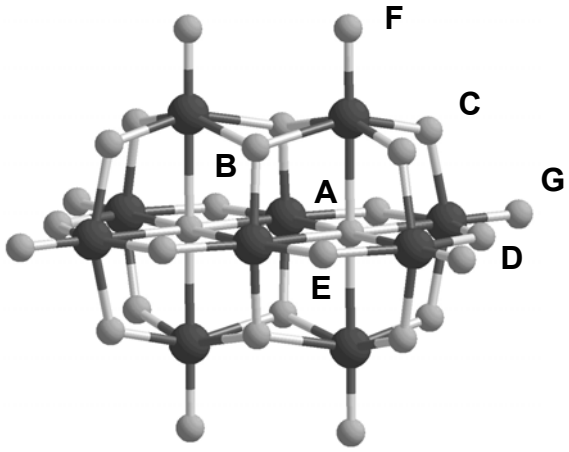

Figure 3.1. Spatial representation for $[V_{10}O_{28}]^{6-}$. The decavanadate anion has six distinct oxygen sites: one OV_3 (B), three OV_2 (C, D and E) and two OV (F, G).

The first attempt to classify the basicity of the various oxygen sites in a POM was reported by Bénard and co-workers at the beginning of the 1990's.[8] The decavanadate ion $[V_{10}O_{28}]^{6-}$ offered an excellent opportunity to compare the basicity of terminal (OV), double-bridging (OV_2) and triple-bridging (OV_3) oxygen sites in the same molecule. ^{17}O NMR spectroscopy for protonated and unprotonated species suggested that sites B and C (Figure 3.1) were the preferred protonation sites. This was confirmed by the crystallographic characterisation of the dimeric species $[H_3V_{10}O_{28}]^{6-}$. At that time, directly determining the protonation energy for a relatively large molecule like decavanadate was unaffordable and Bénard's group discussed the local basicity of a particular site by computing the distribution of Molecular Electrostatic Potentials. Electrophilic species tend to minimise their potential energy by approaching a minimum MESP value as much as possible. The EP distribution computed for the 26 external oxygen sites characterised 20 local minima, which were identified as probable protonation sites. The deepest ones were associated with the four triple-bridging oxygen sites B. Double bridging oxygens C and D were found at relative depths of 10 and 23 kcal mol^{-1}, respectively. According to this MESP distribution, the proton fixation preferentially takes place at the triple coordinated oxygens. The second preferred site is C and the protonation at O(term) is completely unexpected since the deepest minima in the vicinity of a terminal site appeared more than 55 kcal mol^{-1} above the minimum close to site B.

From *ab initio* calculations on fully optimised $M_2W_4O_{19}^{4-}$ (M = Nb and V) Lindqvist anions, Maestre *et al.*[9] determined the relative basicity of the external oxygens by means of three methods. On the one hand, protonation energies were computed for all oxo sites of the cluster and, on the other hand, atomic charges with Bader's population analysis[10] as well as the MESP distribution. The results agree with experimental observations since the deepest minimum of the electrostatic potential distribution is located near the OM_2 oxo site whereas terminal oxygens are the least basic.

Inclusion complexes and host-guest interactions

In a series of papers, Bénard's group analysed the electronic properties of inclusion complexes such as $RCN\subset(V_{10}O_{32})^{4-}$ and electronically inverse systems in which negatively charged species are encapsulated into negatively charged anions. These studies[11-12] have recently been reviewed at

length.[13] Figure 3.2 shows an inclusion complex characterised by the penetration of a nitrile in the hemisphere of a dodecavanadate anion.[14] For the acetonitrile complex, the experimental distance between the nitrile nitrogen and the plane that contains the four vanadium atoms at the bottom of the POM is 2.22 Å. The host-guest interaction between the two subunits remains in solution. The HF stabilisation energies for three R–CN guest molecules (R = H, CH_3 and C_6H_5) were found to have similar energies ranging from –12.8 to –14.4 kcal mol^{-1}.

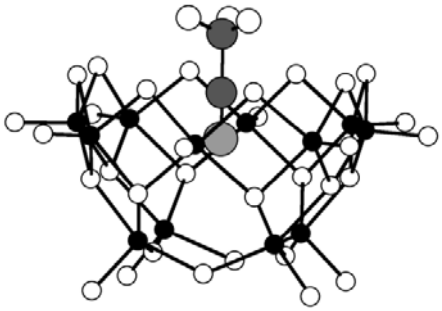

Figure 3.2. The inclusion complex $CH_3CN\subset[V_{12}O_{33}]^{4-}$. The black spheres represent metal atoms

A first analysis of the interaction between the host and guest molecules can be obtained from the MESP distributions of the two separate units. The MESP distribution for the $[V_{12}O_{32}]^{4-}$ cavity showed a saddle point that connects two regions of low potential, one in the bottom of the anion and the other more external. The upper minimum and the saddle point generate a dipolar moment that opposes that of the isolated guest nitrile. The weak stabilising interaction between N_2 and the host vanadate (–5 kcal mol^{-1}) emphasises the importance of a permanent dipole moment in the guest molecule. By superposing the MESP distributions for the host and guest subsystems, the potential minimum facing the N atom in C_6H_5CN coincided exactly with the saddle point in the host cavity. This means that the bonding between the two units follows a *lock* and *key* mechanism in which, as well as the coupling between the two opposing dipole moments, there is an electrostatic interaction between the nitrogen lone pair and the electrophilic region inside the cage. The absence of both a permanent dipole moment and

a lone pair makes C_2H_2 strongly repulsive toward the $[V_{12}O_{32}]^{4-}$ cavity, since its interaction energy was found to be +10.6 kcal mol^{-1}.

By decomposing the stabilisation energy using the CSOV method,[15] the bonding in the two observed inclusion complexes $RCN\subset(V_{10}O_{32})^{4-}$ (R = CH_3 and C_6H_5) and the model system $HCN\subset(V_{10}O_{32})^{4-}$ could be compared. For HCN and CH_3CN, the Steric term, which contains the Pauli repulsion and the Coulombic attraction, is dominated by the attractive interaction between host and guest units (–5.3 kcal mol^{-1} for R = H and –3.7 kcal mol^{-1} for R = CH_3). When the size of R increases, the Pauli repulsion between the substituent R and the anion increases and the Steric term becomes slightly positive (+1.8 kcal mol^{-1}). On the other hand, the guest polarisation and the charge transfer terms are larger for R = C_6H_5, which generally produces similar interaction energies for the three substituents.

Stabilising fields generated by counterions

Highly negative species like POMs only exist in condensed phases, where the external field generated by the solvent molecules or the counterions stabilise the anion. The instability of an *isolated* polyanion is manifested in the high energy of all its molecular orbitals.

Bénard[13] proposed the following procedure to incorporate the effect of the crystal field in quantum chemistry calculations of polyoxoanions:

1. Model the surrounding crystal by a set of point charges that can be determined from a Mulliken partition or from similar procedures.
2. Determine the electrostatic potential generated at the centre of the polyanion by the point charges contained in successive shells of ions until convergence.
3. Define a uniformly charged sphere of 20 Å in diameter, centred on the target anion and with a charge that is fitted to reproduce the potential obtained in the previous step.
4. Carry out a new quantum chemistry calculation with the presence of the charged sphere.

Using this procedure the stabilisation of guest anions inside negatively charged cages was analysed. Typical examples of these electronically inverse host-guest complexes are $Cl@[H_4V_{18}O_{42}]^{9-}$ and $Cl@[V_7O_{12}(O_3PR)_6]^{2-}$, clusters, in which a halogen is encapsulated by the

two anionic cages $[H_4V_{18}O_{42}]^{8-}$ and $[V_7O_{12}(O_3PR)_6]^-$. In agreement with the high negative charge of $[H_4V_{18}O_{42}]^{8-}$, the electrostatic potential at the centre of the cage is –0.57 a.u. This value means that the encapsulation of a negative charge has an associated electrostatic repulsion of +358 kcal mol^{-1}, which makes the encapsulation process of the *isolated* cage non-viable. For the non-protonated model complex $[V_{18}O_{42}]^{12-}$, the electrostatic potential is still more negative and reaches the value of –1 a. u. (–627 kcal mol^{-1}). In the less charged cage $[V_7O_{12}(O_3PR)_6]^-$, the potential at the centre of the cavity is positive (+0.06 a.u.) and therefore attractive towards a negative charge. These results for the electrostatic potential of the isolated cage can explain the formation of the $Cl@[V_7O_{12}(O_3PR)_6]^{2-}$ complex but do not allow us to rationalise the encapsulation of a halogen by a highly charged hollow cage like $[H_4V_{18}O_{42}]^{8-}$. Clearly, the crystal field is needed to achieve the stability of the encapsulation cluster. Bénard and co-workers estimated the lattice potential for $Cs_9(Cl@H_4V_{18}O_{42})$ and showed that it is *positive* at the centre of the cavity, thus overcoming the negative potential generated by the anionic host. An ample review of this subject can be found in reference 13.

One of the most important limitations when determining the lattice field is the disorder in many of the crystals that contain a polyoxoanion. The crystal structure for the salt $(Et_3H)_5(PMo_{12}O_{40}(VO)_2)$ was well solved and the potential due to the crystal could be estimated. The anion $[PMo_{12}O_{40}(VO)_2]^{5-}$ has 8 metal electrons and, unlike an oxidised cluster, this highly reduced system does not need a negative charge to complete the valence shell of oxo ligands. The $[PMo_{12}O_{40}(VO)_2]$ framework, with two VO units capping a Keggin structure, has a high tendency to be negatively charged, even at the gas phase. The total energy of the cluster exhibits a minimum when the net charge of the anion is –2 and –3. These values correspond to a number of 5 and 6 metal electrons over the metal ions, respectively. This means that the $Mo_{12}V_2$ cage has a high propensity to be negatively charged. However, the isolated cage cannot reproduce the optimal number of metal electrons in the cluster (8). The counterions generate a stabilising field (+0.393 a.u. on the central phosphorous) that increases the intrinsic tendency of the cluster to accept electrons: eight are accommodated on the d-metal orbitals.

Electronic structure of $[PMo_{12}O_{40}(VO)_2]^{5-}$

Maestre *et al*. performed DFT calculations on the Keggin-based bicapped $[PMo_{12}O_{40}(VO)_2]^{5-}$ anion.[16] This was synthesised by Hill and co-workers (Figure 3.3).[17] Such a cluster is 8 metallic electrons, and they are distributed between Mo centres and V capping units. Particularity, the two VO's are located at the positions. In this system, a competition between a singlet and a triplet state occurs.[18] The theoretical method utilised to obtain the correct ground state configuration was the Broken-Symmetry approach.[19] From experiments and DFT results it was concluded that each VO fragment has one unpaired electron, and that they are weakly ferromagnetically coupled. The singlet state was computed to be very close in energy, 0.77 kcal mol^{-1} above the ground state triplet state.

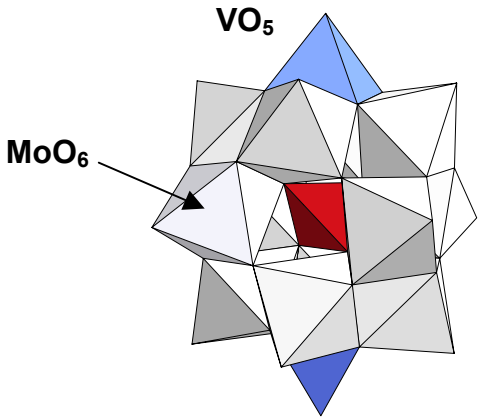

Figure 3.3. Polyhedral view of the $PMo_{12}(VO)_2$ anion, based on a bicapped Keggin framework.

3.3. More Recent Studies

Electronic structure and bonding in fully oxidised POMs

The most representative POM is the Keggin heteropolyanion (HPA), the formula of which is $[XM_{12}O_{40}]^{n-}$, where M is usually W^{6+} or Mo^{6+} and X, the *heteroatom*, is a main group or transition metal ion (P^{V}, Si^{IV}, Al^{III}, Ge^{IV}, Fe^{III}, Co^{II}, Co^{III}, Cu^{I}, Cu^{II}, etc.). The Keggin anion is made of an assembly

of twelve MO_6 octahedrons sharing their corners or edges with a central XO_4 tetrahedron (Figure 3.4). The metal–oxygen bonds in such a framework can be divided into three sets according to whether their oxygen atoms are tetrahedral (tetra), bridging (brid) or terminal (term). There is a fourth M–O bond type between the heteroatom and O(tetra). We will also use the notation O_m, where *m* indicates the number of ions bonded to the oxygen, throughout the text where it is convenient to do so. In the α-isomer, all metal centres are equivalent and the symmetry of the molecule is T_d. Marignac discovered a second isomer, today known as beta and with idealised C_{3v} symmetry. This differs from the α form in that there is a 60º rotation of one of the four edge-sharing M_3O_{13} triads. The common partial reduction of the *addenda* or *peripheral* M centres yields the intensely coloured "heteropoly blues". This term is normally used for reduced polyanions irrespective of their true colour.

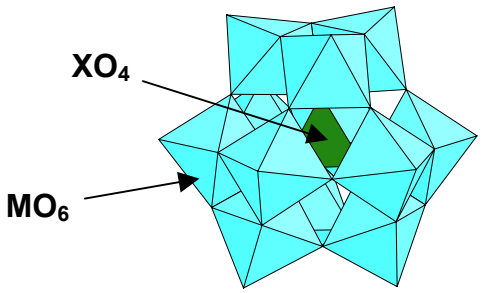

Figure 3.4. Polyhedral representation for an α-$[XM_{12}O_{40}]^{n-}$ Keggin anion. Blue octahedra are MO_6 units and the green tetrahedron contains the XO_4 unit.

Throughout this text we will use an abbreviated notation without oxygen atoms, charge or brackets, e.g., PW_{12} for $[PW_{12}O_{40}]^{3-}$ and $PW_{12}1e$ for $[PW_{12}O_{40}]^{4-}$, where *n*e identifies the number of electrons in the metal orbitals, or *blue* electrons. For clusters with paramagnetic ions, the explicit oxidation state of the heteroatom is given: $Co^{II}W_{12}1e$ represents a heteropolyblue with one delocalised electron among the twelve tungstens and the central cobalt ion in the oxidation state of +2.

In general, DFT calculations reproduce the geometry of HPAs very well. The exception is the M=O(term) bond lengths, which are systematically longer than the experimental ones. A systematic comparison of the theoretical and experimental geometries for several HPAs shows that

the deviation in the M=O(term) bond in Keggin and WD structures is on average 0.05 Å using the BP86 functional (Table 3.1). This discrepancy between the X-ray and the computed geometries is somewhat smaller (~0.03 Å) in isopolyanions such as $[M_6O_{19}]^{2-}$ (M = Mo and W),[20] and $[W_{10}O_{32}]^{4-}$ [21] using local functionals. For the highly charged Lindqvist anions $[Nb_6O_{19}]^{8-}$ and $[Ta_6O_{19}]^{8-}$, the experimental geometries are less well reproduced[20], probably because the crystal field effects are great and are not taken into account in these calculations.

Table 3.1. Comparison of theoretical (BP86/TZP) and X-ray (averaged values) distances (in Å) for a series of heteropolytungstates.

(a)		PW_{12}	SiW_{12}	AlW_{12}	$Co^{III}W_{12}$	$Co^{II}W_{12}$	$Fe^{III}W_{12}$
$X–O_n$	*DFT*	1.574	1.667	1.796	1.821	1.896	1.823
	Expt	1.53	1.64	1.74	1.79	1.90	1.82
X–W	*DFT*	3.579	3.532	3.526	3.565	3.547	3.567
	Expt	3.49	–	3.51	–	3.49	3.53
$W–O_1$	*DFT*	1.727	1.743	1.763	1.771	1.784	1.773
	Expt	1.69	1.71	1.71	1.71	1.71	1.72
$W–O_2$	*DFT*	1.932	1.916	1.930	1.943	1.946	1.944
		1.936	1.937	1.955	1.968	1.978	1.968
	Expt	1.90–1.91	–	1.90–1.96	1.85–1.97	1.88–1.99	1.88–1.96
$W–O_4$	*DFT*	2.424	2.325	2.242	2.265	2.203	2.263
	Expt	2.43	2.35	2.26	–	2.16	–

a) In $W–O_n$, *n* means the number of metal atoms coordinated to the oxygen atom.

In absence of paramagnetic ions, HPAs in general, and Keggin anions in particular, have a *simple* electronic structure in which the doubly occupied orbitals, formally delocalised over the oxo ligands, and the unoccupied set of d-metal orbitals are perfectly separated. In fully oxidised Keggin anions, the latter are symmetry-adapted d-metal orbitals with some antibonding participation of oxygen orbitals,

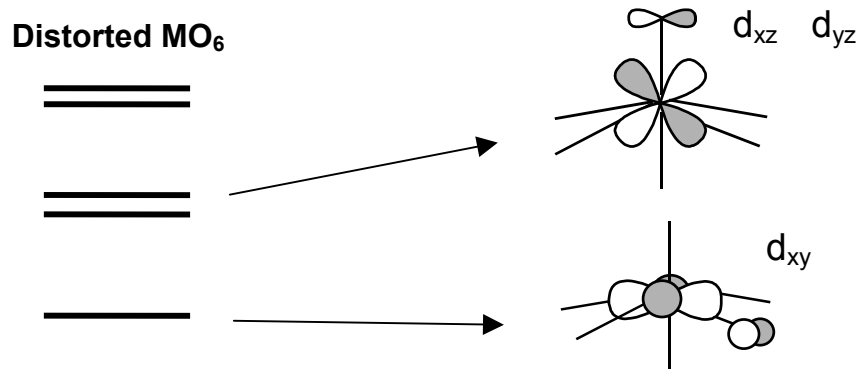

Due to the high oxidation state of metals in POMs, the t_{2g}-like orbitals are the most interesting in these clusters. Provided the MO_6 octahedra are distorted from the ideal O_h symmetry in Keggin anions, the d_{xy}, d_{xz} and d_{yz} orbitals are differently destabilised depending on how effective the antibonding interactions are with neighbouring p-oxygen orbitals. This overlap is more important between d_{xz} and d_{yz} with O(term) because the M=O bond lengths are shorter and the orientations are more favourable. Consequently, the LUMO in POMs are always symmetry-adapted combinations of d_{xy}-like orbitals. A 3D representation of one of the e symmetry components of both the degenerated HOMO and LUMO is given in Figure 3.5.

The energy gap between the occupied and the unoccupied band in Keggin anions without paramagnetic ions has been proven to be independent of X. Using the BP86 functional and a TZP-quality basis set for tungstates, Maestre *et al.* found a constant H-L gap of ~2.8 eV for different X.[22] At the same level of theory, this value decreases to 2 eV for molybdates. There is a direct relationship between the energy of the LUMO and the oxidising power of the POM. Therefore, the lesser energy of the lowest d-metal orbitals in molybdates means that they can generally be more easily reduced than tungstates to produce heteropoly blues. For example, it is well established that $SiMo_{12}$ and $GeMo_{12}$ are more powerful oxidising agents than the homologous tungstates by ~0.5 V. We frequently use the terms *band of unoccupied orbitals* and *oxo band*. It is worth noting though that these sets of orbitals do not form a band in the strict sense, since the orbitals are separated by discrete energies, at least for the relatively small clusters discussed here.

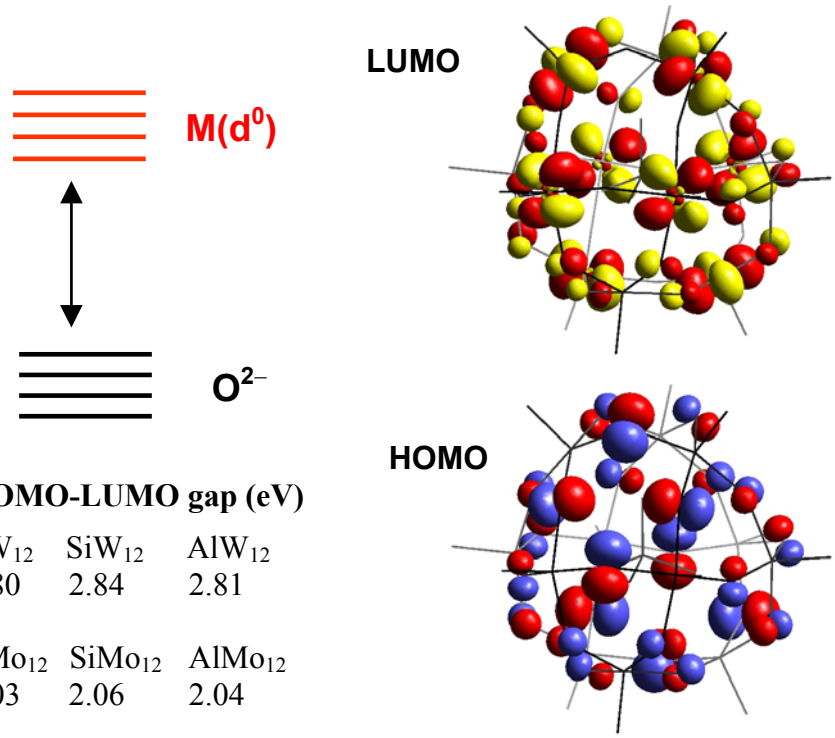

Figure 3.5. Molecular orbitals scheme for an α-Keggin anion. The separation between the M and O^{2-} bands represents the H-L gap, listed for a series of X and M. In $[SiW_{12}O_{40}]^{4-}$ the HOMO is composed in a 95% of p-oxygen orbitals whereas the LUMO has a 73% of d-metal orbitals. 3D-representations of one e component for each MO are showed.

Structure and bonding in single-addenda anions

Bridgeman and Cavigliasso described the nature of the occupied orbitals and bonding in several polyanions.[20-21,23-28] In a recent work, three sets of molecular energy levels were identified in $[M_6O_{19}]^{n-}$ Lindqvist structures: the low-lying orbitals basically composed of nonbonding combinations of s oxygen orbitals, the high-lying set composed of nonbonding combinations of p oxygen orbitals and an intermediate set that corresponds to M–O bonding interactions of essentially M(d)–O(p) character.[20] The gap between the s- and p-oxygen orbital sets is ~10 eV. An equivalent band structure was found for $[W_{10}O_{32}]^{4-}$ [21] and other isopolyanions. In $[TeM_6O_{24}]^{6-}$ and

$[PM_{12}O_{40}]^{3-}$ there is an additional level associated with the heteroatom that lies between the s and p oxo band (~7 eV above the s band). Delocalised σ and π bonds along the interpenetrating M–O closed loops are considered to be a structural-stability factor of a polyanion. For the $[W_{10}O_{32}]$ framework, for instance, two types of closed loops can be considered: the twelve-member W_6O_6 rings that are built along the *axial* direction and the eight-member W_4O_4 rings that lie in the *equatorial* planes.

A measure of the relative bonding capacity and strength of the distinct oxo ligands in an isopolyanion can be obtained through the formation process of a M_xO_y cluster as:

$$[M_xO_{y-1}]^{(n-2)-} + O^{2-} \rightarrow [M_xO_y]^{n-}$$

The average bonding energies (ΔE_B) for terminal, bridging and central oxygen atoms in Lindqvist structures showed that the loss of an O^{2-} ligand in $[M_6O_{19}]^{2-}$ to give the neutral cluster M_6O_{18} is highly endothermic (21–23 eV). These energies presumably would be different in solution since the O^{2-} anion is very unstable in the gas phase.

Table 3.2. Bond Lengths and Mayer Bond Order Indexes for $[M_6O_{19}]^{n-}$ Isopolyanions.[a)]

Molecule	M–O_6			M–O_2			M–O_1		
	LDA	*Expt.*	*B.O.*[a]	*LDA*	*Expt.*	*B.O.*[a]	*LDA*	*Expt.*	*B.O.*[a]
$[Mo_6O_{19}]^{2-}$	2.32	2.32	0.19	1.93	1.92	0.74	1.71	1.68	1.64
$[W_6O_{19}]^{2-}$	2.34	2.33	0.18	1.94	1.92	0.77	1.73	1.69	1.73
$[Nb_6O_{19}]^{8-}$	2.44	2.38	0.30	2.01	2.01	0.77	1.88	1.77	1.51
$[Ta_6O_{19}]^{8-}$	2.44	2.38	0.25	2.02	1.99	0.77	1.90	1.80	1.53

a) Mayer Bond order index.

It is interesting, however, to note the similarities in ΔE_B for the bridging and terminal sites, which show that bonding contributions for these two sites are similar even though they have different bond orders according to the Mayer bond order index[29] (Table 3.2). ΔE_B is somewhat smaller for the central oxygen. We can also see this trend in $[W_{10}O_{34}]^{4-}$, in which the

oxygen linked to five metal ions is again the site with the lowest bonding energy.[21] The connection between the values of the Mayer bond order index and the catalytic properties of a given anion, which are frequently associated with the loss of a terminal or a bridging oxygen, is not direct. One should take into account the effects of the solvent and the relaxation of the lacunary anion, which were not considered by Bridgeman.

Mixed-addenda clusters

Beyond the highly symmetric anions of formula $[XM_{12}O_{40}]^{n-}$, there are many clusters in which one or some $M^{n+}O_6$ octahedra have been formally replaced by another unit usually with a different metal centre like V^{5+}, Nb^{5+}, Ti^{4+}, etc. The distortion generated by this replacement is essentially limited to the region of substitution. Changes in the electronic structure are, however, much more important. The metal substitution modifies the energy and composition of the lowest unoccupied orbitals and, therefore, the redox properties of the molecule. Our group discussed this phenomenon for several mixed HPAs.[22] Although the ionisation energies of isolated metal ions computed suggest that the reduction of mixed-addenda molybdovanadates should occur at the molybdenum centres, the extra electron preferentially goes to a vanadium atom. Therefore, the reduced species $SiMo_{11}V^{IV}$ with one electron localised on the V centre is more stable than the heteropolyblue $SiMo_{11}V1e$ with one electron delocalised among the eleven Mo centres by 0.2 eV. The energy difference for the analogous tungstonvanadate $SiW_{11}V$ is 0.64 eV.[22]

Redox properties of clusters with nonequivalent metal sites

Extended-Hückel calculations[30] performed on the Wells–Dawson anion P_2W_{18} provided a qualitative understanding of the reduction process. It was found that the first metallic electron added to the cluster is belt-centred as experimental observations show. In addition, it was discussed the effect of addenda substitution in the WD framework. The localisation of the LUMO, the orbital directly involved in the first reduction, governs the distribution of the metal electrons.

As in WD structures, the metal atoms in the decatungstate anion $[W_{10}O_{32}]^{4-}$ can also be classified as *axial* and *equatorial* centres (see Figure 3.8). BP, BP86 and B3LYP calculations predict that the LUMO in

$[W_{10}O_{32}]^{4-}$ is an orbital of a_{1u} symmetry mainly delocalised over the equatorial centres.[21] Figure 3.6 shows orbital energies for the four lowest unoccupied orbitals and a plot of the LUMO in $[W_{10}O_{32}]^{4-}$. As expected from the composition of the LUMO, the ground states for the reduced species $[W_{10}O_{32}]^{5-}$ and $[W_{10}O_{32}]^{6-}$ are a doublet and a singlet, respectively, with the additional electrons delocalised among the equatorial sites. The diamagnetism predicted by the calculations for $[W_{10}O_{32}]^{6-}$ fully agrees with the experimental evidence. For the monoreduced species, the reduction at the axial centres (configuration $7b_{1u}^{1}$) was estimated to require ~1eV more than in the equatorial sites. By means of the energy decomposition scheme in terms of electrostatic interaction, Pauli repulsion and orbital mixing, Bridgeman *et al.* showed that the equatorial-reduced states are favoured by orbital mixing and to some extent by electrostatic factors. Otherwise, the states that involve the addition of one electron to the most distant axial sites have a smaller Pauli repulsion. In other words, as Borshch suggested from Extended Hückel calculations,[31] the gain in energy due to delocalisation over the equatorial sites exceeds the loss associated with the larger electronic repulsive effects and is the factor that determines the reduction site.

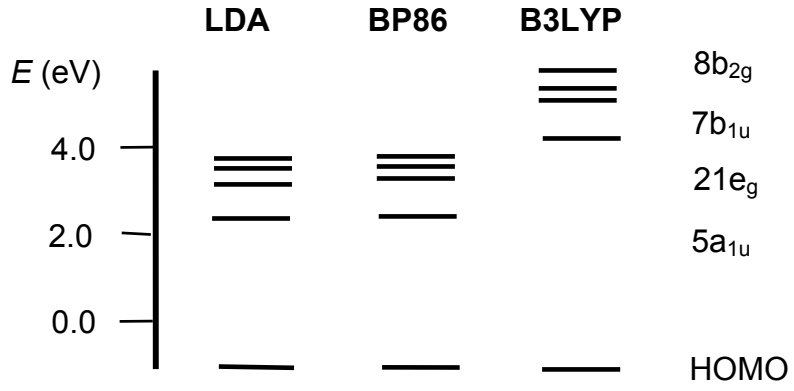

Figure 3.6. Frontier orbital diagram for $[W_{10}O_{32}]^{4-}$ computed with three functionals.

Heteropolyanions with paramagnetic ions

Heteropolyanions may incorporate *central* or *peripheral* paramagnetic transition metal ions. The structure of a Keggin anion, with a paramagnetic ion such as Fe^{III} or Co^{II} occupying the centre of the cluster, is not unlike those in which the heteroatom is a main group element (Table 3.1). A direct consequence of the lack of deformation in the $M_{12}O_{36}$ cage is that the energy gap between the doubly occupied oxo band and the set of unoccupied tungsten orbitals is not modified by the paramagnetic ion in the central tetrahedron. The value of 2.7 eV for the ground state of $Co^{II}W_{12}$ is very similar to the energy gap reported for Keggin clusters with main group heteroatoms, AlW_{12}, SiW_{12} and PW_{12} (2.8 eV). The d-cobalt orbitals appear well separated from the oxo and tungsten band, except for the unoccupied β–t_2 orbital, which is inserted into the tungsten band (Figure 3.7). The spin densities of Table 3.2 confirmed the high localisation of the unpaired electrons in the central tetrahedron XO_4. For $Co^{II}W_{12}$, the spin density is strongly localised in the cobalt centre (+2.56 e) but contributes little to the tetrahedral oxygens (+0.066 e per centre). For two other ions such as Co^{III} and Fe^{III}, the delocalisation of the spin density is somewhat higher.

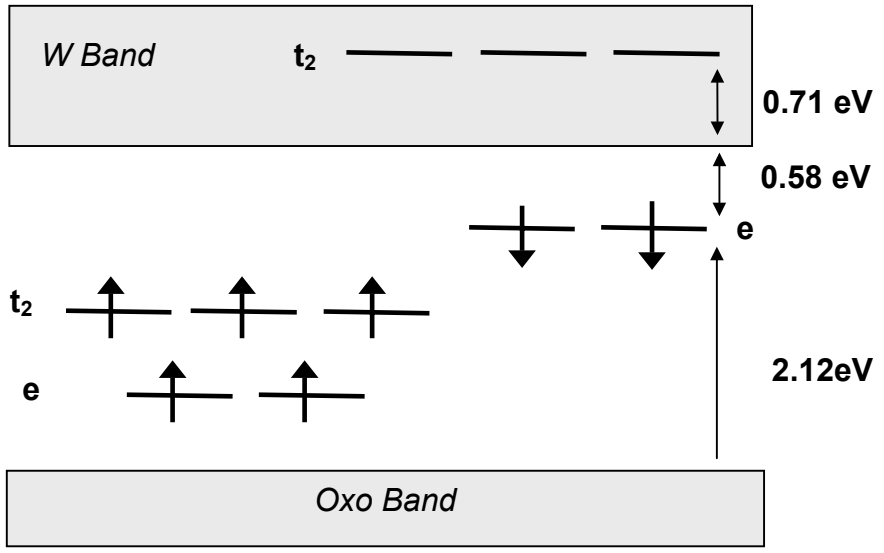

Figure 3.7. Frontier orbital region for the $[Co^{II}W_{12}O_{40}]^{6-}$ anion. The t_2 and e sets of orbitals correspond to the d orbitals of Co^{II}.

Table 3.2. Spin densities of several atoms in Keggin anions with paramagnetic ions in the central position.

	$Co^{III}W_{12}$	$Co^{II}W_{12}$	$Fe^{III}W_{12}$
Fe/Co	+2.867	+2.565	+4.003
W	–0.003	+0.002	–0.001
O_4	+0.226	+0.066	+0.193
O_2	+0.002	+0.001	+0.002
O_2'	+0.015	+0.008	+0.012
O_1	+0.006	+0.002	+0.006

It is well established that the first reduction of $Co^{III}W_{12}$ takes place at the cobalt ion and produces $Co^{II}W_{12}$, whereas the subsequent reduction produces the heteropolyblue $Co^{II}W_{12}1e$ instead of $Co^{I}W_{12}$. On the other hand, the reduction of $Fe^{III}W_{12}$ leads directly to the blue species $Fe^{III}W_{12}1e$. For the ground state of $[CoW_{12}O_{40}]^{6-}$, the promotion of 1e from the highest β Co orbital to the lowest W orbital requires ~1eV. This large amount of energy explains why the blue species $Co^{III}W_{12}1e$ is not the reduction product of $Co^{III}W_{12}$ because the additional electron goes to the cobalt orbital. The subsequent reduction, however, does not occur at the cobalt centre because the blue species $Co^{II}W_{12}1e$ is 0.78 eV more stable than $Co^{I}W_{12}$. This is a product that requires the addition of one electron to the $\beta–t_2$ orbital, which is 0.71 eV above the lowest unoccupied tungsten orbital.

The unrestricted DFT energies computed for an open-shell configuration represent an average of the individual multiplets associated with a given configuration. The energy of a particular multiplet can be formulated as the weighted sum of single determinant energies. With the aid of the STAGEN program for determining the symmetry coefficients for wave functions and energies,[32] Maestre *et al.* computed the multiplet splittings for several excited configurations of $[Co^{II}W_{12}O_{40}]^{6-}$.[33] For the excited $e^3t_2^4$ configuration there are two quadruplets of symmetries $T_2(F)$ and $T_1(F)$ that are at 7126 and 13711 cm^{-1} above the $^4A_2$ ground state, which is associated with the ground configuration $e^4t_2^3$. These energies are too large if we compare them with the assignments made for the permitted Co → Co transition $^4A_2 \rightarrow {}^4T_1$ (7830 cm^{-1}) and the forbidden transition $^4A_2$

$\rightarrow {}^4T_2$ (4600 cm^{-1}). There is strong agreement when a Jahn–Teller relaxation is permitted for the excited configurations. The states $^4T_1$ and $^4T_2$ in the T_d geometry split into the four states $^4B_2$, $^4E(2)$ and $^4A_2$ in the D_{2d} geometry. The lowest state of symmetry B_2 appears at 5275 cm^{-1}, a value that agrees fairly well with the energy expected for the forbidden transition $^4A_2 \rightarrow {}^4T_2$. The energies of the next excited states range between 7700 and 11000 cm^{-1}. These values agree well with the presence of an intense, broad band in the near-infrared region (7000–9000 cm^{-1}) in the electronic spectrum of $[Co^{II}W_{12}O_{40}]^{6-}$. Superposed to the Co $\rightarrow$ Co transitions are charge-transfer transitions from Co to W.

Substituting addenda metal atoms by paramagnetic ions provides highly interesting clusters. Derivatives containing Mo and Fe are one example. The closeness of the redox potentials for Mo^{VI}/Mo^{V} and Fe^{III}/Fe^{II} in oxides allows the equilibrium

$$Fe^{II} + Mo^{VI} \rightarrow Fe^{III} + Mo^{V}$$

when both ions are in octahedral sites. Duclusaud and Borshch studied this process[34] in the Keggin framework through a model cluster including only the region of Fe and two neighbouring Mo atoms. Two minima that differ by less than 1 kcal mol^{-1} were found at the B3LYP level, corresponding to the one-electron-transfer between Fe and Mo. Two configurations were computed: case A is the situation in which all metal electrons are at the iron centre with a high-spin configuration, $t_2{}^4e^2$, and with one β-electron in the orbital. Case B is the configuration in which this β-electron has been transferred to a molybdenum orbital. The only noticeable difference between the geometries of A and B is the coordination sphere around Fe, which is more contracted in B. The small energy difference between the two localisation patterns and the probable absence of an energy barrier between them suggest fast electronic hopping between the states. This would agree with the interpretation of the Mössbauer spectra for this sort of system.[34] A similar model was used to describe the electron transfer between a Keggin unit and an Fe counterion.[35]

Magnetic properties of reduced polyoxoanions

Coupling between blue electrons and paramagnetic ions. POMs are versatile building blocks for constructing molecular magnetic materials.

Many POM-based materials present the coexistence of localised and delocalised magnetic electrons. An example of this situation is given in the heteropolyblue $Fe^{III}W_{12}1e$, in which the five unpaired central electrons are *antiferromagnetically* coupled with the external electron delocalised over the Ws. According to this magnetic behaviour, the low-spin state, determined by the Broken-Symmetry approach, was computed to be 196 cm^{-1} more stable than the high-spin state computed at the unrestricted level. For $Co^{II}W_{12}1e$, the coupling between the external and the three internal cobalt electrons is slightly *ferromagnetic*, with an energy difference between the two spin states of only 21 cm^{-1}.[22]

Duclusaud *et al.*[36] evaluated the magnetism modulated by the nitrosyl derivative of the decamolybdate ion, $[Mo_{10}O_{25}(OMe)_6(NO)]^-$, is affected by the position of the six metoxi ligands. The structure of this anion is related to that of $[Mo_{10}O_{34}]^{4-}$ (Figure 3.8) and may be viewed as a $Mo_{10}O_{34}$ framework in which one terminal oxygen is replaced by a NO group and six bridging oxygens are replaced by six metoxi groups. By modelling the CH_3

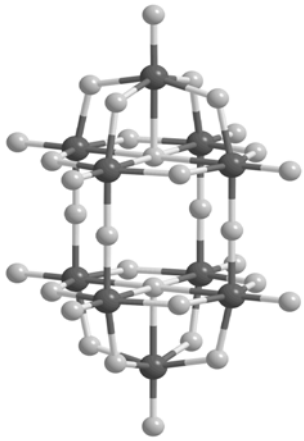

Figure 3.8. Structure of the $[Mo_{10}O_{34}]^{4-}$ anion. One of the axial terminal oxygens was replaced by a NO group, whereas several other oxo positions were substituted to study the changes produced in the MO structure (see text).

groups with H atoms, five positional isomers were studied. As in $[W_{10}O_{34}]^{4-}$, the LUMO for the fully oxidised parent of **I** ($[Mo_{10}O_{25}(OMe)_6(NO)]^+$) is an orbital delocalised over the eight equatorial

Mo ions, and well separated from the next unoccupied level. Consequently, the two additional electrons are accommodated in the LUMO, which gives rise to a diamagnetic ground state for $[Mo_{10}O_{25}(OMe)_6(NO)]^-$. We could modify the diamagnetism of this anion if we could reduce the H-L gap and get an open-shell state (triplet or singlet competitive with the closed-shell configuration). Since the HOMO in $[Mo_{10}O_{25}(OMe)_6(NO)]^-$ is localised on the eight equatorial molybdenum ions, we expect the protonation in the bridging oxygens of the equatorial planes or between the equatorial planes to alter the energy of the HOMO and its separation with respect to the LUMO. See reference 6 for more information. To sum up, Duclusaud and Borshch have proven that the magnetic properties of a reduced cluster can be conveniently tuned by controlling the position of a substituent in POMs.

Ab initio determination of electron-transfer parameters in reduced Keggin anions. Experimentally, it is well established that when Keggin anions contain an even number of delocalised electrons the compound is diamagnetic. Initially, this phenomenon was attributed to a strong antiferromagnetic coupling via a superexchange mechanism.[37] It was later shown through model calculations that electron delocalisation and electron repulsion can stabilise the diamagnetic singlet.[38] Coronado and co-workers recently reported very accurate *ab initio* calculations to evaluate electron-transfer parameters in reduced Keggin anions.[39] Provided that the transfer (hopping) effective integrals are essentially local parameters, fragments can properly model the Keggin framework. These authors used 4W- and 2W-ion fragments (Figure 3.9) to estimate transfer integrals in the one-electron-reduced cluster. Taking into account that the unpaired electrons are delocalised over d_{xy}-like orbitals of W ions, the following four doublets can be defined for the one-electron-reduced 4W-ion fragment,

$$\psi_1 = \frac{d_1 + d_2 + d_3 + d_4}{2},\ \psi_2 = \frac{d_1 - d_2 - d_3 + d_4}{2}$$

$$\psi_3 = \frac{d_1 + d_2 - d_3 - d_4}{2},\ \psi_4 = \frac{d_1 - d_2 + d_3 - d_4}{2}$$

where d_i are the Slater determinants constructed when the extra electron is on the corresponding W_i ions. In this context, the transfer parameters t

(hopping between corner-sharing WO_6 octahedra) and *t'* (hopping between edge-sharing WO_6 octahedra) are then written as:

$$t = \langle d_1 | H | d_4 \rangle \quad t' = \langle d_1 | H | d_2 \rangle$$

These integrals are related to the doublet energies $E_1 - E_4$ by the equations,

$$E_4 - E_1 = -2t - 2t', \quad E_3 - E_2 = -2t + 2t'$$

By precisely determining the E_i energies the values obtained for *t* and *t'* are also very accurate. Contrary to what is commonly accepted, the electron transfer between edge-sharing and corner-sharing WO_6 octahedra was very similar for all methods and fragments used. For the largest fragment, the best calculation was performed at the CASPT2 level, giving a value of –428 meV for *t* and –470 meV for *t'*. The computed values at the same level of accuracy did not differ very much when the smallest 2W-based fragments of Figure 3.9-d (–445 and –490 meV, respectively) were used.

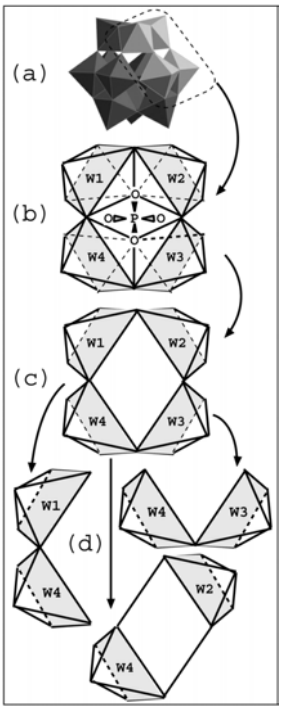

Figure 3.9. (a) Polyhedral representation for a Keggin anion. (b)–(d) Fragments used to compute transfer (hopping) integrals. Reproduced from ref. 39.

For these smaller clusters, t and t' integrals were also calculated with the variational DDCI method, leading to t = –467 meV and t' = –507 meV. When the latter values were introduced into an extended Hubbard Hamiltonian[39], the singlet state for a two-electron-reduced Keggin anion was estimated to be 280 meV more stable than the lowest triplet state. This large energy gap clearly explains the diamagnetism of the two-electron-reduced Keggin anions.

Localisation/delocalisation of the metal electrons in mixed-addenda POMs

Most POMs comprising metal ions in a high oxidation state can be easily reduced without making significant structural changes. It is difficult to unequivocally characterise the number and nature of the reduced centres in a partly reduced cluster and today this is still a matter of debate. Electrochemical reductions and EPR spectroscopy have usually been used to determine the localisation, or delocalisation, of the metal electrons in reduced HPAs. The intense blue colour in reduced POMs is considered to indicate an important delocalisation of the metal electrons.

As we have mentioned above, the monoreduction of the mixed $SiVW_{11}$ anion yields the brown species $SiV^{IV}W_{11}$, not the heteropoly blue, $SiVW_{11}1e$. The first two electrochemical reductions in $SiMoV_2W_9$ and the first three electrochemical reductions in SiV_3W_9 were attributed to $V^V \rightarrow V^{IV}$ steps.[40] Through empirical valence sum calculations based on the X-ray structure of the highly reduced bicapped Keggin complex $[PMo_{12}O_{40}(VO)_2]^{5-}$, two of the eight d electrons were assigned to the two V centres and the other six electrons were considered to be delocalised among the other 12 Mo centres.[41] This distribution was fully confirmed by DFT calculations, which showed that the ground state was a triplet with two V^{IV} ions.[42] The alternative configuration, corresponding to an equipartition of the eight electrons between vanadium and molybdenum centres, was less stable by 1.41 eV. Xu *et al*. synthesised the related tetracapped cluster $[Mo_8V_8O_{40}(PO_4)]^{5-}$ as an anion with eight V^{IV} centres with the other two d electrons delocalised over the eight Mo atoms.[43] When then number of vanadium ions increases, the hypothesis that before accommodating any electron in a Mo orbital all vanadium centres should have at least one electron does not seem to be satisfied. Preliminary calculations carried out by our group on $[Mo_8V_8O_{40}(PO_4)]^{5-}$ indicate that the configuration with eight electrons on the 8 V centres and the two remaining electrons on the 8

Mo atoms is ~2 eV more unstable than the more equilibrated repartition of the electrons i.e. six electrons over the V centres and the other four electrons over the Mo centres.

Using DFT/BP86 calculations, Rohmer and Bénard discussed the nature of the M–M bond in the two-reduced oxothio clusters γ-$[SiW_{10}M_2S_2O_{38}]^{6-}$ (M = Mo, W) recently synthesised by Cadot and Sécheresse.[44] The X-ray characterisation of these structures revealed short M^V–M^V distances (2.832 Å for M = Mo and 2.815 Å for M = W). These values clearly indicate that Mo–Mo and W–W are single bonds. The oxoanions γ-$[SiW_{10}Mo_2O_{40}]^{6-}$ and γ-$[SiW_{12}O_{40}]^{6-}$ were also synthesised but could not be characterised crystallographically. For the four anions a first minimum with a short M–M separation was found. The computed M–M separations in the oxothio anions, 2.998 Å for M = Mo and 2.872 Å for M = W, were somewhat longer than the distances observed but these structures maintained the presence of a metal-metal coupling. The corresponding metal–metal distances for the oxo anions were 2.653 and 2.569 Å. All the complexes have similar electronic structures, an occupied valence O/S band that is well separated from the empty d-Mo/W band and an isolated HOMO localised on the $M_2X_2O_2$ fragment that is typical of a σ_{M-M} bond:

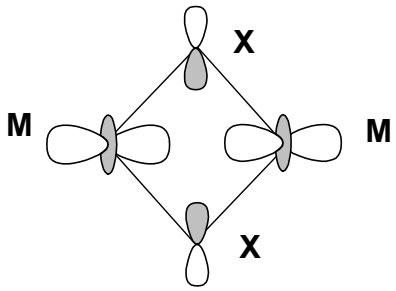

A new minimum characterised by a long M–M distance (>3 Å for X = O and >3.7 Å for X = S) and with the two electrons delocalised over the γ-Keggin tungstate was reported. Except for γ-$[SiW_{12}O_{40}]^{6-}$, the most stable conformation is the one with the short metal-metal distance, with energies ranging from 10.2 to 23.8 kcal mol^{-1}. In the unsubstituted tungstate, the delocalised state is lower in energy by 2.9 kcal mol^{-1} This seems to be consistent with the blue colour of the anion in solution. The other three anions are red or red-brown. The localisation/delocalisation of the two metal

electrons in the γ-$[SiW_{10}M_2X_2O_{38}]^{6-}$ clusters therefore depends on the difference between the electrophilic characters of the Keggin core, γ-$[SiW_{10}O_{36}]^{n-}$, and the flexible dimetallic fragment, $M_2X_2O_2$.[44]

Proton affinity of polyoxoanions

Amoureux and co-workers[45] used BP86 functional and a TZP-quality basis set to study the basicity of single-addenda PM_{12} anions (M = Mo, W). As expected, the protonation in the bridging oxygen sites was preferred. Protonations at terminal (O_1) oxygen were less favoured by 11.5 and 18.4 kcal mol^{-1} for PMo_{12} and PW_{12}, respectively. These values were compared with Rotational Echo Double Resonance (REDOR) NMR data, which detected the protons in $H_3PMo_{12}O_{40}$ and $H_3PW_{12}O_{40}$ at a distance of 5.20±0.20 Å and 5.70±0.20 Å from the central phosphorus, respectively. Both experimental values were rather larger, especially the latter. This seems only consistent with a protonation at a terminal site in H_3PW_{12}. For the first time, the general assumption that the protonation at a terminal oxygen site is only competitive in systems containing Nb, Ti or Cr was called into question. In our opinion, these results are very important because, if confirmed in other systems, they may indicate that solvent and counterions need to be considered to find the local active sites in a POM.

Slightly out of the scope of molecules presented here, let us comment a similar work conducted on a novel tin nanocluster, $[(CH_3Sn)_{12}O_{14}(OH)_6]^{2+}$. Wavefunction-based and DFT calculations[46] were aimed at studying the nature of the interactions between ―anionic and neutral― nucleophilic species and the cited cluster. Molecular electrostatic potentials were computed to confirm the experimental observations on the regioselectivity of the nucleophiles towards the tin cation. The basicity of the oxygen sites of the cluster was investigated by means of the protonation energy and the atomic charge. The hardness/softness principle applied to the system did not probed to describe correctly all the nucleophile-cluster interactions, thus showing that electrostatic considerations and hydrogen bonding are much more important.

Vibrational frequencies in Lindqvist and Keggin anions

The theoretical determination of vibrational frequencies for large molecules is still a non-standard task. In the case of Keggin anions, the calculation of

the second derivatives of the energy is extremely computational demanding despite their tetrahedral symmetry. In a significant study, Bridgeman computed, classified and compared the vibrational frequencies for the series of Keggin anions $[XMo_{12}O_{40}]^{n-}$, X = P^{III}, As^{III}, Si^{IV}, Ge^{IV}, Al^{V} and Ga^{V} and $[PW_{12}O_{40}]^{3-}$ using the B3LYP hybrid functional.[47] We will not describe here the 153 normal modes of vibration of an α-Keggin anion but we should point out that the B3LYP functional with augmented LANL2DZ basis sets reproduces the experimental spectrum of Keggin anions very well. The discrepancy between the calculated and the observed spectra does not exceed a few cm^{-1} for most vibrational modes. For $[PW_{12}O_{40}]^{3-}$, the largest deviation of 71 cm^{-1} takes place in a vibrational mode assigned as a combined stretching and bending Mo–O–Mo mode. Previously, the same group compared the vibrational spectra of various Lindqvist anions at several computational levels. Although DF methods reproduce the vibrational spectral of $[M_6O_{19}]^{n-}$ clusters quite well, the HF method performs very poorly.[48] The fitting between experimental and theoretical spectra was best at the LDA level with the TZP/ZORA approach (triple-ζ Slater basis set with the ZORA method). In comparison, the LDA and B3LYP functionals with GTO basis provide less accurate results. The results with BP86 and BLYP are significantly poorer.[48]

References and Notes

[1] Davidson, E. R. *Chem. Rev.* **2000**, *100*, 351.

[2] Fonseca Guerra, C.; Snijders, J. G.; Te Velde, G.; Baerends, E. J. *Theor. Chem. Acc.* **1998**, *99*, 391 and references therein.

[3] Jansen, S. A.; Singh, D. J.; Wang, S-H. *Chem. Mater*. **1994**, *6*, 146.

[4] Wang, S-H.; Jansen, S. A. *Chem. Mater*. **1994**, *6*, 2130.

[5] Wang, S-H.; Jansen, S. A.; Singh, D. J. *J. Cat*. **1995**, *154*, 137.

[6] Poblet, J. M.; López, X.; Bo, C. *Chem. Soc. Rev.* **2003**, 32, 297.

[7] Bardin, B.; Bordawekar, S. V.; Neurock, M.; Davis, R. J. *J. Phys. Chem. A*. **1998**, *102*, 10817. See also Bardin, B.; Davis, R. J.; Neurock, M. *J. Phys. Chem. B*. **2000**, *104*, 3556.

[8] Kempf, J. Y.; Rohmer, M.-M.; Poblet, J. M.; Bo, C.; Bénard, M. *J. Am. Chem. Soc.* **1992**, *114,* 1136.

[9] Maestre, J. M.; Sarasa, J. P.; Bo, C.; Poblet, J. M. *Inorg. Chem*. **1998**, *37*, 3071.

[10] Bader, R. F. W. *Atoms in Molecules. A Quantum Theory*. Clarendon Press, Oxford, **1990**. Bader, R. F. W. *Chem. Rev*. **1992**, *91*, 893.

[11] Rohmer, M.-M.; Bénard, M. *J. Am. Chem. Soc.* **1994**, *116,* 6959.

[12] Rohmer, M.-M.; Devémy, J.; Wiest, R.; Bénard, M. *J. Am. Chem. Soc.* **1996**, *118,* 13007.

[13] Rohmer, M.-M.; Bénard, M.; Blaudeau, J.-P.; Maestre, J. M.; Poblet, J. M. *Coord. Chem. Rev.* **1998**, *178–180*, 1019.

[14] Day, V. W.; Klemperer, W. G.; Yaghui, O. M. *J. Am. Chem. Soc.* **1989**, *111*, 5959.

[15] Bagus, P. S.; Bauschlicher, C. W.; Nelin, C. J.; Laskowski, B. C. *J. Chem. Phys.* **1984**, *81*, 3594.

[16] Maestre, J. M.; Poblet, J. M.; Bo, C.; Casañ-Pastor, N.; Gómez-Romero, P. *Inorg. Chem.* **1998**, *37*, 3444.

[17] Chen, Q.; Hill, C. L. *Inorg. Chem.* **1996**, *35*, 2403.

[18] Borshch, S. A.; Bigot, B. *Chem. Phys. Lett*. **1993**, *212*, 398.

[19] Noodleman, L. J. *Chem. Phys*. **1981**, *74*, 5737. Noodleman, L.; Davidson, E: R. *Chem. Phys*. **1986**, *109*, 131. Noodleman, L.; Case, D. A. *Adv. Inorg. Chem*. **1992**, *38*, 423. Noodleman, L.; Pen, C. Y.; Case, D. A. Mouesca, J. M. *Coord. Chem. R*ev. **1995**, *144*, 199.

[20] Bridgeman, A.; Cavigliasso, G. *Inorg. Chem.* **2002**, *41*, 1761.

[21] Bridgeman, A.; Cavigliasso, G. *J. Phys. Chem. A*. **2002**, *106*, 6114.

[22] Maestre, J. M.; López, X.; Bo, C.; Poblet, J. M.; Casañ-Pastor, N. *J. Am. Chem. Soc.* **2001**, *123*, 3749.

[23] Bridgeman, A.; Cavigliasso, G. *Polyhedron.* **2001**, *20*, 3101.

[24] Bridgeman, A.; Cavigliasso, G. *J. Phys. Chem. A*. **2001**, *105*, 7111.

[25] Bridgeman, A.; Cavigliasso, G. *J. Chem. Soc., Dalton Trans.* **2001**, 3556.

[26] Bridgeman, A.; Cavigliasso, G. *J. Chem. Soc., Dalton Trans.* **2002**, 2244.

[27] Bridgeman, A. *J. Phys. Chem. A*. **2002**, *106*, 12151.

[28] Bridgeman, A.; Cavigliasso, G. submitted for publication.

[29] Mayer, I. *Chem. Phys. Lett*. **1983**, *97*, 270. Mayer, I. *Int. J. Quant. Chem*. **1984**, *26*, 151.

[30] Keita, B.; Jean, Y.; Levy, B.; Nadjo, L.; Contant, R. *New J. Chem*. **2002**, 1314.

[31] Borshch, S. A. *Inorg. Chem.* **1998**, *37*, 3116.

[32] Daul, C. *Int. J. Quantum Chem*. **1994**, *52*, 867.

[33] Maestre, J. M.; López, X.; Bo, C.; Daul, C.; Poblet, J. M. *Inorg. Chem.* **2002**, *41*, 1883.

[34] Duclusaud, H.; Borshch, S. A. *Inorg. Chem.* **1999**, *38*, 3491.

[35] Borshch, S. A.; Duclusaud, H.; Millet, J. M. *Appl. Cat. A: General*. **2000**, *200*, 103.

[36] H. Duclusaud, S. A. Borshch, *J. Am. Chem. Soc.* **2001**, *123*, 2825.

[37] Casañ-Pastor, N.; Baker, L. C. W. *J. Am. Chem. Soc.* **1992**, *114*, 10384 and references therein.

[38] Borrás-Almenar, J. J.; Clemente-Juan, J. M.; Coronado, E.; Tsukerblat, B. S. *Chem. Phys.* **1995**, *195*, 1.

[39] Suaud, N.; Gaita-Ariño, A.; Clemente-Juan, J. M.; Sánchez-Marín, J.; Coronado, E. *J. Am. Chem. Soc.* **2002**, *124*, 15134.

[40] Cadot, E.; Fournier, M.; Tézé, A.; Hervé, G. *Inorg. Chem.* **1996**, *35*, 282.

[41] Chen, Q.; Hill, C. L. *Inorg. Chem.* **1996**, *35*, 2403.

[42] Maestre, J. M.; Poblet, J. M.; Bo, C.; Casañ-Pator, N.; Gómez-Romero, P. *Inorg. Chem.* **1998**, *37*, 3444.

[43] Xu, Y.; Zhu, H-G.; Cai, H.; You, X.-Z. *Chem. Commun.* **1999**, 787.

[44] Rohmer, M.-M.; Bénard, M.; Cadot, E.; Secheresse, F. *Polyoxometalate Chemistry*. Pope, M. T.; Müller, A., eds., pp. 117–133. Kluwer Academic Publishers. The Netherlands, **2001**.

[45] Ganapathy, S.; Fournier, M.; Paul, J. F.; Delevoye, L.; Guelton, M.; Amoureux, J. P. *J. Am. Chem. Soc.* **2002**, *124*, 7821.

[46] Vivas-Reyes, R.; De Proft, F.; Geerlings, P.; Biesemans, M.; Willem, R.; Ribot, F.; Sanchez, C. *New J. Chem*. **2002**, *9*, 1093.

[47] Bridgeman, A. *Chem. Phys.* **2003**, *287*, 55.

[48] Bridgeman, A.; Cavigliasso, G. *Chem. Phys.* **2002**, *279*, 143.

CHAPTER 4

Electronic Properties of Keggin anions

The Keggin anion, of general formula $XM_{12}O_{40}^{n-}$, has been the focus of much effort for the understanding of the chemistry of POMs. A simple synthetic route as well as the flexibility of its chemical composition makes this compounds the main reference for the knowledge of the general behaviour of metal-oxide clusters and, especially, heteropolyanions. Since 1933, when J. F. Keggin resolved for the first time the X-ray structure of such a molecule, many experiments have detached all the properties and characteristics of this framework. In this chapter we focus on a couple of subjects intimately related to the electronic structure of these anions. Firstly, the structural isomerism occurring in $XM_{12}O_{40}^{n-}$ compounds and the relative stability of the most common forms, namely, α and β. These two isomers are ancient subjects in the literature, and it was established an order of stability for them, although it was shown recently that, in some cases, an inversion of this trend can be observed. We provide here general guidelines to unravel when and why this inversion can take place. The second part of the chapter concerns the chemical effects of metal substitution, one of the most exploited ways to vary the properties of POMs. The main goal here is to connect the features of trisubstituted Keggin anions, $SiM_3W_9O_{40}^{m-}$, with the physical nature of M. For this purpose, the molecular orbitals interpretation is a useful tool that provides complementary information for experimentalists about the affinity to extra electrons and their localisation in the metal-oxide framework.

4.1. Study of the Relative Stability of Single-addenda α/β-Keggin Anions

Historical perspective

The general features of the Keggin anion, $[XM_{12}O_{40}]^{n-}$, were introduced in the previous chapter, stressing on the electronic structure, the composition of the frontier Molecular Orbitals and the clathrate-type structure of the framework. We only were concerned with the α form of the molecule, of T_d symmetry, in which all the metal centres are equivalent. Baker and Figgis[1] proposed that the β structure might be derived from 60º rotation of one of the M_3O_{13} triad about a 3-fold axis of the α anion. Three additional isomers, γ, δ and ε, were postulated resulting from 60º rotation of the remaining triads (Figure 4.1).[2]

It is accepted that these latter structures are less stable than α and β, which are supposed to have similar energies, although the α isomer is probably somewhat more stable since isomerisations on Keggin heteropoly-tungstates and -molybdates all occur in the β → α direction.[3a-c] Starting from the highly-symmetric α form, the other four isomers are formally obtained by successive 60º rotations of the four M_3O_{13} triads about the three-fold axis of symmetry of the α structure. Amongst these five rotational isomers of the Keggin anion, α and β are the most common in the literature as a consequence of their major stability. Conventionally, the α structure appears to be the most stable. The first X-ray characterisation for a β isomer was reported in 1973 for the potassium salt of $[SiW_{12}O_{40}]^{4-}$.[4] Later, Matsumoto *et al.*[5] showed that this compound is kinetically stable. Even though, Weinstock and co-workers[6] reported a detailed study on the equilibrium between α and β isomers for several fully oxidised Keggin anions. They quantify the relative kinetic and thermodynamic stability of β isomers in relation to the α isomers, and it appears to depend on such factors as the heteroatom and the conditions of the solution. A relevant ordering of these β-polyanions stability with X = Al(III) > Si(IV) > P(V) is found, confirming Pope's hypothesis.[7] Previous theoretical calculations carried out by our group[8] on α-Keggin anions supported the hypothesis[9] that a Keggin anion may also be viewed as a neutral $M_{12}O_{36}$ cage that encapsulates the internal charged $[XO_4]^{n-}$ subunit.

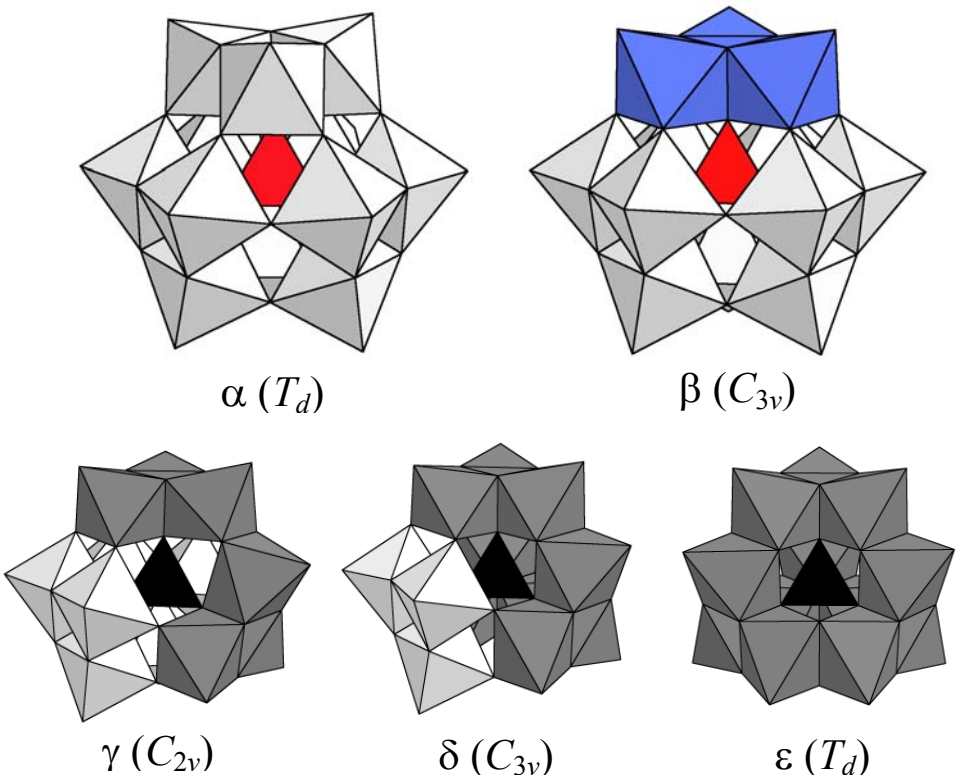

Figure 4.1. Polyhedral representation of the five rotational isomers of the Keggin anion. Shaded are the edge-sharing octahedra involved in the isomerism, which rotate 60º about the four 3-fold axis of the α form.

In the present section we make use of the clathrate model introduced in chapter 1 to study the Keggin molecule. The discussion is addressed to know in which situations this inversion of the traditional stability can occur and what are the factors governing it. The DFT calculations shown were carried out on a series of Keggin anions to analyse the different factors that govern the relative stability of its α and β isomers.

To our knowledge, only a few more β structures have been characterised by X-ray: the fully oxidised tungstates $[GeW_{12}O_{40}]^{4-}$,[10] $[AlW_{12}O_{40}]^{5-}$ [6] and the four-times reduced molybdates $[PMo_{12}O_{40}]^{7-}$ [11a] and $[AsMo_{12}O_{40}]^{7-}$.[11b] Somewhat more abundant are the structures for β mixed-

addenda complexes.[12] An interesting point concerning structures with only one addenda metal type is that reduced β isomers can be more stable than the corresponding α isomers, because β structures reduce at slightly more positive potentials than α structures.[5,7] Tézé *et al.*[13] showed that there is a direct relationship between the oxidising character of Keggin POMs and the number of rotated triads in the $M_{12}O_{36}$ framework: that is to say the reducibility increases in the order $\alpha < \beta < \gamma$. Related to this point, Sécheresse and co-workers reported hydrothermal preparations of reduced β-$SiMo_{12}$ derivatives in low reduction states.[14]

DFT study of fully oxidised clusters

Geometry optimisations under T_d and C_{3v} symmetry constraints for α and β isomers, respectively, were carried out for the $[XM_{12}O_{40}]^{n-}$ series, with X = P, Si, Al, As, Ge, Ga and M = W, Mo. No significant differences were observed between the computed and experimental geometries for the clusters with a known X-ray structure. The calculations show that the β isomer gradually stabilises in the order Al(III) > Si(IV) > P(V) and Ga(III) > Ge(IV) > As(V) for both W and Mo addenda atoms (Table 4.1). The largest stability in favour of the α isomer was found for X = P(V) and M = W with an energy difference of 0.28 eV (+6.5 kcal mol^{-1}). On the other hand, the greater the charge of the cluster, the more stable the β isomer is, particularly for aluminium and gallium tungsto–derivatives, in which the stability is inverted by –0.34 eV (–7.8 kcal mol^{-1}) and by –0.18 eV (–4.2 kcal mol^{-1}), respectively. Only the values for the silico- and germano-tungstates seem to fall outside the expected range of energies for which the difference in energy is slightly above the general tendency. These results are in accordance with the recent studies of Weinstock *et al.*[6] who found that the thermodynamic stability of β isomers in Keggin polytungstates increases in the same order Al(III) > Si(IV) > P(V). However, ΔG for $\alpha \rightarrow \beta$ $[AlW_{12}O_{40}]^{5-}$ isomerization was estimated from kinetic measurements to be positive, +2.1 kcal mol^{-1}. The same authors pointed out that the Gibbs energies for these isomerisation processes are dependent upon the temperature, the solvent, the ionic strength and the nature of the countercation. Therefore, this suggests that absolute Gibbs isomerisation energies in solution and the computed beta–alpha energies, based on isolated anions, are not directly comparable.

Table 4.1. Relevant mean distances, (XO_4) Mulliken charges and β – α energy differences calculated for a series of Keggin heteropolyanions.

X	*M*	*Isomer*	*d(X-O$_4$)*	*d(O$_4$-M)*	*d(M-M)*	*q(XO$_4$)*	$\Delta E_{\beta-\alpha}$[a]	
P	W	α	1.53	2.35	3.44 – 3.71	–1.66	+0.28	(+0.13)
		β	1.58	2.43	3.38 – 3.71	–1.61		
	Mo	α	1.58	2.46	3.47 – 3.75	–1.90	+0.21	
		β	1.59	2.45	3.42 – 3.80	–1.86		
Si	W	α	1.64	2.33	3.35 – 3.70	–2.59	+0.26	(+0.11)
		β	1.67	2.33	3.32 – 3.74	–2.63		
	Mo	α	1.67	2.37	3.41 – 3.75	–2.68	+0.14	
		β	1.68	2.37	3.41 – 3.79	–2.63		
Al	W	α	1.74	2.26	3.32 – 3.73	–3.09	–0.35	(–0.57)
		β	1.81	2.24	3.29 – 3.75	–3.19		
	Mo	α	1.81	2.27	3.35 – 3.77	–3.53	+0.08	
		β	1.81	2.28	3.33 – 3.80	–3.59		
As	W	α	1.75	2.35	3.44 – 3.74	–1.95	+0.16	
		β	1.75	2.35	3.44 – 3.80	–1.93		
	Mo	α	1.75	2.37	3.47 – 3.78	–2.19	+0.11	
		β	1.76	2.37	3.42 – 3.82	–2.17		
Ge	W	α	1.82	2.26	3.36 – 3.73	–3.26	+0.21	
		β	1.83	2.26	3.33 – 3.76	–3.38		
	Mo	α	1.84	2.30	3.42 – 3.79	–3.34	+0.01	
		β	1.84	2.30	3.37 – 3.83	–3.27		
Ga	W	α	1.92	2.19	3.33 – 3.76	–3.53	–0.19	
		β	1.93	2.19	3.30 – 3.77	–3.77		
	Mo	α	1.93	2.22	3.36 – 3.80	–3.80	–0.02	
		β	1.93	2.23	3.34 – 3.84	–3.82		

a) Values in parentheses are for monoreduced species.

For molybdates, the same trend was observed. Nevertheless, the energies range between smaller values. As for the tungstate series, the largest positive $\Delta E_{\beta-\alpha}$ was found for X = P(V) with a value of 0.21 eV, an energy that is 0.07eV smaller than that of the homologous tungstate. In

contrast, for X = Al(III), the β isomer becomes more stable but the α isomer is still the most stable by 0.08 eV. For the gallium derivative, the other group 15 heteroatom considered, both isomers have approximately the same energy. The Mulliken population values in Table 4.1 show that the total charge on the $[XO_4]$ subunit increases as the total charge of the molecule goes from −3 to −5. This increase almost parallels the formal increment except for X = Al where according to Mulliken analysis only ~0.5 electrons are added to $[XO_4]^{n-}$, while the remaining half electron is expected to be over the outer sphere. This general behaviour is also observed in clusters containing paramagnetic heteroatoms. Negative charges of –4.0 e were estimated for the internal tetrahedron in the highly charged clusters $[Fe^{III}W_{12}O_{40}]^{5-}$ and $[Co^{III}W_{12}O_{40}]^{5-}$ and of –4.5 e in $[Co^{II}W_{12}O_{40}]^{6-}$.[8]

In order to get a better understanding of the electronic effects involved in Keggin clusters, we decomposed the interaction energy between the two subunits $[XO_4]^{n-}$ and $M_{12}O_{36}$ by means of the transition state (TS) method developed by Ziegler *et al*.,[15] that is an adaptation of Morokuma's[16] well-known decomposition scheme.

$$E\left(Keggin\right)=E\left(M_{12}O_{36}\right)+E\left(XO_4^{n-}\right)+FIE$$

Once the *Fragment Energies* (*FE*) for the isolated $[XO_4]^{n-}$ and $M_{12}O_{36}$ units (for M = W) in the geometry they adopt in the cluster are calculated, the *Fragment Interaction Energy* (*FIE*) analysis accounting for the interactions between the two fragments is made. The *FIE* itself can be decomposed in two terms:

$$FIE = SR + OI$$

(see chapter 2 for further details). The contributions to the *FIE* are shown in Table 4.2.

Table 4.2. Energy decomposition for a series of Keggin molecules α/β-$[XW_{12}O_{40}]^{n-}$. Absolute values for α isomers and relative values for β isomers are listed in eV.

Isomer	*X*	*Steric Repulsion*	*Orbital Interactions*	*Total Interactions*	*Sum of fragments*
α	P	–10.23	–14.61	–24.84	–429.6
	Si	–13.62	–26.30	–39.92	–414.0
	Al	–8.34	–43.03	–51.37	–395.9
	As	–7.69	–15.78	–23.47	–425.1
	Ge	–9.28	–29.33	–38.61	–409.9
	Ga	–5.54	–44.38	–49.92	–391.1
β	P	+0.12	–0.29	–0.17	+0.44
	Si	+0.26	–0.03	+0.24	+0.02
	Al	+0.35	–1.02	–0.67	+0.33
	As	+0.12	–0.19	–0.07	+0.23
	Ge	+0.28	–0.20	+0.08	+0.14
	Ga	–0.05	–0.72	–0.78	+0.59

An analysis restricted to *FE* shows that this term always slightly favours the α isomer, while the energy of the tetrahedral fragment is, in practice, identical for α and β isomers. In addition, the energy change associated to deformation is fairly dependent on the total charge of the cluster for the geometry of the cage but is small for the tetrahedron. We found that the Deformation Energy[17] (*DE*) of neutral α cages is 2.37 eV for X = P, a value that increases to 4.91 eV for X = Si and to 7.46 eV for X = Al. These energies are very similar to those for beta cages. Such notable *DE*s originate in the change in the cage geometry when the relaxed $M_{12}O_{36}$ encapsulates the anion. The major variations occur in the $W–O_{term}$ bond distances, which increase consistently with the net charge of the anion. Thus, for example, the bond distance between the tungsten atom and the terminal oxygen is 1.727 Å for $[PW_{12}O_{40}]^{3-}$, whereas the corresponding

values for the anions $[SiW_{12}O_{40}]^{4-}$ and $[AlW_{12}O_{40}]^{5-}$ are 1.743 and 1.763 Å, respectively. Differences were smaller for the bridging bonds. On average, the α-$W_{12}O_{36}$ cage is ~0.3 eV more stable than the β cage, a value that is quite similar to the energy difference between the relaxed α and β structures. Therefore, the present calculations confirm the assumed major intrinsic stability of the α organisation of M and O atoms in the $M_{12}O_{36}$ cage.

*FE*s by themselves cannot explain the trend of the α/β relative stability in the series in Tables 4.1 and 4.2. The inversion in the stability of these two isomers has to be actually due to the *FIE*. For all the systems studied, the steric component of this term is dominated by the attractive electrostatic interaction that always overcomes the Pauli repulsion. Neither is the *SR* term responsible for the α/β inversion since in general it favours the α isomer. Only for the Ga derivative the *SR* contribution was found slightly less repulsive for the β isomer. The orbital interaction (*OI*) term, which represents the stabilising energy when the electron density relaxes, is, therefore, the only contribution that is always more stabilising for the β isomer. This term, as well as the Pauli and electrostatic contributions to the *SR* term, increase monotonically with n, the negative charge of the anion $[XM_{12}O_{40}]^{n-}$. For X = P (n = 3) the *SR* term is –10.2 eV. Despite being very large, this energy is smaller than the energy that results from orbital mixing (*OI* energy), which reaches values of up to –14.6 eV, and increases by more than 10 eV when n = 4 and by more than 25 eV for n = 5. It has been mentioned above that the *OI* term includes the $[XO_4]^{n-} \rightarrow M_{12}O_{36}$ charge transfer (*CT*) and the polarisation of both fragments. The electronic transfer from the neutral cage to the central tetrahedron can be neglected. It is not easy to separate these two terms (*CT* and polarisation) in the TS energy decomposition scheme. Some authors have estimated the charge transfer between fragments by selectively removing the virtual orbitals from the molecular orbital fragment set.[18] This method cannot be applied here since it implicitly accepts that the charge is only transferred from the highest occupied orbitals of one of the fragments to the LUMO of the other. Such behaviour cannot be assumed in POMs because of the delocalised nature of metallic orbitals.[8]

Alternatively, the polarisation energy for cage and tetrahedral fragments can be estimated, substituting the atoms of one or the other fragment by point charges. Three sets of atomic charges (formal, Mulliken and CHelpG)

were used to evaluate the cage polarisation by the presence of an $[XO_4]^{n-}$ in its interior. CHelpG charges were calculated to simulate the electrostatic potential generated by the tetrahedral fragment anion.[19] Polarisation energies computed with this model are given in Table 4.3.

Table 4.3. Comparison of the total Orbital Interaction (*OI*) term with the cage ($M_{12}O_{36}$) polarisation energy for the series of X = P, Si and Al. The cage polarisation terms were computed substituting the internal tetrahedron by a set of point charges in the positions of the nuclei. Three types of charges were taken into account for more generality of the results.

	Isomer	*OI*	*Cage Polarisation* [a)]		
			Formal	*Mulliken*	*CHelpG*
$[PW_{12}O_{40}]^{3-}$	α	−14.6	−13.9	−12.2	−12.4
	β	−14.9	−14.2	−12.5	−12.5
$[SiW_{12}O_{40}]^{4-}$	α	−26.3	−24.2	−22.3	−22.8
	β	−26.3	−24.4	−22.7	−23.0
$[AlW_{12}O_{40}]^{5-}$	α	−43.0	−37.6	−35.4	−38.3
	β	−44.0	−38.1	−35.7	−38.6

a) Cage polarisation energies correspond to the stabilisation energy of $M_{12}O_{36}$ when this cage encapsulates an $[XO_4]^{n-}$ anion, which atoms were replaced by point charges, Mulliken, formal, or CHelpG.

Several conclusions emerge from the values in this table.

- *(i)* the three sets of point charges give similar polarisation energies,
- *(ii)* the cage polarisation energy is heavily dependent on the anion charge and
- *(iii)* for all three sets of point charges, the polarisation energies are slightly greater for β than for α cages and this difference is larger for the aluminium derivative.

Moreover, the parallel behaviour of the *OI* term and the cage polarisation contribution and the small difference between these two terms

suggest that the cage polarisation is, very probably, the dominant contribution in the *OI* term. An equivalent analysis for $[XO_4]^{n-}$ polarisation shows that the energies involved are clearly smaller: they range between 3–4 eV for X = P and Si. The corresponding computed value for $[AlO_4]^{5-}$ is very high, about 18 eV. This considerable amount of energy originates in the intrinsic instability of $[AlO_4]^{5-}$ as a free anion. A symptom of this instability is the small energy gap between occupied and unoccupied sets of orbitals for the free $[AlO_4]^{5-}$ anion, which allows these two sets of orbitals to mix easily when the fragment supports an external perturbation such as the electric field generated by the cage. An analysis of the molecular orbitals in the complex does not suggest that there are strong charge transfers from occupied tetrahedron orbitals to the virtual cage orbitals. It is worth mentioning that for X = Al there is a non-negligible mixing between orbitals of both fragments. However, the charge transfer appears in multiple small contributions and this phenomenon is difficult to quantify. All these results seem to confirm, first, the validity of the clathrate model for the Keggin anion, which can therefore also be formulated as $[XO_4]^{n-}@M_{12}O_{36}$ and, second, the higher polarizability of the β framework. The distinct polarizability of α and β neutral $M_{12}O_{36}$ cages is directly related to the different H-L gap for the two clusters (Figure 4.2), which makes the orbital mixing and further cluster stabilisation greater for the β isomer. The H-L gap is smaller when going from the α to the β form because of a symmetry reduction; the LUMO and LUMO+1 in the T_d symmetry belong to the e and t_1 irreducible representations, respectively, while in the C_{3v} point group the symmetries of these molecular orbitals are e and e + a_2. The combination of these two e orbitals stabilises one of them (LUMO) by 0.20 eV, and slightly destabilises the other by 0.14eV. These values correspond to the silicotungstate anion but the same tendency was found for the other systems. The computed gap is ~2.8 eV for α-tungstates, on average 0.18 eV higher than in the β isomer. For molybdates, the gap is notably smaller for both isomers, on average 2.0 eV for α and 1.85 eV for β. Summarising, two opposing forces compete in the formation of Keggin anions: the major intrinsic stability of the α organisation, which favours the α isomer, and the greater polarizability of the β-cage during the process of building the Keggin framework. This latter factor is probably responsible for the greater stability of the β isomer in highly charged, fully oxidised anions.

α/β *Stability in Reduced Clusters*

Let us now analyse the role of metallic electrons in the α/β equilibrium. A Keggin framework has a special ability to accept electrons without decomposing. Actually, the Keggin core is a *reservoir* of electrons that can undergo many electron reduction processes without significantly deforming the framework.[20] It is well known that the β isomer reduces at more positive potentials[7a] and, consequently, reduced β isomers increase their relative stability in relation to α isomers. Calculations carried out on the single-reduced anions $[XW_{12}O_{40}]^{(n+1)-}$, X = P, Si and Al completely agree with this observation since the computed $\Delta E_{\beta-\alpha}$ is more favourable to the β isomer than in the oxidised parents. Thus, for X = Al, the reduction increased the relative stability of the β isomer by 0.22 eV and the $\Delta E_{\beta-\alpha}$ for this reduced species was –0.57 eV. For X = P and X = Si, the reduction also increased the stability of the β isomer quite considerably but the α form was still more stable. This considerable stabilisation of β isomers can also be explained by the lower energy of their LUMO (Figure 4.2).

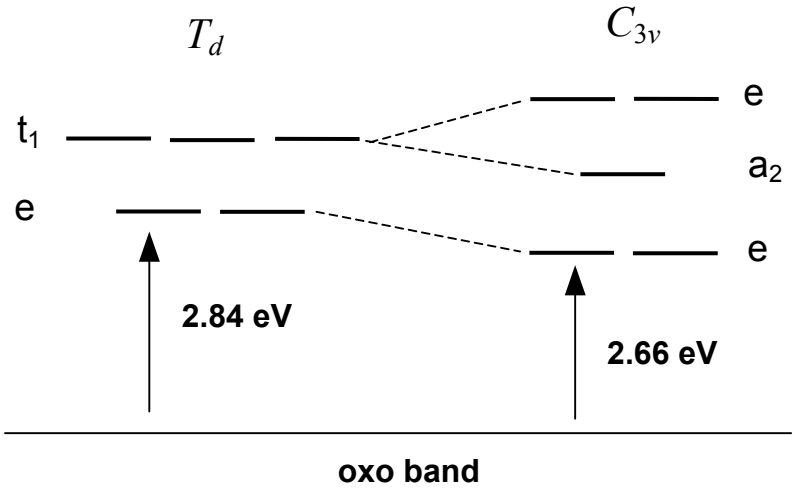

Figure 4.2. Symmetry descent representation from T_d to C_{3v} point groups for the frontier orbitals region of the α and β isomers of $[SiW_{12}O_{40}]^{4-}$. The values are relative to the energy of the HOMO.

In order to determine the factors affecting the stability inversion in reduced species —that is, the number of metal electrons, the central ion and the addenda— we calculated the parameter $\Delta E_{\beta-\alpha}$ for a series of reduced Keggin anions and $M_{12}O_{36}$ cages as a function of the number I of metal electrons, where I was between 0 and 4. Figure 4.3 shows this dependence for the clusters studied. Let us look first at $W_{12}O_{36}$. Although in the neutral cluster the α isomer is initially the most stable by 0.4 eV, after the third reduction both clusters have similar energies ($\Delta E_{\beta-\alpha}$ = –0.02 eV). And when the orbital of e symmetry is filled (I = 4), the stability of the β-cage is 0.14 eV higher. There is almost a linear dependence between this energy difference and the number of metal electrons. When a $[PO_4]^{3-}$ is encapsulated in the interior of the cage, the $\Delta E_{\beta-\alpha}$ values shift toward lower energies, which confirms once again that the presence of an anion inside the cage favours the stability of the β isomer. Thus, for the four-times-reduced $[PW_{12}O_{40}]^{7-}$ complex, the β isomer is more stable by 0.40 eV. In fact, the α/β inversion in the $PW_{12}O_{40}$ framework occurs for I = 2 but the energy difference is only 0.04 eV.

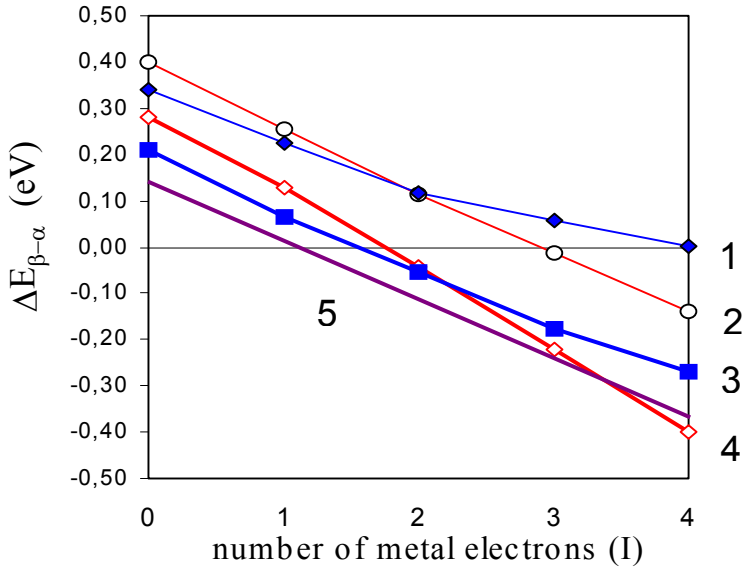

Figure 4.3. Representation of the computed $\Delta E_{\beta-\alpha}$ values for a series of Keggin anions and cages in several reduction states. **1**: $Mo_{12}O_{36}$, **2**: $W_{12}O_{36}$, **3**: $PO_4^{3-}@Mo_{12}O_{36}$, **4**: $PO_4^{3-}@W_{12}O_{36}$, **5**: $SiO_4^{4-}@Mo_{12}O_{36}$.

In general, reduced molybdates behave like their corresponding tungstates but there are some significant differences. Perhaps the greatest of these is that absolute energy differences between the two isomers are smaller. This can be seen in the smaller slope in Figure 4.3. Let us take $Mo_{12}O_{36}$; for $I = 0$, the α form is, as in the homologous tungstate, the lowest in energy but in the molybdate cluster the energy difference between the two forms is 0.06 eV smaller ($\Delta E_{\beta-\alpha}$ = 0.34 eV). The reduction increases the relative stability of the β isomer. However, the increase in stability of this isomer is not enough to induce an inversion of the α/β stability in the isolated $Mo_{12}O_{36}$ cage. The H-L energy gap also makes it possible to rationalise the different behaviour of molybdates and tungstates. Although the descent from T_d to C_{3v} symmetry lowers the H-L gap by 0.14 eV for $W_{12}O_{36}$ and by 0.13 eV for the molybdate cage —a smaller but very similar value— this difference tends to be larger between tungstates and molybdates when metallic electrons are added. For the 4-electron-reduced cages, the H-L gaps are 0.28 eV and 0.18 eV for W and Mo cages, respectively. It is worth noting from Figure 4.3 that the encapsulation of a $[PO_4]^{3-}$ produces almost exactly the same stabilisation in both cages. Therefore, as in the isolated cage, the values for $\Delta E_{\beta-\alpha}$ vary less in the phosphomolybdate cluster than in the analogous tungstate (between +0.21 eV and –0.27 eV for M = Mo and between +0.28 and –0.40 eV for M = W). To our knowledge, the four-times-reduced beta phosphotungstate Keggin cluster has not been reported yet. However, the structure of α-$[PMo_{12}O_{40}]^{7-}$ has been characterised by X-ray spectroscopy.[21] From the structural properties of this cluster, Pope and co-workers proposed no localisation of the four metal electrons.[11a] Present calculations confirm this interpretation since the degenerate e orbital, which accommodates the four additional electrons, is delocalised over the twelve molybdates.

The case in which $Mo_{12}O_{36}$ encapsulates a $[SiO_4]^{4-}$ should be mentioned in particular. The larger negative charge in the internal tetrahedron increases the relative stability of the β isomer by shifting the $\Delta E_{\beta-\alpha}$ energies toward even lower values. A direct consequence is that, for $[SiMo_{12}O_{40}]$, the α/β inversion occurs for I = 1. This result completely agrees with the recent study reported by Sécheresse and coworkers[14], who provided evidence for the greater thermodynamic stability of the β-$[SiMo_{12}O_{40}]$ isomer even when the cluster has one or two metallic electrons. When the internal tetrahedron contains a $[AlO_4]^{5-}$ the beta isomer is more

stabilised than the beta isomer in the analogous silicon derivative ($\Delta E_{\beta-\alpha}$ = –0.1 eV). But both compounds require one–electron reduction undergo inversion of stability. This behaviour is slightly different from that of the homologous tungstate for which the inversion occurs for $I = 0$.

It should be remarked that all the energies shown in Figure 4.3 were computed retaining T_d and C_{3v} symmetries for α and β isomers, respectively. The partial occupation of the doubly degenerate orbitals (Figure 4.2) might yield, however, a Jahn–Teller (J–T) distortion for one- and three-times-reduced anions in both isomers. Keggin clusters are rigid molecules and, in general, J–T distortions are quite small. Previous calculations on α-$[Co^{III}W_{12}O_{40}]^{5-}$, a cluster with a paramagnetic heteroatom, showed that the distortion of the geometry from T_d to D_{2d} only stabilises the anion in 1.4 kcal mol^{-1}.[8] We have checked the eventual importance of J–T distortions in the α/β equilibrium of heteropolyblues performing geometry optimisations for the single reduced $[PW_{12}O_{40}]^{4-}$ cluster, under D_{2d} and C_s symmetry restrictions for α and β isomers, respectively. By means of the strategy suggested by Daul and co-workers,[22] we got consistent energies for the various points on the adiabatic potential surface associated with the J–T distortions. The orbital of *e* symmetry in T_d splits into a_1 and b_1 in D_{2d}, therefore there are two ways for accommodating one electron, $a_1^1\ b_1^0$ and $a_1^0\ b_1^1$. The result of optimising these configurations were two slightly distorted structures, in which the most stable is ~1.1 kcal mol^{-1} lower in energy than the T_d geometry. For the beta form the same process can be followed and the stabilisation reached is ~1.3 kcal mol^{-1}. Furthermore, for two-times-reduced structures, even a minor distortion should occur. Thus, it can be concluded that the $\Delta E_{\beta-\alpha}$ values of Figure 4.3 will remain almost unchanged if heteropolyblues with unpaired electrons are optimised with lower symmetry than that of the fully oxidised parents.

Finally, we would like to point out that the reduction of the cluster does not change the net charge on the internal tetrahedron since the additional electrons go to addenda symmetry-adapted orbitals, which are centred in the outer metal-oxide core. For example, for $[PW_{12}O_{40}]^{4-}$ the unpaired electron is completely localised on the outer sphere and, consequently, the net charge on the internal tetrahedron is only 0.03 e larger than in the parent oxidised cluster. Therefore, according to the clathrate model, fully oxidised Keggin anions may also be formulated as $[XO_4]^{n-}@M_{12}O_{36}$ and the associated reduced clusters as $[XO_4]^{n-}@[M_{12}O_{36}]^{I-}$, where *I* is the reduction state.

As concluding remarks, we claim that the hypothesis[9] that a fully oxidised Keggin anion may be viewed as a $[XO_4]^{n-}$ ion encapsulated by a neutral $M_{12}O_{36}$ was fully confirmed by the calculations, and this model, together with an energy partitioning analysis, enabled us to rationalise the thermodynamic α/β-stability in these important compounds. Although the relative stability of these isomers is governed by a variety of factors, this study illustrates that most of them are related to the relative energy of metallic $M_{12}O_{36}$ orbitals. The calculations led us to formulate the following general rules:

i) in fully oxidised anions the α isomer is, in most cases, the most stable due to the greater intrinsic stability of the α organisation of d^0 metals and oxo ligands,

ii) the relative stability of the β isomer increases as the charge of the cluster localised in the internal tetrahedron increases. This behaviour originates in the higher polarizability of β cage,

iii) there is a strong relationship between the presence of metallic —or blue— electrons in the addenda and the increase in the β–isomer stability,

iv) the energies of α- and β-molybdoderivatives are always more similar than the energies of homologous tungstates,

v) the energy differences between both isomers are larger when X is a third row element.

The α isomer, therefore, displays the largest stability for X = P, M = W and I = 0 (I is the number of metal electrons). $\Delta E_{\beta-\alpha}$ for this cluster was computed to be +0.28 eV. This energy becomes negative for the highly charged fully oxidised systems $[AlW_{12}O_{40}]^{5-}$ and $[GaW_{12}O_{40}]^{5-}$ (–0.35 and –0.19 eV, respectively). For the four–times–reduced clusters $[PW_{12}O_{40}]^{7-}$ and $[SiMo_{12}O_{40}]^{8-}$, the β isomer is ~0.4 eV more stable. Although the largest relative stability of the β isomer was found for the single reduced cluster of the tungstoaluminate derivative (–0.57 eV), successive reductions of this cluster should increase this energy. All these different properties can be inferred from the symmetry reduction when going from α to β and the subsequent decrease in energy of the LUMO, which is responsible for the changes in the relative stability for these two isomers. Current calculations,

however, cannot explain why α-reduced molybdates tend to isomerise to β but α reduced tungstates do not. It is likely that this behaviour will only be understood by taking kinetic considerations into account.

4.2. Mixed-addenda Keggin Anions: A Study of the Redox Properties

Experimental studies

At the end of the 1960's, the work of C. Tourné and G. Tourné[23] created interest in how addenda substitution can affect POMs. Their work permitted a rapid growing of the research in this field in the subsequent decades. Klemperer and co-workers,[9,24] with the aim of obtaining suitable polyoxometalate-supported organometallic derivatives, carried out most research on the Lindqvist isopolyanion. Mixed-addenda HPA research is even more extensive since Keggin- and Dawson-type derivatives can give rise to a greater number of stoichiometries, shapes and aggregates. The addenda W^{VI}, Mo^{VI}, V^{V} and Nb^{V} and the main group heteroatoms P and Si are the most common metal ions in Keggin and W–D HPAs, but other fourth (Ti,[35e,25] Zr[26]), fifth (Ta)[27] and sixth (Cr)[28] row transition metal elements have been incorporated into the POM framework. Lanthanides, actinides[29] and non-transition metal derivatives have also been reported.[35b,g,30] A considerable number of traditionally paramagnetic atoms have been included in the framework of Keggin and W–D anions, as well as in the sandwich-type molecules[31] derived from them. This is a growing area in which rational methods for systematically modifying POM structures have still to be fully developed.[32]

In this section, the general properties of $[SiM_3W_9O_{40}]^{n-}$ Keggin clusters is discussed. A family of compounds with M = Mo, V and Nb were computed and their redox properties analysed. Firstly, the structural characteristics and qualitative results on the electronic structure are discussed. For a quantitative description of the redox properties of this family of molecules, we studied the reduced clusters. Fundamentally, the goal of this section is to discuss the energies of reduction in relation to the substituting element, M. Another relevant feature of these anions is the basicity of their external oxygens. Calculations aimed at describing the

basicity of Keggin anions are presented in chapter 6. The reader shall meet the relationship between the basicity and the ability to dimerise that some clusters have.

Analysis of the geometry and electronic structure of SiM_3W_9 anions

In previous sections we showed that quantum chemistry calculations based on the DFT formalism can be very useful for understanding and rationalising the electronic and magnetic properties of Keggin anions.[8,33] The systematic study of $[XM_{12}O_{40}]^{n-}$ clusters correctly described the redox properties and their magnetic features.[34]

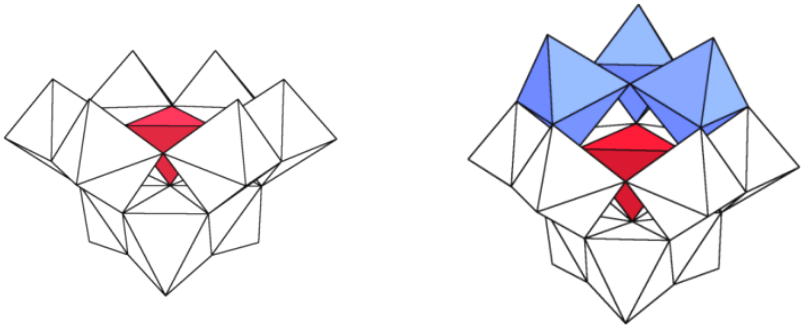

Figure 4.4. Polyhedral representation of the mixed-addenda anion, A-α-$SiM_3W_9O_{40}$, and the parent lacunary form, A-α-SiW_9. The blue polyhedra share corners and contain the M atoms. In the series of molecules discussed here, white polyhedra contain tungsten ions.

Figure 4.4 shows a polyhedral view of a three-times-substituted Keggin tungstosilicate. The chemical composition of the cluster and the shape of the framework define the properties of a POM. For example, the improvement in the catalytic activity of polyanions is closely related to addenda substitution.[35] Like in single-addenda clusters, formally two sets of orbitals are identifiable in substituted clusters without paramagnetic ions: a set of doubly occupied MOs, delocalised over the oxo ligands, and a set of unoccupied d-like addenda orbitals that conform the metallic band. For the present discussion about A-α-SiM_3W_9 systems, with M = Mo, V and Nb,

full geometry optimisations were carried out under C_{3v} symmetry constraints. We assume that present DFT calculations reproduce the geometry of the heteropolyanions well enough for the purpose of the discussion (see Table 4.4).

Table 4.4. Structural parameters computed for the SiM_3W_9 clusters discussed in this section. Distances are in angstrom units.

	$[SiMo_3W_9O_{40}]^{4-}$	$[SiV_3W_9O_{40}]^{7-}$	$[SiNb_3W_9O_{40}]^{7-}$
distance			
$M–O_{term}$	1.74	1.65	1.81
M–M	3.73	3.54	3.77
$M–O_{brid}(M)$	1.91	1.83	1.96
$M–O_{brid}(W)$	1.93	1.99	2.09
Si–M	3.58	3.58	3.72
$M–O_{tetra}$	2.39	2.48	2.56
angle			
$M–O_{brid}–M$	154.5°	150.8°	148.1°

In fact, with the exception of the metal-terminal oxygen bond lengths, that are computed systematically ~0.04 Å longer than the experimental ones, the deviations are in average small. They seem to depend on the net charge in the internal tetrahedron, indeed.

From the DFT results obtained for various SiM_3W_9, the empty set of d-metallic orbitals appears, after the addenda substitution, as a mixture of d-W and d-M orbitals. The order, energy and composition of the molecular orbitals strongly depend on M. There is no doubt that the redox properties of the substituted cluster will be governed by the nature of M. Let us analyse the results concerning the H-L gaps in this series of compounds. In the α-XW_{12}, the H-L gap was computed to be ~2.8 eV at the DFT level (section 4.1). This energy decreases to ~2.0 eV in the homologous molybdates. The lower H-L gap in molybdates means that they are, in general, more easily reduced. Hence, for instance, $SiMo_{12}$ and $GeMo_{12}$ are more powerful

oxidising agents than the corresponding tungstates by ~0.5 V.[36] The other fundamental variable that plays an essential role in the oxidant power is the total negative charge of the anion. Pope and Varga[37] rationalised the first cathodic potential dependence with the negative charge for Keggin anions (Figure 4.5), where the internal atom X fixes the charge. The potential to be applied for reducing a Keggin anion is linearly dependent with the charge of the anion. Thus, the higher the charge, the stronger the potential. This is an important point to be taken into account when calculating and comparing reduction energies for a set of POMs.

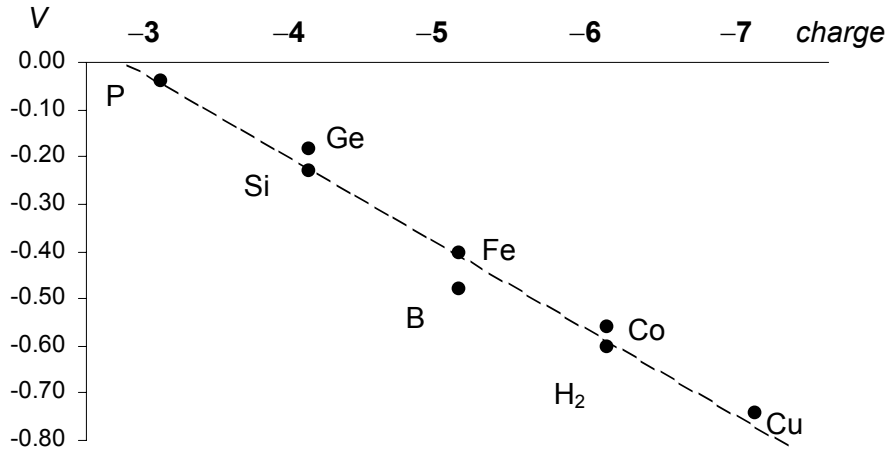

Figure 4.5. Dependence of the first reduction potentials of non-protonated α-$[XW_{12}O_{40}]^{n-}$ clusters (V *vs* sce) with the charge of the anion. Data extracted from references 7a and 37.

Thus, starting from the single-addenda dodecatungstate, the substitution of three tungsten ions by three molybdenum ions modifies the relative energy of the LUMO from 2.8 eV to 2.5 eV in A-α-$SiMo_3W_9$ (Figure 4.6). In the mixed-addenda $SiMo_3W_9$, the LUMO is a degenerate orbital of e symmetry with a larger participation of d-molybdenum orbitals. Since the total charge of the anion does not change, the simple substitution of tungsten by molybdenum increases the oxidising power of the anion. In particular, present DFT calculations indicate that the monoreduction of A-α-$SiMo_3W_9$

is ~0.4 eV more favourable than that of α-SiW_{12}, a value comparable to the previously reported 0.54 V obtained experimentally.[38]

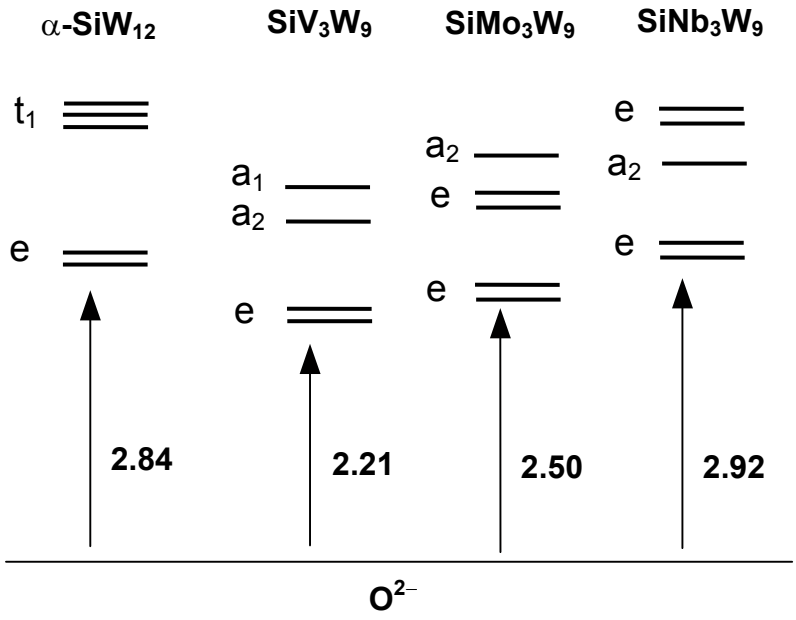

Figure 4.6. Energy-scaled MO diagram for α-$[SiW_{12}O_{40}]^{4-}$ and the series of A-α-$[SiM_3W_9O_{40}]^{n-}$ anions computed for this section. The labelled molecular orbitals are the unoccupied metallic ones. The H-L gaps are showed in eV.

In this series of substituted Keggin anions, the group 5 derivative, A-α-SiV_3W_9, has an H-L gap of 2.21 eV. This is even a lower gap than that computed for A-α-$SiMo_3W_9$. The LUMO in the vanadium derivative, which is a degenerate orbital of e symmetry, and the LUMO+1, which appears ~2.9 eV from the HOMO, are d_{xy}–orbitals essentially localised on the vanadium centres. This means that the vanadotungstate might preferentially be reduced in the vanadium centres, that is, $V^V \rightarrow V^{IV}$ processes would occur before $W^{VI} \rightarrow W^V$. This result is consistent with the electrochemical data obtained by Hervé and co-workers.[39–40] Results concerning the important matter of the reduction sites in mixed-addenda clusters is also discussed in chapter 5 with the Wells–Dawson anion, in which mixed Mo/V

centres compete for the metallic electrons. Another paradigmatic case is shown in chapter 7, where the localisation of the metallic electrons in a capped system containing V and Mo is studied in deep. It shall be shown that the problems of orbital quasi-degeneration need more complicated ways to be solved.

Finally, the analogous niobium derivative has an H-L gap of 2.92 eV (Figure 4.6), which is somewhat larger than the single-addenda dodecatungstate. This behaviour combined with the higher negative charge of the Nb-substituted derivative means that the substitution of W by Nb always decreases the oxidising power of the anion.

Table 4.5. Percentile contributions to the first three unoccupied metallic orbitals of the series of fully oxidised A-α-$[SiM_3W_9O_{40}]^{n-}$ anions computed.

Anion	*% Contribution* [a]		
	LUMO	*LUMO+1*	*LUMO+2*
A-α-$[SiV_3W_9O_{40}]^{7-}$	65/10	64/7	69/5
A-α-$[SiMo_3W_9O_{40}]^{4-}$	46/20	7/57	0/65
A-α-$[SiNb_3W_9O_{40}]^{7-}$	7/59	1/63	17/48

a) In the format (%M)/(%W).

The relative energy and composition of the LUMO is quite well correlated to the electron affinity of each *isolated* M^{n+} ion, which is in the order $Mo^{6+} > V^{5+} > W^{6+} >> Nb^{5+}$. The first reduction potentials are −68.10 eV (Mo^{6+}), −65.72 (V^{5+}), −63.95 eV (W^{6+}) and −49.96 (Nb^{5+}) at the present level of theory. Nb is systematically less willing to gain electrons than any other metal of this series. Figure 4.7 shows the series of reductions starting from the maximum oxidation numbers to the metallic state.

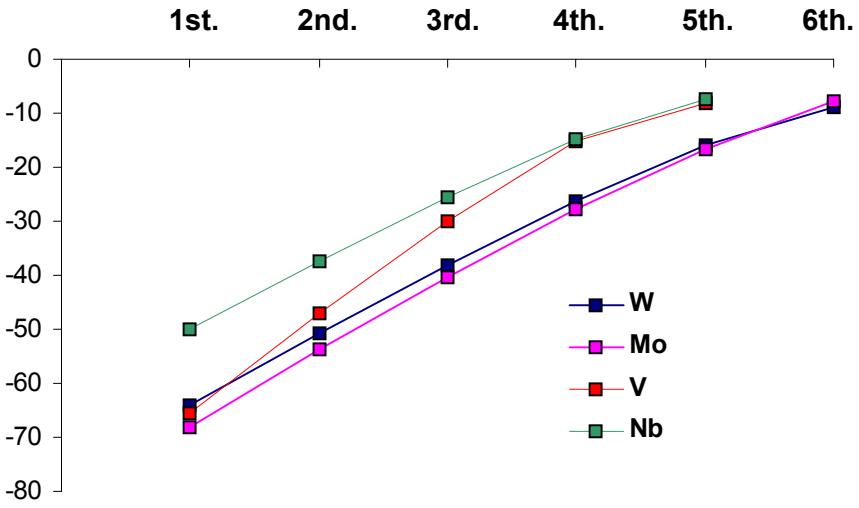

Figure 4.7. First to sixth energies of reduction, in eV, for the addenda cations discussed in this section. The reference oxidation numbers are W^{6+}, Mo^{6+}, V^{5+} and Nb^{5+}. Thus, the x-axis represents the reduction processes *1st.*: $W^{6+} \rightarrow W^{5+}$, *2nd.*: $W^{5+} \rightarrow W^{4+}$, or *1st.*: $V^{5+} \rightarrow V^{4+}$, and so on.

In agreement with these reduction energies, present DFT calculations gave the following LUMO compositions (see Table 4.5): for the niobotungstate, only 7% of Nb and 59% of W contribution. When M = Mo, the sharing of the LUMO is 46/20% for Mo/W and, finally, the LUMO has the largest heteroatom participation, 65%, for SiV_3W_9. The tungsten contribution is 10%. This mixed cluster has the lowest H-L gap.

Unrestricted calculations of single-reduced Keggin anions were performed in order to confirm the predictions made by orbital analysis. J–T effects might take place in monoreduced species since a degenerate *e* orbital is populated with one electron. Nevertheless, previous calculations on single addenda Keggin anions[33] showed that the stabilisation due to the J–T effect is very small and it has not been considered here.

Table 4.6. Spin polarisations for the series of single-reduced A-α-$[SiM_3W_9O_{40}]^{n-}$ anions.

Anion	*Spin polarisation* [a]	
	W_9	M_3
$[SiV_3W_9O_{40}\ 1e]^{8-}$	0.15	1.04
$[SiW_9Mo_3O_{40}\ 1e]^{5-}$	0.20	0.72
$[SiW_9Nb_3O_{40}\ 1e]^{8-}$	0.87	0.13

a) α − β electrons for nine tungstens and three heteroatoms

Spin polarisation given in Table 4.6 reinforce the qualitative predictions based on the molecular orbitals of the oxidised species, which suggest that the additional electron in the monoreduced species A-α -SiW_9V_3 is delocalised over the three vanadium atoms (0.35 spin alpha electrons per V). Some extra polarisation in the molecule yields a population of 0.012 spin alpha electrons per W. In the analogous molybdate, 70% of the additional electron is distributed among the three Mo centres. Finally, when the substituting addenda is the Nb^{5+} ion, the orbitals of the substituting addenda do not participate in the LUMO and the spin density is localised in the W centres in 87%. Although the ionisation energies of isolated metal ions would suggest that the reduction of mixed vanadomolybdates would take place at the molybdenum centres, the extra electron mostly goes to a vanadium atom.[8,39] Notice in Figure 4.5 that the V orbital is the lowest of the four LUMO. The particular behaviour of the Mo^{6+} and V^{5+} pair arises from the different electronic population of d orbitals in fully oxidised clusters, which is larger for Mo atoms.

We conclude, from the results of this section, that two factors govern the redox properties of a POM: the energy and composition of the lowest unoccupied orbitals, being formally symmetry-adapted d_{xy}-type orbitals developed on the addenda atoms and the total charge of the anion. In the α-XM_{12} anion, all metals are equivalent and so they all have the same probability of trapping the additional electron when the cluster is reduced. When the ion W^{6+} in the 1:12 tungstate is substituted by a more electronegative Mo^{6+} ion, the energy of the LUMO decreases and the cluster is more easily reduced, the additional electron going to a Mo orbital. The

same phenomenon takes place when a V^{5+} replaces a W^{6+}: the extra electron goes to the vanadium center. Mixed niobotungstates behave differently since niobium orbitals are energy high lying. They are inserted into the tungsten band and the reduction of $SiNb_3W_9$ for example, yields the *blue* species $SiNb_3W_9$1e and not the cluster $SiNb^{V}_{2}Nb^{IV}W_9$.

References and Notes

[1] Baker, L. C. W.; Figgis, J. S. *J. Am. Chem. Soc.* **1970**, *92*, 3794.

[2] Recent publications on the γ, δ and ε isomers are: Cadot, E.; Béreau, V.; Marg, B.; Halut, S.; Sécheresse, F. *Inorg. Chem*. **1996**, *35*, 3099. Rowsell, J.; Nazar, L. F. *J. Am. Chem. Soc.* **2000**, *122*, 3777. Müller, A.; Beugholt, C.; Kögerler, P.; Bögge, H.; Bud'ko, S.; Luban, M. *Inorg. Chem*. **2000**, *36*, 5176.

[3] (a) Pope, M. T. *Inorg. Chem*. **1976**, *15*, 2068. (b) Tézé, A.; Hervé, G. *J. Inorg. Nucl. Chem*. **1977**, *39*, 2151. (c)Kepert, D. L. *The Early Transition Elements*. Academic Press, New York, **1972**, pp. 46–60, 288–304.

[4] Yamamura, K.; Sasaki, Y. *J. Chem. Soc., Chem. Commun.* **1973**, 648.

[5] Matsumoto, K. Y.; Kobayashi, A.; Sasaki, Y. *Bull. Chem. Soc. Jpn.* **1975**, *48*, 3146.

[6] Weinstock, I. A.; Cowan, J. J.; Barbuzzi, E. M. G.; Zeng, H.; Hill, C. L. *J. Am. Chem. Soc.* **1999**, *121*, 4608.

[7] (a) Pope, M. T. *Heteropoly and Isopoly Oxometalates*. Springer-Verlag. Berlin, **1983**. (b) Hill, C. L. ed. *Chem. Rev.* **1998**, *98*, 1–390 (special issue on Polyoxometalates).

[8] Maestre, J. M.; López, X.; Bo, C.; Casañ-Pastor, N.; Poblet, J. M. *J. Am. Chem. Soc.* **2001**, *123*, 3749.

[9] Day, V. W.; Klemperer, W. G. *Science*. **1985**, *228*, 533.

[10] Tézé, A.; Hervé, G. *J. Inorg. Nucl. Chem.* **1977**, *39*, 999.

[11] (a) Barrows, J. N.; Jameson, G. B.; Pope, M. T. *J. Am. Chem. Soc.* **1985**, *107*, 1771. (b) Müller, A.; Krickemeyer, E.; Penk, M.; Wittneben, V.; Döring, J. *Angew. Chem., Int. Ed. Engl.* **1990**, *29*, 88.

[12] (a) Harrup, M. K.; Kim, G-S.; Johnson, R. P.; VanDerveer, D.; Hill, C. L. *Inorg. Chem.* **1998**, *37*, 5550. (b) Xin, F.; Long, G. J.; Russo, U.; Pope, M. T. *Inorg. Chem.* **1996**, *35*, 1207. (c) Kortz, U.; Jeannin, Y. P.; Tézé, A.; Hervé, G.; Isber, S. *Inorg. Chem.* **1999**, *38*, 3670. (d) Robert, F.; Tézé, A.; Hervé, G.; Jeannin, Y. *Acta Cryst.* **1980**, *B36*, 11. (e) Kawafune, I.; Matsubayashi, G-e. *Bull. Chem. Soc. Jpn.* **1996,** *69*, 359.

[13] Tézé, A.; Canny, J.; Gurban, L.; Thouvenot, R.; Hervé, G. *Inorg. Chem*. **1996**, *35*, 1001.

[14] Dolbecq, A.; Cadot, E.; Eisner, D.; Sécheresse, F. *Inorg. Chem.* **1999**, *38*, 4217.

[15] (a) Ziegler, T; A. Rauk, *Teor. Chim. Acta* **1977**, *46*, 1. (b) Ziegler, T; Rauk, A; *Inorg. Chem.* **1979**, *18*, 1558−1565.

[16] Morokuma, K. *J. Chem. Phys*. **1971**, *55*, 1236.

[17] The Deformation Energy (*DE*) is defined as the energy difference between the fragment energy and the energy of the corresponding subunit in its optimal, fully relaxed conformation. The *DE* for $M_{12}O_{36}$ therefore represents the energy required for transforming this cage from its hypothetical equilibrium structure to the geometry it has in the Keggin anion.

[18] González-Blanco, O.; Branchadell, V. *Organometallics.* **1997**, *16*, 475. González-Blanco, O.; Branchadell, V. *Organometallics.* **1997**, *16*, 5556. González-Blanco, O.; Branchadell, V.; Gree, R.; *Chem. Eur. J.* **1999**, *5*, 1722−1727. González-Blanco, O.; Branchadell,V. *Organometallics*. **2000**, *19*, 4477−4482.

[19] Breneman, C. M.; Wiberg, K. B. *J. Comp. Chem*. **1990**, *11*, 361.

[20] Maestre, J. M.; Bo, C.; Poblet, J.-M.; Casañ-Pastor, N.; Gómez-Romero, P. *Inorg. Chem.* **1998**, *37*, 3444.

[21] Vitoria, P.; Ugalde, M.; Gutiérrez-Zorrilla, J. M.; Román, P.; Luque, A.; San Felices, L.; García-Tojal, J. *New. J. Chem*. **2003**, *2*, 399.

[22] Bruydonckx, R.; Daul, C.; Manoharan, P. T.; Deiss, E. *Inorg. Chem.* **1997**, 36, 4251.

[23] Tourné, C.; Tourné, *G. Bull. Soc. Chim. Fr.* **1969**, 11244.

[24] (a) Klemperer, W. G.; Shum, W. *J. Am. Chem. Soc.* **1977**, *99*, 3544. (b) Klemperer, W. G.; Shum, W. *J. Am. Chem. Soc.* **1978**, *100*, 4891. (c) Filowitz, M.; Ho, R. K. C.; Klemperer, W. G. *Inorg. Chem.* **1979**, *18*, 93. (d) Besecker, C. J.; Klemperer, W. G. *J. Am. Chem. Soc.* **1980**, *102*, 7598−7600. (e) Day, V. W.; Fredrich, M. F.; Thompson, M. R.; Klemperer, W. G.; Liu, R.-S.; Shum, W. *J. Am. Chem. Soc.* **1981**, *103*, 3597–3599. (f) Besecker, C. J.; Klemperer, W. G.; Day, V. W. *J. Am. Chem. Soc.* **1982**, *104*, 6158–6159. (g) Besecker, C. J.; Day, V. W.; Klemperer, W. G.; Thompson, M. R. *J. Am. Chem. Soc.* **1984**, *106*, 4125–4136. (h) Day, V. W.; Klemperer, W. G.; Maltbie, D. J. *Organometallics.* **1985**, *4*, 104. (i) Besecker, C. J.; Day, V. W.; Klemperer, W. G.; Thompson, M. R. *Inorg. Chem.* **1985**, *24*, 44. (j) Day, V. W.; Klemperer, W. G.; Schwartz, C. *J. Am. Chem. Soc.* **1987**, *109*, 6030–6044. (k) Day, V. W.; Klemperer, W. G.; Maltbie, D. J. *J. Am. Chem. Soc.* **1987**, *109*, 2991. (l) Day, V. W.; Klemperer, W. G.; Lockledge, S. P.; Main, D. J. *J. Am. Chem. Soc.* **1990**, *112*, 2031. (m) Day, V. W.; Klemperer, W. G.; Main, D. J. *Inorg. Chem.* **1990**, *29*, 2345–2355. (n) Day, V. W.; Klemperer, W. G.; Main, D. J. *Inorg. Chem.* **1990**, *29*, 2355–2360.

[25] Tourné, C. *C. R. Acad. Sci. Ser. C.* **1968**, *226*, 702–704. Ho, R. K. C.; Klemperer, W. G. *J. Am. Chem. Soc.* **1978**, *100*, 6772–6774. Knoth, W. H.; Domaille, P. J.; Roe, D. C. *Inorg. Chem.* **1983**, *22*, 198–201. Domaille, P. J.; Knoth, W. H. *Inorg. Chem.* **1983**, *22*, 818–822. Maksimov, G. M.; Kuznetsova, L. I.; Matveev, K. I.; Maksimovskaya, R. I.; *Koord. Khim.* **1985**, *11*, 1353–1357. Maksimov, G. M.; Kustova, G. N.; Matveev, K. I.; Lazarenko, T. P.; *Koord. Khim.* **1989**, *15*, 788–796. Keana, J. F. W.; Ogan, M. D.; *J. Am. Chem. Soc.* **1986**, *108*, 7951–7957. Lin, Y.; Weakley, T. J. R.; Rapko, B.; Finke, R. G. *Inorg. Chem.* **1993**, *32*, 5095–5101. Yamase, T.; Ozeki, T.; Sakamoto, H.; Nishiya, S.; Yamamoto, A. *Bull. Chem. Soc. Jpn.* **1993**, *66*, 103–108. Chen, Y. G.; Liu, J. F. *Polyhedron.* **1996**, *15*, 3433–3436. Crano, N. J.; Chambers, R. C.; Lynch, V. M.; Fox, M. A. *J. Mol. Catal. A: Chem.* **1996**, *114*, 65–75. Detusheva, L. G.; Fedotov, M. A.; Kuznetsova, L. I.; Vlasov, A. A.; Likholobov, V. A. *Izv. Acad. Nauk, Ser. Khim.* **1997**, 914–920. Nomiya, K.; Arai, Y.; Shimizu, Y.; Takahashi, M.; Takayama, T.; Weiner, H.; Nagata, T.; Widegren, J. A.; Finke, R. G. *Inorg. Chim. Acta.* **2000**, *300–302*, 285–304.

[26] Finke, R. G.; Rapko, B.; Weakley, T. J. R. *Inorg. Chem.* **1989**, *28*, 1573 and see Barnard, D. L.; Hill, C. L.; Cage, T.; Matheson, J. E.; Huffman, J. H.; Sidwell, R. W. Otto, M. I. Schinazi, R. F. *Intl. Antiviral News.* **1995**, *3*, 159–161.

[27] Torchenkova, E. A.; Nguyen Dieu; Kazanskii, L. P.; Spitsyn, V. I. *Izv. Akad. Nauk. SSSR, Ser. Khim*. **1973**, 734. Radkov, E.; Beer, R. H. *Polyhedron*. **1995**, *14*, 2139. Radkov, E.; Lu, Y-J.; Beer, R. H. *Inorg. Chem.* **1996**, *35*, 551–552.

[28] Wassermann, K.; Lunk, H.-J.; Palm, R.; Fuchs, J. *Acta Crystallogr*. **1994**, *C50*, 348. Wassermann, K.; Palm, R.; Lunk, H.-J.; Fuchs, J.; Steinfeld, N.; Stösser, R.; *Inorg. Chem.* **1995**, *34*, 5029–5036. Wassermann, K.; Lunk, H.-J.; Palm, R.; Fuchs, J.; Steinfeld, N.; Stösser, R.; Pope, M. T. *Inorg. Chem.* **1996**, *35*, 3273–3279.

[29] The first lanthanide complex of a lacunary Wells–Dawson anion was reported by (a) Peacock, R. D.; Weakley, T. J. R. *J. Chem. Soc. A.* **1971**, 1836. See more recent work of (b) Knoth, W.H.; Domaille, P. J.; Harlow, R. L. Inorg. Chem. **1986**, *25*, 1577–1584. (c) Bartis, J.; Dankova, M.; Lessmann, J. J.; Luo, Q-H.; Horrocks, Jr., W. D.; Francesconi, L. C. *Inorg. Chem.* **1999**, *38*, 1042–1053. (d) Luo, Q-H.; Howell, R. C.; Dankova, M.; Bartis, J.; Williams, C. W.; Horrocks, Jr., W. D.; Young, Jr., V. G.; Rheingold, A. L.; Francesconi, L. C.; Antonio, M. R. *Inorg. Chem.* **2001**, *40*, 1894–1901 and references therein.

[30] Knoth, W. H.; Domaille, P. J.; Roe, D. C. *Inorg. Chem.* **1983**, *22*, 198–201. Domaille, P. J.; Knoth, W. H. *Inorg. Chem.* **1983**, *22*, 818–822. Liu, J.; Ortega, F.; Sethuraman, F.; Katsoulis, D. E.; Costello, C. E.; Pope, M. T. *J. Chem. Soc., Dalton Trans.* **1992**, 1901. Xin, F.; Pope, M. T.; Long, G. J.; Russo, U. *Inorg. Chem.* **1996**, *35*, 1207–1213. Cowan, J. J.; Bailey, A. J.; Haintz, R. A.; Do, B. T.; Hardcastle, K, I.; Hill, C. L.; Weinstock, I. A. *Inorg. Chem.* **2001**, 40, 6666–6675.

[31] (a) Weakley, T. J. R.; Evans, H. T.; Showell, J. S.; Tourné, C. M.; Tourné, G. F. *J. Chem. Soc. Chem. Commun.* **1973**, 139. (b) Finke, R. G.; Droege, M.; Hutchinson, J. R.; Gansow, O. *J. Am. Chem. Soc.* **1981**, *103*, 1587–1589. (c) Finke, R. G.; Droege, M. *Inorg. Chem.* **1983**, *22*, 1006–1008. (d) Evans, H. T.; Tourné, C. M.; Tourné, G. F.; Weakley, T. J. R. *J. Chem. Soc. Dalton Trans.* **1986**, 2699–2705. (e) Finke, R. G.; Droege, M. W.; Domaille, P. J. *Inorg. Chem.* **1987**, *26*, 3886–3896. (f) Weakley, T. J. R.; Finke, R. G. *Inorg. Chem.* **1990**, *29*, 1235–1241. (g) Gómez-García, C. J.; Coronado, E.; Borrás-Almenar, J. J. *Inorg. Chem.* **1992**, *31*, 1667. (h) Casañ-Pastor, N.; Bas-Serra, J.; Coronado, E.; Pourroy, G.; Baker, L. C. W. *J. Am. Chem. Soc.* **1992**, *114*, 10380. (i) Gómez-García, C. J.; Coronado, E.; Gómez-Romero, P.; Casañ-Pastor, N. *Inorg. Chem.* **1993**, *32*, 3378. (j) Gómez-García, C. J.; Borrás-Almenar, J. J.; Coronado, E.; Ouahab, L. *Inorg. Chem.* **1994**, *33*, 4016–4022. (k) Zhang, X.; Jameson, G. B.; O'Connor, C. J.; Pope, M. T. *Polyhedron*. **1996**, *15*, 917. (l) Zhang, X.; Chen, Q.; Duncan, D. C.; Campana, C.; Hill, C. L. *Inorg. Chem.* **1997**, *36*, 4208. (m) Zhang, X.; Chen, Q.; Duncan, D. C.; Lachicotte, R. J.; Hill, C. L. *Inorg. Chem.* **1997**, *36*, 4381. (n) Clemente-Juan, J. M.; Coronado, E.; Galán-Mascarós, J. R. Gómez-García, C. J. *Inorg. Chem.* **1999**, *38*, 55 (o) Andres, H.; Clemente-Juan, J. M.; Basler, R.; Aebersold, M.; Güdel, H-U.; Borrás-Almenar, J. J.; Gaita, A.; Coronado, E.; Büttner, H.; Janssen, S. *Inorg. Chem.* **2001**, *40*, 1943–1950.

[32] Anderson, T. M.; Hardcastle, K. I.; Okun, N.; Hill, C. L. *Inorg. Chem.* **2001**, *40*, 6418–6425.

[33] López, X.; Maestre, J. M.; Bo, C.; Poblet, J. M. *J. Am. Chem. Soc.* **2001**, *123*, 9571–9576.

[34] Duclusaud, H.; Borshch, S. A. *J. Am. Chem. Soc.* **2001**, *123*, 2825–2829.

[35] See, for example, (a) Duncan, D. C.; Chambers, R. C.; Hecht, E.; Hill, C. L. *J. Am. Chem. Soc.* **1995**, *117*, 681 and references therein. (b) Cavani, F.; Koutyrev. M.; Trifirò, F. *Catal. Today*. **1996**, *28*, 319–333. (c) Kogan, V.; Aizenshtat, Z.; Neumann, R. *Angew. Chem. Int. Ed.* **1999**, *38*, 3331–3334. (d) Bagno, A.; Bonchio, M.; Sartorel, A. Scorrano, G. *Eur. J. Inorg. Chem.* **2000**, 17–20. (e) Kholdeeva, O. A.; Maksimov, G. M.; Maksimovskaya, R. I.; Kovaleva, L. A.; Fedotov, M. A.; Grigoriev, V. A.; Hill, C. L. *Inorg. Chem.* **2000**, *39*, 3828–3837. (f) Zeng, H.; Newkome, G. R.; Hill, C. L. *Angew. Chem. Int. Ed.* **2000**, *39*, 1771–1774 and ref. 2 therein. (g) Khenkin, A. M.; Shimon, L. J.; Neumann, R. *Eur. J. Inorg. Chem.* **2001**, 789–794. (h) Nishiyama, Y.; Nakagawa, Y.; Mizuno, N. *Angew. Chem. Int. Ed.* **2001**, *40*, 3639–3641.

[36] Hervé, G. *Ann. Chim. (Paris)* **1971**, 6, *219*. *Ibid*, **1971**, 6, *287*. Launay, J. P.; Massart, R.; Souchay, P. *J. Less-Common Met.* **1974**, *36*, 139. Altenan, J.J.; Pope, M.T.; Prados, R.A.; So, H. *Inorg. Chem.* **1975**, *14***,** 417; Maeda, K.; Katano, H.; Osakai, T.; Himeno, S. *J. Electroanal. Chem.* **1995**, *389***,** 167.

[37] Pope, M. T.; Varga, G. M. *Inorg. Chem.* **1966**, *5*, 1249–1254.

[38] Souchay, R.; Hervé, G. *C. R. Acad. Sci., Ser. C*. **1965**, *261*, 2486. Contant, R.; Fruchart, J. M.; Hervé, G.; Tézé, A. *C. R. Acad. Sci., Ser. C*. **1974**, *278*, 199.

[39] Cadot, E.; Fournier, M.; Tézé, A.; Hervé, G. *Inorg. Chem.* **1996**, *35*, 282–288.

[40] Mossoba, M. M.; O'Connor, C. J.; Pope, M. T.; Sinn, E.; Hervé, G.; Tézé, A. *J. Am. Chem. Soc.* **1980**, *22*, 6864–6866.

CHAPTER 5

Electronic Properties of Wells–Dawson Anions

Together with the Keggin anion, studied in previous chapters, the Wells–Dawson molecule is, probably, the second heteropolyanion in popularity. Its structure is somewhat larger and, in general, can be formulated as $X_2M_{18}O_{62}^{n-}$. Some similarities are visible in the shape of Keggin and Wells–Dawson anions. In spite to this, some properties are different, indeed. The main goal of this chapter is to describe, in a systematic way, the geometry and electronic properties related to the structure, and they are compared with regard to the Keggin anion. The redox properties are studied in relation to the electronic structure. Both single- and mixed-addenda compounds are studied and compared for finding general rules of chemical behaviour. The last part of the chapter is devoted to the isomerism. Three isomeric forms are known for the Wells–Dawson anion: α, β and γ. We will focus the attention of the reader in the first two, the most commonly studied, showing what are the major differences compared to Keggin anions. So, the relative stability of the α/β pairs is examined as well as the changes introduced in the reduction potential as we vary the shape or the chemical composition.

5.1. Electronic Structure of α-Wells–Dawson Anions

Fully oxidised structures

We have seen in Chapter 4 that the most common structure amongst all the heteropolyanions, the Keggin structure, has twelve equivalent metal centres in its α form, which confers the experimentally observed T_d symmetry to the framework. A. F. Wells[1] in the middle 40's first postulated the structure for the α-$P_2W_{18}O_{62}^{6-}$ anion. In 1953, Dawson reported the first (low-resolution) X-ray experiment for the same anion,[2] whereas Strandberg[3] and D'Amour[4] later reported more accurately results to determine the structure, now formulated in general as $X_2M_{18}O_{62}^{n-}$. Those reports did not confer full equivalence to the eighteen metal centres, so a distinction was made between polar (α_2 positions or *caps*) and equatorial regions (α_1 positions or *belts*). The two polar fragments are composed of three edge-sharing octahedra (triads), whereas the equatorial M_{12} array is formed via alternative corner- and edge-sharing MO_6 units, as displayed in Figure 5.1.

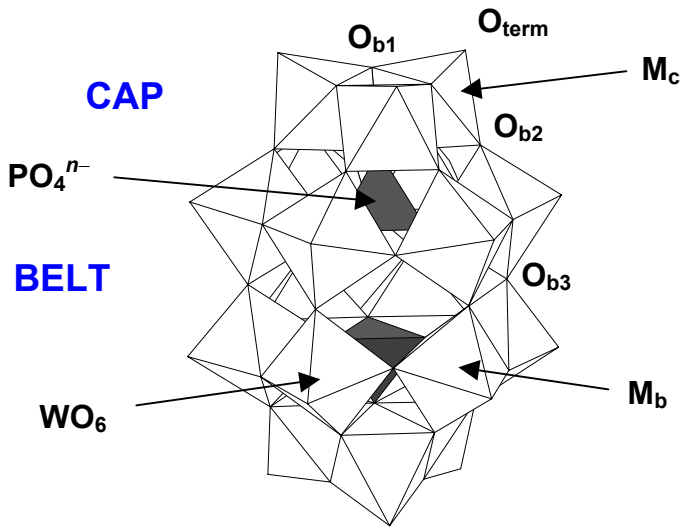

Figure 5.1. Polyhedral representation of the α-$P_2W_{18}O_{62}^{6-}$ Wells–Dawson anion. Two identical fragments or hemispheres are easily identifiable, each composed of one capping triad and one equatorial belt with six WO_6 octahedra. Relevant positions are labelled for further discussion.

Each of the equatorial octahedra is connected to a polar octahedron by a single corner and it shares one edge with a neighbour of the same belt and a corner to the other belt. Two $XO_4^{(n/2)-}$ units are encapsulated inside the formally neutral $M_{18}O_{54}$ cage,[5] containing the greater part of the negative charge of the POM. The structural characterisation of the WD anion is compatible with a D_{3h} point group of symmetry. From the information provided here concerning the nature of the assembly of the octahedra in the WD framework, not only a geometrical distinction but a chemical one can be made for the two different regions of the structure

The WD derivative is may be seen as a derivative of the Keggin structure as follows. The removal of three neighbouring corner-sharing octahedra in, say, α-PW_{12}, produces a lacunary structure, formulated as A-α-PW_9, which is ready to join another equivalent moiety to produce the α-P_2W_{18} assembly (Figure 5.2). ESR and electrochemical studies[6] have shown that WD anions are chemically different compared to the Keggin species in some aspects. To be more concrete, it has been shown that the localisation of extra electrons (metallic electrons) does not obey a strict balanced sharing but there are preferential sites for the trapping of these electrons, differently from the single-addenda α-Keggin case. An explanation to this phenomenon is found in the geometric parameters that make the Keggin and the WD forms different. In this section we will deal only with single-addenda WD structures, introducing the general features like the electronic structure and related properties.

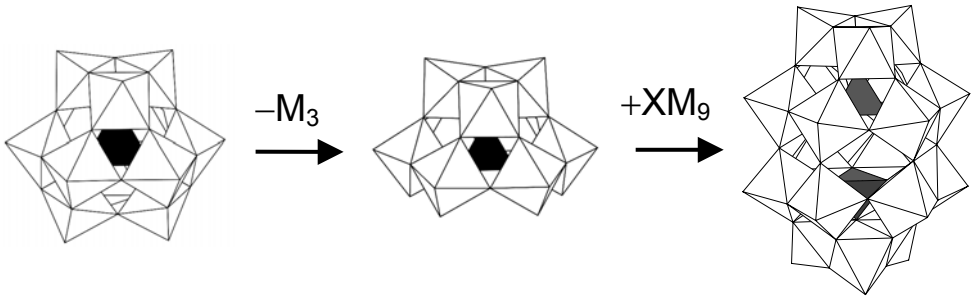

Figure 5.2. Polyhedral representation of the α-XM_{12} Keggin anion, the A-XM_9 lacunary anion derived by removing 3 corner-sharing octahedra, and the Wells–Dawson structure X_2M_{18}, formed by adding an M'$_3$ or another A-XM_9 unit, respectively.

Some structural parameters in WD anions are special. We highlight the M–O–M angle between corner-sharing octahedra of the two belts in the equatorial region. It was computed at the DFT level, being 163º in both P_2W_{18} and P_2Mo_{18} cases. The experimentally measured value is fairly close to that, about 162º.[3] The corresponding M–O–M angle in the cap is close to 125º, the typical value of edge-sharing Keggin-like triads. So, almost linear M–O–M angles appear linking the two halves of the anion and this fact has serious implications in the chemistry of the WD molecule. One of them is

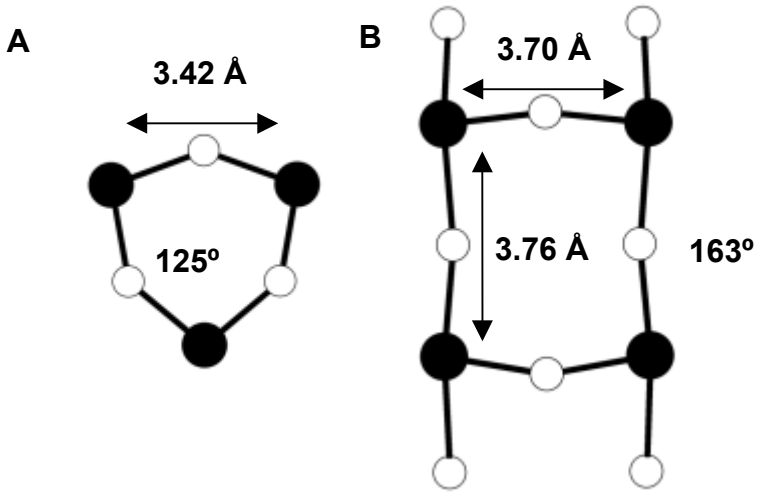

Figure 5.3. Relevant distances and angles for the P_2W_{18} Wells–Dawson anion (black circles–tungsten, white circles–oxygen). In A only metal atoms and bridging oxygens of a polar triad are represented. In B, a part of the equatorial region is shown. Of the four metal atoms represented, those separated by 3.70 Å belong to the same belt, whereas the separation of 3.76 Å is between the two belts.

that metal centres are much more separated, in average by 3.7–3.8 Å, than in polar regions, where the distance between two neighbouring metals is ~3.4 Å, the typical distance in Keggin forms. In the caps, edge-sharing octahedra imply smaller MOM angles and shorter M–M distances (Figure 5.3), whereas in the belt regions, octahedra linked by corners allow metal centres to be farther, and, in addition, MOM angles are bigger. The other structural parameters are somehow common to all the heteropolyanions. In tungstates, all the W=O (terminal) bond lengths were computed to be ~1.74 Å, a value

that is very similar to the W=O distance found for XW_{12} structures[7–8] and it is 0.05 Å longer than the experimental distance. The W–O (bridge) distances are also similar to those found in Keggin anions. They are about 1.90–1.94 Å in the tungstate. In principle, the error introduced in the terminal distances may not alter the reduction properties discussed here since they essentially would affect to the d_{xz}- and d_{yz}-type orbitals that are not involved in the most common reduction processes of these species[8] (see chapter 3). This is so since they do not contribute to the lowest unoccupied MOs. We will see below that some new considerations have to be discussed for the case of 2:18 molybdates.

Table 5.1. Percentile contributions of belt and cap metal centres to the LUMO, LUMO+1 and LUMO+2 for single-addenda WD anions.

Anion	*Sym*	*Belt*	*Cap*	*Belt*	*Cap*	*Belt*	*Cap*
		a_1”		e”		e’	
P_2W_{18}	D_{3h}	70	0.5	61	10	20	48
P_2Mo_{18}	D_{3h}	62	1	54	9	22	40

A deeper analysis of the MO structure of WD anions shows the typical arrangement found in most of the heteropolyanions containing only early transition metals, where the oxo band and the empty set of d_{xy}-metal orbitals are perfectly separated. For comparison, Figure 5.4 contains an energy diagram for the lowest unoccupied orbitals of 1:12 and 2:18 tungstates and the 2:18 molybdate. It is worth noting that the relative energy of the unoccupied set of orbitals is lower in the case of WD anions, compared to the Keggin form displayed. Table 5.1 gives percentile metal contributions to the LUMO, LUMO+1 and LUMO+2 for idealised D_{3h} P_2W_{18} and P_2Mo_{18} structures. All these unoccupied orbitals are formally symmetry adapted d_{xy}-tungsten orbitals with some antibonding participation of the oxygen orbitals (Figure 5.5). Under the constraints of the D_{3h} point group, the symmetries of the first three unoccupied orbitals are a_1”, e” and e’, respectively. The contribution of cap and belt metals to these three orbitals is unequal; the d_{xy}-orbitals centred on the belt metals are the major contributors to the LUMO and LUMO +1. When the energy of the orbital increases the participation of the cap-centred atomic orbitals also increases (from, ~1% in the LUMO to

~48% in the LUMO+2 in the tungstate and to ~40% in the molybdate). A 3D representation of the a_1" orbital (Figure 5.5) shows that the LUMO is only localised over the *belt* tungstens. It should be pointed out that this orbital appears at 2.25 eV above the occupied oxo band, 0.55 eV lower than the relative energy of the degenerate LUMO of e symmetry in PW_{12}. The metal orbitals in PW_{12} and P_2W_{18} have an antibonding character between the metal and oxygen orbitals but also between two adjacent metals. The M–M antibonding interaction is lower when the two adjacent metals belong to two different PW_9 moieties (the metal-metal distances are longer) and therefore the d_{xy}-type orbitals delocalised among the equatorial tungstens have lower energies than the corresponding orbitals in the Keggin structure.

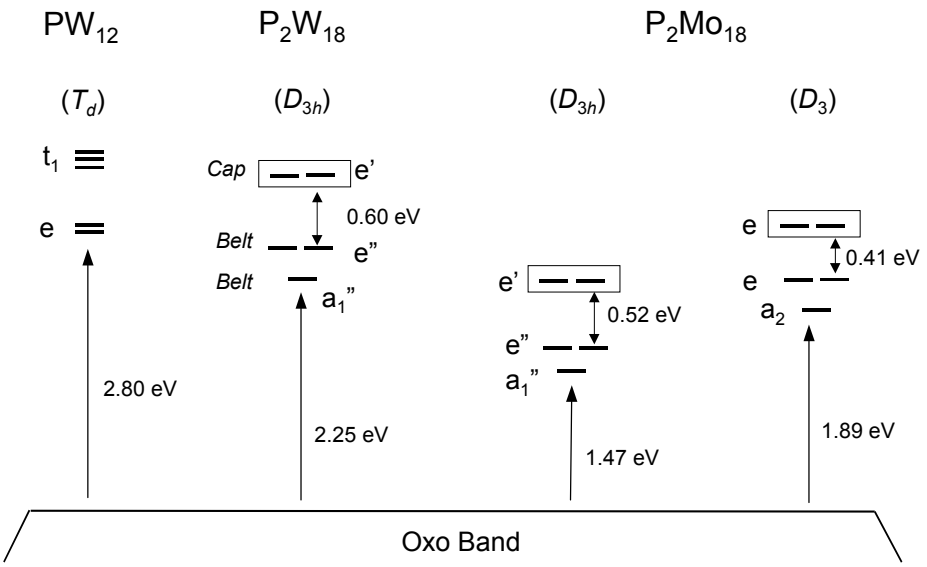

Figure 5.4. Molecular orbitals scheme for the α-PW_{12} anion and the single-addenda WD heteropolyanions with M = W and Mo. In the latter case, we show the orbitals associated to the D_{3h} and D_3 structures. The orbitals in frames are those localised on the polar triads of the corresponding WD structures.

Let us introduce here the case of the molybdate anion. It is well known from experiments that heteropolyanions in general, and 2:18 molybdates in particular, have a very characteristic structure. In fact heteropolymolybdates

in general. Whereas the α-P_2W_{18} anion possesses D_{3h} symmetry, the homologous molybdate is formed of three interpenetrating loops of alternately long and short Mo–O bonds, therefore the structure is distorted. This phenomenon confers chirality to the anion, the symmetry of which is D_3. Experimental evidence of the chirality was obtained from X-ray data,[3-4] ^{17}O NMR,[9] IR spectroscopy and optical rotatory dispersion[10-11] measurements. Both symmetric and distorted geometries were computed at the DFT level for the 2:18 molybdate anion. The bridging Mo–O bonds computed for the D_3 geometry range between

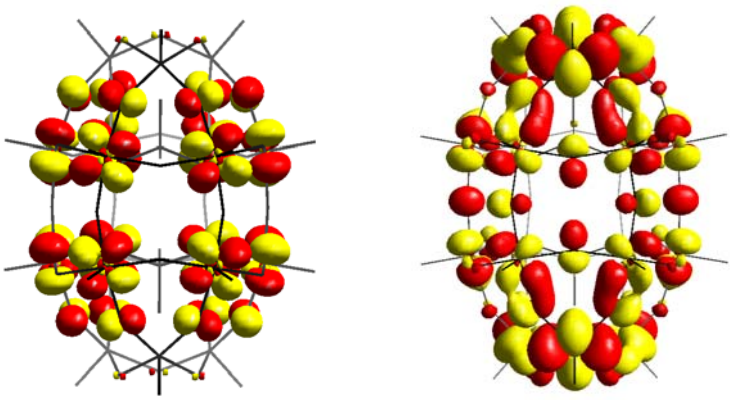

Figure 5.5. It is showed a 3D representation of the LUMO and LUMO+2 (one component) of α-P_2W_{18}. The first one is clearly localised on the equatorial centres, whereas the major contribution of the second orbital comes from the polar regions.

1.84 and 2.12 Å,[12] distances in close agreement with the X-ray data available (1.8–2.1 Å). On the other hand, the Mo=O_{term} distances and all the angles are very close to those of the tungstate anion. The D_{3h}-idealised, highly-symmetric α structure has a LUMO 1.47 eV above the oxo band, an energy that represents again a decrease of 0.56 eV with respect to the H-L gap in PMo_{12}. The equatorial belts maintain the traditional Mo–O distances, of about 1.9 Å. The lowering of the symmetry from D_{3h} to D_3 is accompanied by a considerable stabilisation of 0.32 eV (>7 kcal mol^{-1}) and an enlargement of the H-L gap to 1.89 eV. This value is quite close to the

energy gap of 2.03 eV found for the idealised T_d form of α-PMo_{12}.[8] So, in general, the transformation of a PM_{12} into a P_2M_{18} decreases the H-L gap more in tungstates than in molybdates.

Reduced single-addenda structures

The redox properties of a given molecule are intimately related to the energy and composition of the LUMO. According to the orbital diagram in Figure 5.4, the first reduction in P_2W_{18} and P_2Mo_{18} must take place in the *belt* region. After the exploration of the electronic structure of fully oxidised POMs we can explicitly reduce the clusters to get more precise information about the localisation of the metal electrons and the energy required for carrying out the reductions. Calculations conducted on the reduced structures confirmed the hypothesis that equatorial metals would accept extra electron first, and the ground state for the single reduced P_2W_{18} is a $^2A_1$" with 98% of the spin density localised over the belt metals (Table 5.2).

Table 5.2. Spin polarisation (α – β) and relative energies (in eV) for the first three lowest states in several single-addenda reduced WD Anions.

	Sym	(α – β)		*E*	(α – β)		*E*	(α – β)		*E*
		$^2A_1$			^2E"			^2E'		
		Belt	Cap		Belt	Cap		Belt	Cap	
P_2W_{18}	D_{3h}	0.98	–0.03	0.00	0.87	0.13	0.30	0.26	0.69	0.84
P_2Mo_{18}	D_{3h}	0.89	–0.05	0.00	0.83	0.14	0.20	0.27	0.66	0.69

The first excited state (^2E") has the spin density essentially localised over the belt metal centres (87%) and lies at about 0.30 eV above the ground state. The reduction in the cap sites requires about 0.84 eV more than the ground-state reduction; it involves the addition of one electron to the LUMO+2 (e'). In that case, the associated state is ^2E'. The term ^2E' is characterised by having 0.69 alpha electrons delocalised among the six cap tungsten atoms and 0.26 e among the twelve belt-centres. For the analogous molybdate, the energy associated to the belt ($^2A_1$") and cap (^2E') reductions differs by 0.69 eV for the D_{3h} isomer (exactly the energy gap between the LUMO and the LUMO+2). In the D_3 form, the separation between these

MOs is the same, which suggests that the energy difference between both site reductions should be very close to the value obtained for the D_{3h} form. All these results fully agree with the experimental data of Pope[6b] and Contant[22] who demonstrated that equatorial sites are more easily reduced than polar sites. These values of spin polarisation and electron localisation are in fair accordance with the study of the electronic structure of oxidised clusters, which is the proof that a simple MO analysis is a good approximation to study the features of the reduced molecule.

Calculations carried out for α-P_2W_{18} of symmetry D_{3h} showed that the reduction at the cap sites –addition of one electron to the LUMO+2 (e')– requires 0.84 eV more than the reduction at the belt sites –addition of one electron to the LUMO (a_1").[12] The spin polarisation data confirm that the first metallic electron is delocalised over the *belt* metal centres. For the two-fold-reduced species, both the high- and low-spin electronic configurations were computed. In α-P_2W_{18}, the closed-shell configuration $(a_1")^2$ $(e")^0$ (see Figure 5.10) was found to be 4.0 kcal mol^{-1} more stable than the triplet state $(a_1")^1$ $(e")^1$, which was determined allowing Jahn–Teller relaxation. These results agree with the lack of ESR signal for the two-electron-reduced species.[6c] It is well established that Keggin anions and related structures with an even number of delocalised electrons have a diamagnetic behaviour. Although it was initially attributed to a strong antiferromagnetic coupling via a multiroute superexchange mechanism,[13] recent theoretical studies have shown that electron repulsion and electron delocalization can also stabilise the singlet ground state.[14-16] The theoretical analysis of the coupling of delocalised electrons is a sophisticate problem that, in the case of large systems like POMs, will still need some time to have concluding results.

We can associate now all the features exposed above with the particular structure of WD anions. We saw at the beginning of the chapter what are the main structural differences between P_2M_{18} and PM_{12} molecules. These are centred in the equatorial region, where almost linear M–O–M linkages unite the two belts. First, the antibonding interactions between neighbouring metals from different belts are less effective since they are, in average, 0.3 Å further from each other compared to the M–M distance in a polar triad. Second, there is no contribution of the bridging oxygens (O_{b3}) in this region. Only antibonding interactions appear between belt metals and O_{b2} sites. Neither between belt metals and belt oxygens an antibonding overlapping occurs since there are symmetry restrictions that forbid the p-O_{b3} orbitals to

contribute to the LUMO. Therefore, only a few antibonding p(O)-d(M) interactions appear in the LUMO, and the overall balance for this property allows this MO to be very low in energy.

5.2. Effect of the Chemical Substitution on the Redox Properties of α-Wells–Dawson Anions

After exposing in detail the characteristics of the WD anions with only one type of addenda metal, we can face now the study of more complex clusters, not from a geometrical point of view but concerning the chemical composition. The region of frontier orbitals of a given α-X_2M_{18} anion follows a unique rule; the LUMO and LUMO+1 are composed, nearly exclusively, by contributions of the valence d orbitals centred in the *equatorial* metals plus some contribution of bridging-oxygen p orbitals (see representation in Figure 5.5). On the other hand, the first unoccupied MO localised on the cap octahedra is considerably high in energy. In this section we explore the effect of combining different elements in the same framework, dealing with the most common early transition-metal elements appearing in POMs: W, Mo, V and Nb. The main goal is to describe the MOs of suitable $P_2M_{15}M'_3$ anions and to study their redox properties by means of the knowledge of the electronic structure. In this representation, the three M' centres are all located in the same cap, thus sharing edges. It is expected that the most important changes are introduced in this region, and that a modest influence spreads to other parts of the framework. The principal change in the electronic structure of the WD anion we can think of is one in which the single-addenda (Section 5.1) belt/site reduction order is inverted. We could manage with this task if a more electronegative ion is inserted in the polar region substituting the original addenda metals. Vanadium (in the oxidation state 5+) or molybdenum (VI) are good candidates for this goal, and $P_2W_{15}V_3$ or $P_2W_{15}Mo_3$ are suitable anions for illustrating this phenomenon. In these two clusters, as the three substituting atoms occupy the three neighbouring polar sites of one α-PM_9 moiety, the point group of symmetry is formally reduced from D_{3h} to C_{3v}.

Analysis of $PW_{15}M_3$ derivatives

The first case in study is $P_2W_{15}V_3$. The structural changes introduced in this cluster are limited to the region of substitution. The V=O distances are about 1.65 Å, the bridging V–O–V bonds are 1.85 Å long, and the V–O–W about 1.98 Å. Thus, the shorter V–O–V bonds allow the vanadium centres to be closer, at only 3.24 Å. We may say that this tendency of localisation of the geometrical changes is general in HPAs. The outstanding characteristic of V^{5+} cations is their high affinity to *blue* electrons, especially compared to W^{6+} centres. As we showed for Keggin derivatives containing W and V, vanadium-centred MOs lower their energy and, in the present case, an inversion in the order of belt/cap d_{xy}-like orbitals occurs. The degenerate orbital of e symmetry (e' in the single-addenda species) turns out to be the LUMO in the V-substituted molecule. It is now fairly localised in the cap region with some contribution of the neighbouring belt of Ws. We provide a representation of this orbital in Figure 5.6.

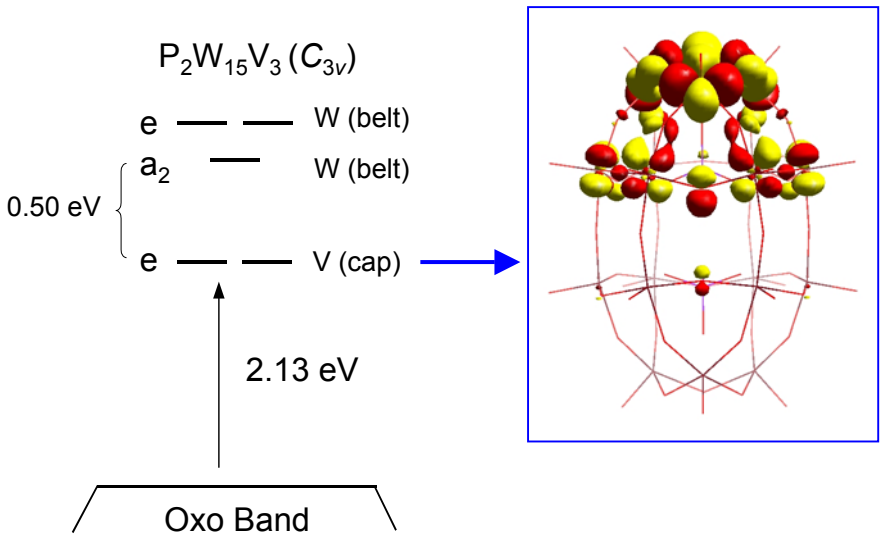

Figure 5.6. Scheme of the molecular orbitals for the V-substituted WD anion, α-$P_2W_{15}V_3$, and 3D representation of the LUMO.

Table 5.3. Percentile contributions of belt and cap metal centres to the LUMO, LUMO+1 and LUMO+2 for mixed-addenda WD anions.

Anion	*Sym*	*Belt*	*Cap*	*Belt*	*Cap*	*Belt*	*Cap*
		LUMO		LUMO+1		LUMO+2	
$P_2W_{15}V_3$	C_{3v}	13	60	65	0	55	10
$P_2W_{15}Mo_3$	C_{3v}	70	2	55	15	49	19
$P_2W_{15}Nb_3$	C_{3v}	66	0	61	7	51	16
$P_2Mo_{15}V_3$	C_{3v}	36	33	59	0	39	26
$P_2Mo_{15}Nb_3$	C_{3v}	60	0	63	3	57	5

Furthermore, it appears well-separated (0.50 eV at the DFT level) from the next two orbitals of a_2 and e symmetry, which are mainly d-W (belt) orbitals (schematic diagram in Figure 5.6). According to this orbital ordering, the first reduction would happen in vanadium cap orbitals and the energy difference between the two site reductions ($^2E - {}^2A_2$) was found to be 0.33 eV. The spin polarisation for the ^2E ground state of $P_2W_{15}V_31e$ confirms that the additional electron is essentially localised on the vanadium centres (Table 5.3), although some residence of the metallic electron is possible over the upper belt of tungstens. We did not study the introduction of V in the equatorial positions. In such a case, the LUMO would be a vanadium orbital with even a larger energy gap between it and the first W-centred MO, since the most electronegative *element* is in the most electronegative *site* (belt). Thus, the first reduction may take place in the belt sites and the difference between the belt and cap reduction would be larger than in the case we studied here. All these results are consistent with the studies of Pope and co-workers, who used cyclic voltammograms to find that the most positive cathodic peak for $P_2W_{17}V$ appears when the vanadium occupies a belt site.[6] The ESR spectra of anions substituted solely at the polar sites, $P_2V^{IV}V^{V}W_{16}$ and $P_2V^{IV}V_2{}^{V}W_{15}$ show that the vanadium centres really trap the metallic electron.[17] Now, two factors —the *most favourable belt position* and the *higher electronegativity* of the V^V ion— strongly compete to capture the additional electron.

Table 5.4. Spin polarisation ($\alpha - \beta$) and relative energies (in eV) for the two lowest states in several reduced mixed-addenda WD anions.

	Sym	($\alpha - \beta$)		*E*	($\alpha - \beta$)		*E*
		Belt	Cap		Belt	Cap	
		^{2}E			$^2A_2$		
$P_2W_{15}V_3$	C_{3v}	0.18	1.00	0.00	0.88	–0.011	0.33
$P_2W_{15}Mo_3$	C_{3v}	0.34	0.61	0.00	0.98	–0.03	–0.018
$P_2W_{15}Nb_3$	C_{3v}	0.87	0.095	0.00	0.90	–0.010	–0.14
$P_2Mo_{15}V_3$	C_{3v}	0.44	0.55	0.00	0.81	–0.020	0.18
$P_2Mo_{15}Nb_3$	C_{3v}	0.91	0.052	0.00	0.83	–0.015	–0.076

The second case of metal substitution studied here is that of $P_2W_{15}Mo_3$. Mo^{5+} is again more electronegative than tungsten(VI), although a priori less than vanadium(V). In this case only slight changes are introduced to the electronic structure. As a matter of fact, no inversion is found in the first three (and more relevant) Kohn–Sham molecular orbitals. The LUMO is still an a_2 belt-centred orbital, with only 2% of d-Mo orbitals. Just above in energy appear two degenerate e orbitals with some contribution of Mo: 15% and 19% for LUMO+1 and LUMO+2, respectively. This means that there is some contribution of cap-metals in both e orbitals. Even though, these contributions are all modest, showing that Mo is notably less electronegative than V in metal-oxide frameworks. So, the polar Mo_3O_{13} triad is not expected to accept the first metallic electron since the equatorial Ws are still in advantage for it. In Table 5.3 are shown the percentile contributions and, in Table 5.4, the spin populations of some states of interest concerning the single-reduced system. The reader may notice that the $^2A_2$ state is slightly more stable; at any rate, as the MO show, a strong competition between this and the ^{2}E" occurs since the LUMO and the next orbital are almost degenerate. A schematic diagram of the levels of energy in the $P_2W_{15}M_3$ WD anions computed is in Figure 5.7.

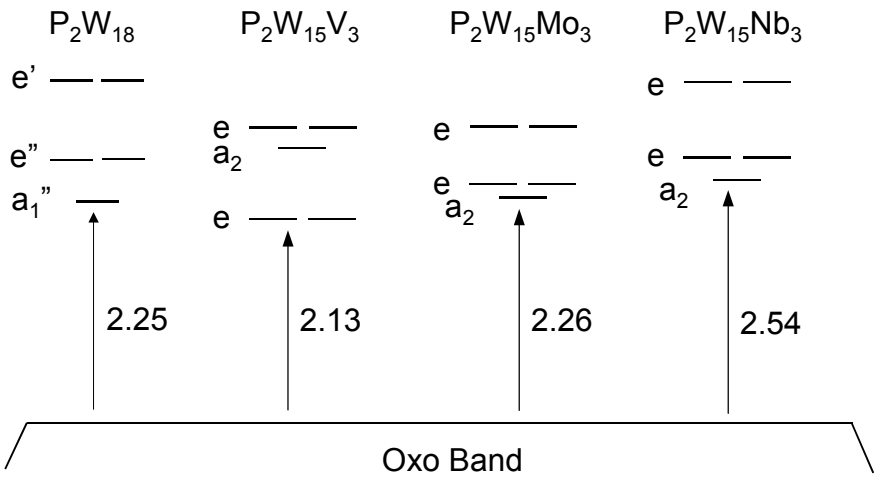

Figure 5.7. Schematic diagram of the frontier orbitals for the series of $P_2W_{15}M_3$ anions computed, with M = V, Mo and Nb. The H-L gaps are represented in eV for comparison.

The third tungsto-derivative studied is $P_2W_{15}Nb_3$. This derivative has the particularity that contains niobium(V), which is known to be less electronegative than W in its highest oxidation state. Probably the novel feature introduced by Nb in this set of WD anions is that the H-L gap is bigger than the parent P_2W_{18} form by 0.3 eV. Although the LUMO is absolutely centred on the belt Ws (66% W, 0% Nb), the presence of Nb in the polar region is more than tangible. We may expect that the oxidising power is decreased when Nb replaces W. The homologous $P_2Mo_{15}Nb_3$ is expected to behave similarly since Nb occupies the cap region and the most EN element is Mo.

One case of special interest is the vanadomolybdate, $P_2Mo_{15}V_3$, where there is a considerable competition between vanadium and molybdenum for the extra electrons. The most electronegative centre occupies the least favoured position in front of reduction and *vice versa*. As Table 5.3 shows, the LUMO of e symmetry in $P_2Mo_{15}V_3$ is not localised in one of the regions of the molecule and the participation of belt Mo (36 %) and cap V (33 %) orbitals is similar. The next metallic orbital of a_2 symmetry is only separated from the LUMO by 0.19 eV and is basically a belt orbital (59 %). This competition between Mo and V orbitals yields a spin density distribution in

the reduced complex of 0.55 e for cap V atoms and 0.44 e for belt Mo atoms. The energy difference between the two states ^2E and $^2A_2$ was computed to be only 0.18 eV. This competition is still more important in $P_2W_{15}Mo_3$ since those two states associated to the first reduction in cap (^2E) and belt ($^2A_2$) sites were found degenerate, result that does not fully match with the fact that the first reductions in $P_2W_{15}Mo_3$ are restricted to the Mo centres.[18-19] Although the origin of this discrepancy is unclear, we believe that present DFT calculations probably exaggerate the energy gap between cap and belt reductions for a given metal. We provide molecular orbital diagrams in Figure 5.8 the mixed-addenda WD systems derived from the 2:18 molybdate, in which three neighbouring capping octahedra were substituted.

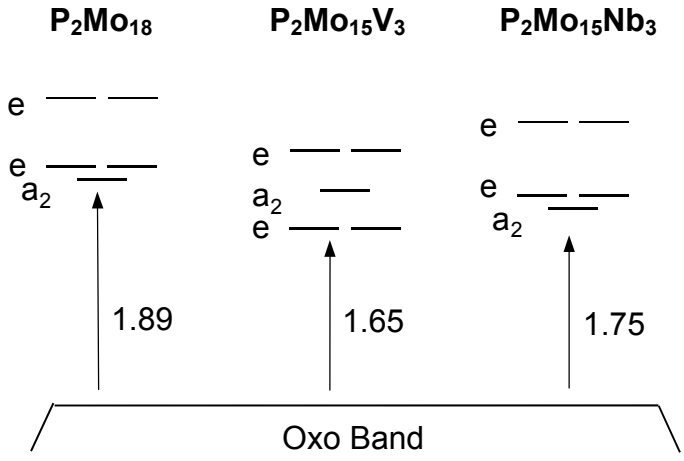

Figure 5.8. Schematic diagram of the frontier orbitals for the series of $P_2Mo_{15}M_3$ anions computed, with M = V and Nb. The H-L gaps are represented in eV.

5.3. Study of the Relative Stability of α/β-Wells–Dawson Anions

Introduction

The comprehension of the rotational isomerism occurring in some heteropolyanions is of great interest for the understanding and the applications of POMs. Although the relative instability of β isomers compared to α be accepted as a general rule, recent experimental and theoretical studies have shown that the differences in stability between the two isomers may be quite small.[20] In chapter 4 we made a detailed analysis of the factors that govern the relative stability of the α and β isomers of the Keggin anion, $[XM_{12}O_{40}]^{n-}$, with M = W, Mo and X a main group element.[8] The α isomer has T_d symmetry and the β isomer, of C_{3v} symmetry is derived from a 60º rotation of one M_3O_{13} triad about a three-fold axis of the α form (Figure 4.1).[21] DFT calculations also showed that the metallic (*blue*) electrons incorporated in the $M_{12}O_{36}$ framework and the greater stability of the β isomer are closely related. This gain in stability of the β isomer may be because there is a reduction in symmetry when going from α to β and a subsequent decrease in the energy of the LUMO. The rotational isomerism of Keggin structures also takes place in WD heteropolyanions. Pope, in the middle 60's,[6] and Contant's group[22] explored the electrochemistry of X_2M_{18} and mixed-addenda derivatives. They found that β anions also gain electrons at more positive potentials than the α forms although the difference is smaller than in α/β-Keggin pairs. Here we extend the previous study of section 5.1 on α-WD heteropolyanions[12] to analyse the α/β isomerism in WD structures. In particular, we focus on the relative stability of these isomers for $[P_2Mo_{18}O_{62}]^{6-}$, $[P_2W_{18}O_{62}]^{6-}$ and $[P_2W_{15}V_3O_{62}]^{9-}$, as well as the effect of the reduction processes on this equilibrium. The redox properties of the α isomer of WD structures were presented in sections 5.1-2. For the β isomer, we can conduct the same procedure to explore the reduction energies. As well as the Keggin anion, WD heteropolyanions can undergo structural isomerisations. If instead of two A-α-PW_9 moieties to give the α-P_2W_{18} framework we formally put together one A-α- and one A-β-PW_9 form, the result is the β-P_2W_{18} anion. This is characterised by having one α- and one β-Keggin-like half. In addition, it exists another isomeric

form, the so-called γ-P_2W_{18}. In this case, both PW_9 subunits are A-β forms. They are not discussed here.

Structure of $P_2W_{15}M_3$ anions

Geometry optimisations performed on the α and β[21,23] isomers of the title anions led to the structures listed below. The α isomer of P_2W_{18} was computed under the constraints of D_{3h} symmetry group whereas, for the corresponding β isomer, the symmetry of the molecule is C_{3v} (representations in Figure 5.9). The reader shall see below that the analogous molybdates have less symmetry.

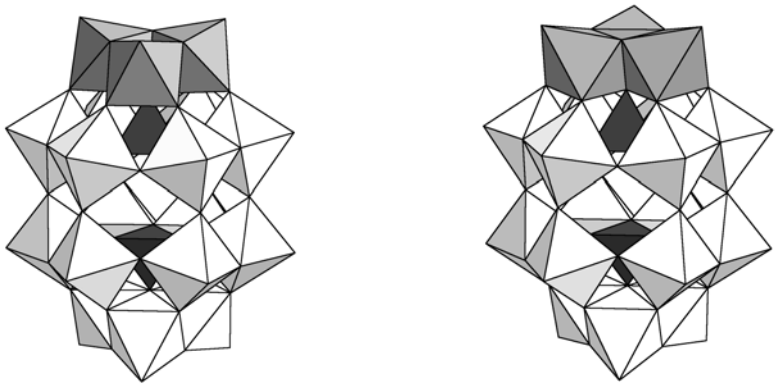

α-$P_2W_{15}M_3$ (D_{3h}) **β-$P_2W_{15}M_3$** (C_{3v})

Figure 5.9. Polyhedral representation of α- and β-$P_2W_{15}M_3$. A 60º rotation of one of the polar triads (shaded) about the vertical three-fold axis of symmetry of the alpha form leads to the beta one.

As it was already commented above, the geometries of the heteropolyanions are very well reproduced at the present level of theory. The largest discrepancy always appears in the W–O_{term} oxygen bonds, which are systematically underestimated by an average of 0.05 Å.[2,4] Deviations in the terminal bonds should not modify the reduction properties discussed here since they would essentially affect the energy of the d_{xz}- and d_{yz}-type orbitals, which are not the lowest. The reader will notice from Table

5.5 that the geometrical differences between isomers of the same formula are very small. Only the $M_b–O_{b3}–M_b$ angle appears to be always 4–5º bigger in the β form.

Table 5.5. Computed angles (in degrees) and interatomic distances (in Å) for a series of fully oxidised α and β Wells–Dawson anions. See Figure 5.1 for the labelling of metal and oxygen sites.

Anion (Sym.)	$M_c–O_{term}$	$M_c–O_{b1}$	$M_c–O_{b2}$	$M_b–O_{b2}$
α-P_2W_{18} (D_{3h})	1.74–1.75	1.94	1.90	1.95
β-P_2W_{18} (C_{3v})	1.74–1.75	1.94	1.90	1.95
α-P_2Mo_{18} (D_3)	1.74	1.89–2.04	1.84–2.05	1.85–2.12
β-P_2Mo_{18} (C_3)[a]	1.74–1.75	1.88–2.05	1.84–2.05	1.86–2.12
α-$P_2W_{15}V_3$ (C_{3v})	1.76–1.77 (W) 1.65 (V)	1.96 (W) 1.85 (V)	1.89 (W) 1.98 (V)	2.01 (W) 1.84 (V)
β- $P_2W_{15}V_3$ (C_{3v})	1.76–1.77 (W) 1.65 (V)	1.96 (W) 1.84 (V)	1.89 (W) 1.98 (V)	2.01 (W) 1.84 (V)

Anion (Sym.)	$M_c–M_c$	$M_b–M_b$[a]	$M_b–O_{b3}–M_b$
α-P_2W_{18} (D_{3h})	3.42	3.70 3.76	163º
β-P_2W_{18} (C_{3v})	3.41–3.42	3.69–3.74 3.78	166º
α-P_2Mo_{18} (D_3)	3.46	3.42–3.74 3.89	163º
β-P_2Mo_{18} (C_3)[b]	3.45–3.47	3.40–3.78 3.88	167–169º
α-$P_2W_{15}V_3$ (C_{3v})	3.46 (W) 3.24 (V)	3.62–3.73 3.84	164º
β- $P_2W_{15}V_3$ (C_{3v})	3.46 (W) 3.25 (V)	3.31–3.41 3.85	168º

a) β-P_2Mo_{18} was optimised without symmetry constraints

b) First values concern two metals on the same belt, whereas the second number is the distance between two metals of different belts.

The substitution of three neighbouring tungsten atoms by vanadiums in one of the polar triads induces some structural changes restricted to the replaced octahedrons. Typically, all the V–O bonds are shorter than the homologous W–O. As a consequence, the V···V distances in the substituted triad are also shorter (3.24 Å) than the typical W···W separation (3.42 Å).

Electronic properties

The discussion of the α/β isomerism in WD clusters might be introduced with regard to that of the Keggin anion. In a first step, a qualitative study of the electronic structure can be of help for understanding their redox properties. Let us show a correlation diagram of the frontier orbitals for the most and least symmetric PW_{12} and P_2W_{18} isomers (Figure 5.10).

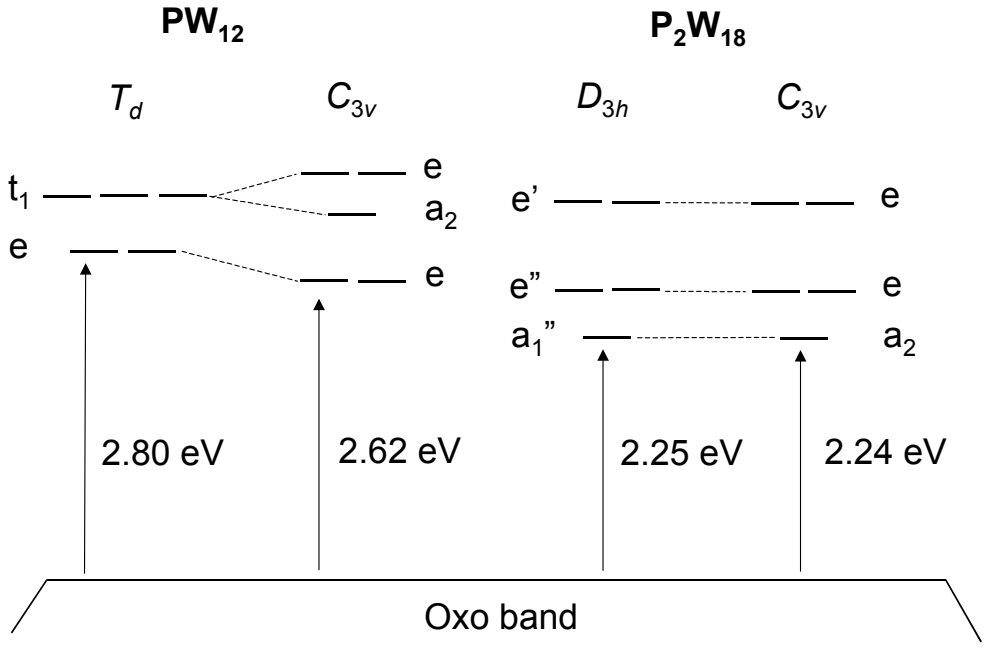

Figure 5.10. Relative energies of the lowest metallic orbitals of the α and β isomers of PW_{12} and P_2W_{18} anions.

The frontier orbitals e and t_1 (LUMO and LUMO+1, respectively) of the α-Keggin split into e and e + a_2 after one W_3O_{13} triad is rotated in the T_d structure to give the β isomer. Mixing the orbitals of the same symmetry leads to a decrease in the H-L gap from 2.80 eV in the T_d geometry to 2.62 eV in the C_{3v} geometry. Consequently, the β forms are always more easily reduced than the corresponding α forms. The formal substitution of three octahedrons in α-XM_{12} anions by a XM_9 unit (to give the WD anion) breaks the equivalence of all metals and two types of metal ions appear in an α-X_2M_{18} framework. Cap and belt metals do not participate in the lowest unoccupied orbitals equally. Whereas the d_{xy} orbitals centred on the twelve *belt* metals are the major contributors to the LUMO (a_1") and LUMO+1 (e"), the LUMO+2 (e') is mainly composed of d_{xy} orbitals centred on the six cap metals. According to this orbital composition, the first reduction in the WD anions takes place in the belt region. The 3D representation of the LUMO is given in Figure 5.11.

From Figure 5.10, it arises that the energy of WD anion frontier orbitals do not change significantly when one of the cap triads is rotated and, therefore, the redox properties of β-P_2W_{18} are expected to be similar to those of the α isomer. By studying the reduced species we can confirm the predictions made from molecular orbital analysis of the oxidised anions. If n is the number of blue electrons in the lowest metallic orbital (a_1" and a_2 for the D_{3h} and C_{3v} isomers, respectively), the energy difference between the isomers hardly changes with n. The magnitude $\Delta E_{\beta-\alpha}$ is 1.83 kcal mol^{-1} for n = 0 and decreases by only 0.13 kcal mol^{-1} for n = 1 and 0.72 kcal mol^{-1} for n = 2. These positive values for $\Delta E_{\beta-\alpha}$ clearly indicate that the α isomer is the most stable but the difference in stability between the two isomers is quite small. The relative thermodynamic stabilities of the α and β of $[P_2W_{18}O_{62}]^{6-}$ were recently established both in solid state by differential scanning calorimetry and in solution by ^{31}P NMR.[24] Both techniques give that the α isomer is more stable than the β one by ~4 kcal mol^{-1}. Taking into account that the theoretical calculations were carried out with the isolated anions the agreement between experimental and theoretical results can be considered excellent.

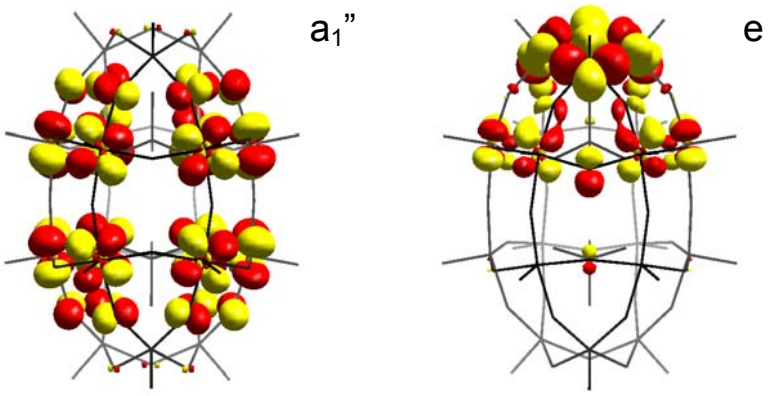

Figure 5.11. 3D representations for the LUMO of α-$[P_2W_{18}O_{62}]^{6-}$ (orbital of a_1” symmetry delocalised over the belt metal atoms) and α-$[P_2W_{15}V_3O_{62}]^{9-}$ (one of the components of the e symmetry orbital centred at the vanadium cap ions).

We presented above the characteristics of the molybdate WD anions. The α structure is quite well studied by means of different techniques but, to our knowledge, there is no experimental evidence about the shape of the β isomer. Perhaps the most significant data concerns its reduction properties, which are quite similar to those of the α counterpart.[6b] For the β isomer, two structures were explored: a non-distorted C_{3v} structure, similar to the one optimised for β-P_2W_{18}, and a structure with alternate Mo–O bonds of C_3 symmetry (Figure 5.12). Considerable computational effort was made to optimise the latter because the C_3 point group is not available in the ADF package, and the geometry had to be optimised without symmetry constraints. As in the α isomer, the structure with an alternate arrangement of the Mo–O bonds is clearly more stable than the most symmetric form. The energy difference between the C_3 and C_{3v} structures is 8.2 kcal mol^{-1}. Also as in the α isomer, the Mo–O distances are between 1.83 and 2.12 Å. These relatively important energies strongly suggest that the two α and β forms of P_2Mo_{18} have similar structures, with series of short and long Mo–O bonds. We looked for a possible chiral structure for the α-2:18 tungstate, however, the optimisation process always yield the most symmetric D_{3h} form. This finding seems in agreement with the observation of chiral structures only in molybdates.[10-11]

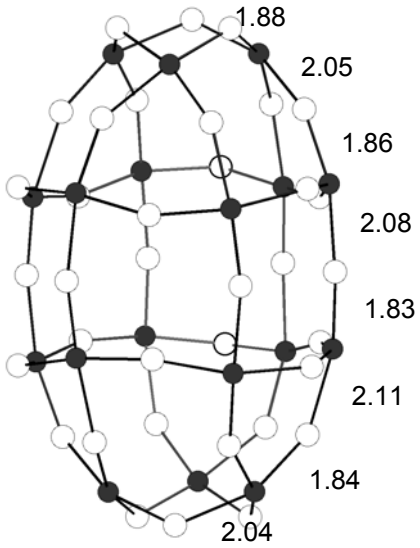

Figure 5.12. Ball-and-stick view of the DFT computed geometry of the β-P_2Mo_{18} anion with formal C_3 symmetry. White and black spheres represent oxygen and molybdenum atoms, respectively. The two internal PO_4 units, as well as the terminal oxygens, are not included for clarity. The distances (in Å) highlight the alternative disposition of long and short Mo–O bonds forming three interpenetrating loops.

If a more electronegative ion, like V^{5+}, is incorporated into a polar site, there is an inversion of the traditional belt/cap site reduction order. We analysed the effect that the reduction may have on the equilibrium of the α/β-$P_2W_{15}V_3$ species, where the three Vs occupy three sites in the same triad (shaded octahedrons in Figure 5.9). The substitution of W by the more electronegative V inverts the order of belt/cap d_{xy}-like orbitals and then the LUMO in $P_2W_{15}V_3$ is an orbital of e symmetry mainly centred on the three equivalent vanadium atoms[17] (60% V orbitals – 10% belt W orbitals, Figure 5.11). The LUMO+1 is composed of 65% belt tungsten orbitals and the LUMO+2 of 48% belt W and 10% V orbitals. The shape and energy of the β-form orbitals resemble those of the α-form orbitals. The H-L gap is similar in both structures. This is important because although the substitution reduces a metal ion directly involved in the rotation, it does not significantly alter the α/β equilibrium in WD anions. As the values in Table

5.6 show, the computed $\Delta E_{\beta-\alpha}$ are only slightly higher than those found for the non-substituted P_2W_{18} cluster. Moreover, the effect of the single reduction on the α/β equilibrium in $P_2W_{15}V_3$ does not exceed the 0.5 kcal mol^{-1}.

Table 5.6. Experimental reduction potentials and calculated relative stabilities for several heteropolyanions.

	Reduction Potentials[a] *(in V)*		
Compound	α	β	$\Delta V_{\beta-\alpha}$
Keggin			
AlW_{12}	–0.62 (1)	–0.45 (1)	0.17
SiW_{12}	–0.26 (1)	–0.14 (1)	0.12
PMo_{12}	+0.36 (2)	+0.55 (2)	0.19
Wells–Dawson			
P_2W_{18}	+0.045 (1)	+0.059 (1)	0.014
P_2Mo_{18}	+0.46 (2)	+0.53 (2)	0.07
	$\Delta E_{\beta-\alpha}$ *(in kcal* mol^{-1}*)* [b]		
	$n = 0$ [c]	$n = 1$ [c]	$n = 2$ [c]
Keggin			
PW_{12}	+6.46	+3.00	+0.92
SiW_{12}	+6.00	+2.54	–3.30
PMo_{12}	+4.84	+1.49	–2.59
Wells–Dawson			
P_2W_{18}	+1.83	+1.70	+1.11
P_2Mo_{18}	+2.92	-	+0.60
$P_2W_{15}V_3$	+2.54	+2.03	+2.31

a) Values in parentheses are the number of metallic electrons added
b) Positive values for $\Delta E_{\beta-\alpha}$ mean that the α isomer is the most stable
c) Number of metal or blue electrons in the framework

For the α/β equilibrium in 2:18 molybdates, we found an energy difference of 2.9 kcal mol^{-1} between the fully oxidised forms. This is

smaller than the difference computed for PMo_{12} (4.8 kcal mol^{-1}) and PW_{12} (6.5 kcal mol^{-1}), but somewhat larger than the one found for P_2W_{18} (1.8 kcal mol^{-1}). The LUMO in the chiral α (D_3) isomer of P_2Mo_{18} is 1.86 eV above the oxygen band. The 60º rotation of one capping triad decreases the energy of the LUMO by 0.17 eV, whereas the same transformation in the D_{3h} structure of P_2W_{18} reduces the stabilisation of the LUMO to a mere 0.01 eV. This reduction favours the stability of the β form. Hence, after the second reduction, the C_3 structure is only 0.60 kcal mol^{-1} less stable than the D_3 one. The relative stability of α and β isomers fully agrees with the reduction potentials given in Table 2. In general, the β isomers reduce at more positive potentials than the α counterparts, and this behaviour is much more significant in the most symmetric Keggin frameworks than in the WD anions. For these latter anions, the polarographic data suggest that the gain in stability of the β form due to the reduction is somewhat larger for molybdates than tungstates.[6]

References and Notes

[1] Wells, A. F. *Structural Inorganic Chemistry*. Clarendon Press. Oxford, U. K., 1945.

[2] Dawson, B. *Acta Crystallogr., Sect. B*. **1953**, *6*, 113.

[3] Strandberg, R. *Acta Chem. Scand., Ser. A.* **1975**, *29*, 350.

[4] D'Amour, H. *Acta Cryst., Sect C.* **1976**, *32*, 729.

[5] Day, V. W.; Klemperer, W. G. *Science.* **1985**, *228*, 533.

[6] (a) Pope, M. T.; Papaconstantinou, E. *Inorg. Chem.* **1967**, *6*, 1147. (b) Papaconstantinou, E.; Pope, M. T. *Inorg. Chem.* **1967**, *6*, 1152. (c) Varga, G. M.; Papaconstantinou, E.; Pope, M. T. *Inorg. Chem.* **1970**, *9*, 662. (d) Papaconstantinou, E.; Pope, M. T. *Inorg. Chem.* **1970**, *9*, 667.

[7] López, X.; Maestre, J. M.; Bo, C.; Poblet, J. M. *J. Am. Chem. Soc.* **2001**, *123*, 9571–9576.

[8] Maestre, J. M.; López, X.; Bo, C.; Casañ-Pastor, N.; Poblet, J. M. *J. Am. Chem. Soc.* **2001**, *123*, 3749–3758.

[9] Kazanskii, L. P.; Fedotov, M. A. *J. Chem. Soc., Chem. Commun*. **1980**, 644.

[10] Pope, M. T. *Inorg. Chem.* **1976**, *15*, 2008.

[11] Garvey, J. F.; Pope, M. T. *Inorg. Chem.* **1978**, *17*, 1115.

[12] López, X.; Bo, C.; Poblet, J. M. *J. Am. Chem. Soc.* **2002**, *124*, 12574.

[13] Kozik, M.; Baker, L. C. W. *J. Am. Chem. Soc.* **1987**, *109,* 3159. Casañ-Pastor, N.; Baker, L. C. W. *J. Am. Chem. Soc.* **1992**, *114,* 10384 and references therein.

[14] Suaud, N; Gaita-Ariño, A.; Clemente-Juan, J. M.; Sánchez-Marín, J.; Coronado, E. *J. Am. Chem. Soc.* **2002**, *124,* 15134.

[15] Borrás-Almenar, J. J.; Clemente-Juan, J. M.; Coronado, E.; Tsukerblat, B. S. *Chem. Phys.*, 1995, **195**, 1.

[16] Borshch, S. A.; Bigot, B.; *Chem. Phys. Lett.* **1993**, *212*, 398.

[17] Harmalker, S. P.; Pope, M. T. *J. Am. Chem. Soc.* **1981**, *103*, 7381–7383.

[18] Kozik, M.; Hammer, C. F.; Baker, L. C. W. *J. Am. Chem. Soc.* **1986**, *108,* 2748. *ibid.* **1986**, *108*, 7627.

[19] Kozik, M.; Baker, L. C. W. *J. Am. Chem. Soc.* **1990**, *112,* 7604.

[20] Weinstock, I. A.: Cowan, J. J.; Barbuzzi, E. M. G.; Zeng, H.; Hill, C. L. *J. Am. Chem. Soc.* **1999**, *121*, 4608.

[21] Baker, L. C. W.; Figgis, J. S. *J. Am. Chem. Soc.* **1970**, *92*, 3794.

[22] Some recent publications are: Keita, B.; Belhouari, A.; Nadjo, L.; Contant, R. *J. Electroanal. Chem.* **1998**, *442*, 49. Keita, B.; Girard, F.; Nadjo, L.; Contant, R.; Canny, J.; Richet, M. *J. Electroanal. Chem.* **1999**, *478*, 76. Keita, B.; Lu, Y. W.; Nadjo, L.; Contant, R.; Abbessi, M.; Canny, J.; Richet, M. *J. Electroanal. Chem.* **1999**, *477*, 146. Contant, R.; Abbessi, M.; Canny, J.; Richet, M.; Keita, B.; Belhouari, A.; Nadjo, L. *Eur. J. Inorg. Chem.* **2000**, 567. Keita, B.; Lu, Y. W.; Nadjo, L.; Contant, R. *Eur. J. Inorg. Chem.* **2000**, 2463.

[23] Acerete, R.; Harmalker, S.; Hammer, C. F.; Pope, M. T.; Baker, L. C. W. *J. Chem. Soc., Chem. Commun.* **1979**, 777. Massart, R.; Contant, R.; Fruchart, J. M.; Ciabrini, J. P. Fournier, M. *Inorg. Chem.* **1977**, *16*, 2916.

[24] Anderson, T. M.; Hill, C. L. *Inorg. Chem.* **2002**, *41*, 4252.

CHAPTER 2

Theoretical Approach and Computational Details

This chapter is an overview of the first-principles-based theoretical chemistry of current use, without any attempt at rigour in the mathematical description. After a short introduction, section 2.2 describes the elementary topics and mathematical formulation of the well-known Hartree–Fock approximation, the density functional theory and the role of the basis set. Section 2.3 revisits the strong and weak points of both theories in a comparative fashion. In section 2.4 we present the general characteristics of the functionals used in the framework of calculations arising from first-principles theories. It also contains computational details of this particular study. Finally, in section 2.5, the reader shall meet a few important tools for analysis in theoretical chemistry. The features derived from these tools are studied in becoming chapters.

2.1. Introduction to Quantum Chemistry

After the birth of the Quantum Mechanics in the early 1900's, the application of the new quantum concepts to the study of atomic and molecular systems experienced a growing acceptance. Some semi-empirical approximations were developed in a first stage, like the Hückel model for calculating the orbital energies of organic molecules or, at a higher level, the extended-Hückel method, both making use of empirical parameters. First-principles quantum mechanical methods are, on the other hand, aimed at solving the Schrödinger equation with neither an approximation nor additional parameters. That is, to solve equation (1) *ab initio*:

$$H\Psi = E\Psi \tag{1}$$

$$H = -\frac{1}{2}\nabla_i^2 - \sum_{i=1}^{N}\sum_{A=1}^{M}\frac{Z_A}{r_{iA}} + \sum_{i=1}^{N}\sum_{j>1}^{N}\frac{1}{r_{ij}} \tag{2}$$

where H is the full time-independent electronic Hamiltonian. The first term is the electronic kinetic energy, the second one is the electron-nucleus coulombic attraction, and the third one accounts for the electron-electron repulsion. Even though, theoreticians realised that the exact solution of (1) is only attainable for monoelectronic systems, so only when Ψ describes the motion of one electron (hydrogen-like systems). However, the interest on monoelectronic systems amongst the scientific community is rare, and the efforts to obtain accurate results for polyelectronic systems started soon. Therefore, approximate methods were developed in order to obtain an estimate for the energy of the system and other molecular magnitudes. In a way, especially in a first stage of this new theory, the main problem was the complicated way to find the solution to the equations arising from that theory. The fundamentals for the modern methods of computation were established during the 1930-50's. Since the decade of 1960's, with the introduction of the primitive computing machines, the development of more and more efficient algorithms for solving the equations involved in the motion of electrons allowed to obtain the first relevant results.

Many-body theories are those aimed at describing in a mathematical way the motion (or the behaviour, in general) of more than two interacting particles. Models of increasing complexity have been developed attempting to reproduce as better as possible the features of molecules. In section 2.2

we present a few basic aspects of the mathematical formulation used throughout the text without any attempt at completeness or rigor. For this purpose a vast literature is available.[1-3] Only the most outstanding aspects of the theory are discussed, those that are necessary for further understanding of the performance of the model and the accuracy and meaning of the results.

2.2. Fundamentals of Computational Chemistry

2.2.1. The Hartree-Fock approximation

The wavefunction-based *ab initio* methods were the preferred ones to be used for solving the Schrödinger equation until the late 80's. The starting point for all of them is the Hartree–Fock (HF) approximation. Let us consider some of the basic ideas underlying this method. A simple antisymmetric wavefunction, used to describe the ground state of an *N*-electron system, is constructed with one-electron spin orbitals, χ_i (exact solutions of (1)) to form a single determinant, also called Slater determinant, represented as

$$\Psi_0 = |\, \chi_1 \chi_2 \cdots \chi_N \rangle \tag{3}$$

The variational principle can find the best wavefunction of this form, simply forcing it to give the lowest possible energy

$$E_0 = \langle \Psi_0 | H | \Psi_0 \rangle \tag{4}$$

E_o is the lowest expected value for the energy of the ground state taking Ψ_o as the reference function. The flexibility in the wavefunction can be introduced choosing the spin orbitals. Obviously, the better the approximation to Ψ_o, the lower the energy. So, an improvement of the wavefunction by means of better spin orbitals always leads to an energy closer to the exact result. This is the basis of the variational principle and has a great relevance, especially for more complex wavefunction-based methods. So, if we minimise E_o with respect to the χ_i's we obtain the

Hartree–Fock equation, thus determining the optimal spin orbitals. This is again an eigenvalue problem of the form

$$f_i\chi(\mathbf{x}_i) = \varepsilon_i\chi(\mathbf{x}_i) \tag{5}$$

with

$$f(i) = -\frac{1}{2}\nabla_i^2 - \sum_{A=1}^{M}\frac{Z_A}{r_{iA}} + v^{HF}(i) \tag{6}$$

and

$$v^{HF}(i) = \sum_b J_b(i) - K_b(i)$$

v^{HF} is the two-electron term of the Fock operator, $f(i)$. So, the $v^{\mathrm{HF}}(i)$ is the average potential experienced by the i-th electron due to the presence of the other N–1 electrons. J_b is a *local* operator accounting for the classical Coulomb repulsion that each electron experiences by the effect of the remaining N–1 electrons, and K_b is the attractive exchange term. This one has no simple classical interpretation because is concerned with the spin of particles, and arises due to the antisymmetric nature of the determinantal wavefunction. The exchange operator is *non-local* and is approximated as a mean-field, averaged effect of the mutual interaction of the electrons of the same spin. In terms of the spin orbitals, these contributions are written in the form

$$J_b(1)\chi_a(1) = \left[\int \chi_b^*(2)\, r_{12}^{-1}\chi_b(2)d\mathbf{x}_2\right]\chi_a(1), \text{ Coulomb}$$

$$K_b(1)\chi_a(1) = \left[\int \chi_b^*(2)\, r_{12}^{-1}\chi_a(2)d\mathbf{x}_2\right]\chi_b(1), \text{ Exchange}$$

It will be shown below the importance of these two expressions in the evolution of computational chemistry.

Introduction of basis sets

In 1951, Roothaan[4] introduced the use of a set of spatial basis functions to solve the differential equations of the HF approximation. Thus, the differential equations were converted into a set of algebraic equations that could be solved by matrix techniques. A given basis set is formed by an

ensemble of functions that describe the motion of the electrons in space. The choice of the basis set is very important since it governs the correct functioning of the machinery of calculation. Lots of basis sets are available nowadays. They were developed with the aim of improving the behaviour of electrons by stressing some characteristics. It is not the goal of this text to discuss exhaustively those sets. It is worth showing the two types of functions that are of most common use for computation. Their mathematical differences are of much importance in the implementation for computation. The Slater-type orbitals (STO) are defined, in general, as

$$\varphi^{STO} = Nx^l y^m z^n e^{-\zeta r}$$

whereas Gaussian-type orbitals (GTO) are

$$\varphi^{GTO} = Nx^l y^m z^n e^{-\zeta r^2}$$

x, y and z describe the angular part of the orbital, and the ζ factor, which affects the exponential radial function, fixes how much contracted the orbital is.

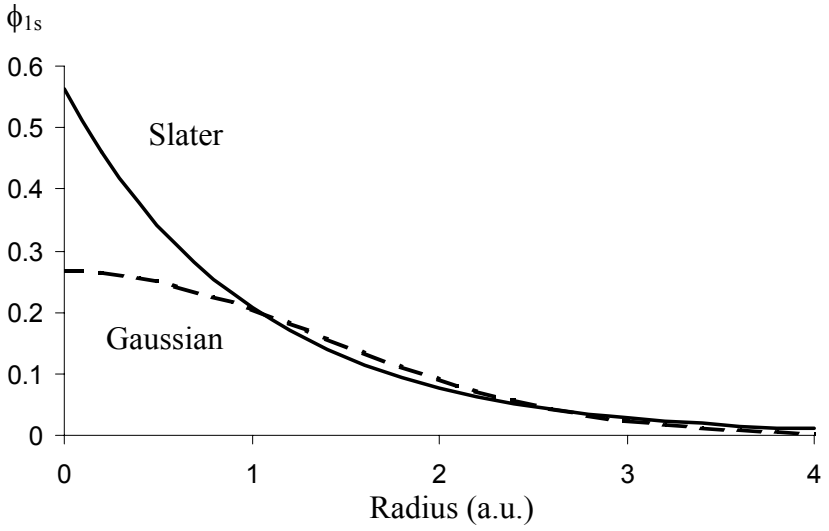

Figure 1.1. Comparison of a Slater function with ζ = 1.0, and a single Gaussian function (α = 0.27095) for a 1s orbital.

The only difference between STO's and GTO's is the dependence with *r* of the exponential term. Even though, this has dramatic implications in the treatment of data. GTO's enable the efficient calculation of molecular multi-center integrals by an analytical procedure. On the other hand, STO's, which are used in a few computational chemistry packages like ADF, MOPAC and others, are more adequate for numerical integration since no efficient analytical algorithms are known yet. Even though, and as a general rule, the accuracy achieved by a single STO is similar to that of about three GTOs. This fact arises from the behaviour of each type of orbital in the $r \rightarrow 0$ region. STOs are advantageous from this point of view since they reproduce very well the necessary conditions of electronic behaviour around a nucleus. They are actually the exact solutions of the Schrödinger equation for the hydrogen atom. Contrarily to wavefunction-based methods, where Gaussian-type functions are commonplace (because of the advantages they offer to the calculation of four-centre-two-electron integrals), there is no need of combinations or contractions of functions to reproduce the cusp behaviour at $r \rightarrow 0$. See Figure 1.1 for comparison of Slater- and Gaussian-type functions.

Another type of functions, not so extended amongst the theoretical community but employed under certain circumstances in DFT calculations, is the so-called plane-waves. They are sometimes used in periodic calculations since they implicitly contain the features of periodic boundary conditions.

Every basis set can be classified in terms of the quality. It depends on the number of functions describing each atomic orbital. The simple rule is "more is better". But, recalling in the mathematical shape of GTO's and STO's, with the angular and the radial parts, we can carefully choose the shape of these orbitals. If we increase the number of functions by varying the exponential factor ζ, we get simple- ζ, double- ζ, ...*n* ζ basis sets. This factor governs how much *diffuse* is each function. The second characteristic describes the angular part of the function. That is, the complexity of the nodal structure of ϕ_i, and it is sometimes required for introducing some additional electronic correlation. For a better description of the electronic structure, ϕ_i's with different values of ζ and polarisation functions may be used. Of course, the more extended the basis is, the more time-demanding the calculation becomes, but the better the result is. Even though, with the

fast evolution of hardware and mathematical algorithms implemented, large basis sets are routinely used.

The essence of the HF approximation is, thus, to replace the complicated expression for the many-electron problem by a one-electron, mean-field formulation of the electronic repulsion. Provided that the averaged field for the *i*-th electron depends itself on all the spin orbitals, the HF equation must be solved iteratively. Such a procedure is the Self-Consistent-Field (SCF) method.[5] This is a typical eigenvalue problem. The procedure for solving it yields a set of eigenvalues with an associated set of eigenvectors, which is the sequence of molecular orbitals. The HF method determines the best single-determinant wave function. At this level of theory, the improvement of the wavefunction is linked to the quality of the basis set.

It is worth mentioning that the HF method itself does not properly account for the Coulomb hole. It is associated to the repulsion that two electrons experience for being charged particles. This is the main failure of this approximation since the motion of the electrons is then poorly described. In fact, the HF wavefunction only incorporates the exchange hole, which arises from the nature of fermions. It is also known as the Fermi hole. Consequently, it gives too much importance to electron pairing and to ionic structures. On average, two electrons are closer at the HF level than they should be.

One way to improve the pioneering but modestly accurate electronic description introduced with the HF approximation is to enlarge the trial wavefunction or to make it more flexible. This is possible by means of two strategies. One is the perturbation method, and the other is the configuration interaction (CI) method. They constitute the post-HF methods, which were developed with the main goal of introducing electronic correlation. They are, in general, very computationally demanding since the number of variables to handle grows very fast as we enlarge Ψ. Most of the CI techniques developed for introducing the correlation effects to get better energies and wavefunctions use the *brute force*, in the sense that, in general, they use larger (linear combination of *N*-electron Slater determinants) trial functions. The CI methods make use of a multi-determinantal trial wave function, which can be formulated as

$$|\psi_0\rangle = c_0 |\Phi_0\rangle + \sum_{i=1} c_i \, |\Phi_i\rangle$$

where Φ_o is a Slater determinant and the Φ_i terms represent other electronic configurations, with an associated weight, c_i, each. These terms in the above expression are the expansion of the *uncorrelated* function. If no truncation were made, we would obtain the exact solution Ψ_o within the chosen basis set—the so-called Full Configuration Interaction (FCI) solution. In fact, the application of CI techniques is restricted to small systems due the extraordinary scaling with the molecular size. Furthermore, the convergence of the correlation effects with the size of the trial function is slow. Computational chemists apply some variants of such CI techniques daily, but rarely to medium or large systems.

2.2.2. Density functional theory

Hohenberg-Kohn theorems and Kohn-Sham formulation

Let us now introduce an alternative way for describing the many-electron problem. It is formulated introducing the electron correlation *locally*. This idea constitutes the fundamental idea of Density Functional Theory (DFT). This theory is based on the assumption that the ground state electronic density, ρ_0, contains all the information of the chemical system. Such a method was built on the basis of the famous first Hohenberg–Kohn theorem,[6] which states that there is a one-to-one correspondence between an external potential (the nuclear field) $v(\mathbf{r})$, the particle density $\rho(\mathbf{r})$ and the ground state wavefunction, $\Psi(\mathbf{r})$. This is, indeed, a consequence of the variational principle. In addition, the energy of the ground state is a functional of $\rho(\mathbf{r})$,

$$E[\rho] = T[\rho] + V[\rho] + W[\rho]$$

with

$$T = -\frac{1}{2}\nabla^2(i);\quad V = -\sum_{i=1}^{N}\sum_{A=1}^{M}\frac{Z_A}{r_{iA}};\quad W = \sum_{i<j}^{N}\frac{1}{r_{ij}}$$

where T is the electronic kinetic energy, V is the electron-nucleus Coulomb potential, and W is the electron-electron interaction energy. The latter term can be split into two contributions, the classical electron-electron Coulomb

repulsion and the exchange-correlation term, *XC,* for which the mathematical nature as a functional of ρ is unknown

$$W[\rho] = W_{Coul}[\rho] + W_{XC}[\rho]$$
$$W_{XC}[\rho] = W_X[\rho] + W_C[\rho]$$

W_{XC} contains all the terms remaining from the electron-electron interactions not included in W_{Coul}. The *XC* part is artificially decomposed into exchange + correlation, although it has no much physical significance. However the theoretical study of both effects seems to be easier in that way. The second Hohenberg-Kohn theorem[6] predicts that we can apply the variational principle, at a fixed external potential, *v*, to the electronic density

$$E_v[\rho] = \langle \Psi[\rho] | T + V + W | \Psi[\rho] \rangle \geq E_0$$

Almost all the modern DF-based applications make use of the DFT formulation of Kohn and Sham[7] (KS). It was postulated the existence of an auxiliary system of *noninteracting* electrons moving in an external and unique potential $v_s(\mathbf{r})$. This potential has the property of having a wavefunction associated yielding exactly the same density than the interacting system. In addition, that wavefunction is a Slater determinant. The exact energy may be written as

$$E = \int_{1 \to 1'} -\frac{1}{2}\nabla^2(1)\gamma(1,1')d1 + \int \rho(\mathbf{r})v(\mathbf{r})d\mathbf{r} + \frac{1}{2}\int r_{12}^{-1}\Gamma(1,2)d1d2$$
$$\Gamma(1,2) = \rho(1)\rho(2) + \Gamma_{XC}(1,2)$$

$\Gamma(1,2)$ is the correlated probability of finding two electrons at 1 and 2. It is decomposed into the uncorrelated part, $\rho(1)\rho(2)$, and the remainder that accounts for the exchange and correlation parts of the correlated probability.

From this formulation we obtain the KS orbitals, in which the optimisation of the density is a straightforward procedure since it is derived after solving a set of one-electron equations. The problem at this point is that the exact mathematical form connecting the energy and the total electronic density is yet unknown. Hence, approximations should be introduced in order to have an analytic expression to be evaluated. The

primitive *XC* part of $E[\rho]$ is the central battlefield for theoreticians that try to improve the performance of the model.

Local Density Approximation

Let us discuss here the central model that gave birth to the DFT. It is the simplistic but surprisingly good uniform electron gas approximation (or homogeneous gas model) proposed in the middle 1920's by Thomas and Fermi.[8] Such a model can be mathematically formulated as an energy functional that accounts for the local value of ρ at each point in space (regardless of any other one). For the homogeneous gas approximation, the first analytic expression obtained for the electron correlation part was reported in the early 80's by Vosko, Wilk and Nusair (VWN)[9] which fitted energy values obtained from Monte Carlo simulations by Ceperley and Alder.[10] The exchange part of this functional was approximated, in a simple form, with the *X*α method of Slater[11]

$$E_{X\alpha}[\rho] = -\frac{9}{8}\left(\frac{3}{\pi}\right)^{\frac{2}{3}} \alpha \int \rho(\vec{r_1})^{\frac{4}{3}} d\vec{r_1}$$

where α is a semi-empirical adjustable parameter. The *XC* part of the energy functional within the Local Density Approximation (LDA) consists in these two parts

$$E_{XC}^{LDA} = E_X^{X\alpha} + E_C^{VWN}$$

We will see below that more complex functionals can be proposed.

Generalised Gradient Approximation

The modestly accurate results of the LDA applied to molecules forced the search of more accurate expressions for describing the motion of electrons. The central idea is to take into account not only the value of the electron density at each point in space but also what is the value of its first derivative. This constitutes the so-called *non-local* or generalised gradient approximations, GGA. The gradient corrections are added to the local definition of *X* and *C*, thus redefining the E_{XC} and, in most of the cases,

improving the performance of the model. In general, we have that gradient corrections are functionals of the density and of its first derivative:

$$E_{XC}^{NLDA}[\rho] = \int f(\rho, \nabla\rho) d\vec{r}$$

The density gradient is typically included in the form $\frac{|\nabla\rho|^2}{\rho^{\frac{4}{3}}}$.

The *non-local* term, NLDA, together with the LDA part of *XC* leads to mathematical expressions for the corrected $E_{XC}^{GGA}[\rho]$ functionals

$$E_C^{GGA}[\rho] = E_C^{LDA}[\rho] + E_C^{NLDA}[\rho] \text{ for correlation}$$

$$E_X^{GGA}[\rho] = E_X^{LDA}[\rho] + E_X^{NLDA}[\rho] \text{ for exchange}$$

All the efforts concerned with the development of DFT are aimed at improving and testing the exchange and correlation corrections for the *NLDA* part. There is an inherent problem beneath the current status of the model. Provided that the exact form of $E[\rho]$ is unknown (it is indeed what we are looking for), we can not say much about the performance of the new functionals until they are tested with chemical systems. So, there is no systematic way to get better functionals and, a priori, a new formulation of the E_{XC} part is not better than a previous one. There are many *XC* expressions in the literature.[12] The functionals enjoying of a spread acceptance nowadays are the Becke[13] exchange functional and the Perdew[14] and Perdew–Wang[15] correlation functionals. There is a different class of functionals, the so-called hybrid functionals, like the Lee–Yang–Parr[16] (LYP) for correlation that combined with the Becke's three-parameter method (B3),[17] led to the popular B3LYP exchange-correlation functional. They were introduced with the aim of including the exact exchange energy as a contribution from the correct HF exchange. This latter mathematical approach have proven to be accurate for many systems, although somewhat more time demanding than non-hybrid *XC* functionals like the BP or the BP86. This is so since the calculation of the two-electron integrals in the HF exchange (the bottleneck of quantum chemistry) is avoided.

2.3. DFT vs. HF Methods

Compared to the HF-based methods, the DFT is conceptually more difficult to be improved. The way to account for the correlation effects in the framework of the DFT does not pass through enlarging the trial wavefunction. It is the unknown Hamiltonian that is improved, indeed. As we pointed out before, no systematic procedure is known to date to improve the performance of the model. Luckily, better functionals do not imply more expensive calculations (with the exception of those that include a part of the HF exchange). Thus, new pure (non-hybrid) functionals can be tested regardless of how much time-consuming they are. After more than fifteen years of work concerning the mathematical expression of $E[\rho]$, some conclusions about the performance and current status of the DFT-based methods arise. Here we divide the discussion in three main points: molecular energies, accuracy of the geometries and electronic properties (molecular orbitals structure).

Total Molecular Energies. Care must be taken when we analyse the molecular energies with different functionals. Provided that the variational principle is not applicable in the framework of the DFT (the exact functional connecting E and ρ is unknown), it is impossible to know *a priori* whether a GGA method will give a lower (better) energy than the LDA. Thus, a simpler functional does not imply a worse energy, there is not such a direct connection in DFT energies. Even though, the use of the same functional for the study of relative values of binding energies is, in the context of the accuracy of the functional, perfectly applicable. In this compilation, it is a constant way to evaluate chemical problems to compare pairs of energies to elucidate relative stabilities.

Molecular Geometries. Not much experience has been achieved yet in the calculation of large transition-metal-based clusters compared to the smaller metal-ligand or organic compounds. For these cases, compared to experimental data, LDA and GGA geometries proved to be in better agreement than HF ones. The latter method, in general, overestimates the Metal–Ligand (M–L) distance, which is an effect of the inherent deficiencies in the treatment of electron correlation. On the other hand, equilibrium geometries computed by the LDA tend to be underestimate bond distances. Nevertheless, LDA deviations have been reported smaller

than HF ones. For large systems like polyoxometalates, with many heavy atoms, the performance of the DFT can be considered excellent. Experimental geometries are very well reproduced with medium-size basis sets and GGA functionals, so at low cost. With the BP86 exchange-correlation functionals, some elongation of the LDA-computed bond distances is achieved, thus reducing the average deviation in M–L distances. The inclusion of some exact exchange (HF exchange) in the energy functional (say, by means of the B3LYP) can improve the equilibrium geometries although at a major computational cost.

Electronic Properties. Most of the present work deals with the analysis of electronic properties in terms of molecular orbital energies. The conventionally accepted idea in which electrons are disposed in a well-defined sequence of energetic levels facilitates the rationalisation of plenty of the features of molecular systems. The original idea (or we might say, perhaps, the main goal) of the DFT gets rid off electrons as the basic unit of the machinery. Instead, it makes use of an electron gas. Even though, the current formalism in use (the Kohn–Sham approach) forced the implementation, in density functional-based methods, of molecular orbitals containing the electrons, the KS orbitals. They are trivially connected to the density via

$$\rho(r) = \sum_i \left|\varphi_{i,KS}\right|^2$$

After recent reports in favour of the physical significance of the KS orbitals, their use in the context of the density functional scheme is welcome,[18-22] and their application for rationalising chemical phenomena is justified. The molecular orbital theory has been routinely used as a tool for the analysis of the electronic structure.

Chemists are being familiarised with the discussion of properties related with the Highest Occupied Molecular Orbital (HOMO) and the Lowest Unoccupied Molecular Orbital (LUMO) and their spatial shape. The linked value HOMO-LUMO (H-L) gap, the energetic separation between both orbitals, is an indicator of the stability of the cluster. Comparison of H-L gaps in various systems is a good guess for advancing the electronic affinity of each one. Must we warn the reader that, in highly charged clusters like those discussed in chapters 4-8, the energy of the molecular

orbitals can be dramatically shifted to unrealistic levels. The fact that the HOMO (or some occupied orbitals) appears at positive energies is a signal of failure of both the DFT and the HF approximation. This energy upshift is indicative of instability and is reflected in the total binding energy, being less negative than it should be. In chapter 7, a way to arrange this error is used to equalise HOMO energies in several clusters, thus giving somewhat comparable orbital energy values and electron transfer energies.

To resume this section, we schematise several considerations concerning the general features, failures and advantages of the HF and the DFT methods.[23]

DFT weak points:

- ► The DFT energy is not variational with v_{XC}. The HF method was formulated within the framework of an exact Hamiltonian, so the variational principle is applicable. The only way to improve the performance of the DFT is formulating better *XC* potentials. However, there is no systematic procedure to do that. In wavefunction-based methods, the trial function is enlarged to improve the results. The better the function, the closer we are to the exact result (more correlation energy is included).
- ► The complex electronic configurations (those that are clearly multi-determinantal) are troublesome. The mono-determinantal nature of the DFT formalism can not handle them within the framework of the current KS implementation. Post-HF techniques are the tool to be used in such cases.
- ► Highly negatively charged molecules display artificially upshifted occupied molecular orbitals. In general, HOMO-LUMO gaps are smaller at the DFT level than in the HF approximation.

DFT strong points:

- ► In principle, the DFT formulation only deals with ρ, which depends on 3 variables irrespective of the size of the system. In wavefunction-based methods, like the HF, Ψ is a function of 3*N* variables.
- ► Gradient-corrected density functionals applied to POMs far surpass HF in accuracy. The electronic correlation is introduced at low cost, whereas including correlation to the HF method is highly expensive.

► DFT is cheaper than HF at similar performance.
► The shape, symmetry and energetic sequence of the KS orbitals coincide with those obtained at the HF level.
► In principle, DFT can include *all* the electronic correlation, whereas HF can not.
► The total electronic density is an observable. The wavefunction Ψ is not.
► Nowadays, it is the method to be used in large systems, like POMs. DFT geometries are proven to be very good. Even with medium-quality basis sets, the experimental geometries are well reproduced. Only double-bonded metal-oxygen distances in POMs are modestly calculated.

Resuming, before the decade of the 80's, the conventional *ab initio* methods were the only way to include correlation effects in quantum calculations. The Density Functional Theory (DFT) represents an alternative way for introducing the electronic correlation effects for solving the electronic Schrödinger equation. In the last fifteen years, the application of the DFT-based methods was popularised amongst the computational chemists since they permit the calculation of systems of medium and large size with low computational cost. Furthermore, the accuracy reached is generally comparable to the expensive post-Hartree–Fock methods. For the large systems studied here, the DFT is the optimal tool to achieve a good accuracy in the results with modest computational demands.

2.4. Computational Details

The density-functional

In order to achieve a general consistency of the work for further comparison of the results, the same computational accuracy was kept to obtain the results presented here. With this policy we can avoid artificial differences due to mere aspects of the calculation. Where a different computational level or method is applied, the motivation for doing that and a detailed explanation are highlighted.

The DFT calculations presented in this thesis were carried out with the ADF package of programs[24] (versions 2.3, 1999 and 2000). The local density approximation (LDA) characterised by the homogeneous electron gas exchange (the $X\alpha$ method[11]) together with the Vosko–Wilk–Nusair[9]

(VWN) parameterisation for correlation were used. The gradient-corrected Becke[13] and Perdew[14] functionals (BP86 *XC* functional) for exchange and correlation are included, respectively. All these features are resumed in this chapter above.

One way to simplify the computation when heavy atoms are involved passes through discarding some electrons of each atom from first-principles calculations. They are the lowest-lying, internal and most inert ones, or *core* electrons. They can be considered frozen or, otherwise, they can be treated by means of effective core potentials. The energy and orbital sequence of such electrons can be computed in a previous stage of the procedure. In the process of searching the total electron density of the system (orΨ), they do not account for bonding more than in the extent in which they affect the energy of the *valence* electrons. (Quasi)relativistic corrections are applied to core electrons since their kinetic energy is much larger than that of the valence shells. They were introduced alongside the Pauli formalism with corrected core potentials. The quasirelativistic frozen core shells were generated with the auxiliary program DIRAC,[24] included in the ADF package.

The choice of the basis set and the functional utilised in this work has its fundament in the good balance between accuracy and time. Taking the reference of the previous works published by authors concerned with similar systems,[25-26] STO basis sets of triple-ζ + polarisation quality were used to describe the valence electrons of all the atoms. The electrons treated as frozen core shells are listed in Table 2.1.

Table 2.1. Complete list of the elements appearing in the calculations of chapters 4–8, together with their respective core electrons, classified as p- or d-elements.

p-series		*transition-metals*	
element	core electrons	element	core electrons
O	1s	Ti, V	1s–2sp
Al, Si, P	1s–2s	Nb, Mo	1s–3spd
Ga, Ge, As	1s–2sp	W	1s–4spd

All the electrons included in the core are described by means of a single Slater-type orbital each.[27-28]

2.5. Tools for Analysis

It was discussed before the importance of the total electronic density, ρ, in the DFT formulation. In principle, all the molecular properties can be extracted from this unique function. Here we briefly point out some outstanding properties derived from ρ that reveal characteristics of the molecular system.

Atomic charge analysis

Although the atomic charge is not an observable magnitude, its values can indicate a tendency if they are properly taken into account in relative terms. There is no experimental chance to measure the charge of an atom in a molecule. Even though, such an analysis can easily link the quantum chemical calculations with concepts like bonding and valence, but a qualitative level. Amongst many other methods for obtaining the atomic charge, the Mulliken population analysis[29] is a standard method to have a guess to this magnitude. The net charge of an atom is calculated as follows:

$$q_A = Z_A - \sum_{\mu(A)} (\mathbf{PS})_{\mu\mu}$$

where Z_A is the nuclear charge, **P** is the electron density in matrix form and **S** represents the overlap matrix between atomic orbitals. Their elements are constructed by

$$P_{\mu v} = \sum_{a}^{N} C_{\mu a}^{\alpha} (C_{va}^{\alpha})^{*}$$

$$S_{\mu v} = \int \phi_{\mu}(1)^{*} \phi_{v}(1) dr_1$$

respectively. $(\mathbf{PS})_{\mu\mu}$ can be interpreted as the number of electrons associated to the atomic orbital ϕ_μ. This partition of the charge is strongly dependent on the basis set, in addition to other serious deficiencies of the method. So, the meaning of absolute values of atomic charge does not make sense. Only for comparing purposes atomic charges might be computed, and some parts of this work make use of this. In a particular case, another method is applied (see chapter 4) for the calculation of atomic charges. It is the CHelpG

method,[30] in which atomic charges are calculated to reproduce the same electrostatic potential generated by the electronic density and nuclear distributions in the molecule.

If an unrestricted calculation have been carried out, the spatial parts for α and β electrons are treated separately. For a further population analysis, both sets combined adequately hold information of *spin polarisation*. Apart of the total electric charge attributed to a single atom in a molecule, we can have a guess of the spin polarisation in case of unpaired electrons by means of the same Mulliken population analysis. This will provide the excess of α vs. β electrons in each atom and, consequently, in different regions of the molecule. The mathematical procedure is equivalent to that of the closed-shell restricted case, although two density matrices shall be constructed, one for each set of electrons.

Decomposition of the energy

In many cases, especially when some units take part in a complex molecule, special phenomena can be studied. This is the case of, say, adsorption, encapsulation or coordination. These three cases show at least two fragments: adsorbate + substrate, host + guest or metal + ligand. For the study of these systems, theoreticians can artificially split the molecule in order to compute the energy of the fragments separately. Afterwards, their mutual interaction is computed. Then, a general expression for the total energy is in terms of the energy of the fragments is

$$E(molecule) = \sum_{i=1}^{N} E(i) + FIE$$

where *E(i)* is the energy of the *i*-th isolated (and thus distorted) and *FIE* is the energy of interaction between the fragments. The decomposition of the *FIE*, which accounts for the stabilisation of the whole system when the fragments are united adopting the geometry of the real cluster, can be carried out by means of several strategies. The Constrained Space Orbital Variation (CSOV) method, developed by Bagus,[31] performs a decomposition of the fragments interaction in various contributions in terms of a given orbital interaction scheme.[32]

Another decomposition method of the *FIE* is that formulated by Morokuma[33] and later adapted by Ziegler *et al.* in their Transition State method.[34] According to this formulation

$$FIE = SR + OI$$

Here, *SR* is the steric repulsion, consisting of two components: the classical electrostatic interaction between the *N* unperturbed charge distributions of the interacting fragments, and the so-called exchange or Pauli repulsion. This latter term accounts for the 4-electron destabilising interactions between occupied orbitals in the fragments. The orbital interaction (*OI*) term recover the energy variation due to charge transfer between fragments as well as the mutual electronic density polarisation of each fragment as an effect of the presence of the other. With this scheme one can study how fragments affect each other and what is the nature of this interaction, the magnitude of the charge transfer, etc.

In chapter 1 we introduced the clathrate concept associated to a family of POMs as special feature of this set of molecules. For further analysis of clathrate-like frameworks, the interaction between the fragments (say, the *cage* and the *internal ion*) is highly valuable. We will see in chapter 4 how the application of this scheme of decomposition can contribute to unravel highly interesting problems concerning the relative stability of a set of molecules.

Deformation density maps

Somehow related to the previous point there are the Deformation Density Maps,[35] DDM in brief. It is a tool for qualitative analysis. The fundamentals of this method lie in the deformation of two electronic densities upon interaction. The calculation of, say, two isolated fragments leads to ρ_1 and ρ_2, whereas the whole cluster provides ρ_{super}. Obviously, the sum of the densities of the isolates fragments does not equal ρ_{super}, the density of the supersystem. The difference between them is the deformation density,

$$\Delta\rho = \rho_{super} - (\rho_1 + \rho_2)$$

The magnitude of change, $\Delta\rho$,[36] is induced by the mutual polarisation + charge transfer. With DDM we can detect regions of charge accumulation or

charge depletion after interaction. We shall see in chapter 3 how the analysis of a DDM provides information related to the magnitude of the charge accumulation depending on the variation of one fragment.

Molecular electrostatic potential

For the study of fundamental aspects of the molecular structure and the reactivity, the interpretation of molecular electrostatic potentials (MESP) is of much importance. The electrostatic potential is defined as the energy experienced by a positive unitary charge put in position **r** in space under the effect of an electric field. The electrostatic potential (EP) is defined at each point of space with

$$V(\mathbf{r}) = \sum_{A=1}^{N} \frac{Z_A}{|\mathbf{r} - \mathbf{R}_A|} - \int \frac{\rho(\mathbf{r}')}{|\mathbf{r} - \mathbf{r}'|} d^3 r'$$

where **r** is a spatial position. The charge distribution of a molecule is composed of the positively charged nuclei and the negative charge density of electrons. Thus, the first term of the sum corresponds to the nuclear contribution (positive charges, Z_A) and the second one to the effect of the negative electronic distribution that is integrated over all space since ρ(**r**') is formally a continuous function. The values of $V(\mathbf{r})$ provide information about the electro- or nucleophilicity of the different regions of a molecule.[37] Provided that we can calculate the value of $V(\mathbf{r})$ at any point of space, a good way to represent this function in a friendly way is to plot it over a 3-dimensional isodensity surface of the molecule, thus giving a 4-dimensional coloured plot.

The major utilisation of MESP in the present work is concerned with the study of the basicity in Keggin clusters. This is, in some sense, the analysis of an electrophilic attack of an incoming H^+ to form an O–H bond in a cluster. For this purpose, an atomic charge analysis is sometimes proposed but from the discussion carried out before in this section, the latter tool is not as reliable as the MESP function. The reader shall notice in next chapters that the atomic charges of individual nucleophilic centres have shown no correspondence with their respective basicities. This is so for two reasons: the basicity is a property much more complicated than the simple study of the (artificial) atomic charges and, second, the calculation of atomic charges is inherently erroneous.

References and Notes

[1] Parr, R. G.; Yang, W. *Density Functional Theory of Atoms and Molecules*. Oxford University Press. New York, **1989**.

[2] Dreizler, R. M.; Gross, E. K. U. *Density Functional Theory: An Approach to the Many-Body Problem*. Springer-Verlag. Berlin, **1990**.

[3] Koch, W.; Holthausen, M. C. *A Chemist's Guide to Density Functional Theory*, 2nd. edition, Wiley, Weinheim, **2001**.

[4] Roothaan, C. C. J. *Rev. Mod. Phys*. **1951**, *23*, 69.

[5] Szabo, A.; Ostlund, N. S. *Modern Quantum Chemistry: Introduction to Advanced Electronic Structure Theory*, 2nd. edition. McGraw-Hill. New York, **1989**.

[6] Hohenberg, H.; Kohn, W. *Phys. Rev. B*. **1964**, *136*, 864.

[7] Kohn, W.; Sham, L. J. *Phys. Rev A*. **1965**, *140*, 1133.

[8] Thomas, L. H. *Proc. Camb. Phil. Soc*. **1927**, *23*, 542. Fermi, E. *Rend. Accad. Lincei.* **1927**, *6*, 602.

[9] Vosko, S. H.; Wilk, L.; Nusair, M. *Can. J. Phys.* **1980**, *58*, 1200.

[10] Ceperley, D. M.; Alder, B. J. *Phys. Rev. Lett.* **1980**, *45*, 566.

[11] Slater, J. C. *Quantum Theory of Molecules and Solids.* Vol. 4. McGraw–Hill, New York, **1974**.

[12] Perdew, J.P.; Burke, K.; Ernzerhof, M. *Phys. Rev. Lett*. **1996**, *77*, 3865. Filatov, M.; Thiel, W. *Mol. Phys.* **1997**, *91*, 847. Filatov, M.; Thiel, W. *Int. J. Quant. Chem*. **1997**, *62*, 603. Hamprecht, F. A.; Cohen, A. J.; Tozer, D. J.; Handy, N. C. *J. Chem. Phys.* **1998**, *109*, 6264.

[13] Becke, A. D.; *J. Chem. Phys*. **1986**, 84, 4524; *Phys. Rev. A*. **1988**, *38*, 3098.

[14] Perdew, J. P. *Phys. Rev. B*. **1986**, *33*, 8822; Perdew, J. P. *Phys. Rev. B*. **1986**, *34*, 7406.

[15] Perdew, J. P.; Wang, Y. *Phys. Rev. B*. **1986**, *33*, 8800.

[16] Lee, C.; Yang, W.; Parr, R. G. *Phys. Rev. B*. **1988**, *37*, 785.

[17] Becke, A. D. *J. Chem. Phys.* **1993**, *98*, 5648.

[18] Baerends, E. J.; Gritsenko, O. V. *J. Phys. Chem*. **1997**, *101*, 5383.

[19] Kohn, W.; Becke, A. D.; Parr, R. G. *J. Phys. Chem*. **1996**, *100*, 12974.

[20] Zhao, Q.; Parr, R. G. *Phys. Rev. A.* **1992**, *46*, 2337.

[21] Zhao, Q.; Parr, R. G. *J. Chem. Phys.* **1993**, *98*, 543.

[22] Stowasser, R.; Hoffmann, R. *J. Am. Chem. Soc.* **1999**, *121*, 3414.

[23] Andrés, J.; Beltrán, J., eds. *Química Teórica y Computacional*. Biblioteca de la Universitat Jaume I, Castelló, **2000**.

[24] ADF 2000.01. Department of Theoretical Chemistry. Vrije Universiteit. Amsterdam. Baerends, E. J.; Ellis, D. E.; Ros, P. *Chem. Phys.* **1973**, *2*, 41. Versluis, L.; Ziegler, T. *J. Chem. Phys.* **1988**, *88*, 322. Te Velde, G.; Baerends, E. J. *J. Comput. Phys.* **1992**, *99*, 84. Fonseca Guerra, C.; Snijders, J. G.; Te Velde, G.; Baerends, E. J. *Theor. Chem. Acc.* **1998**, *99*, 391.

[25] Maestre, J. M.; Poblet, J. M.; Bo, C.; Casañ-Pastor, N.; Gómez-Romero, P. *Inorg. Chem*. **1998**, *37*, 3444.

[26] Maestre, J. M.; López, X.; Bo, C.; Poblet, J. M.; Casañ-Pastor, N. *J. Am. Chem. Soc.* **2001**, *123***,** 3749.

[27] Snijders, J. G.; Baerends, E. J.; Vernooijs, P.; *At. Nucl. Data Tables,* **1982**, 26**,** *483*. Vernooijs, P.; Snijders, J. G.; Baerends, E. J. *Slater type basis functions for the whole periodic system,* Internal Report, Free University of Amsterdam, The Netherlands, **1981**.

[28] Rosa, A.; Ricciardi, G.; Baerends, E. J.; Stufkens, D. J. *Inorg. Chem.* **1996**, *35***,** 2886.

[29] Mulliken, R. S. *J. Chem. Phys*. **1955**, *23*, 1833.

[30] Breneman, C. M.; Wiberg, K. B. *J. Comp. Chem*. **1990**, *11*, 361.

[31] Bagus, P. S.; Bauschlicher, C. W.; Nelin, C. J.; Laskowski, B. C. *J. Chem. Phys.* **1984**, *81*, 3594.

[32] Hoffmann, R. *Solids and surfaces.* VCH, New York, **1988**. Schustorovich, E.; Baetzold, R. C. *Science.* **1985**, *227,* 1985.

[33] Morokuma, K. *J. Chem. Phys.* **1971**, *55*, 1236.

[34] Ziegler, T.; Rauk, A. *Theor. Chim. Acta.* **1977**, *46*, 1. Ziegler, T.; Rauk, A. *Inorg. Chem.* **1979**, *18*, 1558.

[35] Coppens, P.; Stevens, E. D. *Adv. Quantum Chem.* **1977**, *10*, 1. Coppens, P.; Hall, M. B., eds. *Electron distributions and the chemical bond*. Plenum Press, New York, **1982**. Breitenstein, M.; Dannhöl, H.; Meyer, H.; Schweig, A.; Seeger, R.; Seeger, U.; Zittlau, W. *Int. Rev. Phys. Chem.* **1983**, *3*, 335. Bader, R. F. W.; Nguyen-Dang, T. T. *Adv. Quantum Chem.* **1981**, *14*, 63.

[36] Schwarz, W. H. E.; Ruedenberg, K.; Mensching, L. *J. Am. Chem. Soc.* **1989**, *111***,** 6926.

[37] The basis of both concepts of '-philicity' lie on simple electrostatic considerations without taking into account quantum features like bonding or orbitals.